

WATER COMPATIBLE IONIC AND POLAR ORGANIC SEMICONDUCTORS FOR BIOELECTRONICS

Von der Universität Bayreuth
zur Erlangung des Grades eines
Doktors der Naturwissenschaften (Dr. rer. nat.)
genehmigte Abhandlung

von

Martina Margarete Schmidt

aus Pegnitz / Deutschland

1. Gutachter Prof. Dr. Mukundan Thelakkat
2. Gutachter Prof. Dr. Georg Papastavrou

Tag der Einreichung: 20.12.2017

Tag des Kolloquiums: 17.04.2018

Die vorliegende Arbeit wurde in der Zeit von September 2013 bis Dezember 2017 in der Arbeitsgruppe Angewandte Funktionspolymere am Lehrstuhl für Makromolekulare Chemie I der Universität Bayreuth unter der Betreuung von Prof. Dr. Mukundan Thelakkat angefertigt.

Amtierender Direktor der Graduiertenschule: Prof. Dr. Dirk Schüler

Dissertation eingereicht am: 20.12.2017

Wissenschaftliches Kolloquium: 17.04.2018

Prüfungsausschuss:

Prof. Dr. Mukundan Thelakkat (Gutachter)

Prof. Dr. Georg Papastavrou (Gutachter)

Prof. Dr. Andreas Greiner (Vorsitzender)

PD Dr. Richard Hildner

Für meinen Vater

*“Imagination is more important than knowledge.
Knowledge is limited. Imagination encircles the world. “*

Albert Einstein

TABLE OF CONTENTS

Summary.....	1
Zusammenfassung.....	4
1 Introduction.....	7
1.1 Organic Bioelectronics.....	7
1.2 Bioelectronic applications of organic semiconductors.....	11
1.3 Organic semiconductor materials	20
1.4 References	43
2 Objective of the thesis.....	56
3 Overview of the thesis.....	58
4 Smaller counter cation for Higher transconductance in anionic conjugated polyelectrolytes	73
5 Conjugated polyelectrolytes biased in aqueous electrolytes: mechanism of ion exchange and oxidation.....	101
6 Conjugated Polyelectrolyte Blends for Highly Stable Accumulation Mode Electrochemical Transistors	123
7 Conjugated Polyelectrolyte Blend as Photonic Probe of Biomembrane Organization	150
8 Eco-friendly processable fullerene derivatives with high electron mobility	182
List of publications.....	202
Acknowledgement.....	203
Danksagung	205

SUMMARY

This thesis focuses on the design and synthesis of novel semiconductor materials, highly suited for bioelectronics applications. The prototype of bioelectronics device studied here is organic electrochemical transistors (OECTs). This thesis also studies the physicochemical processes in OECTs based on conjugated polyelectrolytes (CPEs). The standard doped semiconductor layers in OECTs lead to devices operating in depletion mode. For applications, such as sensors, the devices operating in accumulation mode are preferred, as the power consumption is reduced. Nevertheless, materials that function in accumulation mode are rare, since the charge transport mobility and conductivity of undoped systems under low voltages is usually very low. One promising material, which has been already published as active layer in OECTs, is the conjugated polyelectrolyte poly(6-(thiophene-3-yl)hexane-1-sulfonate) tetrabutylammonium (PTHS⁻TBA⁺). This material requires further structural studies to improve its performance.

To improve the performance of PTHS⁻TBA⁺, first the processes in OECTs need to be understood in detail, which constitutes the first part of this thesis. The influence of counterions attached to the anionic CPEs on the properties such as optical characteristics, solubility, spectroelectrochemical behaviour, ionization potentials, capacitances, swelling capability and the device performance was investigated. Three different CPEs with the same polythiophene backbone, but with different counter ions, were synthesized. The counter ions varied in size: from the bulky tetrabutylammonium (TBA⁺) over tetraethylammonium (TEA⁺) to the smallest tetramethylammonium (TMA⁺) ion. Recorded absorbance and spectroelectrochemical spectra of the pristine as well as of the cross-linked CPEs showed that PTHS⁻TMA⁺ led to a higher aggregation degree, a faster diffusion of ions into the film and a faster recovery from oxidized state than the other two CPEs. Electrochemical impedance spectroscopy and cyclic voltammetry revealed that PTHS⁻TMA⁺ converted more dopant ions to electrical charges. Consequently, PTHS⁻TMA⁺ led to the best performing OECT devices.

This result brings up the question, which ions of the CPE and liquid electrolyte influence the ion-diffusion in anionic CPEs such as PTHS⁻X⁺ or what the fundamental steps of physicochemical processes are once the CPE film comes into contact with aqueous medium under bias. Via combination of spectroelectrochemical and elemental analysis, this question was addressed in this thesis. Cross-linked CPE films on ITO were immersed in different electrolytes with and without bias. Spectroelectrochemical spectra were used to detect the redox processes in the films. Afterwards, the elemental composition of the films was investigated via energy dispersive

X-ray spectroscopy (EDX). These measurements showed that ion exchange between the CPE and the electrolyte happens as soon as both got into contact. Application of additional bias and the immersion time did not influence the ion exchange process. Nevertheless, an influence of the nature of the electrolyte medium on the degree and kinetics of the CPE oxidation was noticed. The results contributed to a better understanding about redox processes, ion diffusion mechanism and the influence of the electrolyte solution on these and this allows future research to optimize material-electrolyte combinations for more efficient OECTs.

A further approach to improve the performance of PTHSTBA⁺ in OECTs was done by blending a conducting and a semiconducting CPE. The blend was rendered hydrophobic by counter ion exchange in the conducting CPE with the bulky dioctylammonium cation. Due to the hydrophobicity of the blended film, it showed an increased stability in aqueous environment. The electronic states of the blend were unaffected. Conductance measurements revealed that the threshold voltage was modified by the blending and the cation exchange. In OECTs the blends achieved transconductances up to 15.3 mS and switching times of around 79 ms (ON) and 11 ms (OFF). Consequently, an improvement of OECT stability and device performance was obtained by the blending of the CPEs and the cation exchange.

In the second part of this thesis the synthesis of new materials to be used as semiconductor layer in OECTs was the main focus. For example, biomembranes as active layers in OECTs can give a deeper insight into biological processes, e.g. the activity of ion channels. Therefore, the biomembrane has to be coupled with conducting/semiconducting CPEs without changing its assembled state. This can be verified by a photonic probe. Contrary to already known photonic probes, a hydrophobic blend of two CPEs was developed, which could be incorporated into the hydrophobic lipid shell of the biomembrane. The physical state of the different assemblies of membranes and CPEs were recorded via absorption measurements. As one of the CPEs showed good emission properties, the blend was suitable for imaging different physical states in vesicles via confocal microscopy experiments.

Further, the synthesis of an active material for n-type OECTs was demonstrated. To achieve high electron mobility, good swelling in aqueous conditions and processability from non-toxic solvents, swallow-tail oligo ethylene glycol groups were attached to C₆₀ and C₇₀ cores via Bingel-Hirsch reaction. Optimization of the reaction conditions led to a malonate to fullerene ratio of 0.7 to 1 and to iodine as halogenating reagent to obtain a good yield of monoadducts. The monoadducts showed a high solubility in polar solvents. Nevertheless, the fullerene derivatives were insoluble in water, which is suitable for bioelectronics. Therefore, no cross-linker will be needed to stabilize films in aqueous environment. The electron mobility of the derivatives were

determined by space charge limited current method and we obtained values up to $2.80 \cdot 10^{-2} \text{ cm}^2 \text{ V}^{-1} \text{ s}^{-1}$. Thus, the modified fullerene derivatives are promising candidates for bioelectronic applications.

In summary, this thesis paves the way to improve the performance of CPE materials in OECTs, as the processes in these devices are closely investigated and fundamental physicochemical insight is elucidated. Beside an approach to tune the operating mode of an OECT, new materials were synthesized and characterized, which constitute very promising candidates for bioelectronic applications.

ZUSAMMENFASSUNG

Die vorliegende Dissertation beschäftigt sich mit der Entwicklung und Synthese neuer Halbleitermaterialien, die für bioelektronische Anwendungen geeignet sind. Organische elektrochemische Transistoren (OECTen) wurden dabei als Prototyp verwendet. Darüber hinaus wurden die physikochemischen Prozesse in OECTen, die auf konjugierten Polyelektrolyte (KPE) basieren, untersucht. Bisher wurden gedopte Halbleitermaterialien als Standard in OECTen verwendet. Diese führen zu Bauteilen, die eine Verarmungsschicht aufweisen. Für viele Anwendungen, z.B. für Sensoren, ist jedoch ein Transistor mit Anreicherungsschicht von Vorteil, da diese weniger Energie verbrauchen. Allerdings sind Materialien, die eine Verarmungsschicht bilden, selten, da die Mobilität der Ladungsträger und die Leitfähigkeit ungedopter Materialien in der Regel bei geringer Spannung sehr niedrig ist. Ein bereits publiziertes, vielversprechendes Material stellt der konjugierte Polyelektrolyt Tetrabutylammonium Poly(6-(thiophen-3-yl)hexan-1-sulfonat) (PTHSTBA⁺) dar. Um die Leistung dieses Materials als aktive Schicht in OECTs zu verbessern, sind jedoch weitere Untersuchungen notwendig.

Um eine Leistungssteigerung von auf PTHSTBA⁺ basierenden OECTen zu erzielen, ist es notwendig zunächst die in OECTen ablaufenden Prozesse im Detail zu verstehen. Dies wird im ersten Teil dieser Dissertation behandelt. Der Einfluss der Gegenionen des anionischen konjugierten Polyelektrolyten auf dessen Eigenschaften wie optisches und spektroelektrochemisches Verhalten, Löslichkeit, Ionisationspotential, Kapazität, Schwellung und Leistung als aktive Schicht in OECTen wurde betrachtet. Hierfür wurden drei KPEs synthetisiert. Diese bestanden aus demselben Polythiophenrückgrat, wiesen aber in der Größe variierende Gegenionen auf: vom sterisch anspruchsvollen Tetrabutylammonium (TBA⁺), über Tetraethylammonium (TEA⁺) zum kleinsten Tetramethylammonium (TMA⁺) Gegenion. Absorptions- und spektroelektrochemische Messungen an reinen und vernetzten KPE Filmen zeigten, dass PTHSTMA⁺ den höchsten Aggregationsgrad, die schnellste Ionendiffusion in den Film, sowie die schnellste Regeneration vom oxidierten in den Grundzustand im Vergleich zu den anderen beiden KPEs erreichte. Darüber hinaus wurde mit elektrochemischer Impedanzspektroskopie und zyklischer Voltammetrie nachgewiesen, dass PTHSTMA⁺ ebenfalls die meisten dotierenden Ionen in elektrische Ladungen umwandeln konnte. Mit PTHSTMA⁺ wurde somit die beste Leistung in OECTen erzielt.

Diese Ergebnisse warfen die Frage auf, ob die im Elektrolyten vorhandenen Ionen einen Einfluss auf die Ionendiffusion in anionischen KPEs wie PTHS⁻X⁺ haben und was die grundlegenden

physikochemischen Schritte sind, sobald der KPE Film mit wässriger Lösung unter Spannung in Berührung kommt. Dieser Frage wurde hier mittels Kombination von spektroelektrochemischen und elementarer Analyse auf den Grund gegangen. Vernetzte KPE Filme wurden hierfür auf ITO Substraten aufgebracht und anschließend in unterschiedliche Elektrolytlösungen getaucht. Einige Filme wurden zusätzlich durch das Anlegen einer Spannung oxidiert. Spektroelektrochemische Aufnahmen detektierten die ablaufenden Redoxprozesse in den Filmen. Anschließend wurde die elementare Zusammensetzung der Filme mittels energiedispersiver Röntgenspektroskopie untersucht. Auf diese Weise wurde gezeigt, dass ein Ionenaustausch zwischen Film und Elektrolyt bei Kontakt sofort stattfindet. Weder ein zusätzlicher Stromfluss noch eine Veränderung der Eintauchdauer beeinflusste diesen Ionenaustauschprozess. Allerdings konnte ein Einfluss der Elektrolytlösung auf den Oxidationsgrad und die Oxidationskinetik festgestellt werden. Diese Ergebnisse tragen wesentlich zu einem besseren Verständnis der Redoxreaktionen, der Ionendifusionsmechanismen und des Einflusses der Elektrolytlösung bei und bereiten somit den Weg für weitere Optimierungen der Material-Elektrolyt-Zusammensetzung für noch effizientere OECTen.

Ein weiterer Ansatz zur Verbesserung KPE-basierter OECTen bestand aus der Vermischung eines halbleitenden mit einem leitenden KPE. Dieser Blend wurde durch Gegenionenaustausch der Protonen im leitenden KPE gegen Dioctylammonium hydrophob. Aufgrund der Hydrophobizität wurde eine höhere Stabilität in wässrigen Lösungen erhalten. Die elektronische Struktur des Blends wurde dabei nicht beeinflusst. Die Schwellenspannung konnte durch Modifizierung der Blendzusammensetzung und durch Ionenaustausch beeinflusst werden. Der optimierte Blend lieferte OECTen mit Transkonduktanzen von bis zu 15,3 mS und Schaltzeiten von 79 ms (ON) und 11 ms (OFF). Durch Mischung der beiden KPE und Ionenaustausch wurde schließlich eine Verbesserung der Leistung als auch der Stabilität von OECTen erzielt.

Der zweite Teil dieser Dissertation beschäftigte sich mit der Synthese von neuen Materialien für den Einsatz als aktive Schicht in OECTen. Um biologische Prozesse wie beispielsweise die Aktivität von Ionenkanälen besser zu verstehen, sind Biomembranen als aktive Schichten in OECTen besonders interessant. Hierfür ist es nötig, die Biomembranen mit leitenden/halbleitenden KPEs zu koppeln ohne deren physischen Zustand zu beeinflussen verändern. Dies kann durch photonische Sonden verifiziert werden. Im Gegensatz zu den gebräuchlichen photonischen Sonden, wurde ein hydrophober Blend aus zwei KPEs entwickelt, der in den hydrophoben Lipidkern der Biomembran positioniert werden kann. Der physische Zustand von Biomembranen konnte durch die jeweiligen Absorptionsspektren des eingebauten Blends sicht-

bar gemacht werden. Da der halbleitende KPE Emission aufwies, war der Blend zusätzlich zur Abbildung verschiedener physischer Zonen in Vesikeln durch konfokale Mikroskopie geeignet.

Darüber hinaus beschäftigt sich diese Dissertation mit der Synthese eines aktiven Materials für elektronenleitende OECTen. Um hohe Elektronenmobilität, gutes Schwellverhalten in wässriger Lösung und Verarbeitbarkeit aus ungiftigen Lösungsmitteln zu gewährleisten, wurden Schwalbenschwanz Oligoethylenglykolgruppen mittels Bingel-Hirsch Reaktion an C₆₀ und C₇₀ addiert. Als optimale Reaktionsbedingungen wurde ein Malonat zu Fulleren Verhältnis von 0,7 zu 1 und die Verwendung von Iod als Halogenierungsmittel ermittelt. Unter diesen Bedingungen konnten hohe Ausbeuten an Monoaddukt erzielt werden. Die synthetisierten Monoaddukte zeigten eine hohe Löslichkeit in polaren Lösungsmitteln. In Wasser zeigten sie jedoch keine Löslichkeit. Dies ist für bioelektronische Anwendungen von Vorteil, da keine zusätzliche Vernetzung notwendig ist, um die Filme in wässriger Lösung zu stabilisieren. Die Elektronenmobilität der Fullerenderivate wurde mit Messungen des durch Raumladung begrenzten Stroms bestimmt und lieferte Werte bis zu $2,80 \cdot 10^{-2} \text{ cm}^2 \text{ V}^{-1} \text{ s}^{-1}$. Demzufolge sind die hier untersuchten Fullerenderivate vielversprechende Materialien für bioelektronische Anwendungen.

Zusammenfassend trägt diese Dissertation durch das hinzugewonnene Verständnis der in OECTen ablaufenden physikochemischen Prozesse zu einer Leistungssteigerung von konjugierten Polyelektrolyten in OECTen bei. Darüber hinaus wurde eine Methode gefunden, die Betriebsart von OECTen anzupassen Außerdem wurden vielversprechende elektronenleitende Materialien für bioelektronische Anwendungen synthetisiert und charakterisiert.

1 INTRODUCTION

1.1 Organic Bioelectronics

The field of bioelectronics can be traced back to Luigi Galvani's famous experiments in the 1780s at the University of Bologna. In those experiments he showed that application of electricity on a detached leg muscle of a frog induces muscular activity. Galvani suggested that this phenomenon requires some "animal electricity", a form of intrinsic electricity present in animals. On the contrary, Alessandro Volta, a physicist at the University of Pavia, claimed that the muscular movement was induced by external electricity originating from metal contacts. This controversy between Volta and Galvani counts as one of the most important scientific disagreements in history, which end in the invention of the electrical battery by Volta and the basis of electrophysiology by Galvani. The crucial experiments, which turned Galvani to the founder of electrophysiology, were performed in 1794 and 1797: To corroborate his theory of "animal electricity" he induced the muscle activity of the frog's leg by directly connecting nerves and muscles without any metal involved (Figure 1-1 A). However, Volta was not convinced and claimed that dissimilar bodies that are brought in contact can also generate electricity. Finally, Galvani proofed his hypothesis of "animal electricity" by connecting corresponding nerves of the same frog, as there were no dissimilar bodies involved (Figure 1-1 B).^[1,2]

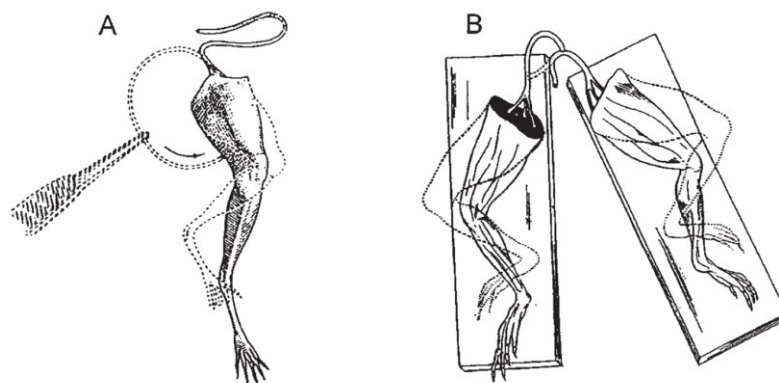


Figure 1-1: Experiments of Galvani on a detached frog leg. (A) Nerve sections brought in contact with the leg muscle led to contraction of the frog leg. This experiment was performed in 1794. (B) In the experiment of 1797, Galvani connected sciatic nerves of the legs of the same frog resulting in a contraction of both legs. Figure reproduced from Ref. [1].

Later, Galvani's theory of an intrinsic electricity in animals is verified by subsequent studies and the field of bioelectronics arose.^[1,2] Bioelectronics can be seen as translator between biomaterials and electronic elements (Figure 1-2). On the one hand, biological systems and

reactions can be recorded and studied by electronic elements, which convert the signals into electronically displayable values. On the other hand, electronic elements can be used to influence the biochemical processes happening in biological systems (Figure 1-2).^[3] Therefore, bioelectronics can improve the quality of life of patients, enhance clinical diagnostics and help to understand biological processes. Implantable cardioverters-defibrillators (ICDs),^[4] pacemakers^[5] and cochlear implants^[6] are examples for bioelectronics, which are already in clinical use. Applications such as electroencephalogram (EEG), which records brain activities, helps to understand the functioning of the brain and to diagnose tumors or epilepsy.^[7] Electrical stimulation is successfully used for treating epilepsy and Parkinson's disease.^[8-10] Biosensors are a special part of bioelectronics. Here, a biological element, e.g. enzyme or tissue, reacts with a target analyte and produces an electrical, thermal or optical signal, which can be detected and depends on the concentration of the analyte.^[11] Biosensors can be used for clinical diagnosis,^[12] analysis of environmental samples^[13] and food quality,^[14] control of industrial processes^[15] and detection of pathogens.^[16] A well-studied example for biosensors is the glucose sensor, which helps diabetics to have a better control on their blood sugar level.^[17]

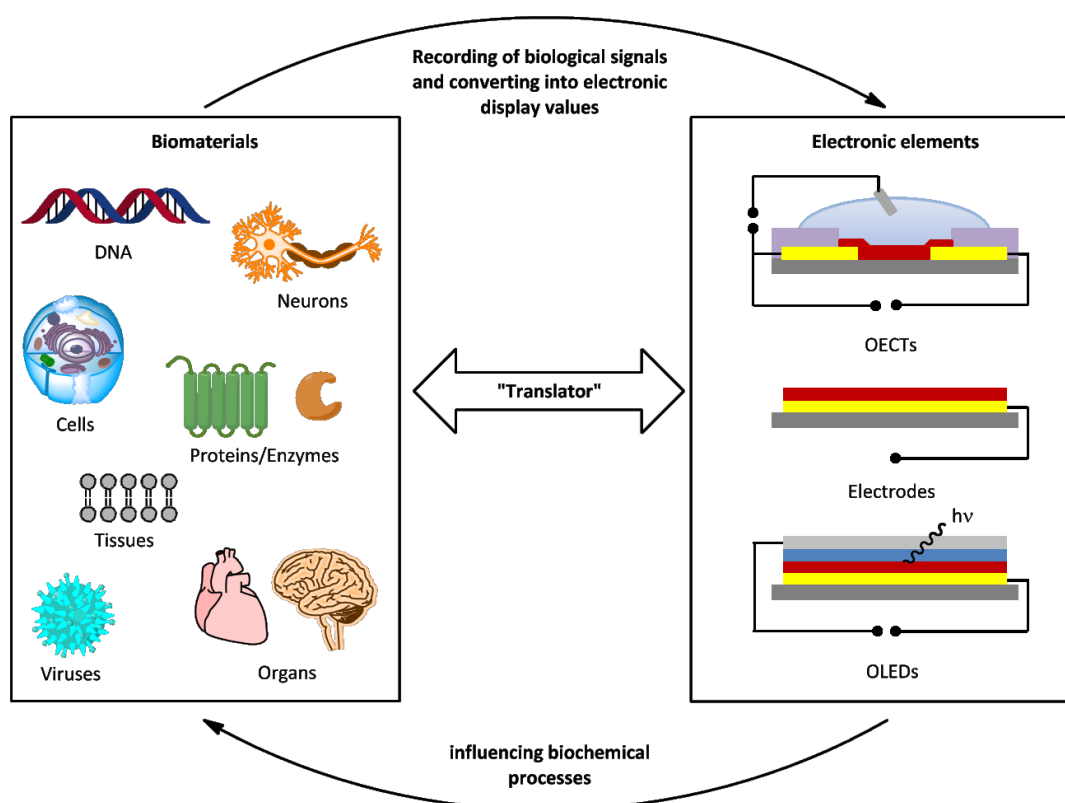


Figure 1-2: Schematic illustration of bioelectronics as translator between biomaterials and electronic elements. Biological signals are recorded and converted into electronic signals by electronic elements. Furthermore, electronic elements can influence biochemical processes. Figure adapted from Ref. ^[3].

The electrical contact between the abiotic side (i.e. electrodes, devices and components) and the biotic side (e.g. cells, tissues, organs) is a crucial factor for bioelectronic applications.^[18] Therefore, materials for bioelectronics are limited to the ones which are able to transduce signals across the biotic/abiotic interface.^[19] Conventional used materials for electronics, such as metals, cannot efficiently convert ionic signals used in biological signaling to electrical signals or vice versa. The impedance is an indicator for these conversions. Conducting polymers were used as electrode coatings, as they increase the accessible interfacial area and can be easier infiltrated by ions.

This leads to a decreased impedance and thereby to an improved conversion.^[20–24] Consequently, neural depth probes coated with conducting polymers gained a higher signal-to-noise ratio compared to conventional electrodes.^[25–27] A decrease of impedance also reduces the needed voltages for electrical stimulation and as a result the likeliness of harmful electrochemical side reactions.^[18,22] Inflammations, triggered by insertion of a device, can be reduced by the coating, as it is able to deliver anti-inflammatory drugs.^[28,29] Finally, a trend from organic coatings to organic devices arose. A main advantage of organic semiconductor materials compared to classical inorganic materials such as silicon is their ability to conduct electrons as well as ions.^[30] This ability derives from their soft nature and compatibility with biological systems. Inorganic layers consist of a covalently bound network and an oxide top layer, through which hydrated ions cannot easily diffuse. In contrary, organic semiconductor materials build networks, which are hold together only by weak van der Waals interactions enabling an efficient ion diffusion through the films. As organic materials do not form oxide layers, they furthermore provide direct contact with the biological environment (Figure 1-3). As the soft mechanical properties of organic electronic materials mimic those of biological structures, the formation of scar tissue by mechanical stress is reduced.^[19,30–32]

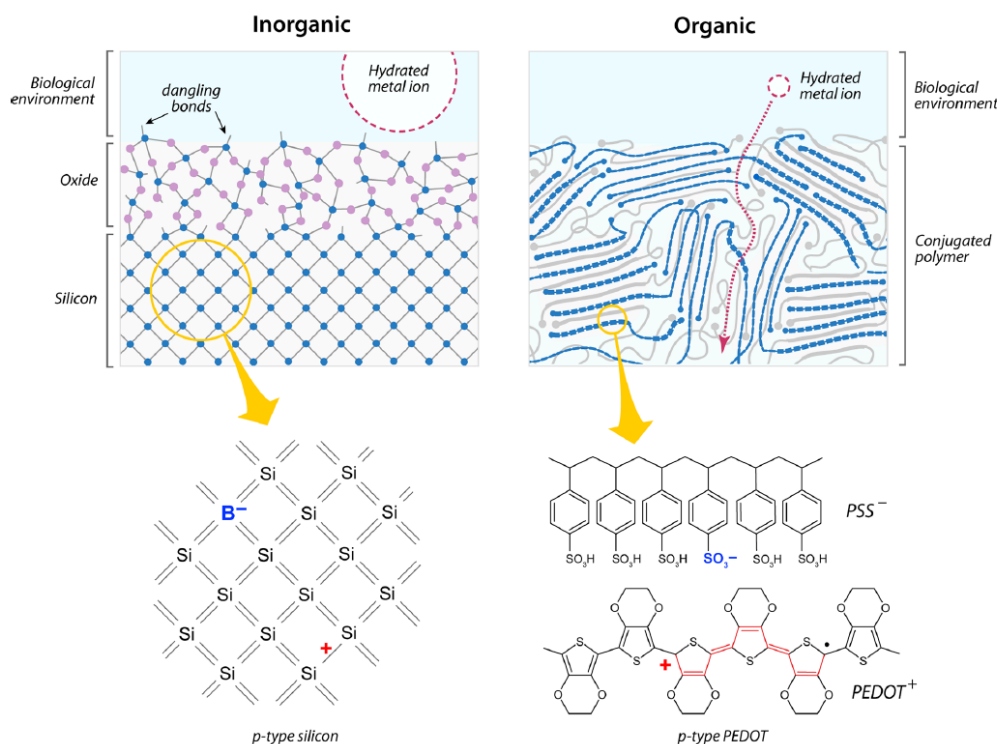


Figure 1-3: Schematic comparison of ion diffusion through an inorganic and an organic semiconductor layer. A *p*-type silicon layer and a PEDOT:PSS layer in direct contact with biological environment are used as examples. As the silicon layer consists of a covalently bound network and an oxide top layer, hydrated ions cannot easily diffuse through the silicon layer. In contrast, PEDOT:PSS forms a network, which is held together by weak van der Waals interactions, which enables the ions to diffuse through the network. Figure reproduced from Ref. [19].

The transparency of organic materials enables the use of optical analysis techniques and imaging applications.^[31] Organic materials can be deposited at room-temperature and can be synthesized cost-effectively. This is not possible for conventional electronics.^[19] The conductivity of organic electronic materials can be tuned from semiconducting to semi-metallic or even metallic.^[30,33,34] The biological properties can be tailored by functionalizing the compounds with molecular side-groups such as proteins or anchoring groups.^[18,31] By means of chemical synthesis also the mechanical and electronic properties can be influenced. Due to their versatility, organic electronic materials face a lot of potential applications in the field of bioelectronics. In 2007 the term “organic bioelectronics” was coined for the research of bioelectronics based on organic electronics.^[19,31] In the next part bioelectronic applications of organic semiconductors will be considered in more detail.

1.2 Bioelectronic applications of organic semiconductors

1.2.1 Organic electrochemical transistor (OECT) devices

Wrighton's group reported the first organic electrochemical transistor (OECT) in 1984, in which transistor geometry of a device is achieved by biasing through an electrolyte with a reference electrode as gate electrode. The setup consists of three gold electrodes coated with polypyrrole and immersed in an electrolyte. It is a fundamental property of a transistor to amplify a signal, that varies the resistance between two contacts.^[35,36] Based on polyaniline, this OECT acted as a sensor for redox reagents and pH value, as both parameters change the conductivity of the polymer.^[37] Different conjugated polymers were tested as active material in OECTs, like polythiophenes^[38–42] and polycarbazoles.^[43,44] Nowadays, poly(3,4-ethylenedioxythiophene):poly(styrene sulfonic acid) (PEDOT:PSS) is the most common active material used in OECTs, as it combines high environmental stability with improved processability and performance.^[18,36,43]

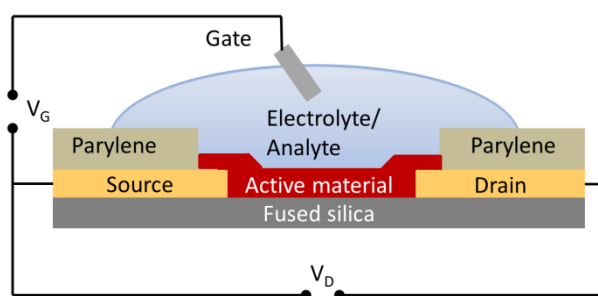


Figure 1-4: Cross-sectional schematic of an OECT.

A cross-sectional schematic of a typical OECT is shown in Figure 1-4. The active material is cast in the channel located between the source and the drain electrodes. The gate electrode is separated from the channel through the electrolyte. Application of a gate voltage causes ion motion between the electrolyte and the active layer of the device. This ion motion influences the conductivity of the active layer due to redox processes.^[45] As it is presumed that the ions diffuse into the active layer via application of a gate voltage, the geometry (width, length and volume) of the channel has a high impact on the transistor performance.^[18,46] For instance, a small-sized channel will lead to a faster response down to several milliseconds.^[47–49] However, the modulation of the drain current will be less obvious than for devices with larger channel.^[18,49] The material used for the gate electrode is also crucial for the performance of an OECT. Lin et al. showed that OECTs with the same geometry and active layer, but different gate electrode materials, differ in their characteristics. Reason for that are the altered properties of the

electrode/electrolyte interface and the associated differences in the potential drop at these interfaces.^[43]

The electrolyte in an OECT can be a solid, a liquid or a gel.^[50] As the ions within the electrolyte modulate the conductivity and consequently the drain current, I_D , of the OECT, the transistor characteristics depend on the ion concentration in the electrolyte, as well.^[43] By increasing the ion concentration, the current modulation will be more drastic.^[43]

As ion-to-electron transducers, OECTs enable the translation of a biological (ionic) into an electronic signal.^[51] The transconductance g is the figure-of-merit for this transduction and is defined as

$$g = \frac{\partial I_D}{\partial V_G}$$

with I_D as the drain current and V_G as the gate voltage.^[46] As the dedoping/doping of the active layer takes place within the bulk of the material, the whole material is involved in producing signal and therefore the transconductance is among the highest in all transistor technologies.^[52]

The low operational gate voltage (below 1 V) and thus the possibility to use OECTs in aqueous environment render this type of transistor suitable for applications in biology. Biological systems require low voltages to avoid redox reactions of water or biomolecules.^[36,48] OECTs can act as sensor for ions^[43,53], DNA^[54], bacteria^[55], enzymes^[56,57], cells^[58] etc. Furthermore, they enable “lab on a chip” systems, as they can be easily integrated into microfluidic channels.^[59] Due to the possibility to fabricate OECTs on flexible substrates, stretchable devices for wearable electronics and implantable devices can be produced.^[60,61] It was shown that even after mechanical deformation of a flexible OECT, the transistor characteristics remain unchanged.^[49,60] Besides, the integrity of tissues can be examined with OECTs.^[18] This is useful for screening of drugs as the ability of drugs to cross a barrier tissue can be read through the OECT current.^[62,63]

As demonstrated by Fromherz et al., transistors can record electrical signals of neurons and stimulate them extracellularly. Using field effect transistors (FET) based on silicon, in vitro signals from neuronal cell cultures could be detected.^[64,65] Compared to classical electrodes that are passive elements, an increased signal-to-noise ratio was obtained with FETs. This is due to the ability of the FET to amplify small changes in electrical field generated by neurons. Further improvement of the signal-to-noise ratio can be achieved by the use of OECTs due their high transconductance. In silicon based FETs, an oxide layer separates the active layer from the cells and ions can interact only with a thin layer of the film. In OECTs, on the other hand, the electrolyte (cell culture) is in direct contact with the channel, which enables excellent amplification.^[66]

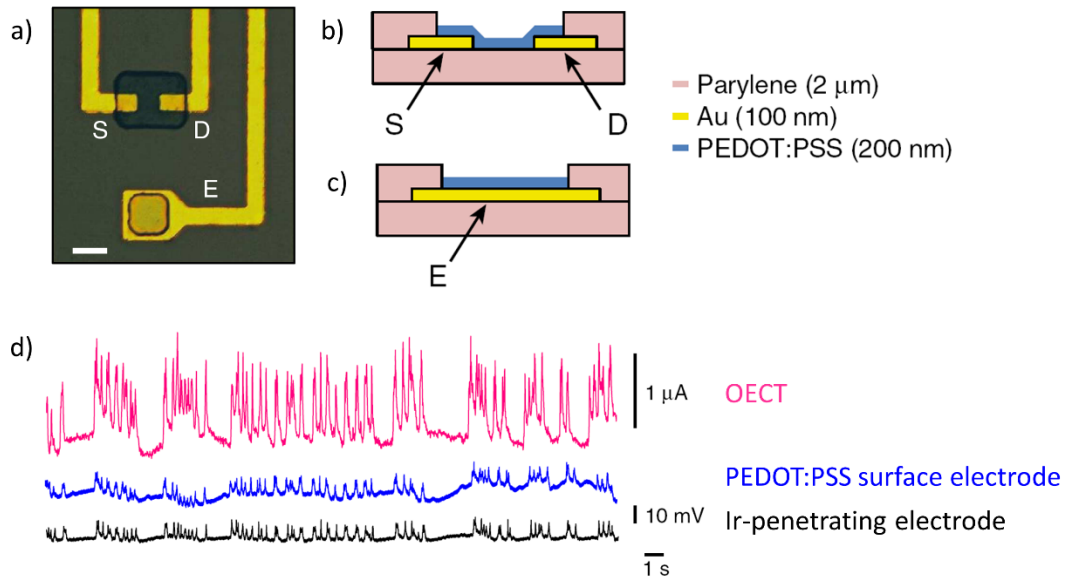


Figure 1-5: a) Optical microscopy photos of an ECoG probe based on a PEDOT:PSS OECT and electrode (Scale bar: 10 μm). The source (S), drain (D) and the electrode pad (E) consist of gold (Au). b) Cross-sectional schematic of the OECT and c) the electrode nearby. PEDOT:PSS layer is ca. 200 nm in both devices. d) Neural recordings of the OECT, the nearby electrode and a penetrating iridium electrode. Figure reproduced from Ref. ^[66].

A comparison of electrocorticography (ECoG) recordings obtained from the somatosensory cortex of rats using PEDOT:PSS based electrodes and OECTs is shown in Figure 1-5.^[66] With an OECT based on PEDOT:PSS, a high local amplification of neural signals is achieved leading to an excellent signal-to-noise ratio. Moreover, the electrophysiological signals obtained from an Ir-penetrating electrode are shown in Figure 1-5 d. The quality of the signals obtained using the OECT from the surface of the brain is superior compared to that obtained with an electrode which penetrates the brain.^[66]

OECTs can operate in two different modes: the depletion mode and the accumulation mode. Up to date most OECTs work in depletion mode. In this mode, when no bias is applied, the OECT is in the ON state (high I_D values) and can be turned OFF (low or negligible values of I_D) by application of gate voltage. PEDOT:PSS, is the golden standard of doped semiconductor used in OECTs. OECTs based on it work in depletion mode. To operate a PEDOT:PSS based OECT, a positive gate voltage has to be applied (cations penetrating into the channel deplete holes).^[50] An example for I_D - V_g transfer characteristics and transconductance of an OECT operating in depletion mode is shown in Figure 1-6 a. Here, a modified form of PEDOT:PSS, namely PEDOT:PSTFSILi, was used as active material, in which lithium is used as counter ion and the sulfonate side groups of the dopant polymer PSS is replaced by (trifluoromethylsulfonyl)sulfonylimide (TFSI).^[67] For accumulation mode OECTs, on the other hand, the channel material should exhibit low conductivity in its pristine state (no applied V_g). Consequently, the device is initially

OFF, while a negative (positive) bias at the gate creates holes (electrons) in the semiconductor and switches the device ON.^[50] Accumulation mode OECTs are still rare and typically, need high operation voltages due to high barriers of ion injections and energy levels of the polymer.^[66] The first example of an accumulation mode OECT with high transconductance was shown in a joint work between Malliaras group and our group. In Figure 1-6 b the I_D - V_g transfer characteristics and the transconductance of this accumulation mode OECT based on poly(6-(thiophene-3-yl)hexane-1-sulfonate) tetrabutylammonium is shown.^[40]

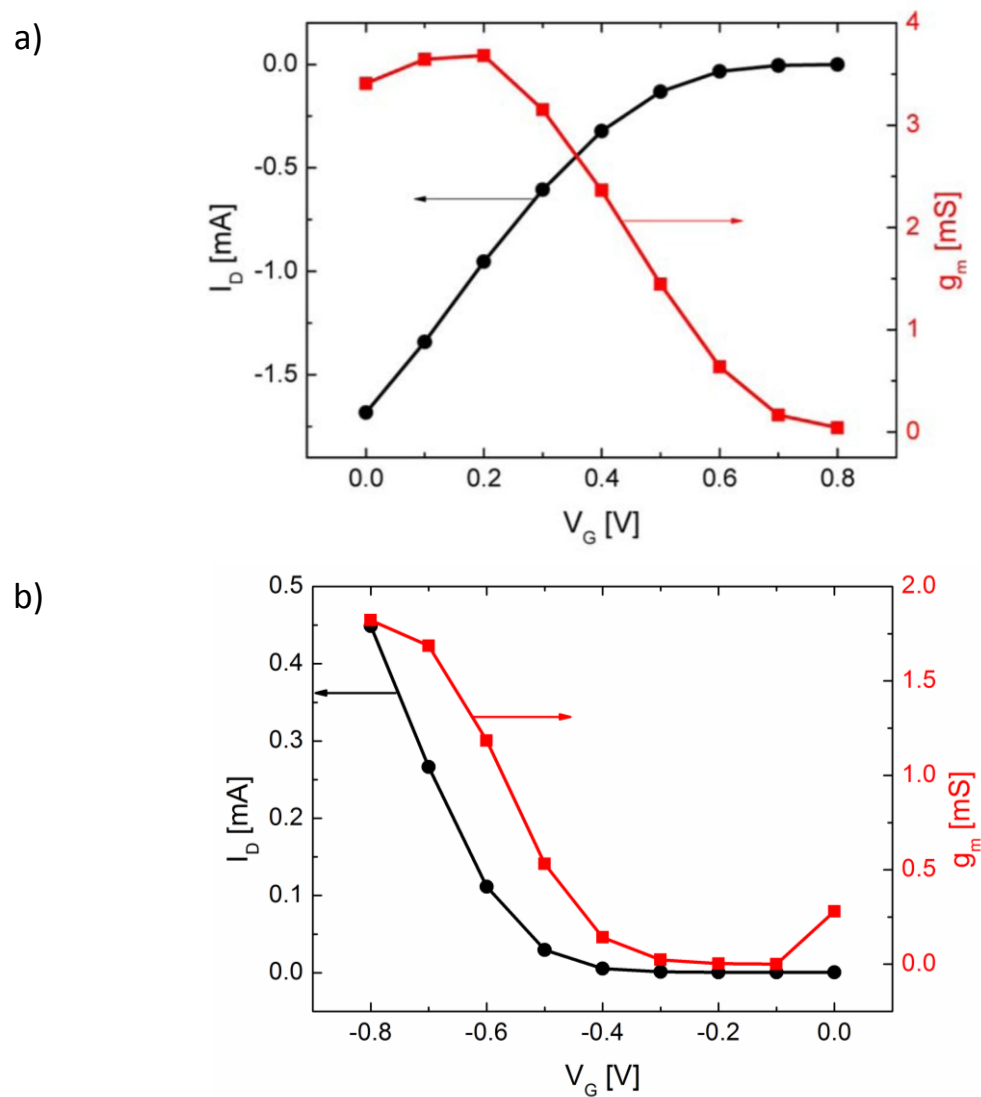


Figure 1-6: Examples of I_D - V_g transfer characteristics and transconductances of an (a) depletion mode and an (b) accumulation mode OECT. The OECT in figure (a) ($W = 100 \mu\text{m}$, $L = 10 \mu\text{m}$, $d = 200 \text{ nm}$, $V_D = -0.8 \text{ V}$), is based on PEDOT:PSTFSLI, a modified form of the golden standard PEDOT:PSS, and is reproduced from Ref. ^[67]. Figure (b) shows the results for an OECT based on crosslinked poly(6-(thiophene-3-yl)hexane-1-sulfonate) tetrabutylammonium comprising 5 vol% ethylene glycol ($W = 250 \mu\text{m}$, $L = 5 \mu\text{m}$, $d = 60 \text{ nm}$, $V_D = -0.6 \text{ V}$), which was published in a joint work between Malliaras group and our group.^[40]

Since the focus of scientific research has traditionally been on p-type semiconductors (most likely due to their presence), the OECTs rely on hole transport materials. In fact, a major problem

for the use of n-type materials in OECTs is the aqueous operation regime, which often leads to degradation of the material and readily oxidation.^[68,69] Just recently, Giovannitti et al. showed the first stable n-type OECT based on a 2,6-dibromonaphthalene-1,4,5,8-tetracarboxylic diimide (NDI) polymer.^[69]

1.2.2 Photonic probe for biomembranes

As lipid bilayers are the fundamental structure of all biological membranes, they are typically used as model systems for bioimaging.^[70] Lipid bilayers are built of phospholipids, which consist of two hydrophobic tails (acyl chains) and a hydrophilic head with a phosphate group (Figure 1-7). The hydrophobic tails are normally fatty acids and differ in their saturation degree and length.^[71]

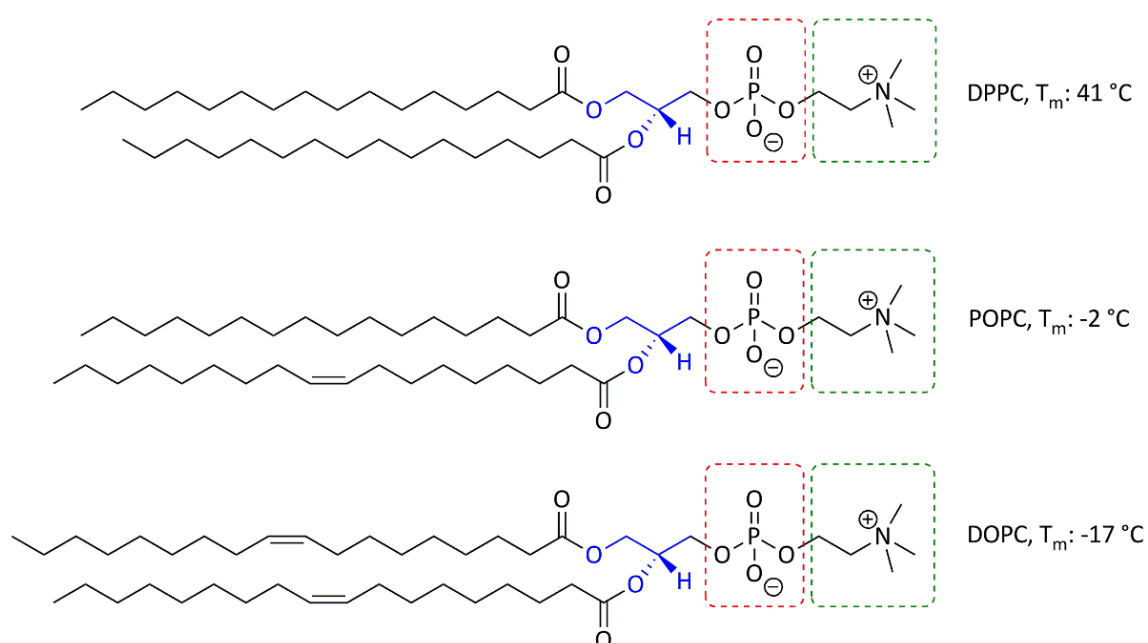


Figure 1-7: Chemical structures of three phospholipids, which vary only in the saturation degree of the fatty acids (drawn in black). The phase transition temperature T_m of these phospholipids are changing with the degree of saturation in the hydrophobic tails: The saturated 1,2-dipalmitoyl-sn-glycero-3-phosphocholine (DPPC) has a T_m of 41 °C, 1-palmitoyl-2-oleoyl-sn-glycero-3-phosphocholine (POPC) (one unsaturated group) of -2 °C and 1,2-dioleoyl-sn-glycero-3-phosphocholine (DOPC) (two unsaturated groups) of -17 °C. The blue marked part build together with the red and the green box the hydrophilic phospholipid head. The blue marked structure is glycerol, in the red box the phosphate group and in the green a choline group can be found.

Due to their amphiphilic (also called amphipathic) nature, phospholipids self-assemble in polar solvents to form vesicles called liposomes (Figure 1-8). The hydrophilic head is orientated towards the polar media, whereas the hydrophobic tails interact with each other and try to keep the surface with the polar media as small as possible.^[72] Lipid bilayers function as barrier for ions, as ions have trouble to diffuse through the hydrophobic core of the bilayer. The permeability of bilayers towards sodium and potassium ions is in the order of 10^{-5} nm/s and for

chloride around 10^{-3} nm/s. Liposomes can be classified into small unilamellar vesicles (SUV) (20 - 100 nm), large unilamellar vesicles (LUV) (> 100 nm) and giant unilamellar vesicles (GUV) (> 1000 nm). Furthermore multilamellar vesicles (LMV) (> 500 nm) can be formed, in which the bilayers are separated by layers of polar medium.^[73-75]

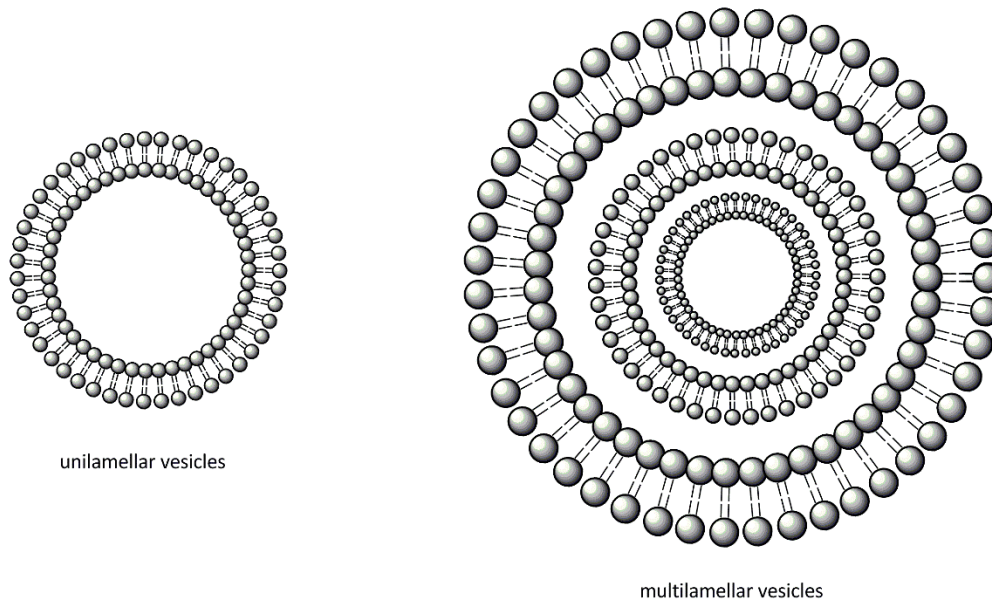


Figure 1-8: Structure of a phospholipids arranged as uni- and multilamellar vesicle.

Lipid bilayers can be in the liquid disordered, fluid (L_{dis} or L_d) state or in the solid ordered-gel phase (S_{ord} or S_o). Dependent on the lipid type (degree of unsaturation and length of the acyl chain, type of the head group) the phase transition will take place at a different temperature (Figure 1-7). This temperature is called the phase transition or melting temperature T_m .^[76]

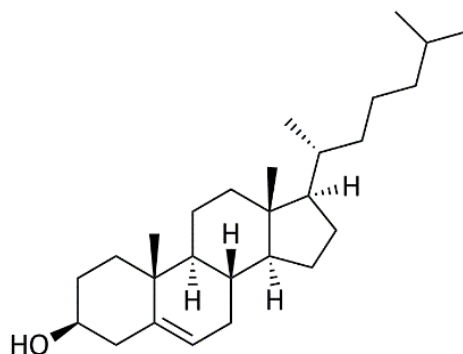


Figure 1-9: Chemical structure of cholesterol.

Furthermore, small molecules are part of biomembranes. These molecules also influence the physical state of the bilayer. Cholesterol (Figure 1-9) is an important component, which will keep biomembranes fluid independent of temperature variations. As example a phase diagram of DPPC in dependence of cholesterol content is shown in Figure 1-10. At high cholesterol content,

the DPPC will be in a liquid ordered state (L_{ord} or L_o). Furthermore, membrane microdomains can exist, such as L_d besides L_o or S_o besides L_o .^[77]

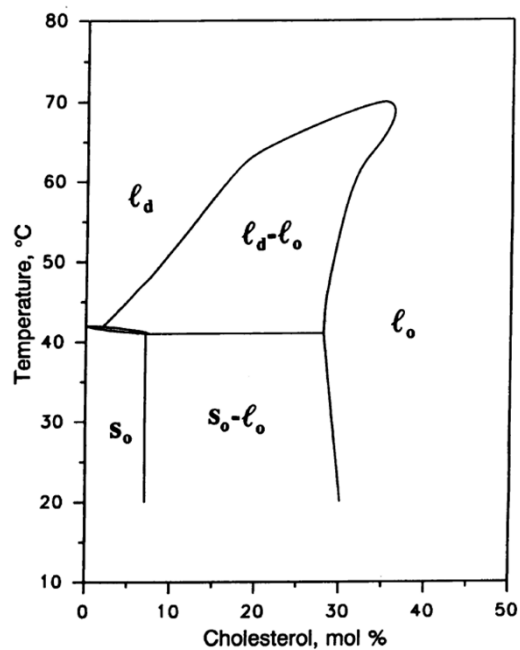


Figure 1-10: Phase diagram of DPPC plotted as a function of cholesterol content and temperature. Figure reproduced from Ref.^[77].

Additionally, the affinity of cholesterol varies for different phospholipids.^[78] Consequently, in model membranes consisting of various phospholipids, microscopic domains can be obtained. These domains, that are called rafts, were proposed just in 1997.^[79] They are supposed to induce several membrane processes, like cell motility and polarization, signal transduction, protein cluster formation and endocytosis.^[80-83]

But still membrane rafts are controversial discussed. The mechanism behind the formation of such rafts and how they influence membrane processes are still not understood, as the detection methods are a long way off to ideal. Thus, new techniques were developed to enable the examination of L_{ord} and L_{dis} phases. Especially optical techniques are relevant, as they are noninvasive, fast and sensitive. Furthermore, optical methods can be used in situ on live cells. Besides the improvement of microscopy techniques, new fluorescent probes were investigated to optically image the physical states of membranes.^[83-87]

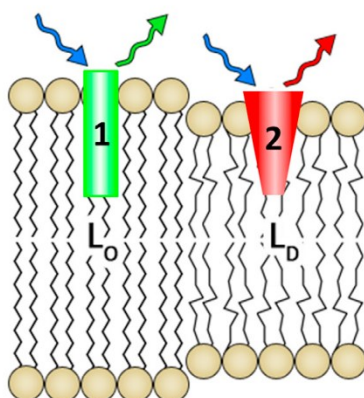


Figure 1-11: Schematic scheme illustrating the principle of partitioning probes. 1 and 2 representing lipophilic fluorescent molecules. Molecule 1 preferences partition in the liquid ordered phase, whereas molecule 2 prefers the disordered phase. Figure reproduced from Ref. ^[83].

Due to photonic probes, that are staining the membrane with a fluorescent material, the physical state of the liposomes can be visualized. Visualization is based on selective partitioning or on the sensitivity of the fluorescent material towards changes in polarity of its environment. Probes, based on the selective partitioning, consist of lipophilic fluorescent molecules that have a preference to partition either into the liquid ordered or the liquid disordered phase. There they provide their specific staining and indicate the respective phase (Figure 1-11). Generally, most probes are segregated from the liquid ordered phase, as the requirements on the spatial structure of the probe are high to fit into the tightly packed L_o phase. ^[83,88,89]

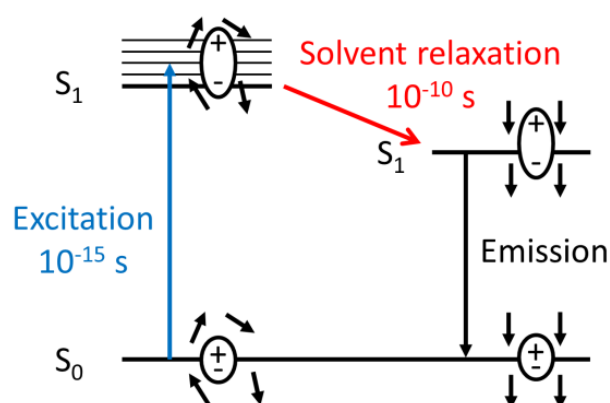


Figure 1-12: Schematic illustration of solvent relaxation. The little arrows symbolize the dipole moment of surrounded solvent molecules. In the excited state (S_1) fluorophores exhibit a larger dipole than in ground state (S_0). Solvent relaxation, i.e. the reorientation of the solvent dipoles, leads to a decrease of the excited state S_1 and therefore to a shift in the emission spectrum. The excitation (absorption) occurs in less than 10^{-15} s. Normally, solvent relaxation is finished within 10^{-10} s. ^[90-92]

On the contrary, probes, based on environment-sensitive fluorescent molecules, partition into both phases. Due to changes in the environment, the color, intensity or the lifetime of the

obtained fluorescence will vary. The changes can be of solvatochromic nature: In general, fluorophores exhibit a larger dipole moment in their excited state than in their ground state. As fluorescence occurs for a relatively long timescale, polar solvent molecules can rearrange around the dipole created by excitation. This reorientation leads to a decrease of the energy of the state and therefore to a shift of the emission spectrum to longer wavelengths (Figure 1-12). As water molecules possess dipoles, the presence of water will lead to such a solvent relaxation. Given that lipid bilayers in L_{dis} phase will absorb more water, L_{dis} and L_{ord} phases can be distinguished by a shift of the emission spectrum. A famous example for an environment-sensitive fluorescent molecule is 2-dimethylamino-6-lauroylnaphthalene, which is better known as Laurdan and belongs to the first used probes in lipid biomembranes (Figure 1-13). In the liquid ordered phase, the emission maximum of Laurdan occurs at a wavelength of 440 nm, whereas in the liquid disordered phase the maximum can be found at 490 nm (Figure 1-13).^[264,270,272,274]

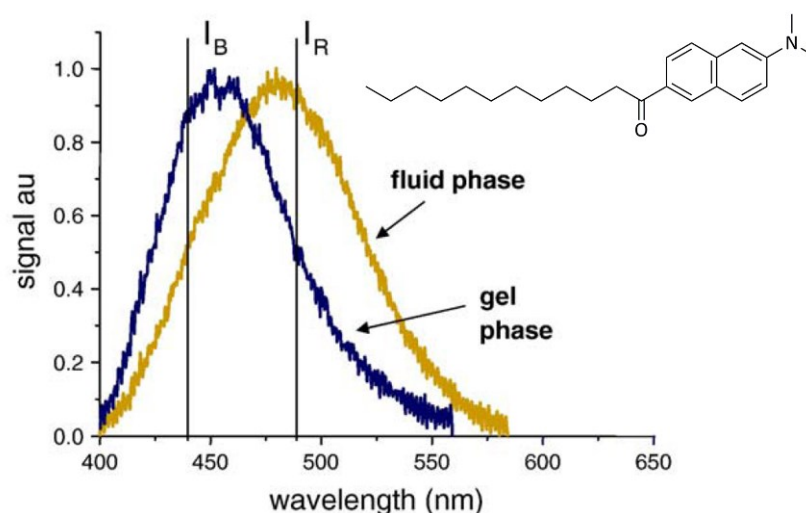


Figure 1-13: Emission spectra of laurdan in gel phase (i.e. L_{ord}) and in fluid phase (i.e. L_{dis}) reproduced from Ref.^[94]. The inset shows the chemical structure of Laurdan.

Beside small fluorescent molecules, fluorescent proteins and quantum dots (QD) have been used as photonic probe. However, the application of proteins and small molecules was restricted by their low photobleaching threshold.^[95–97] Whereas, QDs show good photostability, but introduce cytotoxic heavy metals like cadmium or selenium into the biological system and are therefore not suitable for in vivo bioimaging.^[98,99] On the contrary, CPEs show low cytotoxicity, high sensitivity and versatile surfaces. They possess good photostability, which enables the use of confocal microscopy.^[88,97,100] Because of the amphiphilic nature of CPEs, they can be added to lipid bilayers from aqueous solution and can be incorporated to a certain degree into the lipid bilayer. So far, only few examples for the usage of CPEs as photonic probe for biomembranes are

presented in literature.^[76,88] In membranes in the disordered phase, the conjugated backbone of CPEs will be twisted, leading to a decrease in conjugation length and thus to a blue-shift of the emission maximum (see chapter 1.3.2 for more detail). Contrary, a planarization of the CPE backbone in ordered phase membranes will lead to a red-shift of the emission spectra.^[76,101–103]

1.3 Organic semiconductor materials

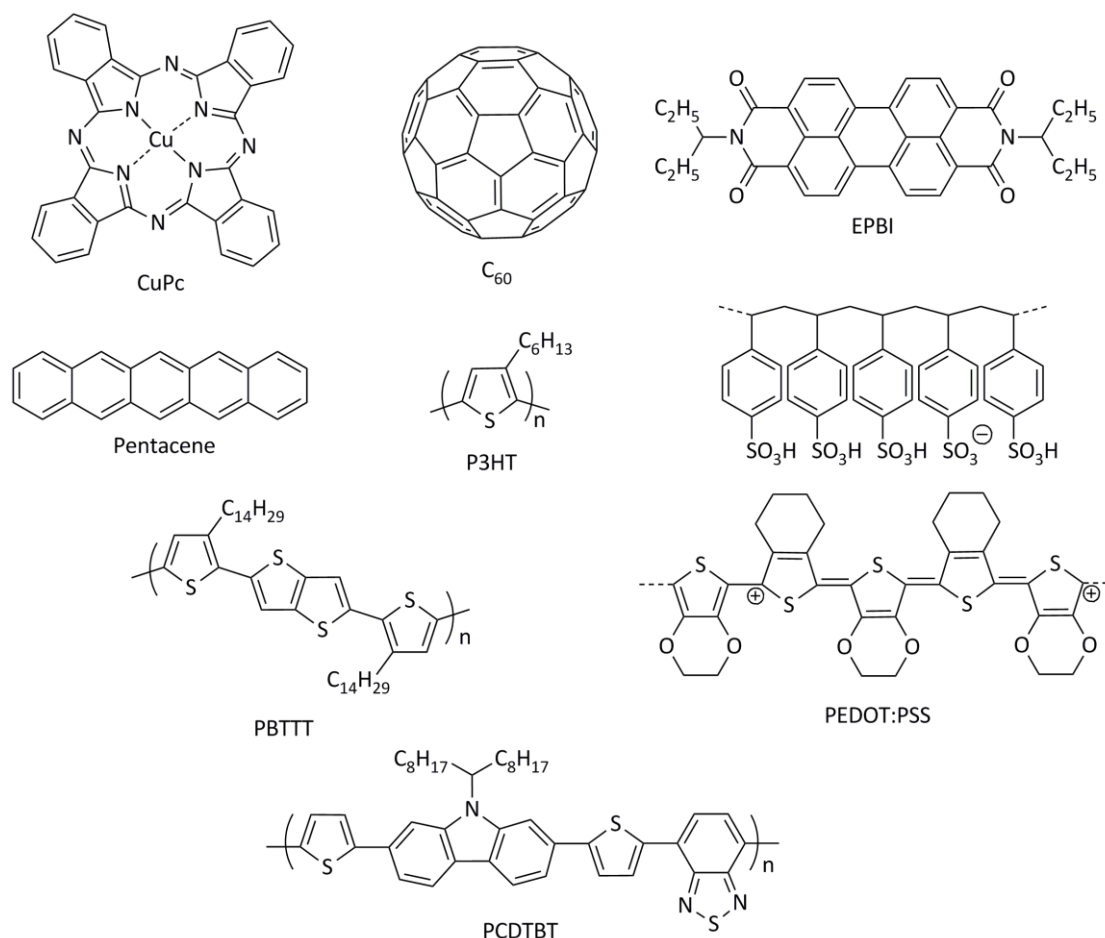


Figure 1-14: Chemical structures of commonly used organic semiconductors: copper phthalocyanine (CuPc), fullerene C_{60} , N,N'-bis(1-ethylpropyl)perylene-3,4,9,10-bis(dicarboximide) (EPBI), pentacene, poly(3-hexylthiophene) (P3HT), Poly(3,4-ethylenedioxythiophene):poly(styrene sulfonic acid) (PEDOT:PSS), poly(2,5-bis(3-tetradecylthiophen-2-yl)thieno[3,2,-b]thiophene) (PBTTT), poly(N-9'-heptadecanyl-2,7-carbazole-*alt*-5,5'-(4',7'-di-2-thienyl-2',1',3'-benzothiadiazole) (PCDTBT).

Organic semiconductors can be classified into polymer and small-molecule semiconductors. All of these materials have in common that they are based mainly on carbon atoms (Figure 1-14). Alternation of single and double bonds between the atoms lead to a π -conjugated system with delocalized electrons in π -orbitals among the sp^2 hybridized atoms. This delocalization is responsible for the charge transport, oxidizability and conductivity of the materials. The degree of electrical conductivity of an organic semiconductor is influenced by the charge carrier mobility

and the density of charge carriers and can therefore cover a wide range. As the charge carriers can be either holes or electrons, organic semiconductors can be furthermore subdivided as electron-donor (hole transporting) or electron-acceptor (electron transporting) semiconductor. In the next section, conjugated polymers are described, followed by a section on the small-molecule organic semiconductor fullerene and its derivatives.

1.3.1 Conjugated polymers

In 2000 Alan J. Heeger, Alan G. MacDiarmid and Hideki Shirakawa were awarded the Nobel Prize for the discovery and development of conducting polymers.^[104] In the 1970s, by doping the semiconductor polyacetylene (Figure 1-15) with halogens, Heeger et al. induced permanent charges into the conjugated π -system turning the semiconductor conductive.^[105] The halogen removed an electron (oxidation) of the polymer backbone leaving a positive charged hole. This hole can be transported along the conjugated chain (intramolecular) as well as between different chains (intermolecular).^[106–109] The intermolecular transport of charges is also referred to as hopping process. As conjugated polymers can be doped to a high density of charge carriers, an increase of conductivity over several orders of magnitude can be obtained.^[105,110,111] In most cases, doping of conjugated polymers is induced either chemically, like Heeger et al. did, or electrochemically. The molecular structures of some of the first developed conjugated polymers are shown in Figure 1-15.

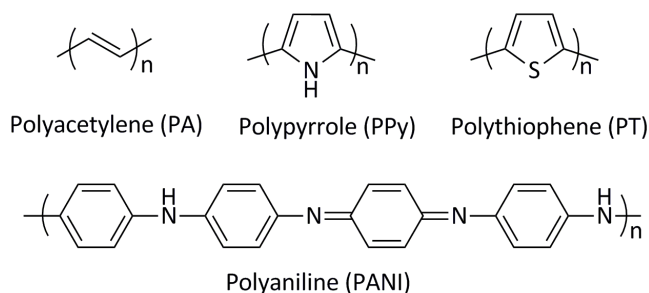


Figure 1-15: Molecular structures of some of the first conjugated polymers: Polyacetylene (PA), polypyrrole (PPy), polythiophene (PT) and polyaniline (PANI).

Although, the doping processes in inorganic and organic semiconductors are different, conjugated polymers are categorized in p- and n-type semiconductors in analogy to inorganic semiconductors. Polymers, which can be oxidized (electron-donor), are therefore often referred as p-type, whereas polymers, which are easier to be reduced, are called n-type (electron-acceptor) semiconductors. Conjugated polymers as p-type materials, are more widely known than the n-type counterparts.^[112,113] Nevertheless, a few conjugated polymers with high electron affinity can accept and conduct electrons (n-type).^[114,115]

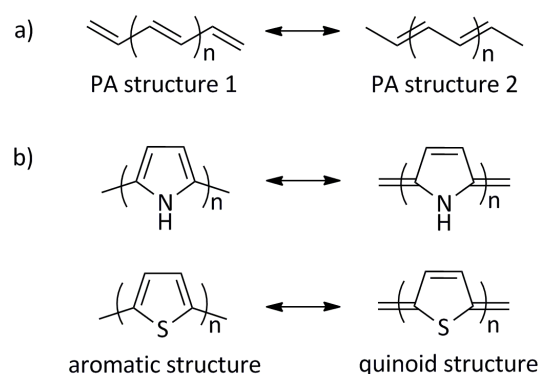


Figure 1-16: Chemical structures for PA (a), PPy and PT (b). PA possess two geometric structures, which have the same energy. They differ from each other by the position of the single and double bonds. PA is a degenerated polymer. On the contrary, PPy and PT exist in aromatic structure or in quinoid structure. The aromatic structure is the state with less energy and therefore forms the ground state geometry. PPy and PT are non-degenerated polymers.

Additionally, conjugated polymers are classified into geometrical structure features such as degenerate (of equal energy) and non-degenerate electronic structures. A polymer possesses degenerate structures, if the polymer has two identical geometrical ground state structures with the same energy. A common example for a degenerate polymer structure is polyacetylene (Figure 1-16 a). Non-degenerate polymers possess two different structures, which have different energies.^[116,117] Polypyrrole and polythiophene are common used polymers of this category.^[117] As in this thesis derivatives of polythiophene are used, the following part will concentrate on the doping processes of non-degenerate, aromatic structures. Polymers consisting of ring-structures can be existent in the aromatic ground-state or in quinoid-like geometric structure, which has a higher total energy (Figure 1-16 b). By removing one electron from the backbone (p-type doping), a radical cation with a spin of $\frac{1}{2}$ is created. As the quinoid structure possesses a lower ionization potential as well as a larger electron affinity than the ground-state, the structure of the chain changes to the quinoid-like structure locally around the introduced charge (Figure 1-17).^[117,118] This distortion of the lattice results in localized electronic states in the energy gap, which are termed polaron states (Figure 1-18). Further oxidation of the polymer creates a spinless bipolaron (a dication in the case of oxidation/p-type doping). The local lattice distortion of a bipolaron is stronger than for polarons. Therefore, the distance of the electronic states to the band edges are smaller for polarons than for bipolarons (Figure 1-18).^[117] The formation of sub-bands is accompanied with a reduction of the energy gap leading to a change in absorbance and color of the polymer.^[112,119–121] The combination of spectroscopy with electrochemistry, which is called spectroelectrochemistry, is a powerful technique to study the doping (redox) behavior and creation of electronic states. Spectroelectrochemistry will be discussed in detail in chapter 1.3.4.

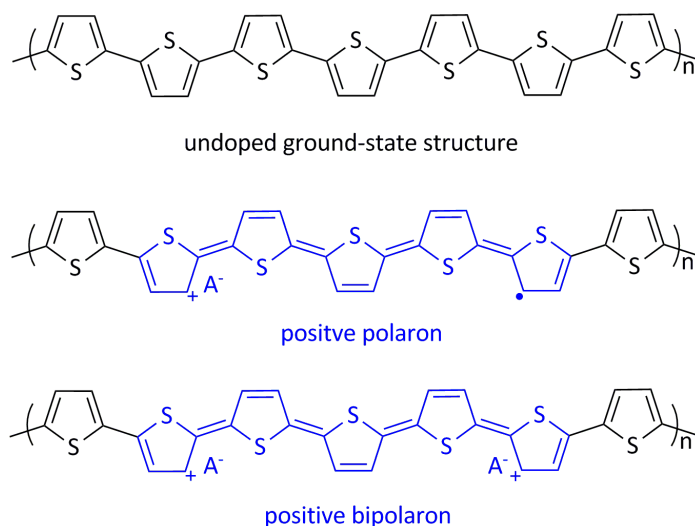


Figure 1-17: Chemical structure of PT in the undoped ground-state, with a positive polaron and a positive bipolaron after p-type doping. A^- denotes the introduced counteranion to preserve charge neutrality. Figure adapted from Ref. ^[118].

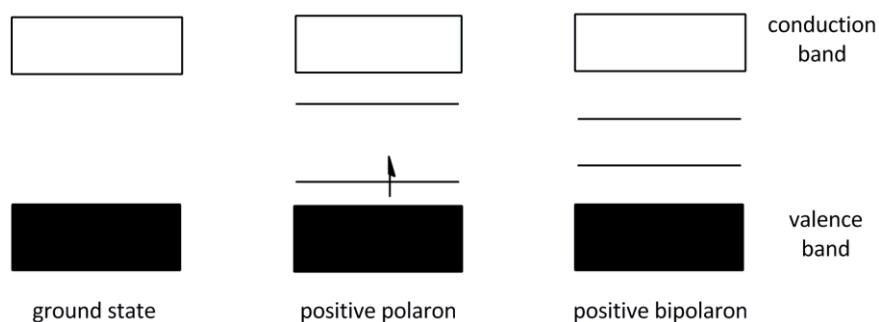


Figure 1-18: Schematic energy level diagram for a conducting polymer in ground state, and with the formed sub-bands in a positive polaron and a positive bipolaron after p-type doping. The polaron has a spin of $\frac{1}{2}$, whereas the bipolaron is spinless.

To preserve charge neutrality during doping processes, introduced charges are neutralized by counterions, which diffuse into the polymer during charging (doping) and out of the polymer during discharging (dedoping).^[113,122] The insertion of counterions leads to an osmotic expansion of the polymer matrix as well as to a change in the bond lengths and in the conformation of the backbone.^[123] Thus, a volumetric change (swelling/deswelling) is obtained. As the ions diffuse inside the polymer matrix, conjugated polymers are able to conduct not only electrons but also ions.

During doping conjugated polymers retain flexibility and light weight. Nevertheless, the relatively strong interchain electron-transfer interactions (hopping of electrons) render the first reported conjugated polymers insoluble and difficult to process. Introduction of side-chains, which are covalently bound to the conjugated backbone, leads to an increase of the entropy and weakens the interchain interactions making these polymers soluble.^[104,124] With the possibility to fabricate semiconductor films from solution, organic electronics have gained increasing

attention. Conjugated polymers are used in organic-light emitting diodes (OLED),^[125,126] organic photovoltaics (OPV),^[127,128] organic field-effect transistors (OFET)^[129,130] and sensors.^[131,132] As these polymers are electrochromic, they can function in so called “smart glasses”, which can be switched electrochemically between two states (colored and colorless), which allow the tuning of light transmission or reflection. Smart glasses can be used in a variety of applications like eyeglasses,^[133] self-darkening windows in buildings,^[134] anti-glare rear-view mirrors^[135] and flexible electrochromic displays.^[136] The volumetric change enables the usage as actuators like artificial muscles.^[137,138] Furthermore, they function as corrosion protection^[139] and coatings for electrodes.^[140,141]

Synthesis of conjugated polymers

The first reported conjugated polymer was polyacetylene, which was synthesized via an ill-defined Ziegler-Natta polymerization. Later, aromatic conjugated polymers like polypyrrole and polythiophene, which showed higher stability, were synthesized and investigated.^[142] In 1979 Gardini et al. successfully synthesized a highly conducting polypyrrole (in its oxidized state) via oxidative electropolymerization as thin-films in an one-step reaction.^[143] Polypyrrole is very reactive in its neutral state, as it reacts even with a tiny amount of oxygen.^[144] On the contrary, polythiophenes, both in doped and undoped state, showed a good stability at ambient conditions.^[145] Therefore, polythiophenes became the model polymer for charge transport studies of conjugated polymers.^[145] Besides electropolymerization^[146,147] and oxidative polymerization^[148], polythiophenes were synthesized by creating an active Grignard reagent of a 2,5-dibromothiophene monomer in combination with a transition metal catalyst like $[\text{NiCl}_2(\text{bpy})]$ (bpy: 2,2'-bipyridine)^[149] or the better soluble $\text{Ni}(\text{acac})_2$ (acac = acetylacetonate)^[150]. Using Kumada cross-coupling^[151] reaction, 2,5-coupling of the monomer units is observed predominantly.^[152] Solubility of polythiophene was gained by introduction of alkyl chains on the thiophenes.^[124,153] Due to the asymmetry of substitution of thiophene using alkyl groups at position 3, the resulting poly(3-alkylthiophene) have regioisomers.^[154] Figure 1-19 shows the possible regiochemical couplings. The carbon atom on position 2 of 3-alkylthiophene is termed “head” (H), whereas the one on position 5 is called “tail” (T) position. In general, different regioisomeric polymers can be obtained depending on the control of sequence of H and T couplings. If the polymer backbone is completely regioregular, all monomer units are coupled in H-T fashion. In contrary to regioirregular polymers, regioregular poly(3-alkylthiophenes) remain planar like polythiophene. In irregular isomers the steric repulsion of the alkyl chains in position 3 lead to twists in the backbone. The planar regioregular poly(3-alkylthiophenes) enables an efficient π -stacking of the chains suitable for crystallization, which leads to red shift of

absorption. Both factors are responsible for the higher charge carrier mobility of regioregular compared to irregular poly(3-alkylthiophenes) and the different optical characteristics.^[106,155–157]

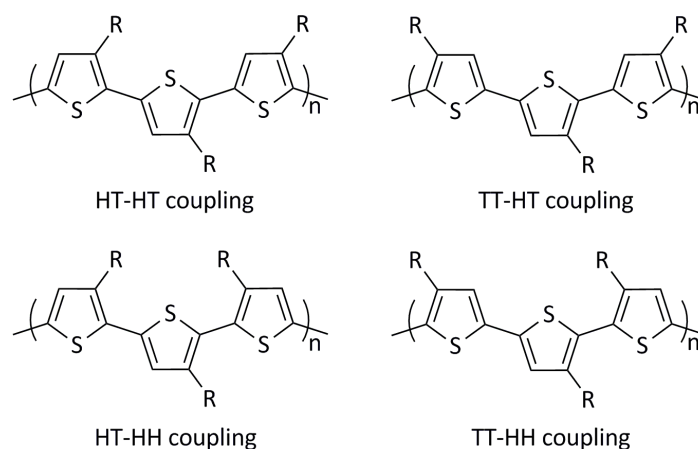


Figure 1-19: Possible regiochemical couplings in poly(3-alkylthiophenes).

The first synthesized poly(3-alkylthiophenes) were irregular, as the so far used polymerization reactions (Kumada cross-coupling^[124,153,158], oxidative polymerization^[158–161] and electrochemical polymerization^[160,162]) did not control the coupling of the monomer units. In 1992 McCullough and Lowe were the first to present a synthesis route, which lead to high regioregular poly(3-alkylthiophenes) with 91 % HT couplings in their polymer backbone.^[156] Although the polymerization is based on the Kumada cross-coupling reaction as well, here a control of regioregularity is obtained by a selective metalation of the monomer, 2-bromo-3-alkylthiophene. In the same year Rieke and Chen claimed to have synthesized a completely regioregular HT coupled poly(3-alkylthiophene) via an alternative synthesis route (Negishi coupling) containing highly reactive “Rieke zinc”.^[163] As both methods are performed under cryogenic temperatures (McCullough’s method -60 °C^[156], Rieke’s method -78 °C^[164]) and need long reaction times, they were not suitable for large scale production of poly(3-alkylthiophenes). In 1999 McCullough et al. developed a synthetic route for regioregular poly(3-alkylthiophene), which does not need cryogenic temperatures or expensive reagents like $ZnCl_2$ ^[163,165] and $MgBr_2$ ^[156]. On top of this, the polymerization is fast and poly(3-alkylthiophenes) are obtained in high yields.^[166] Even though all the polymers obtained in this way had reasonable molecular weights (M_n of 20±35 kDa, polydispersity index (PDI) of 1.20 to 1.47), and very high HT-HT couplings, the real mechanism of this reaction was not clear at that time and the broad PDI and end group analysis suggested a typical Ni-catalyzed step-growth polymerization mechanism.^[167] It took some years to get a clear evidence for the mechanism, which was first suggested in 2004 independently by McCullough’s^[168] and Yokozawa’s^[169] groups as “catalyst-transfer polycondensation with a chain growth mechanism”.^[170] The mechanism of the reaction is shown in Figure 1-20.

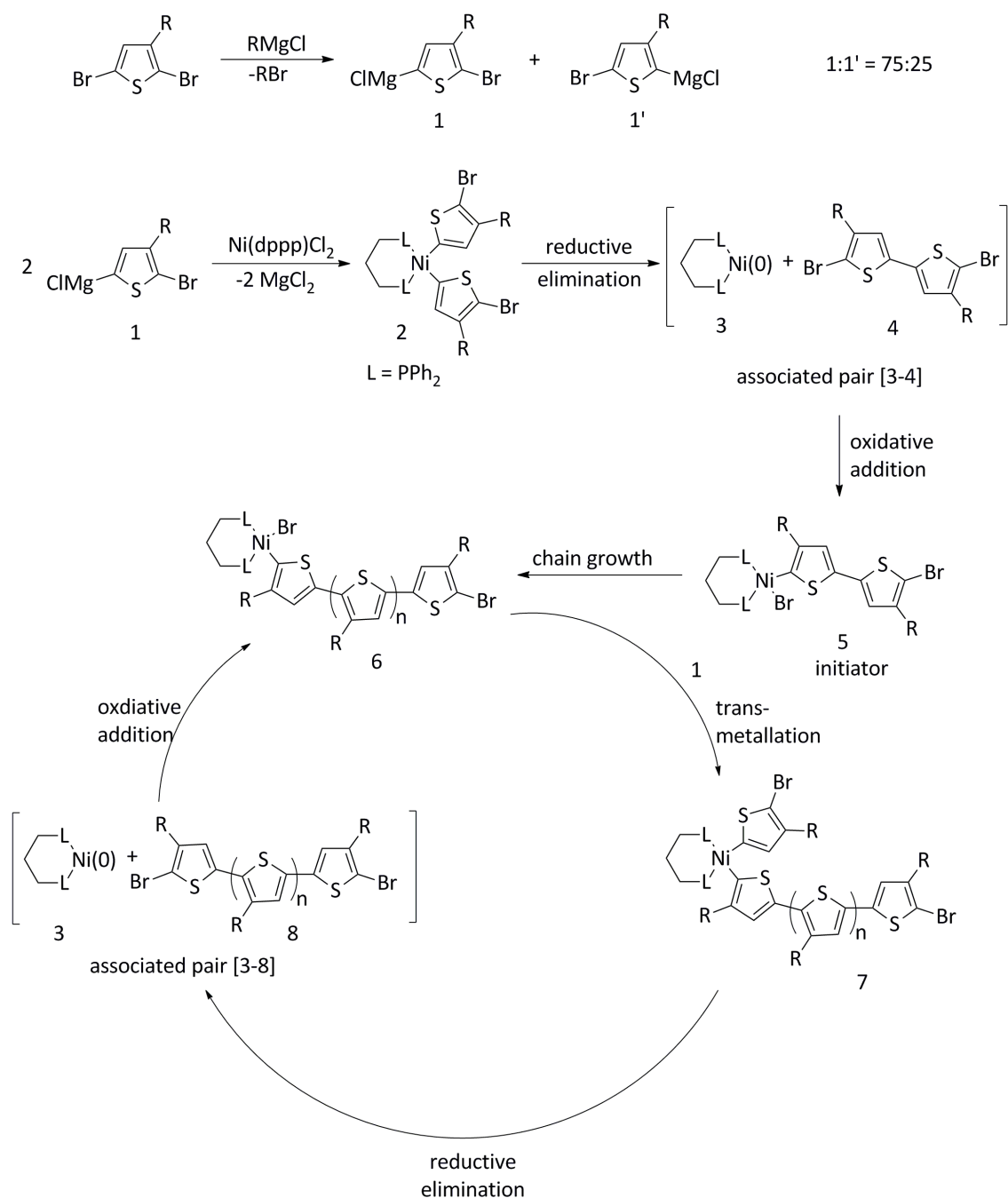


Figure 1-20: Mechanism of the Gringard methathesis polymerization of poly(3-alkylthiophene). Figure adapted from Ref. ^[171]

The first step involves a Grignard methathesis (GRIM) of 2,5-dibromo-3-alkylthiophene with one equivalent alkylmagnesium chloride (RMgCl). Due to the exchange of bromide against magnesium chloride two regioisomers 1 and 1' are obtained. The ratio of 1:1' is about 75:25, if prepared at room temperature. The nickel-catalyst Ni(dppp)Cl_2 (dppp: 1,3-diphenylphosphino-propane) reacts with two equivalents of the monomer 2-bromo-5-chloromagnesium-3-alkylthiophene (1) to a bis(organonickel) compound (2). Here the less sterical hindered tail-tail conformation is built. Ni(0) (3) and a dimer (4) is obtained via reductive elimination of nickel. The

initiator compound of the polymerization (5) is created by oxidative addition of the dimer (4) to the Ni (0) (3). Now multiple cycles containing transmetallation, reductive elimination and intramolecular oxidative addition generate the polymer chain. As the insertion of the undesired regioisomer 1' is sterically hindered, only the regioisomer 1 is embedded in the chain. Consequently, just one tail to tail coupling per polymer chain is created leading to a high regioregularity of around 98 %.^[168,171]

1.3.2 Conjugated polyelectrolytes

As a natural consequence of synthesis of conducting polymers, it was also tried to realize water or alcohol soluble conjugated polymers. Processing from these non-toxic and eco-friendly solvents would pave the way for large-scale production like roll-to-roll process. Furthermore, water compatible conjugated polymers would be of great interest for applications in biological systems. The first water-soluble conjugated polymers were synthesized by Heeger et al. in 1987 (Figure 1-21), in which an ionic side chain was introduced to a conjugated polymer in each repeating unit to get conjugated polyelectrolytes (CPEs).^[172]

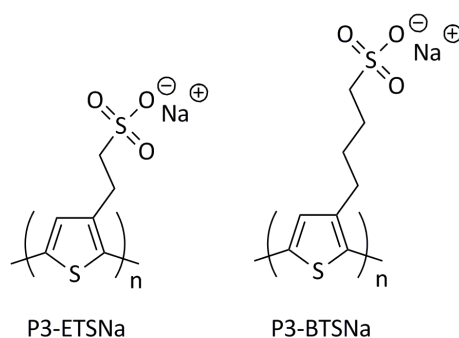


Figure 1-21: Structures of the first water-soluble conjugated polymers: poly(3-(2-ethanesulfonate)thiophene) (P3-ETSNa) and poly(3-(4-butanesulfonate)thiophene) (P3-BTSNa).

CPEs can be classified into anionic, cationic and zwitterionic CPEs dependent on the nature of the attached groups. Typical ionic groups of anionic CPEs include sulfonates,^[172,173] carboxylates^[172,174] and phosphonates,^[175,176] whereas quaternary ammonium^[177–179] and pyridinium^[180,181] salts are used for cationic CPEs. Zwitterionic CPEs contain anionic as well as cationic groups. In contrast to anionic and cationic CPEs, zwitterionic CPEs do not have mobile counter ions, as all ions are covalently bound to the polymer backbone. Therefore, during doping of neutral conjugated polymers or zwitterionic CPEs ambient counterions have to diffuse in and out of the polymer matrix to ensure neutrality of charges. On the contrary, created charges in anionic or cationic CPEs can be compensated by expulsion or insertion of their ionic bound counterions (in Figure 1-21 Na^+).^[182,183] Thus, cationic and anionic CPEs are also termed self-

doped polymers, if oxidation or reduction of the conjugated backbone takes place.^[184] Some examples for anionic, cationic and zwitterionic CPEs are shown in Figure 1-22.

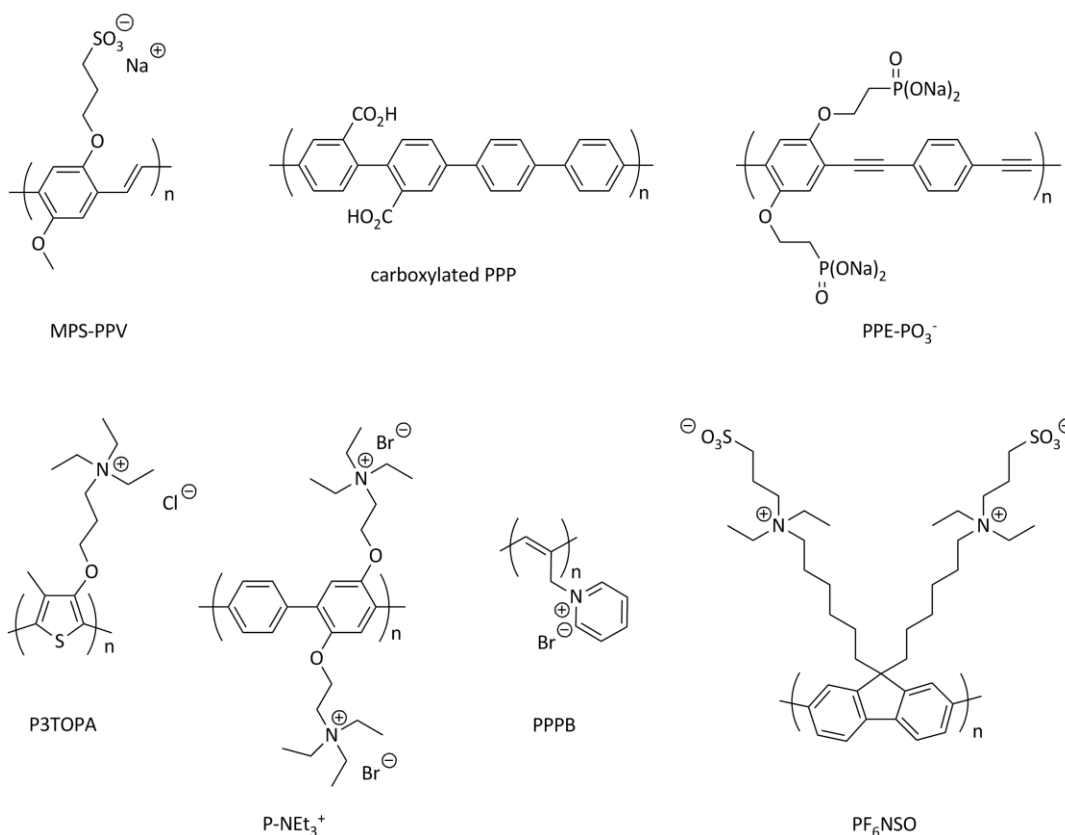


Figure 1-22: Chemical structures of some conjugated anionic (MPS-PPV: sodium poly(5-methoxy-2-(3-sulfopropoxy)-1,4-phenylenevinylene),^[173] carboxylated PPP: poly(p-quaterphenylene-2,2'-dicarboxylic acid),^[174] PPE-PO₃⁻: sodium poly(1,4-bis(2-phosphonoethoxy)-p-phenyleneethynylene)^[175]), cationic (P3TOPA: poly(3-(3'-thienyloxy)propyltriethylammonium) chloride,^[178] P-NEt₃⁺: poly(2,5-bis(3-{N,N,N-triethylammonium}-1-oxapropyl)-1,4-phenylene-alt-1,4-phenylene) dibromide,^[177] PPPB: poly(propargyl pyridinium bromide)^[180]) and zwitterionic polyelectrolytes (PF₆NSO: poly(9,9-bis((N-(3-sulfonate-1-propyl)-N,N-diethylammonium)-hexyl)-2,7-fluorene)^[185]).

In general, there are two ways to synthesize CPEs: An ionic monomer can be directly polymerized^[178,186] or functional groups on the side chain of a polymer precursor can be converted into ionic groups (post-polymerization functionalization).^[172,187] Most CPEs are synthesized using the last described method, as many polymerizations are sensitive to the presence of ionic groups and solvents suitable for polyelectrolytes, like water. Furthermore, the neutral precursor polymer facilitates the purification of the product and can be characterized by well-known techniques in common organic solvents.^[188,189]

Interactions of CPEs with the solvent as well as electrostatic correlations influence the aggregation and therefore the optical properties.^[190] In polar solvents such as water, most CPEs tend to aggregate. Consequently a red-shift of the absorption bands and fluorescence quenching can be traced due to the obtained π - π interactions in the aggregated state. Depending on the chemical structure, in solvents such as DMSO or methanol, the polymer chains are dissolved on

molecular level. Therefore, just limited intermolecular interactions are possible, leading to a blue-shifted absorption maxima.^[191–193] As the ionic groups of CPEs can interact with ambient chemical or biological compounds, their presence can be detected by changes in the absorption and fluorescence spectrum of the CPE. Consequently, CPEs function as optical sensor for those compounds.^[194] Because of the sensitivity of CPEs to their ambient conditions, also the temperature, the pH value of the solution and the concentration of CPE influence the aggregation and the absorption and fluorescence spectra.^[175,195,196] Moreover, CPEs have been studied as interfacial layer in organic devices, like solar cells, OFETs or OLEDs.^[197–203] They cause a reduction of the energy barrier for charge injection/extraction. This effect is induced by a combination of two processes: On the one hand, permanent interfacial dipoles are created between the electrode and the CPE layer resulting in a reduction of the work function of the electrode. On the other hand, external electric fields cause ion migration or molecular reorientation in the CPE layer leading to an internal field redistribution within the device.^[189,204–210] As the organic photoactive layer is typically soluble in nonpolar organic solvents, CPEs can be deposited without re-dissolution of the underlying photoactive layer.

1.3.3 Fullerene and its derivatives

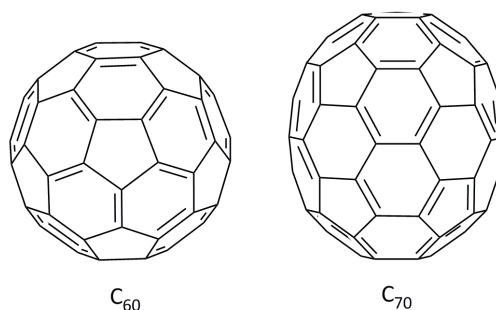


Figure 1-23: Chemical structure of the two widely studied fullerenes: C₆₀ and C₇₀.

Fullerenes and their derivatives are an important group of organic acceptor semiconductors. At their discovery in September 1985, Curl, Kroto and Smalley were not aware of the versatility of potential applications, which evolved out later. During an experiment, in which graphite was heated and evaporated by a laser, the scientists obtained a signal of a stable molecule in the mass spectra. This molecule had the weight of 60 carbon atoms. As they were not able to identify this molecule with the known structures and modifications of carbon, they proposed a closed polyhedral structure. Theoretical calculations of Jones (1966) and Osawa (1970) had already shown that this structure should be possible and stable. The development of a process,

which enabled the production of C_{60} in gram quantities, resulted in the proof of the structure and built the base for further research in this field. ^[211–216]

Fullerene can consist of 20 up to several 100 carbon atoms. The carbon atoms are arranged in pentagons and hexagons, which assemble in a polyhedral structure (Figure 1-23). Contrary to graphene, fullerenes are completely closed systems without free bounds. According to Euler, a polyhedron composed of pentagons and hexagons must contain exactly 12 pentagons to build a closed system. Consequently, C_{20} is the smallest possible fullerene consisting of exactly 12 pentagons. Depending on the number of additional hexagons, molecules of different sizes are obtained. Strong surface flexion accompanied by warping of the bounds with neighbored pentagons is responsible for the instability of many fullerenes. C_{60} is the smallest stable fullerene, as it consists of completely surrounded pentagons, in a combination of 12 pentagons and 20 hexagons. ^[214,217,218]

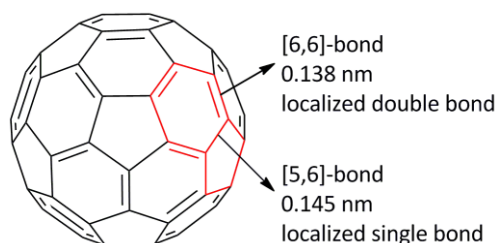


Figure 1-24: Most stable Kekulé structure of C_{60} . A pentagon and a hexagon are highlighted in red to show the different bonding characteristics.

In fullerenes two different chemical bonds can be noticed: On the one hand, a [6,6]-bond between two hexagons, on the other hand a [5,6]-bond between a pentagon and a hexagon. Via X-ray crystal structure studies, a bond length of around 0.145 nm for [5,6]-bonds and 0.138 nm for [6,6]-bonds were determined. Therefore, localization of double bonds between two hexagons and of single bonds fusing a pentagon with a hexagon lead to the most stable Kekulé structure for C_{60} (Figure 1-24). ^[219–222] C_{60} molecules crystalize in a face-centered cubic lattice. As just Van-der-Waals interactions are effective between the single molecules, fullerenes are expected to be soluble in many solvents. However, the energy, which is needed to break intermolecular linkages of solvent molecules, cannot be compensated by the interaction of solvent with fullerene. Furthermore, dissolved fullerene molecules hinder the formation of an intermolecular structure in the solvent, which are created by intermolecular interactions such as hydrogen bonds. Hence, C_{60} is not soluble in polar solvents like acetone, tetrahydrofuran or water. Due to strong π - π interactions with aromatic units, fullerenes are better soluble in aromatic than polar aliphatic solvents. ^[223,224]

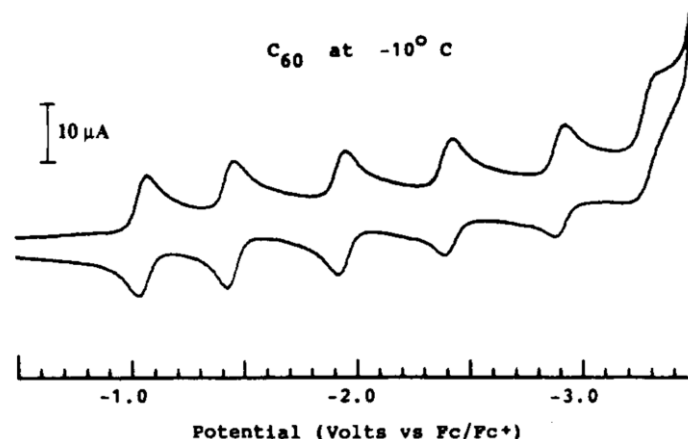


Figure 1-25: Cyclic voltammogram of C_{60} in a solvent mixture of 15-20 vol% of acetonitrile in toluene at $-10\text{ }^{\circ}\text{C}$ and a scan rate of 100 mV/s. Figure reproduced from Ref. ^[225].

Despite the low solubility, fullerenes are interesting for different applications due to their unique electrochemical properties. C_{60} is a molecule with high electron affinity and can collect up to six electrons (Figure 1-25). Reason for that is the lowest unoccupied molecular orbital (LUMO), which is degenerated triply and has a comparable small energy. Two successive reduction processes show an invariable potential distance of around 450 ± 50 mV in cyclic voltammetry measurements. Fullerene anions are exceedingly stable and enable charge separated states. C_{60} is difficult to oxidize. The difference between the first oxidation and the first reduction potential amounts 2.32 V. The highest occupied molecular orbital (HOMO) is fivefold and has a closed-shell configuration. ^[225-229]

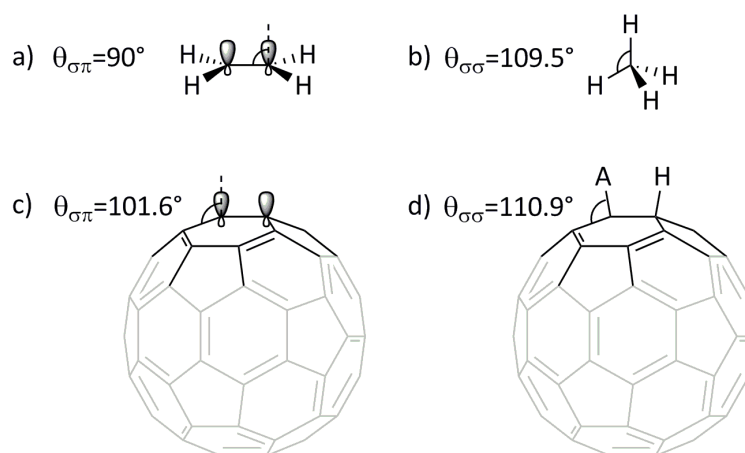


Figure 1-26: Comparison of the angles of simple carbon molecules (a) Ethene $\theta_{\sigma\pi}$ and b) methane $\theta_{\sigma\sigma}$) with the angles in c) pristine C_{60} fullerene ($\theta_{\sigma\pi}$) and d) after addition of AH ($\theta_{\sigma\sigma}$). Addition of AH leads to conversion of sp_2 into sp_3 hybridized carbon atoms and to reduction of cyclic stress in the fullerene.

C_{60} molecules are more reactive than other saturated systems. Reason for that are the geometrical requirements. Double bonds have to deviate from their usually planar (Figure

1-26a) to a pyramidal structure (Figure 1-26b). This leads to a huge stress in the molecule. In most chemical reactions of fullerenes a conversion of sp_2 into sp_3 hybridized carbon atoms occurs (Figure 1-26d).^[230,231]

Generally, fullerenes undergo redox or addition reactions. The stress relaxation in the fullerene cage is the major driving force for chemical reactions. As carbanions favor a tetrahedral geometry, reduction of fullerenes also cause an energy release. Via reduction reactions fullerene salts are obtained (Figure 1-27a), whereas addition reactions lead to covalently-bound, exohedral adducts (Figure 1-27b). Further conversions of activated adducts yield heterofullerenes (Figure 1-27c), endohedral fullerenes (Figure 1-27d), fullerenes with open structure (Figure 1-27e) or degradation products (Figure 1-27f).^[230,231]

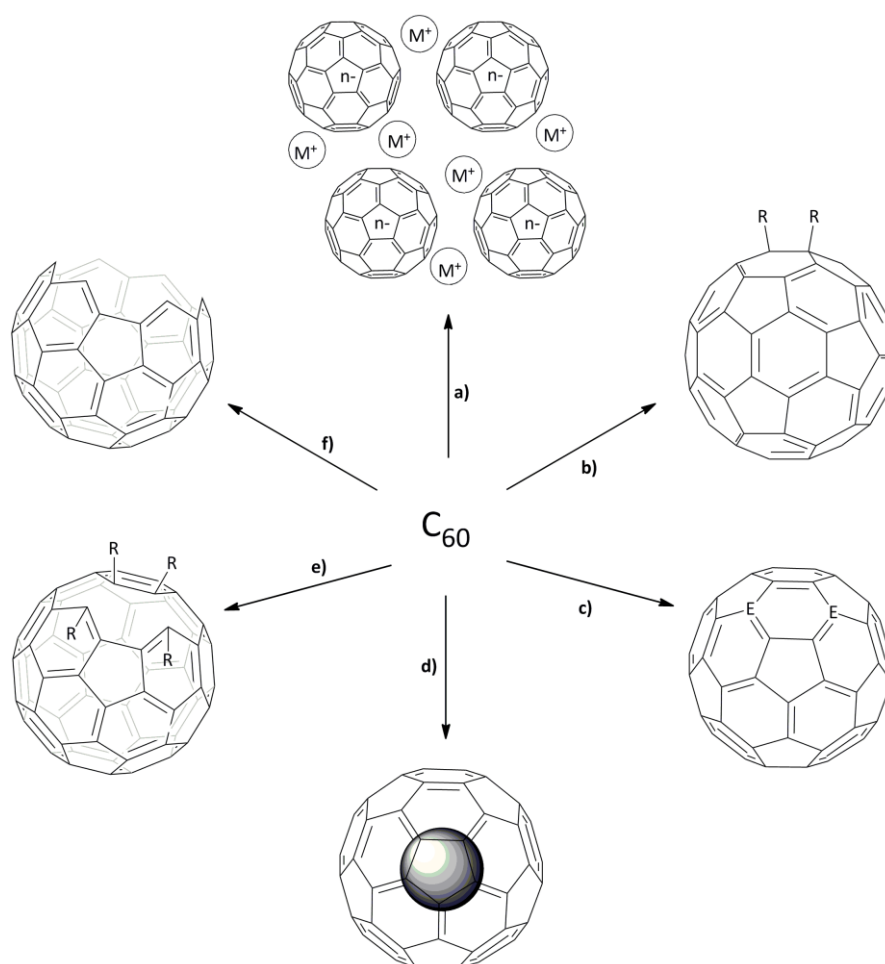


Figure 1-27: Possible C_{60} derivative types: a) fullerene salt, b) exohedral adduct, c) heterofullerene, d) endohedral fullerene, e) fullerene with open structure and f) degradation products. Figure adapted from Ref. ^[232].

Additions to fullerene cages usually take place on double bonds, that is on [6,6]-bonds. The generation of a [5,6]-double bond would need energy input of around 8.5 kcal/mol.^[233,234] Figure 1-28 shows the possible isomers of C_{60} after monoaddition. Unfavorable structure elements are

marked in red color. The most stable isomer is a ring-closed system with a bridged [6,6]-bond. Also [5,6]-open structures can be found in reaction mixtures. The [5,6]-open structure is 6 kcal/mol less stable than the [6,6]-closed one. Here the double bonds, which have to be built next to the bridgeheads, are energetically unfavorable according to Bredt's rule. A tiny amount of [5,6]-closed structures can also be found in some reaction mixtures. This structure is 21 kcal/mol less stable than the most stable [6,6]-closed isomer. Fullerenes aim to have as less double bonds between pentagons and hexagons as possible to be energetically favourable. In [5,6]-closed structures, however, two double bonds at those position have to be created. This leads to the less stability compared with the [6,6]-closed isomer. Another possible isomer is a [6,6] ring-opened structure. Here, even three double bonds between pentagons and hexagons have to be built. Furthermore, two double bonds need to be created next to the bridgeheads. As the [6,6]-open isomer is energetically unfavorable, it could not be found in reaction mixtures so far.^[231,235,236]

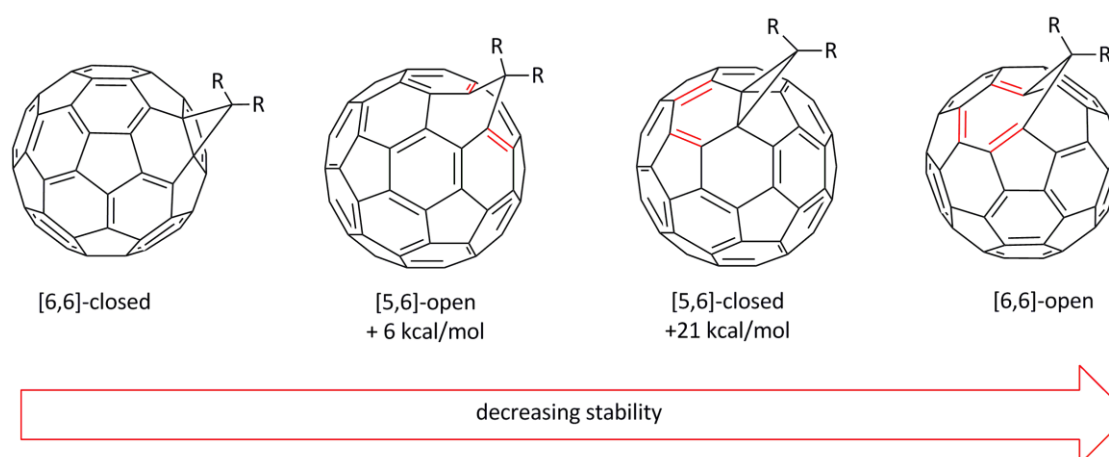


Figure 1-28: Possible isomers of C_{60} after monoaddition. For the isomers [5,6]-open and [5,6]-closed the relative energies to the most stable isomer [6,6]-closed are given. Unfavorable structure elements are marked in red color. Figure adapted from Ref.^[235]

In 1993 Bingel published an efficient method to synthesize and isolate cyclopropanated fullerenes.^[237] Because of good yields, mild reaction conditions, and the tolerance towards various functional groups, this method is still the most used for functionalization of fullerenes. In the first step of the initially reported Bingel reaction, sodium hydride (NaH) deprotonates a α -bromomalonate (Figure 1-29, 1). The resulting α -bromo-carbanion (2) is added to the C_{60} cage (3) and intramolecularly substituted by the created anionic centrum of the fullerene cage (4). Using the Bingel reaction exclusively [6,6]-closed isomers are obtained.^[235,237,238]

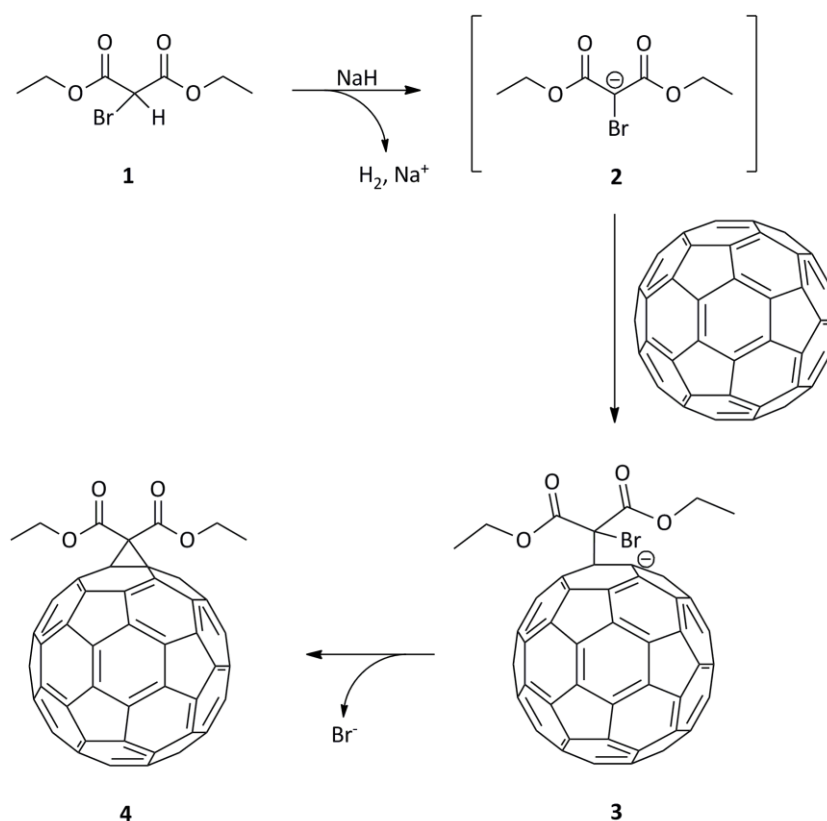


Figure 1-29: Mechanism of the cyclopropanation of C₆₀ via Bingel. Figure adapted from Ref. ^[231].

As the synthesis and isolation of more complex halogenated malonates is difficult due to their instability, Hirsch et al. modified the synthesis. They generated the α -halogenmalonate in situ in the presence of tetrabromomethane or iodine and an auxiliary base. It is important that the base is not nucleophilic to avoid addition reactions of the base on the fullerene cage. 1,8-Diazabicyclo[5.4.0]undec-7-ene (DBU) is often used here. Using this modified reaction, nowadays called Bingel-Hirsch reaction, good yields of 30-60 % of monoadduct are obtained.^[231,238–240]

As C₆₀ provides 30 reactive [6,6]-double bonds, also multiadducts are possible. That is the reason, why complex mixtures of monoadducts and several multiple adducts are obtained for addition reactions on C₆₀. With increasing number of additions, also the number of possible isomers increases. These isomers are very similar in their chromatographic properties. Thus, they cannot be separated very easily. Normally, reactions are aimed for monoadducts, as they do not possess isomers and can be separated from higher addition products and unreacted C₆₀ by chromatography. For each added group, the conjugated system of the fullerene cage is reduced, which leads to an increase of the LUMO energy. In addition, each added group decreases the number of potential reduction steps by one. As a result, the easiness of reduction

drops from mono to hexakis adducts. Depending on the type and amount of added groups, the solubility and other characteristics of fullerenes can be influenced. ^[221,234,241]

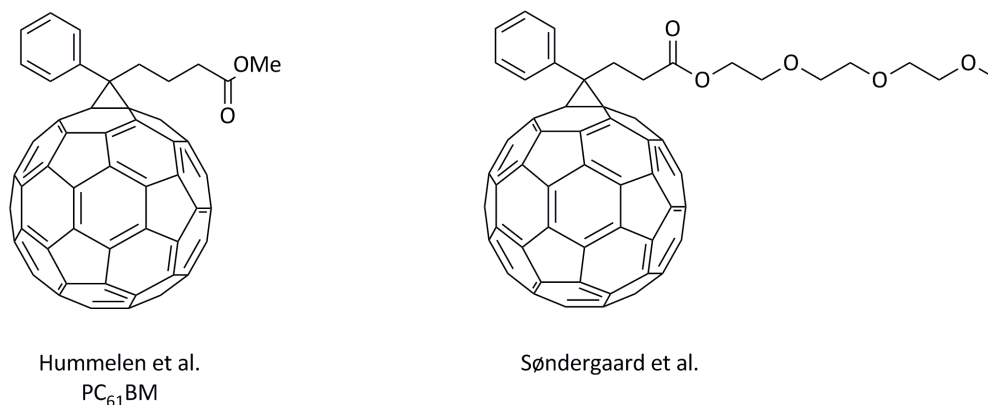
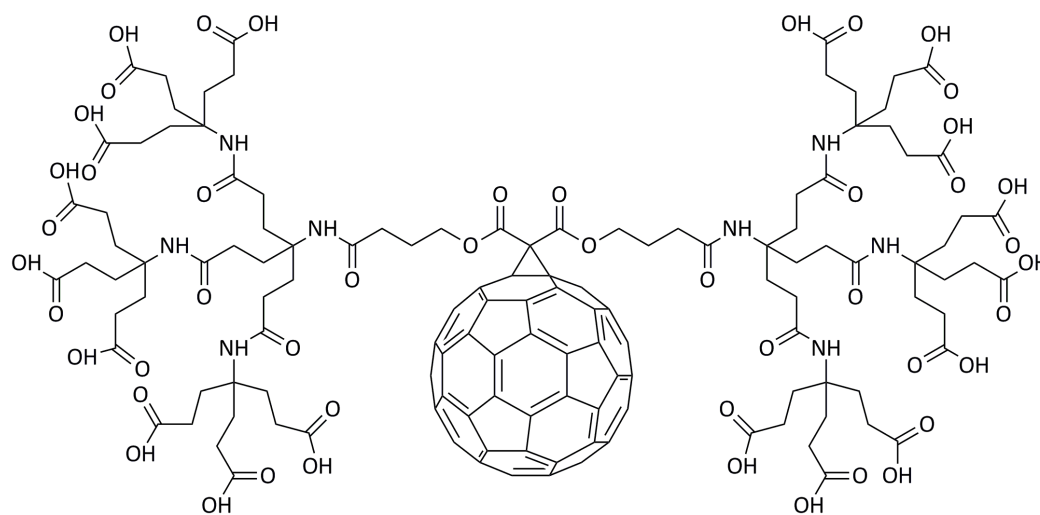


Figure 1-30: Chemical structures of the most famous fullerene derivative PC61BM and the THF soluble phenyl-C61-2-(2-(2-methoxyethoxy)ethoxy)ethyl butanoate.

The most famous fullerene derivative is phenyl-C₆₁-butyric acid methyl ester (PC₆₁BM), which is commonly used as electron acceptor material for organic photovoltaics. ^[242] Hummelen et al. aimed for the addition of a functional group to the C₆₀ cage, which enables the attachment of a big range of different molecules. It is important that the functional group does not react with the electronegative C₆₀ cage. The carboxyl group is one of the few groups, which comply that. Furthermore, it is one of the most versatile functional groups. As a result, Hummelen et al. decided to add this group as the handle on a spacer. As spacer the flexible and inert trimethylene was used, as it is long enough to solubilize the product. A phenyl ring is added on the spacer, because a phenyl ketone is more stable and easier to synthesize. ^[243] PC₆₁BM provides a good solubility in organic solvents such as chloroform (28.8 mg/mL), chlorobenzene (59.5 mg/mL) and dichlorobenzene (42.1 mg/mL). ^[244]

For large-scale processing in industry a large amount of solvents are used. Because of the bad environmental compatibility of aromatic and chlorinated solvents, fullerene derivatives, which are sufficiently soluble in relatively nonhazardous solvents such as dimethyl sulfoxide (DMSO), acetone, ethyl acetate or tetrahydrofuran (THF) are interesting. Solubility of fullerene derivatives in water is especially interesting for applications in medicine and biology. Søndergaard et al. prepared a fullerene derivative similar to PC₆₁BM, which obtained instead of the methyl ester substituent a triethyleneglycol mono methyl ester. This phenyl-C₆₁-2-(2-(2-methoxyethoxy)-ethoxy)ethyl butanoate is highly soluble in DMSO and THF. This fullerene derivative is not soluble in water itself. Nevertheless, it can be processed in aqueous surroundings. ^[245]



Brettreich and Hirsch

Figure 1-31: Water-soluble dendro[60]fullerene developed by Brettreich and Hirsch.

A water soluble fullerene derivate was developed by Brettreich and Hirsch (Figure 1-31). By addition of a dendrimer containing 18 carboxyl groups, they preserve the easiness of reduction of monoadducts, but still have a sufficient amount of soluble groups attached to the fullerene. This dendro[60]fullerene has a solubility of 34 mg/mL in aqueous solution with a pH value of 7.4. In basic solution (pH 10) the solubility increases to at least 254 mg/mL.^[246]

Fullerenes can be used as electron acceptor in solar cells. Most commonly used are PC₆₁BM and PC₇₁BM.^[247] Derivatives of C₇₀ are not very common compared to derivatives of C₆₀, because of the high cost and less availability of C₇₀. For the application in solar cells, mostly mono-adducts are used, to make use of their favorable electronic properties and charge transport. A lot of fullerene derivatives were tested in bulk heterojunction organic solar cells. Ganesamoorthy et al. just published a good review about, showing a variety of used fullerene derivatives.^[248] Furthermore fullerenes and fullerene derivatives can be used as chromatographic stationary phase. Strong π - π interactions between the fullerenes and the analytes lead to retention and therefore to separation of polycyclic aromatic hydrocarbons (PAHs). The fullerenes are immobilized for example on silica, which acts just as support material. Only the fullerenes take place in the separation process.^[249,250] Due to its extraordinary characteristics, fullerenes and their derivatives can be used in biological and medicinal applications, as well. As the fullerenes can be reduced easily, they react with free radical species. As radical-scavengers they can be used against apoptosis and neurodegenerative diseases.^[251-254] Antibacterial and antiviral activity of fullerenes and their derivatives are well-known nowadays.^[255-258] Furthermore, fullerenes can block the receptor site of human immunodeficiency virus-1 (HIV-1) protease due to its spherical shape and hydrophobic surface. Consequently, HIV replication and infection is

stopped, as the cleavage of proteins is prevented.^[259–263] Because of the ability of fullerenes to generate singlet oxygen after irradiation, fullerenes can be used to cleave nucleic acids and to oxidize lipids.^[251,264] In addition, application of fullerenes as drug delivery carriers is discussed. Foley et al. showed that fullerenes and their derivatives can cross cell membranes and can deliver drug molecules to the target cells.^{[265][266]}

1.3.4 Characterization methods

Determination of charge carrier mobility via space charge limited current method

The bulk charge transport properties of organic semiconductors depend on the molecular structure as well as on intermolecular interactions. It is moreover dependent on the charge density of the sample. The electrical conductivity σ_c in a material is correlated to charge carrier mobility as

$$\sigma_c = n \cdot e \cdot \mu$$

with n is the number of charge carriers, e the electronic charge and μ the charge carrier mobility. The charge carrier mobility as a material property plays a key role in defining the switching time of electronic devices. Charge carrier mobility values as high as $1 \text{ cm}^2\text{V}^{-1}\text{s}^{-1}$ have been reported for organic semiconductors. Nevertheless, these charge carrier mobilities are much lower than the ones in single crystalline inorganic semiconductors. In organic materials charge carriers are transported both via intramolecular and intermolecular pathways, where the transfer rate is much slower than the band transport in inorganic semiconductors. The charges in organic materials hop from one molecule to another. Thus, amongst others, the molecular packing, impurities, degree of disorder, extend and depth of charge trap states and the temperature have influence on the charge carrier mobility.^[109,115,267–269] The charge carrier mobility can be written as

$$\mu = \frac{v}{E}$$

where v is the carrier drift velocity and E the applied electric field. Hence, the charge carrier mobility defines the distance, over which the charge carriers can be transported due to the electric field E . μ can be determined by various techniques. Practically, the final determined charge carrier mobility values depend on a method, geometry and the thickness of the sample. For measurements with time-of-flight (TOF) and space charge limited current (SCLC) method, the sample is sandwiched between two electrodes. Thus, the charge carrier mobility is determined in bulk in a perpendicular direction to the substrates. In contrast, in an organic field effect

transistor (OFET), the lateral charge carrier mobility values along the plane of substrates over some μm are measured ^[267,268]

The electric current of a single carrier organic device is limited either by the space charge developed inside the device (SCLC) or by the number of charge carriers (injection-limited current) injected from the electrodes. Consequently, the injection barrier height of the electrode to the organic semiconductor is crucial. If the barrier at the interface is greater than 0.3 eV, injection-limited current is observed. Contrary, SCLC appears for injection barriers less than 0.3 eV. In this case, charges are injected efficiently into the device. ^[268,270–272] A typical current density-voltage (J-V) curve of a non-injection limited device contains three different regions (Figure 1-32): At low voltages, the current density increases linearly (ohmic region), as the current density is limited by the background charge carrier concentration. The SCLC region is reached for higher voltages. Here, the current density is quadratically dependent on the voltage. Usually in this region, enough carriers are injected from the electrode than the material can transport. In the trap-free region all traps in the material are filled. As high voltages are needed to reach this region, the trap-free region is generally not detected as heat dissipation in the device can destroy the organic semiconductor. ^[267,270]

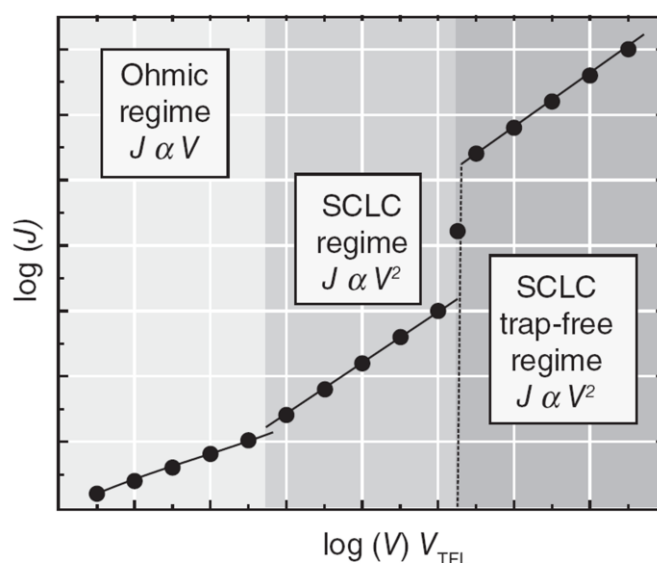


Figure 1-32: Schematic of a typical current density-voltage curve of a non-injection limited device. The ohmic and the SCLC regimes are indicated. V_{TFL} indicate the trap-filled limit voltage. Figure reproduced from Ref. [273].

For determination of the charge carrier mobility via SCLC method, the organic semiconductor is sandwiched between two suitable electrodes. The current-voltage characteristics of such a device are recorded in the dark. The resulting I-V curve depends on the charge carrier mobility and concentration of charge carriers as well as on the electric field. The choice of the electrodes is crucial for the SCLC method: The injecting electrode must form an ohmic contact with the

respective energy level of the semiconductor. In hole-only devices, in which the mobilities of holes are investigated, the highest occupied molecular orbital (HOMO) of the semiconductor has to be considered for the charge injection. Likewise, in electron-only devices the electrode must be able to inject required electrons into the lowest unoccupied molecular orbital (LUMO). As already mentioned, the injection barrier height should be smaller than 0.3 eV to ensure SCLC conditions. The counter electrode should be selected in such a way, that the charge carriers can leave the organic semiconductor without hindrance and opposite charge carriers cannot enter from it. In this manner, the transport of charge carriers is limited by the charge carrier mobility of the organic semiconductor. As the injection of charge carriers is not restricted, the number of injected carriers will reach a maximum as soon as their electrostatic potential prevents the injection of further charge carriers. Because of the accumulation of charges at the injecting electrode, this method is called “space charge limited current” (SCLC) method.^[109,115,267,268,270–272,274]

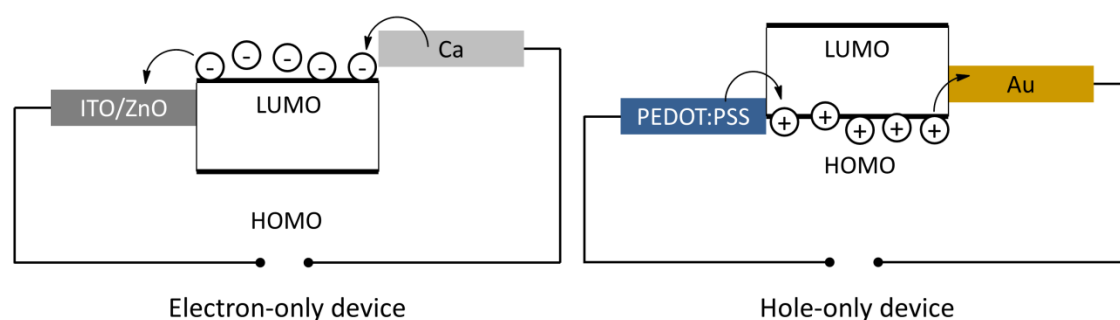


Figure 1-33: Schematics of an electron-only and a hole-only device.

In Figure 1-33, schematics of an electron-only device and a hole-only device are shown. Here, common electrode pairs were chosen: zinc oxide and calcium for the electron-only device, PEDOT:PSS and gold (Au) for the hole-only device. Nevertheless, the selection of the electrode should be considered for each organic semiconductor individually.

If the concentration of traps is low compared to the amount of free charge carriers and the charge carrier mobility is not a function of electric field (at very low fields), the charge carrier mobility can be calculated from the Mott-Gurney equation:

$$J = \frac{9}{8} \cdot \epsilon_0 \cdot \epsilon_r \cdot \mu \cdot \frac{V^2}{L^3}$$

where J is the current density, ϵ_0 the vacuum permittivity, ϵ_r the dielectric constant of the organic semiconductor, V the applied voltage and L the layer thickness of the semiconductor between the electrodes. As the charge carrier mobility and density can depend on the electric field, Murgatroyd modified the Mott-Gurney equation to:

$$J = \frac{9}{8} \cdot \epsilon_0 \cdot \epsilon_r \cdot \mu_0 \cdot e \left(0.89 \cdot \gamma \cdot \sqrt{\frac{V}{L}} \right) \cdot \frac{V^2}{L^3}$$

Where μ_0 is the charge carrier mobility at zero electric field and γ is the field activation parameter.^[268,275,276] To ensure SCLC conditions, several devices, which vary in the thickness of the organic semiconductor layer, should be considered. As charge injection becomes more crucial in thin films, a minimum layer thickness exists, at which reliable results can be achieved.^[274] For every device based on the same organic semiconductor, the same charge carrier mobility μ should result independent from the film thickness L . Additionally, the quadratic dependence of J and V as well as the L^{-3} dependence have to be valid for a correct evaluation of J-V curves using the SCLC method.^[109] Furthermore, a built-in potential (V_{bi}), which originates from the different work functions of the two electrode, should be considered for the calculation of μ . The effective voltage V across a device is given by

$$V = V_{app} - V_{bi}$$

where V_{app} is the applied voltage.^[109,274]

Spectroelectrochemistry

Spectroelectrochemistry (SEC) combines the reaction-oriented electrochemistry with the species-focused spectroscopy. Conventional electrochemistry provides information about concentrations, redox potentials and reaction kinetics. In combination with spectroscopy, unknown species formed during the redox reactions and their structural details can be spectroscopically identified. Depending on the requirements, different spectroscopic methods can be used in spectroelectrochemistry: absorption spectroscopy in the UV-vis region is used for the examination of electronic transitions, in the infrared (IR) region for vibrational transitions. Also Raman scattering can be used for vibrational transitions. Unlike IR spectroscopy, it can be used also for aqueous media, which is important for the measurement of bioelectronic systems. Electron paramagnetic resonance (EPR) can be used to obtain information about unpaired electrons during electrochemical redox processes. Furthermore, these methods require different radiation energies and differ in their timescales. In general, absorption spectroscopy in the UV-vis-NIR (near infrared) region is used for the examination of electronic structures and changes due to redox processes.^[277–282]

Spectroelectrochemical measurements can be executed in two-electrode mode, composed of a working electrode and a counter electrode, or three-electrode mode, in which a reference electrode is accessorially added. In the three-electrode mode, the applied potential on the working electrode is regulated in relation to the reference electrode, which leads to an accurate potential control. In contrary, the two-electrode setup may simulate practical applications more

faithfully. If the spectroelectrochemical characteristics of a film should be examined, the film is directly prepared on a transparent, conductive substrate, which functions as working electrode. Typically, quartz slides coated with indium tin oxide (ITO) are used. A platinum wire can act as working electrode for measurements of solutions. The counter electrode should have a surface area, which is equal or larger than the one of the working electrode. This ensures that the reaction at the counter electrode is fast enough and is not a limiting factor of the electrochemical reaction at the working electrode, at which the crucial reaction takes place. Therefore, the use of a platinum mesh, which comprises a huge surface area, would be a good choice. In a three-electrode setup typical reference electrodes are the saturated calomel electrode (SCE) or an Ag/AgCl-wire. To affect any electrochemical phenomena charge transport between the working and the counter electrode has to be possible. If films are measured, usually dissolved ionic salts are used. For spectroelectrochemical measurements of solutions, addition of conductive salts is necessary, only if the conductivity of the solution is not sufficient. The solvent has to enable the spectroscopic measurement in the desired region without influencing the results.^[279,280,283]

If the spectroscopic response is recorded, while the electrical potential is applied between the working and the counter electrode simultaneously, it is called "in situ". In contrary, in "ex situ" spectroelectrochemical measurements, the working electrode is removed from the electrochemical cell before it is spectroscopically examined. On the one hand, ex situ measurements enable characterizing the film with various methods without considering the geometrical issues. On the other hand, the nature of the film (swelling, incorporated ions etc.) may change upon removal from the electrochemical cell. Hence, in situ measurements are more common in practice.^[284,285]

Time resolved spectroelectrochemical measurements show the switching times between the undoped and highly doped state created by redox reactions. The switching time depends among others on the film thickness, the used electrolyte, the applied potential and, in the case of polymers, the molecular weight.^[286,287] Information about the electroactivity of a material can be obtained, as well. Electroactive materials can transduce ionic to electronic signals due to redox processes. Therefore, an inter-diffusion of ions or biological media into the material under study is required. The inter-diffusion leads to doped/dedoped states in the material, which can be recorded spectroscopically.^[288,289] For conducting polymers in general, a broad bipolaron band is obtained, as the chain length, the packing and the conformational order are not sharply defined.^[283] For small well-defined molecules, such as fullerenes, sharp absorption peaks can be

obtained.^[290] Isobestic points indicate the reversibility of doping processes, as they represent the transition from undoped to doped states.^[278,284]

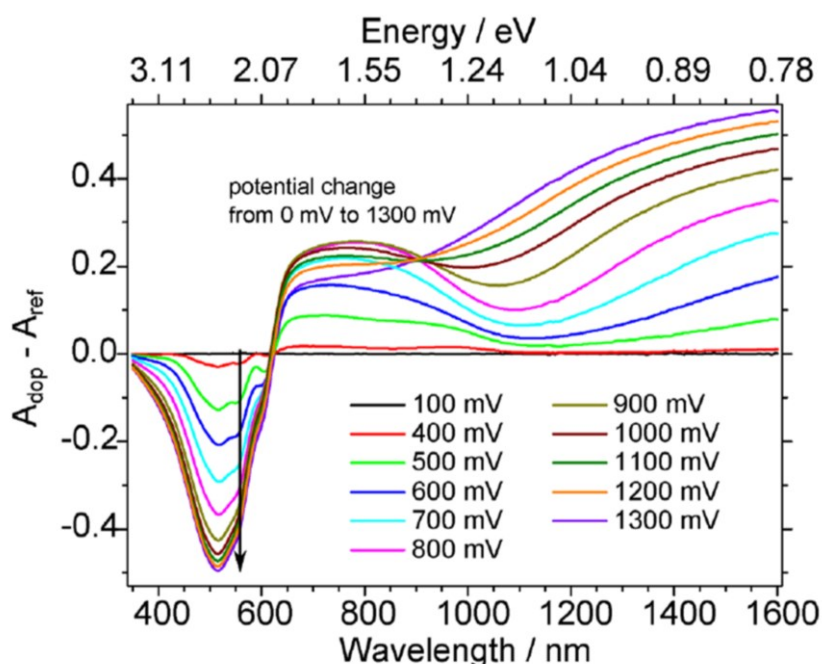


Figure 1-34: In situ measured spectroelectrochemical data of P3HT plotted as difference spectra with the undoped, pristine spectrum as reference. The electrochemical oxidation of P3HT was created by application of a potential from 0 to 1300 mV. The spectrum at 0 mV is taken as reference spectrum. The direction of spectral changes is indicated by an arrow. The isobestic point is located at around 600 nm. Figure reproduced from Ref. [118].

Spectroelectrochemical data are in general presented as multispectral graph, where the changes in the absorption are shown in dependence of the applied voltage. Another common way is plotting difference spectra with the undoped, pristine spectra as reference.^[278,283] In Figure 1-34 spectroelectrochemical data of an in situ measured P3HT are shown as an example for a difference spectra plot as well as for the broad bipolaron bands obtained for conducting polymers.

1.4 References

- [1] M. Piccolino, *Trends Neurosci.* **1997**, *20*, 443.
- [2] M. Piccolino, *Brain Res. Bull.* **1998**, *46*, 381.
- [3] *Bioelectronics*; Willner, I.; Katz, E., Eds.; WILEY-VCH Verlag GmbH & Co. KGaA: Weinheim, 2005.
- [4] M. Mirowski, P. R. Reid, M. M. Mower, L. Watkins, V. L. Gott, J. F. Schauble, A. Langer, M. S. Heilman, S. A. Kolenik, R. E. Fischell, M. L. Weisfeldt, *N. Engl. J. Med.* **1980**, *303*, 322.
- [5] R. Elmqvist, J. Landegren, S. O. Pettersson, A. Senning, G. William-Olsson, *Am. Hear. J.* **1963**, *65*, 731.
- [6] B. S. Wilson, M. F. Dorman, *Hear. Res.* **2008**, *242*, 3.
- [7] A. Rashid, S. Tahir, A. S. Ch, I. M. Qureshi, *Int. J. Appl. Math. Electron. Comput.* **2015**, *3*, 78.
- [8] R. L. Testerman, M. T. Rise, P. H. Stypulkowski, *IEEE Eng. Med. Biol. Mag.* **2006**, *25*, 74.
- [9] P. Limousin, P. Pollack, A. Benazzouz, D. Hoffman, J.-F. Le Bas, E. Broussolle, J. E. Perret, A.-L. Benabid, *Lancet* **1995**, *345*, 91.
- [10] R. S. Fisher, A. L. Velasco, *Nat. Rev. Neurol.* **2014**, *10*, 261.
- [11] B. Nagel, H. Dellweg, L. M. Gierasch, *Pure Appl. Chem.* **1992**, *64*, 143.
- [12] M. Mascini, S. Tombelli, *Biomarkers* **2008**, *13*, 637.
- [13] K. R. Rogers, *Biosens. Bioelectron.* **1995**, *10*, 533.
- [14] P. D. Patel, *TrAC - Trends Anal. Chem.* **2002**, *21*, 96.
- [15] N. Massad-Ivanir, G. Shtenberg, N. Raz, C. Gazenbeek, D. Budding, M. P. Bos, E. Segal, *Sci. Rep.* **2016**, *6*, 38099.
- [16] P. D. Skottrup, M. Nicolaisen, A. F. Justesen, *Biosens. Bioelectron.* **2008**, *24*, 339.
- [17] J. Wang, *Electroanalysis* **2001**, *13*, 983.
- [18] D. T. Simon, E. O. Gabrielsson, K. Tybrandt, M. Berggren, *Chem. Rev.* **2016**, *116*, 13009.
- [19] J. Rivnay, R. M. Owens, G. G. Malliaras, *Chem. Mater.* **2014**, *26*, 679.
- [20] D.-H. Kim, M. Abidian, D. C. Martin, *J. Biomed. Mater. Res. - Part A* **2004**, *71*, 577.
- [21] M. R. Abidian, D. C. Martin, *Adv. Funct. Mater.* **2009**, *19*, 573.
- [22] R. A. Green, P. B. Matteucci, R. T. Hassarati, B. Giraud, C. W. D. Dodds, S. Chen, P. J. Byrnes-Preston, G. J. Suaning, L. A. Poole-Warren, N. H. Lovell, *J. Neural Eng.* **2013**, *10*, 16009.
- [23] X. Cui, V. A. Lee, Y. Raphael, J. A. Wiler, J. F. Hetke, D. J. Anderson, D. C. Martin, *J. Biomed. Mater. Res.* **2001**, 261.
- [24] K. A. Ludwig, J. D. Uram, J. Yang, D. C. Martin, D. R. Kipke, *J. Neural Eng.* **2006**, *3*, 59.

- [25] M. R. Abidian, K. A. Ludwig, T. C. Marzullo, D. C. Martin, D. R. Kipke, *Adv. Mater.* **2009**, *21*, 3764.
- [26] M. R. Abidian, D. C. Martin, *Biomaterials* **2008**, *29*, 1273.
- [27] X. Cui, J. F. Hetke, J. A. Wiler, D. J. Anderson, D. C. Martin, *Sens. Actuators, A* **2001**, *93*, 8.
- [28] M. R. Abidian, D. H. Kim, D. C. Martin, *Adv. Mater.* **2006**, *18*, 405.
- [29] C. S. Reinhard, M. L. Radomsky, W. M. Saltzman, J. Hilton, H. Brem, *J. Control. Release* **1991**, *16*, 331.
- [30] F. Cicoira, C. Santato, *Organic Electronics*; WILEY-VCH Verlag GmbH & Co. KGaA: Weinheim, 2013.
- [31] M. Berggren, A. Richter-Dahlfors, *Adv. Mater.* **2007**, *19*, 3201.
- [32] A. Williamson, M. Ferro, P. Leleux, E. Ismailova, A. Kaszas, T. Doublet, P. Quilichini, J. Rivnay, B. Rózsa, G. Katona, C. Bernard, G. G. Malliaras, *Adv. Mater.* **2015**, *27*, 4405.
- [33] C. K. Chiang, C. R. Fincher, Y. W. Park, A. J. Heeger, H. Shirakawa, E. J. Louis, S. C. Gau, A. G. MacDiarmid, *Phys. Rev. Lett.* **1977**, *39*, 1098.
- [34] O. Bubnova, Z. U. Khan, H. Wang, S. Braun, D. R. Evans, M. Fabretto, P. Hojati-Talemi, D. Dagnelund, J.-B. Arlin, Y. H. Geerts, S. Desbief, D. W. Breiby, J. W. Andreasen, R. Lazzaroni, W. M. Chen, I. Zozoulenko, M. Fahlman, P. J. Murphy, M. Berggren, X. Crispin, *Nat. Mater.* **2014**, *13*, 190.
- [35] H. S. White, G. P. Kittlesen, M. S. Wrighton, *J. Am. Chem. Soc.* **1984**, *106*, 5375.
- [36] L. Kergoat, B. Piro, M. Berggren, G. Horowitz, M.-C. Pham, *Anal. Bioanal. Chem.* **2012**, *402*, 1813.
- [37] E. W. Paul, A. J. Ricco, M. S. Wrighton, *J. Phys. Chem.* **1985**, *89*, 1441.
- [38] C. B. Nielsen, A. Giovannitti, D. T. Sbircea, E. Bandiello, M. R. Niazi, D. A. Hanifi, M. Sessolo, A. Amassian, G. G. Malliaras, J. Rivnay, I. McCulloch, *J. Am. Chem. Soc.* **2016**, *138*, 10252.
- [39] D. J. Macaya, M. Nikolou, S. Takamatsu, J. T. Mabeck, R. M. Owens, G. G. Malliaras, *Sens. Actuators, B* **2007**, *123*, 374.
- [40] S. Inal, J. Rivnay, P. Leleux, M. Ferro, M. Ramuz, J. C. Brendel, M. M. Schmidt, M. Thelakkat, G. G. Malliaras, *Adv. Mater.* **2014**, *26*, 7450.
- [41] E. Zeglio, M. M. Schmidt, M. Thelakkat, R. Gabrielsson, N. Solin, O. Inganäs, *Chem. Mater.* **2017**, *29*, 4293.
- [42] J. W. Thackeray, H. S. White, M. S. Wrighton, *J. Phys. Chem.* **1985**, *89*, 5133.
- [43] P. Lin, F. Yan, H. L. W. Chan, *ACS Appl. Mater. Interfaces* **2010**, *2*, 1637.
- [44] V. Rani, K. S. V. Santhanam, *J. Solid State Electrochem.* **1998**, *2*, 99.

- [45] D. A. Bernardis, G. G. Malliaras, *Adv. Funct. Mater.* **2007**, *17*, 3538.
- [46] J. Rivnay, P. Leleux, M. Ferro, M. Sessolo, A. Williamson, D. A. Koutsouras, D. Khodagholy, M. Ramuz, X. Strakosas, R. M. Owens, C. Benar, J.-M. Badier, C. Bernard, G. G. Malliaras, *Sci. Adv.* **2015**, *1*, 1400251.
- [47] D. Khodagholy, M. Gurfinkel, E. Stavrinidou, P. Leleux, T. Herve, S. Sanaur, G. G. Malliaras, *Appl. Phys. Lett.* **2011**, *99*, 163304.
- [48] C. Liao, M. Zhang, M. Y. Yao, T. Hua, L. Li, F. Yan, *Adv. Mater.* **2015**, *27*, 7493.
- [49] D. Khodagholy, J. Rivnay, M. Sessolo, M. Gurfinkel, P. Leleux, L. H. Jimison, E. Stavrinidou, T. Herve, S. Sanaur, R. M. Owens, G. G. Malliaras, *Nat. Commun.* **2013**, *4*, 2133.
- [50] M. Nikolou, G. G. Malliaras, *Chem. Rec.* **2008**, *8*, 13.
- [51] G. Tarabella, F. Mahvash Mohammadi, N. Coppedè, F. Barbero, S. Iannotta, C. Santato, F. Cicoira, *Chem. Sci.* **2013**, *4*, 1395.
- [52] M. Sessolo, J. Rivnay, E. Bandiello, G. G. Malliaras, H. J. Bolink, *Adv. Mater.* **2014**, *26*, 4803.
- [53] D. A. Bernardis, G. G. Malliaras, G. E. S. Toombes, S. M. Gruner, *Appl. Phys. Lett.* **2006**, *89*, 1.
- [54] P. Lin, X. Luo, I.-M. Hsing, F. Yan, *Adv. Mater.* **2011**, *23*, 4035.
- [55] R.-X. He, M. Zhang, F. Tan, P. H. M. Leung, X.-Z. Zhao, H. L. W. Chan, M. Yang, F. Yan, *J. Mater. Chem.* **2012**, *22*, 22072.
- [56] S. Y. Yang, F. Cicoira, R. Byrne, F. Benito-Lopez, D. Diamond, R. M. Owens, G. G. Malliaras, *Chem. Commun.* **2010**, *46*, 7972.
- [57] D. Khodagholy, V. F. Curto, K. J. Fraser, M. Gurfinkel, R. Byrne, D. Diamond, G. G. Malliaras, F. Benito-Lopez, R. M. Owens, *J. Mater. Chem.* **2012**, *22*, 4440.
- [58] M. Ramuz, A. Hama, M. Huerta, J. Rivnay, P. Leleux, R. M. Owens, *Adv. Mater.* **2014**, *26*, 7083.
- [59] J. T. Mabeck, J. A. DeFranco, D. A. Bernardis, G. G. Malliaras, S. Hocdé, C. J. Chase, *Appl. Phys. Lett.* **2005**, *87*, 13503.
- [60] S. Zhang, E. Hubis, G. Tomasello, G. Soliveri, P. Kumar, F. Cicoira, *Chem. Mater.* **2017**, *29*, 3126.
- [61] C. Liao, C. Mak, M. Zhang, H. L. W. Chan, F. Yan, *Adv. Mater.* **2015**, *27*, 676.
- [62] S. A. Tria, M. Ramuz, M. Huerta, P. Leleux, J. Rivnay, L. H. Jimison, A. Hama, G. G. Malliaras, R. M. Owens, *Adv. Healthc. Mater.* **2014**, *3*, 1053.
- [63] *Handbook of Bioelectronics: Directly Interfacing Electronics and Biological systems*; Carrara, S.; Iniewski, K., Eds.; Cambridge University Press: Cambridge, 2015.

- [64] P. Fromherz, A. Offenhäusser, T. Vetter, J. Weis, *Science* **1991**, 252, 1290.
- [65] P. Fromherz, A. Stett, *Phys. Rev. Lett.* **1995**, 75, 1670.
- [66] D. Khodagholy, T. Doublet, P. Quilichini, M. Gurfinkel, P. Leleux, A. Ghestem, E. Ismailova, T. Hervé, S. Sanaur, C. Bernard, G. G. Malliaras, *Nat. Commun.* **2013**, 4, 1575.
- [67] S. Inal, J. Rivnay, A. I. Hofmann, I. Uguz, M. Mumtaz, D. Katsigiannopoulos, C. Brochon, E. Cloutet, G. Hadziioannou, G. G. Malliaras, *J. Polym. Sci. Part B Polym. Phys.* **2016**, 54, 147.
- [68] J. E. Anthony, A. Facchetti, M. Heeney, S. R. Marder, X. Zhan, *Adv. Mater.* **2010**, 22, 3876.
- [69] A. Giovannitti, C. B. Nielsen, D.-T. Sbircea, S. Inal, M. Donahue, M. R. Niazi, D. A. Hanifi, A. Amassian, G. G. Malliaras, J. Rivnay, I. McCulloch, *Nat. Commun.* **2016**, 7, 13066.
- [70] Y. Zhang, S. Inal, C.-Y. Hsia, M. Ferro, M. Ferro, S. Daniel, R. M. Owens, *Adv. Funct. Mater.* **2016**, 26, 7304.
- [71] M. Zein, R. Winter, *Phys Chem Chem Phys* **2000**, 2, 4545.
- [72] M. O. Eze, *Biochem. Educ.* **1991**, 19, 204.
- [73] A. Akbarzadeh, R. Rezaei-Sadabady, S. Davaran, S. W. Joo, N. Zarghami, Y. Hanifehpour, M. Samiei, M. Kouhi, K. Nejati-Koshki, *Nanoscale Res. Lett.* **2013**, 8, 102.
- [74] A. Laouini, C. Jaafar-Maalej, I. Limayem-Blouza, S. Sfar, C. Charcosset, H. Fessi, *J. Colloid Sci. Biotechnol.* **2012**, 1, 147.
- [75] R. Milo, R. Phillips, *Cell Biology By the Numbers*; Garland Science, 2015.
- [76] J. E. Houston, M. Kraft, U. Scherf, R. C. Evans, *Phys. Chem. Chem. Phys.* **2016**, 18, 12423.
- [77] M. B. Sankaram, T. E. Thompson, *Proc. Natl. Acad. Sci. U. S. A.* **1991**, 88, 8686.
- [78] O. Engberg, V. Hautala, T. Yasuda, H. Dehio, M. Murata, J. P. Slotte, T. K. M. Nyholm, *Biophys. J.* **2016**, 111, 546.
- [79] K. Simons, E. Ikonen, *Nature* **1997**, 387, 569.
- [80] V. Michel, M. Bakovic, *Biol. Cell* **2007**, 99, 129.
- [81] D. A. Brown, E. London, *J. Biol. Chem.* **2000**, 275, 17221.
- [82] K. Simons, D. Toomre, *Nat. Rev. Mol. Cell Biol.* **2000**, 1, 31.
- [83] A. S. Klymchenko, R. Kreder, *Chem. Biol.* **2014**, 21, 97.
- [84] M. Bates, S. A. Jones, X. Zhuang, *ICold Spring Harb. Lab. Protoc.* **2013**, 498.
- [85] A. S. Shaw, *Nat. Immunol.* **2006**, 7, 1139.
- [86] J. A. Allen, R. A. Halverson-Tamboli, M. M. Rasenick, *Nat. Rev. Neurosci.* **2007**, 8, 128.
- [87] E. London, *Curr. Opin. Struct. Biol.* **2002**, 12, 480.
- [88] Z. Kahveci, M. J. Martínez-Tomé, R. Mallavia, C. R. Mateo, *Biomacromolecules* **2013**, 14, 1990.
- [89] M. Dal Molin, S. Matile, *Org. Biomol. Chem.* **2013**, 11, 1952.

- [90] M. Sauer, J. Hofkens, J. Enderlein, *Handbook of Fluorescence Spectroscopy and Imaging*; WILEY-VCH Verlag GmbH & Co. KGaA: Weinheim, 2011.
- [91] J. R. Lakowicz, *Principles of Fluorescence Spectroscopy*; 3rd ed.; Springer Science+Business Media, LLC: New York, 2006.
- [92] L. A. Bagatolli, In *Fluorescent Methods to Study Biological Membranes. Springer Series on Fluorescence (Methods and Applications), Vol. 13*; Mély, Y.; Duportail, G., Eds.; Springer: Berlin, Heidelberg, 2012.
- [93] E. Sezgin, T. Sadowski, K. Simons, *Langmuir* **2014**, *30*, 8160.
- [94] L. A. Bagatolli, *Biochim. Biophys. Acta* **2006**, *1758*, 1541.
- [95] A. M. Koch, F. Reynolds, M. F. Kircher, H. P. Merkle, R. Weissleder, L. Josephson, *Bioconjug. Chem.* **2003**, *14*, 1115.
- [96] J. Zhang, R. E. Campbell, A. Y. Ting, R. Y. Tsien, *Nat. Rev. Mol. Cell Biol.* **2002**, *3*, 906.
- [97] G. Feng, D. Ding, B. Liu, *Nanoscale* **2012**, *4*, 6150.
- [98] U. Resch-Genger, M. Grabolle, S. Cavaliere-Jaricot, R. Nitschke, T. Nann, *Nat. Methods* **2008**, *5*, 763.
- [99] X. Michalet, F. F. Pinaud, L. A. Bentolila, J. M. Tsay, S. Doose, J. J. Li, G. Sundaresan, A. M. Wu, S. S. Gambhir, S. Weiss, *Science* **2005**, *307*, 538.
- [100] S. Wang, F. Lv, *Functionalized Conjugated Polyelectrolytes - Design and Biomedical Applications*; Springer, 2013.
- [101] H. Ho, A. Najari, M. Leclerc, *Acc. Chem. Res.* **2008**, *41*, 168.
- [102] B. Liu, G. C. Bazan, *Chem. Mater.* **2004**, *16*, 4467.
- [103] K. P. R. Nilsson, P. Hammarström, F. Ahlgren, A. Herland, E. A. Schnell, M. Lindgren, G. T. Westermark, O. Inganäs, *ChemBioChem* **2006**, *7*, 1096.
- [104] A. J. Heeger, *J. Phys. Chem. B* **2001**, *105*, 8475.
- [105] H. Shirakawa, E. J. Louis, A. G. MacDiarmid, C. K. Chiang, A. J. Heeger, *J. C. S. Chem. Comm.* **1977**, 578.
- [106] H. Sirringhaus, P. J. Brown, R. H. Friend, M. M. Nielsen, K. Bechgaard, B. M. W. Langeveld-Voss, A. J. H. Spiering, R. A. J. Janssen, E. W. Meijer, P. Herwig, D. M. de Leeuw, *Nature* **1999**, *401*, 685.
- [107] D. Hertel, H. Bässler, U. Scherf, H. H. Hörhold, *J. Chem. Phys.* **1999**, *110*, 9214.
- [108] A. Moliton, R. C. Hiorns, *Polym. Int.* **2004**, *53*, 1397.
- [109] A. Köhler, H. Bässler, *Electronic Processes in Organic Semiconductors*; WILEY-VCH Verlag GmbH & Co. KGaA: Weinheim, 2015.
- [110] A. J. Heeger, *Angew. Chem. Int. Ed. Engl.* **2001**, *40*, 2591.

- [111] M. S. Freund, B. A. Deore, *Self-doped Conducting Polymers*; John Wiley & Sons, Ltd, 2007.
- [112] T.-H. Le, Y. Kim, H. Yoon, *Polymers* **2017**, *9*, 150.
- [113] J. Heinze, B. A. Frontana-Urbe, S. Ludwigs, *Chem. Rev.* **2010**, *110*, 4724.
- [114] A. Babel, S. A. Jenekhe, *Adv. Mater.* **2002**, *14*, 371.
- [115] V. Coropceanu, J. Cornil, D. A. da Silva Filho, Y. Olivier, R. Silbey, J.-L. Bredas, *Chem. Rev.* **2007**, *107*, 926.
- [116] J. L. Bredas, R. R. Chance, R. Silbey, *Phys. Rev. B* **1982**, *26*, 5843.
- [117] J. L. Brédas, G. B. Street, *Acc. Chem. Res.* **1985**, *18*, 309.
- [118] C. Enengl, S. Enengl, S. Pluczyk, M. Havlicek, M. Lapkowski, H. Neugebauer, E. Ehrenfreund, *ChemPhysChem* **2016**, *17*, 3836.
- [119] R. J. Mortimer, *Chem. Soc. Rev.* **1997**, *26*, 147.
- [120] P. R. Somani, S. Radhakrishnan, *Mater. Chem. Phys.* **2002**, *77*, 117.
- [121] J. M. Leger, *Adv. Mater.* **2008**, *20*, 837.
- [122] M. Farajollahi, A. Usgaocar, Y. Dobashi, V. Woehling, C. Plesse, F. Vidal, F. Sassani, J. D. W. Madden, *IEEE ASME Trans. Mechatronics* **2017**, *22*, 705.
- [123] L. Bay, T. Jacobsen, S. Skaarup, K. West, *J. Phys. Chem. B* **2001**, *105*, 8492.
- [124] K.-Y. Jen, G. G. Miller, R. L. Elsenbaumer, *J. Chem. Soc., Chem. Commun.* **1986**, 1346.
- [125] J. H. Burroughes, D. D. C. Bradley, A. R. Brown, R. N. Marks, K. Mackay, R. H. Friend, P. L. Burns, A. B. Holmes, *Nature* **1990**, *347*, 539.
- [126] F. Guo, A. Karl, Q. Xue, K. C. Tam, K. Forberich, C. J. Brabec, *Light Sci. Appl.* **2017**, *6*, e17094.
- [127] Y. Liu, J. Zhao, Z. Li, C. Mu, W. Ma, H. Hu, K. Jiang, H. Lin, H. Ade, H. Yan, *Nat. Commun.* **2014**, *5*, 5293.
- [128] L. Lucera, F. Machui, H. D. Schmidt, T. Ahmad, P. Kubis, S. Strohm, J. Hepp, A. Vetter, H.-J. Egelhaaf, C. J. Brabec, *Org. Electron.* **2017**, *45*, 209.
- [129] L. Van Tho, W.-T. Park, E.-Y. Choi, Y.-Y. Noh, *Appl. Phys. Lett.* **2017**, *110*, 163303.
- [130] S. Holliday, J. E. Donaghey, I. McCulloch, *Chem. Mater.* **2014**, *26*, 647.
- [131] D. Khim, G.-S. Ryu, W.-T. Park, H. Kim, M. Lee, Y.-Y. Noh, *Adv. Mater.* **2016**, *28*, 2752.
- [132] B. Li, S. Santhanam, L. Schultz, M. Jeffries-El, M. C. Iovu, G. Sauv e, J. Cooper, R. Zhang, J. C. Revelli, A. G. Kusne, J. L. Snyder, T. Kowalewski, L. E. Weiss, R. D. McCullough, G. K. Fedder, D. N. Lambeth, *Sens. Actuators, B* **2007**, *123*, 651.
- [133] C. Ma, M. Taya, C. Xu, *Polym. Eng. Sci.* **2008**, *48*, 2224.
- [134] D. R. Rosseinsky, R. J. Mortimer, *Adv. Mater.* **2001**, *13*, 783.
- [135] F. Carpi, D. De Rossi, *Opt. Laser Technol.* **2006**, *38*, 292.

- [136] H. Pagès, P. Topart, D. Lemordant, H. Page, *Electrochim. Acta* **2001**, *46*, 2137.
- [137] L. Bay, K. West, P. Sommer-Larsen, S. Skaarup, M. Benslimane, *Adv. Mater.* **2003**, *15*, 310.
- [138] R. H. Baughman, *Mater. Sci.* **2005**, *308*, 63.
- [139] P. P. Deshpande, N. G. Jadhav, V. J. Gelling, D. Sazou, *J. Coatings Technol. Res.* **2014**, *11*, 473.
- [140] Y. Yang, G. Yu, J. J. Cha, H. Wu, M. Vosgueritchian, Y. Yao, Z. Bao, Y. Cui, *ACS Nano* **2011**, *5*, 9187.
- [141] Y. Yao, N. Liu, M. T. McDowell, M. Pasta, Y. Cui, *Energy Environ. Sci.* **2012**, *5*, 7927.
- [142] P.-O. Morin, T. Bura, M. Leclerc, *Mater. Horiz.* **2016**, *3*, 11.
- [143] A. F. Diaz, K. K. Kanazawa, G. P. Gardini, *J. Chem. Soc., Chem. Commun.* **1979**, 635.
- [144] A. Pron, P. Rannou, *Prog. Polym. Sci.* **2002**, *27*, 135.
- [145] J. Roncali, *Chem. Rev.* **1992**, *92*, 711.
- [146] K. Kaneto, K. Yoshino, Y. Inuishi, *Solid State Commun.* **1983**, *46*, 389.
- [147] K. Kaneto, Y. Kohno, K. Yoshino, Y. Inuishi, *J. Chem. Soc. Chem. Commun.* **1983**, 382.
- [148] K. Yoshino, S. Hayashi, R.-I. Sugimoto, *Jpn. J. Appl. Phys* **1984**, *23*, L899.
- [149] T. Yamamoto, K. Sanechika, A. Yamamoto, *J. Polym. Sci. Polym. Lett. Ed.* **1980**, *18*, 9.
- [150] J. W.-P. Lin, L. P. Dudek, *J. Polym. Sci. Polym. Chem. Ed.* **1980**, *18*, 2869.
- [151] K. Tamao, K. Sumitani, M. Kumada, *J. Am. Chem. Soc.* **1972**, *94*, 4374.
- [152] *P3HT Revisited – from Molecular Scale to Solar Cell Devices*; Ludwigs, S., Ed.; Springer-Verlag: Heidelberg, 2014.
- [153] R. L. Elsenbaumer, K. Y. Jen, R. Oboodi, *Synth. Met.* **1986**, *15*, 169.
- [154] T. Yamamoto, K. Sanechika, A. Yamamoto, *Bull. Chem. Soc. Jpn.* **1983**, *56*, 1497.
- [155] P. J. Brown, D. S. Thomas, A. Köhler, J. S. Wilson, J.-S. Kim, C. M. Ramsdale, H. Sirringhaus, R. H. Friend, *Phys. Rev. B* **2003**, *67*, 64203.
- [156] R. D. McCullough, R. D. Lowe, *J. Chem. Soc., Chem. Commun.* **1992**, 70.
- [157] R. D. McCullough, *Adv. Mater.* **1998**, *10*, 93.
- [158] J.-E. Österholm, J. Laakso, P. Nyholm, H. Isotalo, H. Stubb, O. Inganäs, W. R. Salaneck, *Synth. Met.* **1989**, *28*, C435.
- [159] S. Hotta, M. Soga, N. Sonoda, *Synth. Met.* **1988**, *26*, 267.
- [160] M. Leclerc, F. M. Diaz, G. Wegner, *Makromol. Chem.* **1989**, *190*, 3105.
- [161] M. Pomerantz, J. J. Tseng, H. Zhu, S. J. Sproull, J. R. Reynolds, R. Uitz, H. J. Arnott, M. I. Haider, *Synth. Met.* **1991**, *41–43*, 825.
- [162] M. Sato, H. Morii, *Macromolecules* **1991**, *24*, 1196.
- [163] T.-A. Chen, R. D. Rieke, *J. Am. Chem. Soc.* **1992**, *114*, 10087.

- [164] T.-A. Chen, X. Wu, R. D. Rieke, *J. Am. Chem. Soc.* **1995**, *117*, 233.
- [165] L. Zhu, R. M. Wehmeyer, R. D. Rieke, *J. Org. Chem.* **1991**, *56*, 1445.
- [166] R. S. Loewe, S. M. Khersonsky, R. D. McCullough, *Adv. Mater.* **1999**, *11*, 250.
- [167] J. Liu, R. S. Loewe, R. D. McCullough, *Macromolecules* **1999**, *32*, 5777.
- [168] E. E. Sheina, J. Liu, M. C. Iovu, D. W. Laird, R. D. McCullough, *Macromolecules* **2004**, *37*, 3526.
- [169] A. Yokoyama, R. Miyakoshi, T. Yokozawa, *Macromolecules* **2004**, *37*, 1169.
- [170] R. Miyakoshi, A. Yokoyama, T. Yokozawa, *J. Am. Chem. Soc.* **2005**, *127*, 17542.
- [171] R. H. Lohwasser, M. Thelakkat, *Macromolecules* **2011**, *44*, 3388.
- [172] A. O. Patil, Y. Ikenoue, F. Wudl, A. J. Heeger, *J. Am. Chem. Soc.* **1987**, *109*, 1858.
- [173] S. Shi, F. Wudl, *Macromolecules* **1990**, *23*, 2119.
- [174] T. I. Wallow, B. M. Novak, *J. Am. Chem. Soc.* **1991**, *113*, 7411.
- [175] M. R. Pinto, B. M. Kristal, K. S. Schanze, *Langmuir* **2003**, *19*, 6523.
- [176] A. Viinikanoja, J. Lukkari, T. Ääritalo, T. Laiho, J. Kankare, *Langmuir* **2003**, *19*, 2768.
- [177] B. S. Harrison, M. B. Ramey, J. R. Reynolds, K. S. Schanze, *J. Am. Chem. Soc.* **2000**, *122*, 8561.
- [178] H.-A. Ho, M. Boissinot, M. G. Bergeron, G. Corbeil, K. Doré, D. Boudreau, M. Leclerc, *Angew. Chem. Int. Ed.* **2002**, *41*, 1548.
- [179] G. Zotti, S. Zecchin, G. Schiavon, A. Berlin, *Macromolecules* **2001**, *34*, 3889.
- [180] C. Zhou, Y. Gao, D. Chen, *J. Phys. Chem. B* **2012**, *116*, 11552.
- [181] C. Tan, N. Liu, B. Yu, C. Zhang, W. Bu, X. Liu, Y.-F. Song, *J. Mater. Chem. C* **2015**, *3*, 2450.
- [182] Y. Ikenoue, N. Uotani, A. O. Patil, F. Wudl, A. J. Heeger, *Synth. Met.* **1989**, *30*, 305.
- [183] J. R. Reynolds, N. S. Sundaresan, M. Pomerantz, S. Basak, C. K. Baker, *J. Electroanal. Chem.* **1988**, *250*, 355.
- [184] A. O. Patil, Y. Ikenoue, N. Basescu, N. Colaneri, J. Chen, F. Wudl, A. J. Heeger, *Synth. Met.* **1987**, *20*, 151.
- [185] C. Duan, L. Wang, K. Zhang, X. Guan, F. Huang, *Adv. Mater.* **2011**, *23*, 1665.
- [186] E. Li, L. Lin, L. Wang, M. Pei, J. Xu, G. Zhang, *Macromol. Chem. Phys.* **2012**, *213*, 887.
- [187] L. Zhai, R. D. McCullough, *Adv. Mater.* **2002**, *14*, 901.
- [188] A. Laschewsky, *Curr. Opin. Colloid Interface Sci.* **2012**, *17*, 56.
- [189] W. Lee, J. H. Seo, H. Y. Woo, *Polymer* **2013**, *54*, 5104.
- [190] M. R. Pinto, K. S. Schanze, *Synthesis* **2002**, *9*, 1293.
- [191] C. Tan, E. Atas, J. G. Müller, M. R. Pinto, V. D. Kleiman, K. S. Schanze, *J. Am. Chem. Soc.* **2004**, *126*, 13685.

- [192] C. Tan, M. R. Pinto, K. S. Schanze, *Chem. Commun.* **2002**, 446.
- [193] X. Zhao, M. R. Pinto, L. M. Hardison, J. Mwaura, H. Jiang, D. Witker, V. D. Kleiman, J. R. Reynolds, K. S. Schanze, *Macromolecules* **2006**, *39*, 6355.
- [194] H. Jiang, X. Zhao, K. S. Schanze, *Langmuir* **2006**, *22*, 5541.
- [195] P. Kaur, H. Yue, M. Wu, M. Liu, J. Treece, D. H. Waldeck, C. Xue, H. Liu, *J. Phys. Chem. B* **2007**, *111*, 8589.
- [196] Q.-L. Fan, Y. Zhou, X.-M. Lu, X.-Y. Hou, W. Huang, *Macromolecules* **2005**, *38*, 2927.
- [197] W. Ma, P. K. Iyer, X. Gong, B. Liu, D. Moses, G. C. Bazan, A. J. Heeger, *Adv. Mater.* **2005**, *17*, 274.
- [198] J. Park, C. V. Hoven, R. Yang, N. Cho, H. Wu, T.-Q. Nguyen, G. C. Bazan, *J. Mater. Chem.* **2009**, *19*, 211.
- [199] S.-H. Oh, S.-I. Na, J. Jo, B. Lim, D. Vak, D.-Y. Kim, *Adv. Funct. Mater.* **2010**, *20*, 1977.
- [200] C. He, C. Zhong, H. Wu, R. Yang, W. Yang, F. Huang, G. C. Bazan, Y. Cao, *J. Mater. Chem.* **2010**, *20*, 2617.
- [201] J. Luo, H. Wu, C. He, A. Li, W. Yang, Y. Cao, *Appl. Phys. Lett.* **2009**, *95*, 43301.
- [202] J. H. Seo, A. Gutacker, Y. Sun, H. Wu, F. Huang, Y. Cao, U. Scherf, A. J. Heeger, G. C. Bazan, *J. Am. Chem. Soc.* **2011**, *133*, 8416.
- [203] L. Hu, F. Wu, C. Li, A. Hu, X. Hu, Y. Zhang, L. Chen, Y. Chen, *Macromolecules* **2015**, *48*, 5578.
- [204] A. Garcia, R. C. Bakus II, P. Zalar, C. V Hoven, J. Z. Brzezinski, T.-Q. Nguyen, *J. Am. Chem. Soc.* **2011**, *133*, 2492.
- [205] C. Hoven, R. Yang, A. Garcia, A. J. Heeger, T.-Q. Nguyen, G. C. Bazan, *J. Am. Chem. Soc.* **2007**, *129*, 10976.
- [206] C. V Hoven, R. Yang, A. Garcia, V. Crockett, A. J. Heeger, G. C. Bazan, T.-Q. Nguyen, *Proc. Natl. Acad. Sci.* **2008**, *105*, 12730.
- [207] C. V. Hoven, J. Peet, A. Mikhailovsky, T.-Q. Nguyen, *Appl. Phys. Lett.* **2009**, *94*, 33301.
- [208] J. H. Seo, A. Gutacker, B. Walker, S. Cho, A. Garcia, R. Yang, T.-Q. Nguyen, A. J. Heeger, G. C. Bazan, *J. Am. Chem. Soc.* **2009**, *131*, 18220.
- [209] B. H. Lee, I. H. Jung, H. Y. Woo, H.-K. Shim, G. Kim, K. Lee, *Adv. Funct. Mater.* **2014**, *24*, 1100.
- [210] A. Duarte, K.-Y. Y. Pu, B. Liu, G. C. Bazan, *Chem. Mater.* **2011**, *23*, 501.
- [211] H. W. Kroto, J. R. Heath, S. C. O'Brien, R. F. Curl, R. E. Smalley, *Nature* **1985**, *318*, 162.
- [212] R. E. Smalley, *Angew. Chem.* **1997**, *109*, 1666.
- [213] R. F. Curl, *Angew. Chem.* **1997**, *109*, 1636.

- [214] W. Krätschmer, K. Fostiropoulos, *Phys. unserer Zeit* **1992**, 23, 105.
- [215] H. W. Kroto, *Angew. Chem. Int. Ed.* **1992**, 31, 111.
- [216] W. Krätschmer, L. D. Lamb, K. Fostiropoulos, D. R. Huffman, *Nature* **1990**, 347, 354.
- [217] H. Prinzbach, A. Weiler, P. Landenberger, F. Wahl, J. Wörth, L. T. Scott, M. Gelmont, D. Olevano, B. v. Issendorff, *Nature* **2000**, 407, 60.
- [218] W. Krätschmer, *Phys. Bl.* **1992**, 48, 553.
- [219] W. I. F. David, R. M. Ibberson, J. C. Matthewman, K. Prassides, T. J. S. Dennis, J. P. Hare, H. W. Kroto, R. Taylor, D. R. M. Walton, *Nature* **1991**, 353, 147.
- [220] K. Hedberg, L. Hedberg, D. S. Bethune, C. A. Brown, H. C. Dorn, R. D. Johnson, M. De Vries, *Science* **1991**, 254, 410.
- [221] M. Prato, *J. Mater. Chem.* **1997**, 7, 1097.
- [222] M. Bühl, A. Hirsch, *Chem. Rev.* **2001**, 101, 1153.
- [223] N. Sivaraman, R. Dhamodaran, I. Kaliappan, T. G. Srinivasan, V. Rao, C. K. Mathews, *J. Org. Chem.* **1992**, 57, 6077.
- [224] R. S. Ruoff, D. S. Tse, R. Malhotra, D. C. Lorents, *J. Phys. Chem.* **1993**, 97, 3379.
- [225] Q. Xie, E. Pérez-Cordero, L. Echegoyen, *J. Am. Chem. Soc.* **1992**, 114, 3978.
- [226] X.-B. Wang, C.-F. Ding, L.-S. Wang, *J. Chem. Phys.* **1999**, 110, 8217.
- [227] L. Echegoyen, L. E. Echegoyen, *Acc. Chem. Res.* **1998**, 31, 593.
- [228] R. C. Haddon, L. E. Brus, K. Raghavachari, *Chem. Phys. Lett.* **1986**, 125, 459.
- [229] Q. Xie, F. Arias, L. Echegoyen, *J. Am. Chem. Soc.* **1993**, 115, 9818.
- [230] R. C. Haddon, *Science* **1993**, 261, 1545.
- [231] A. Hirsch, M. Brettreich, *Fullerenes: Chemistry and Reactions*; WILEY-VCH Verlag GmbH & Co. KGaA: Weinheim, 2005.
- [232] A. Hirsch, *Top. Curr. Chem.* **1999**, 199, 1.
- [233] N. Matsuzawa, D. A. Dixon, T. Fukunaga, *J. Phys. Chem.* **1992**, 96, 7604.
- [234] A. Hirsch, *Synthesis* **1995**, 8, 895.
- [235] F. Diederich, L. Isaacs, D. Philp, *Chem. Soc. Rev.* **1994**, 23, 243.
- [236] C. Bellavia-Lund, F. Diederich, A. Hirsch, W. K. Hsu, J. C. Hummelen, H. W. Kroto, M. Prato, Y. Rubin, M. Terrones, C. Thilgen, D. R. M. Walton, F. Wudl, *Topics in current chemistry*; Hirsch, A., Ed.; Springer-Verlag Berlin Heidelberg, 1999.
- [237] C. Bingel, *Chem. Ber.* **1993**, 126, 1957.
- [238] X. Camps, A. Hirsch, *J. Chem. Soc., Perkin Trans.* **1997**, 1, 1595.
- [239] J.-F. Nierengarten, J.-F. Nicoud, *Tetrahedron Lett.* **1997**, 38, 7737.
- [240] J.-F. Nierengarten, V. Gramlich, F. Cardullo, F. Diederich, *Angew. Chem.* **1996**, 108, 2242.

- [241] A. Hirsch, I. Lamparth, T. Grösser, *J. Am. Chem. Soc.* **1994**, *116*, 9385.
- [242] C. J. Brabec, S. Gowrisanker, J. J. M. Halls, D. Laird, S. Jia, S. P. Williams, *Adv. Mater.* **2010**, *22*, 3839.
- [243] J. C. Hummelen, B. W. Knight, F. LePeq, F. Wudl, J. Yao, C. L. Wilkins, *J. Org. Chem.* **1995**, *60*, 532.
- [244] F. Machui, S. Langner, X. Zhu, S. Abbott, C. J. Brabec, *Sol. Energy Mater. Sol. Cells* **2012**, *100*, 138.
- [245] R. Søndergaard, M. Helgesen, M. Jørgensen, F. C. Krebs, *Adv. Energy Mater.* **2011**, *1*, 68.
- [246] M. Brettreich, A. Hirsch, *Tetrahedron Lett.* **1998**, *39*, 2731.
- [247] I. Etxebarria, J. Ajuria, R. Pacios, *Org. Electron.* **2015**, *19*, 34.
- [248] R. Ganesamoorthy, G. Sathiyam, P. Sakthivel, *Sol. Energy Mater. Sol. Cells* **2017**, *161*, 102.
- [249] A. Speltini, D. Merli, A. Profumo, *Anal. Chim. Acta* **2013**, *783*, 1.
- [250] J. R. Baena, M. Gallego, M. Valcárcel, *trends Anal. Chem.* **2002**, *21*, 187.
- [251] S. Bosi, T. Da Ros, G. Spalluto, M. Prato, *Eur. J. Med. Chem.* **2003**, *38*, 913.
- [252] L. L. Dugan, D. M. Turetsky, C. Du, D. Lobner, M. Wheeler, C. R. Almli, C. K.-F. Shen, T.-Y. Luh, D. W. Choi, T.-S. Lin, *Proc. Natl. Acad. Sci. U. S. A.* **1997**, *94*, 9434.
- [253] Y.-L. Huang, C. K.-F. Shen, T.-Y. Luh, H. C. Yang, K. C. Hwang, C.-K. Chou, *Eur. J. Biochem.* **1998**, *254*, 38.
- [254] H. Jin, W. Q. Chen, X. W. Tang, L. Y. Chiang, C. Y. Yang, J. V. Schloss, J. Y. Wu, *J. Neurosci. Res.* **2000**, *62*, 600.
- [255] H. Yilmaz, L. Ahmed, B. Rasulev, J. Leszczynski, *J. Nanoparticle Res.* **2016**, *18*, 123.
- [256] R. Bakry, R. M. Vallant, M. Najam-ul-Haq, M. Rainer, Z. Szabo, C. W. Huck, G. K. Bonn, *Int. J. Nanomed.* **2007**, *2*, 639.
- [257] T. Da Ros, M. Prato, F. Novello, M. Maggini, E. Banfi, *J. Org. Chem.* **1996**, *61*, 9070.
- [258] S. Bosi, T. Da Ros, S. Castellano, E. Banfi, M. Prato, *Bioorganic Med. Chem. Lett.* **2000**, *10*, 1043.
- [259] D. I. Schuster, S. R. Wilson, R. F. Schinazi, *Bioorg. Med. Chem. Lett.* **1996**, *6*, 1253.
- [260] G. L. Marcorin, T. Da Ros, S. Castellano, G. Stefancich, I. Bonin, S. Miertus, M. Prato, *Org. Lett.* **2000**, *2*, 3955.
- [261] S. H. Friedman, D. L. DeCamp, R. P. Sijbesma, G. Srdanov, F. Wudl, G. L. Kenyon, *J. Am. Chem. Soc.* **1993**, *115*, 6506.
- [262] I. Rašović, *Mater. Sci. Technol.* **2017**, *33*, 777.
- [263] R. Sijbesma, G. Srdanov, F. Wudl, J. A. Castoro, C. Wilkins, S. H. Friedman, D. L. DeCamp, G. L. Kenyon, *J. Am. Chem. Soc.* **1993**, *115*, 6510.

- [264] A. S. Boutorine, H. Tokuyama, M. Takasugi, H. Isobe, E. Nakamura, C. Hélène, *Angew. Chemie Int. Ed. English* **1994**, *33*, 2462.
- [265] S. Foley, C. Crowley, M. Smaihi, C. Bonfils, B. F. Erlanger, P. Seta, C. Larroque, *Biochem. Biophys. Res. Commun.* **2002**, *294*, 116.
- [266] A. Montellano, T. Da Ros, A. Bianco, M. Prato, *Nanoscale* **2011**, *3*, 4035.
- [267] S. Tiwari, N. C. Greenham, *Opt. Quantum Electron.* **2009**, *41*, 69.
- [268] A. Kokil, K. Yang, J. Kumar, *J. Polym. Sci. Part B Polym. Phys.* **2012**, *50*, 1130.
- [269] P. Stallinga, A. R. V Benvenho, E. C. P. Smits, S. G. J. Mathijssen, M. Cölle, H. L. Gomes, D. M. de Leeuw, *Org. Electron. physics, Mater. Appl.* **2008**, *9*, 735.
- [270] P. López Varo, J. A. Jiménez Tejada, J. A. López Villanueva, J. E. Carceller, M. J. Deen, *Org. Electron. physics, Mater. Appl.* **2012**, *13*, 1700.
- [271] G. G. Malliaras, J. C. Scott, *J. Appl. Phys.* **1999**, *85*, 7426.
- [272] P. S. Davids, I. H. Campbell, D. L. Smith, *J. Appl. Phys.* **1997**, *82*, 6319.
- [273] O. D. Jurchescu, In *Handbook of Organic Materials for Optical and (Opto)electronic Devices*; Ostroverkhova, O., Ed.; Woodhead Publishing Limited, 2013; pp. 377–397.
- [274] J. C. Blakesley, F. A. Castro, W. Kylberg, G. F. A. Dibb, C. Arantes, R. Valaski, M. Cremona, J. S. Kim, J.-S. Kim, *Org. Electron.* **2014**, *15*, 1263.
- [275] P. N. Murgatroyd, *J. Phys. D. Appl. Phys.* **1970**, *3*, 151.
- [276] W. Brütting, *Physics of Organic Semiconductors*; WILEY-VCH Verlag GmbH & Co. KGaA: Weinheim, 2005.
- [277] A. J. Bard, L. R. Faulkner, *Electrochemical Methods: Fundamentals and Applications*; 2nd ed.; John Wiley & Sons, Inc., 2001.
- [278] W. Kaim, J. Fiedler, *Chem. Soc. Rev.* **2009**, *38*, 3373.
- [279] W. R. Heineman, *J. Chem. Educ.* **1983**, *60*, 305.
- [280] P. Ceroni, A. Credi, M. Venturi, *Analytical Methods in Supramolecular Chemistry*; Schalley, C. A., Ed.; 2nd ed.; WILEY-VCH Verlag GmbH & Co. KGaA, 2012.
- [281] W. Kaim, B. Sarkar, G. K. Lahiri, In *Spectroelectrochemistry*; Kaim, W.; Klein, A., Eds.; Royal Society of Chemistry, 2008; pp. 68–90.
- [282] P. R. Murray, L. J. Yellowlees, In *Spectroelectrochemistry*; Kaim, W.; Klein, A., Eds.; Royal Society of Chemistry, 2008; pp. 207–231.
- [283] P. Chandrasekhar, *Conducting Polymers, Fundamentals and Applications: a practical approach*; Springer Science+Business Media, LLC, 1999.
- [284] S. Enengl, C. Enengl, P. Stadler, H. Neugebauer, N. S. Sariciftci, *ChemPhysChem* **2015**, *16*, 2206.

- [285] L. Kavan, L. Dunsch, *ChemPhysChem* **2007**, *8*, 974.
- [286] K. Hyodo, *Electrochim. Acta* **1994**, *39*, 265.
- [287] M. Trznadel, A. Pron, M. Zagorska, R. Chrzaszcz, J. Pielichowski, *Macromolecules* **1998**, *31*, 5051.
- [288] C. M. Pacheco-Moreno, M. Schreck, A. D. Scaccabarozzi, P. Bourgun, G. Wantz, M. M. Stevens, O. J. Dautel, N. Stingelin, *Adv. Mater.* **2017**, *29*, 1604446.
- [289] A. V. Volkov, S. K. Singh, E. Stavrinidou, R. Gabrielsson, J. F. Franco-Gonzalez, A. Cruce, W. M. Chen, D. T. Simon, M. Berggren, I. V Zozoulenko, *Adv. Electron. Mater.* **2017**, *3*, 1700096.
- [290] P. Rapta, A. Bartl, A. Gromov, A. Staško, L. Dunsch, *ChemPhysChem* **2002**, *4*, 351.

2 OBJECTIVE OF THE THESIS

The research field of organic electrochemical transistors (OECTs) is growing rapidly, since the discovery in 1984. OECTs can function as sensors or signal amplifier for a variety of applications. Nowadays, PEDOT:PSS, a dispersion of two polymers, is mainly used as active material in depletion mode OECTs. The main focus of current research was on the optimization of device setups and on PEDOT:PSS layers to gain a better performance, such as an improved transconductance or shorter response time. Recently, a new π -conjugated polyelectrolyte, namely poly(6-(thiophene-3-yl)hexane-1-sulfonate) tetrabutylammonium (PTHSTBA⁺), was synthesized in our research group and successfully applied as active layer in an OECT. Contrary to PEDOT:PSS, this new p-type material functions as active material for OECTs in accumulation mode. Accumulation mode devices have the advantage of lower power consumption compared to depletion mode devices.

However, devices based on PTHSTBA⁺ were not able to reach the good performance of PEDOT:PSS based OECTs, which are highly optimized in different groups. To improve OECTs using CPEs as active layer, the knowledge about the processes proceeding as soon as CPEs are immersed in aqueous media, with and without applied bias, is crucial. So a detailed study of ion diffusion is planned in this thesis. Furthermore, the influence of ions in the electrolyte as well as the counterions of the CPE has to be considered. Especially, the influence of a systematic variation of the counter cations from tetramethylammonium to tetraethylammonium and tetrabutylammonium on transconductance and response time of OECTs will be undertaken. Another question is the tuning of hydrophobicity/hydrophilicity as well as the mode of operation (depletion vs. accumulation mode) in blends of two CPEs (in situ doped and undoped).

Therefore, the aims of the first part of this thesis are to contribute to a better understanding of the processes in CPE based OECTs and to systematically optimize the device performance.

OECTs function as interface between electronic elements and biomaterials. But the active layers in OECTs are in general based on p-type semiconductors. To improve the connection between biology and electronics, the use of biomembranes as active material is desirable. This enables the sensing and stimulation of biological processes like the activity of ion channels. For this purpose, the transduction of ionic to electronic current has to be enabled through the biomembrane. As pristine biomembranes have insulating properties, their conductivity has to be modified. This could be obtained by incorporation of an electric conductive material. CPEs are perfectly matching the mechanical properties of lipid membranes because of their hydrophobic

backbone. It is crucial, that the polymer backbones are near enough to each other inside the membrane to enable intermolecular hopping process of charges and, consequently, conduction. The visualization of the conductive material in the membrane as well as the imaging of occurring changes in the lipid core of the membrane are further aims of this thesis. This can lead to the usage of CPEs as photonic probes, which would pave the way for the application of biomembranes as active layers in OECTs.

As the usage of only p-type materials hinders the variety of OECTs and their applications, water compatible n-type materials will also be synthesized and studied in this thesis. The first n-type OECT was recently published in 2016. Here, the active material was a semiconducting polymer, which can transport holes as well as electrons along its backbone. Typically organic n-type materials are fullerene derivatives, which possess high electron mobilities and are already discussed for medical applications. To obtain a pure n-type OECT, the last part of this thesis aims for designing water compatible fullerene derivatives for the application in bioelectronic devices.

Overall, this thesis will contribute to a better understanding of OECTs based on CPEs and pave the way for new semiconductor materials for OECTs, such as conductive biomembranes and water-compatible organic n-type semiconductors.

3 OVERVIEW OF THE THESIS

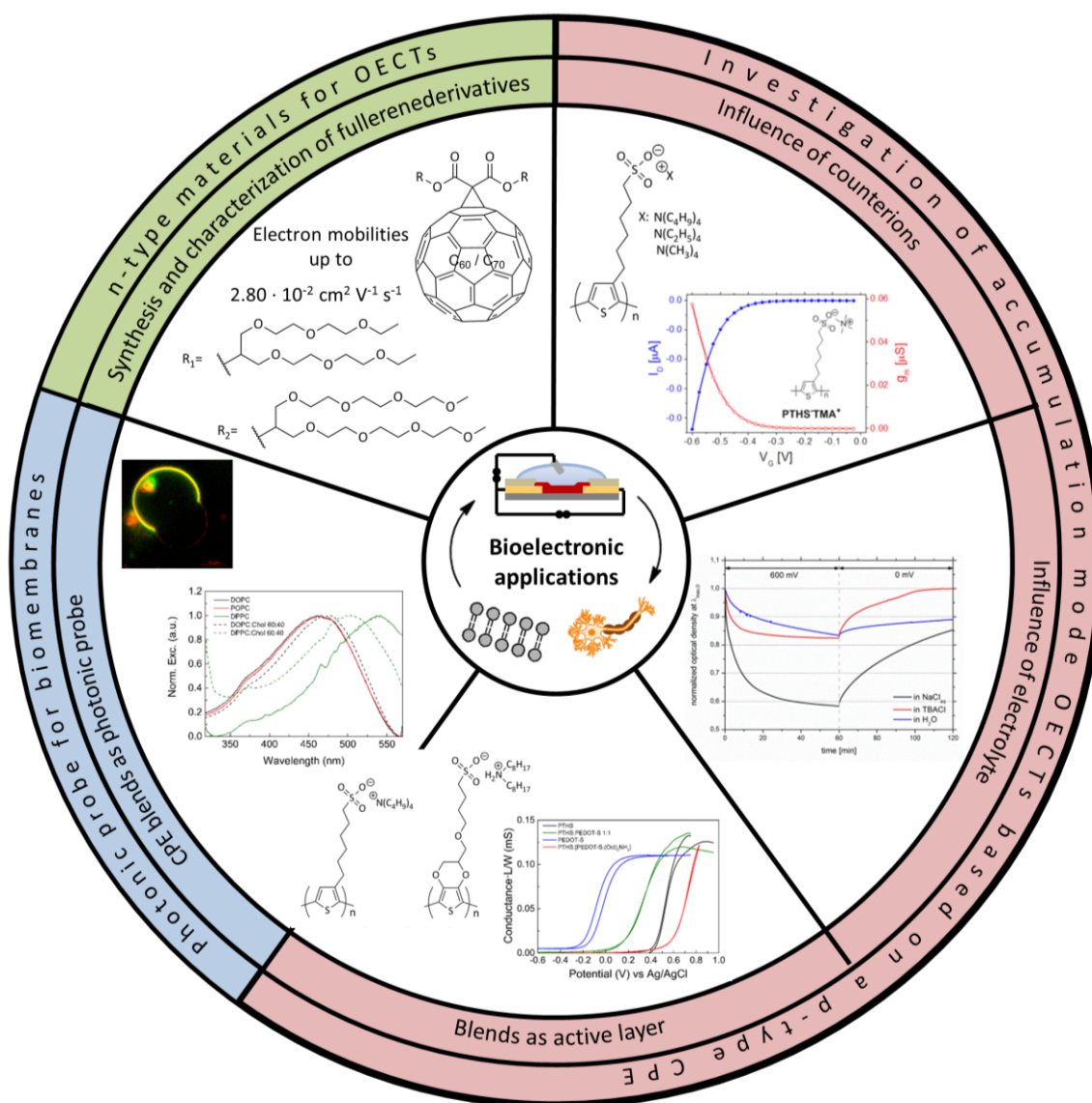


Figure 3-1: Schematic overview of the thesis. The thesis can be divided into three main parts: The investigation of accumulation mode OECTs based on a p-type CPE, the study of photonic probes for biomembranes and the synthesis of n-type materials for the use as active layers in OECTs. In the first main part the influence of CPE counterions and electrolyte ions under bias on the performance of the CPE were studied. Furthermore, the blend of a semiconducting and a conducting CPE was tested in OECTs. The second main part includes the investigation of CPE blends as photonic probe for biomembranes. The last part deals with the synthesis and characterization of new n-type semiconductor materials for the application in bioelectronics. Here, fullerene derivatives are presented, which met the demands of an active material in OECTs under aqueous conditions.

This thesis focuses on the investigation of the ionic and electronic processes occurring in CPE based OECTs. Moreover, blends of CPEs will be studied to use them as conductive biomembranes and new n-type semiconductors will be synthesized suitable for bioelectronic

applications. The cumulative thesis consists of five papers: Three of them are already published and two are prepared for submission.

As shown in the schematic overview in Figure 3-1, the thesis can be divided into three main parts: the study of the working principle and improvement of already known accumulation mode OECTs based on a p-type CPE, investigation of tunable CPE blends as photonic probe for biomembranes, and the synthesis and characterization of n-type semiconductors suitable for bioelectronic applications. Furthermore, the first part is subdivided into three chapters: Investigation of the influence of counterion (chapter 4) and the mechanism of doping and ion diffusion in presence of electrolyte (chapter 5) on the characteristics of the material and OECT performance, as well as improvement of OECTs via blending of two CPEs (chapter 6). The second part consists of a chapter about CPEs as photonic probe for lipid bilayers (chapter 7) and the third part of a chapter on the synthesis and characterization of water-compatible n-type semiconductors, which are suitable for bioelectronic applications (chapter 8). The main parts of this thesis are briefly outlined in the following.

Investigation of accumulation mode OECTs based on p-type CPEs

In the first part of this thesis, the processes happening in p-type accumulation mode OECTs were studied. Therefore, conjugated polyelectrolytes based on PTHS⁻ backbone was used as channel material, as PTHSTBA⁺ was the first CPE presented as active layer in OECTs. The knowledge about processes will help to improve the performance of those OECTs.

Up to now, it was not completely understood, if the counter ions in CPEs have an impact on the characteristics (e.g. optical characteristics, solubility, spectroelectrochemical behaviour, ionization potentials, capacitances, swelling capability) and thus, on their performance in electronic devices. To answer these questions, the influence of the counter ion X⁺ in PTHSX⁺ was studied in chapter 4. Besides the already known PTHSTBA⁺, two more CPEs, namely PTHS⁻TEA⁺ with tetraethylammonium and PTHSTMA⁺ with tetramethylammonium as counter ions, were synthesized. Thus the counter ion X⁺ was varied in size and, hence, in diffusion ability, whereas the PTHS⁻ backbone remained unchanged. Differences in aggregation, swelling and electronic properties were examined. A clear tendency of the dependence of the device performance on the size of the ions could be observed. The results provided the explanation, why the CPE with the smallest counter ion led to the best performing OECT.

After investigation of the counter ion influence on the characteristics of PTHSX⁺, chapter 5 addresses the question, if there is an influence of external ions and applied bias voltage in electrolyte on PTHSTBA⁺ films, as well. By combination of spectroelectrochemical and elemental analysis, the ion composition of the film was determined after different treatments. Beside

immersion of the film in different electrolyte solutions with various durations, the application of bias was studied. Our results led to the conclusion, that ion exchange between the CPE and the electrolyte took place as soon as they were brought in contact and that the exchange is independent of the application of bias. However, the degree and kinetics of the exchange depends on the used electrolyte. These fundamental basics will pave the way for the optimization of semiconductor layer-electrolyte combinations for forthcoming OECT research.

Another approach to diversify the application of PTHS⁻TBA⁺ based OECTs is presented in chapter 6. PTHS⁻TBA⁺ was blended with the conducting CPE poly(4-(2,3-dihydrothieno[3,4-b]-[1,4]dioxin-2-yl-methoxy)-1-butanefulfonic acid) (PEDOT-S), which is highly doped. PTHS⁻TBA⁺ based OECTs are working in accumulation mode, whereas PEDOT-S based OECTs are typically operating in depletion mode. The blend of both CPEs led to accumulation mode OECTs, as well. As shown in chapter 4, counter ion exchange in CPEs influences the characteristics, such as solubility. This knowledge was used to increase the stability of OECTs based on blends: as both CPEs, PTHS⁻TBA⁺ and PEDOT-S, are water-soluble, the counter ion protons in PEDOT-S were exchanged with an alkyl ammonium salt to render it insoluble in aqueous media. Besides the stability of the blended OECT, this also influences the threshold voltage. Testing different CPE ratios, with and without cation exchange in PEDOT-S, the influence of self-assembly on the device performance was investigated. This knowledge will contribute to an improvement of OECT performance and stability.

Overall, the first part of this thesis accounts for the understanding of the redox processes in OECTs, which are based on p-type CPEs. Considering the acquired knowledge, the first part of the thesis presents possibilities to improve the performance of OECTs.

Investigation of tunable CPE blend as photonic probe for biomembranes

The usage of conductive biomembranes as active layer opens the way for a lot of promising applications, as it can stimulate the activity of ion channels. First, the intrinsically nonconductive biomembrane have to be rendered conductive. This could be obtained by incorporation of a semiconducting or conducting CPE. The CPE backbones have therefore be near enough to each other to enable the intermolecular hopping of charges. To visualize, where the conductive material in the membrane is localized, the already mentioned blend of PTHS⁻TBA⁺ and PEDOT-S was tested as photonic probe. The optical properties of CPEs depend on the backbone conformation, which is dependent on the interactions with the surrounding media. Thus, absorption and emission spectra of CPEs change due to interaction with biological systems. The exchange of counter ions in PEDOT-S with alkylammonium salt rendered the blend hydrophobic

and enables the incorporation of the blend in the core of lipophilic membranes. The usage of pristine PTHSTBA⁺ led to a photonic probe with only limited sensitivity to changes in the biomembrane, whereas pristine PEDOT-S lacks of fluorescence. The optimal stoichiometry of the blend to obtain an efficient photonic probe was investigated in chapter 7. This photonic probe is planned to be inserted in biomembranes for OECTs and enables the visualization of the physical state of the lipid biomembrane core.

Synthesis of new materials as semiconductor layers

In chapter 8 the synthesis and characterization of n-type semiconductors for bioelectronic applications is reported. A well-known electron acceptor class are fullerenes and their derivatives. A high electron mobility, but also a bad solubility, are significant for these semiconductors. For the usage in OECTs, however, the materials have to be water-compatible and should be soluble in non-toxic solvents. Via Bingel-Hirsch reaction, oligo ethylene glycol chains were attached to C₆₀ and C₇₀ fullerene cores. The oligo ethylene glycol groups provide a good swelling behaviour in aqueous conditions. To test the applicability for OECTs, the fullerene derivatives were tested regarding their solubility, thermal stability, electron affinity and charge carrier mobility in bulk. The obtained results are very promising for the application of those fullerene derivatives as active layers in n-type OECTs. The final step of testing the materials in OECT devices is still ongoing and will not be presented herein.

The most important results of each chapter are summarized in the following. A detailed description of the experiments, the results and the conclusions are given in the individual chapters 4-8, which are either published, submitted or prepared for submission.

Influence of counter cations and surrounding electrolytes on electronic properties and oxidation of anionic conjugated polyelectrolytes (chapter 4 and chapter 5)

As already shown by a joint work of our research group and Malliaras group, PTHSTBA⁺ is a promising material for the application as semiconductor in accumulation mode OECTs. But still the performance of those OECTs cannot reach the ones of heavily doped PEDOT:PSS devices which work in depletion mode. To improve the OECT devices based on PTHSTBA⁺, it is necessary to understand the redox processes proceeding in those devices. In these redox processes two different ion sources can participate: on the one hand the counter ions of the CPE, on the other hand ions present in the electrolyte solution.

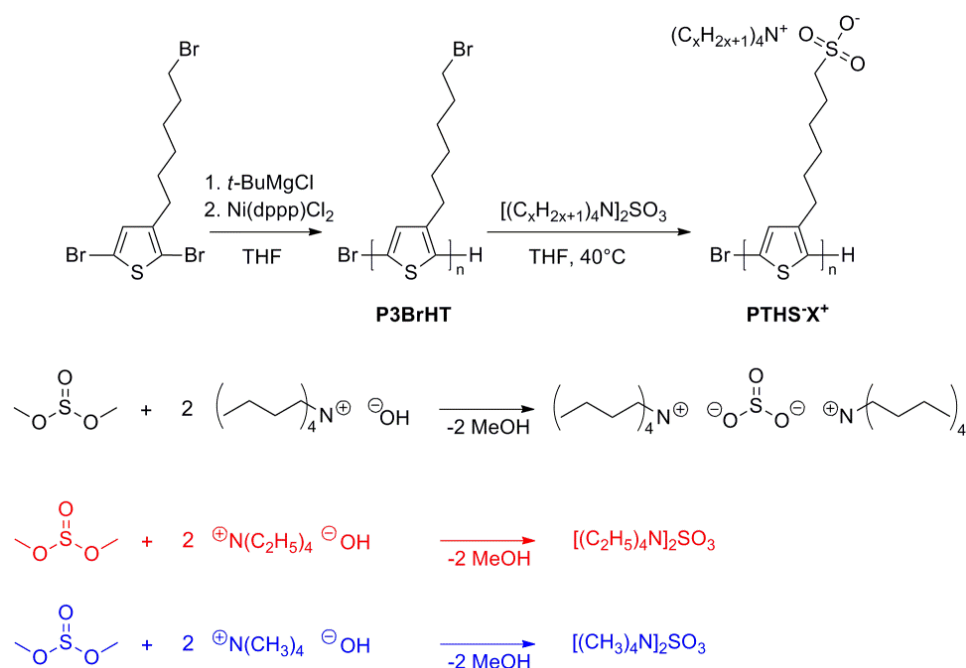


Figure 3-2: Kumada catalyst transfer polycondensation of the precursor polymer, poly(3-(6-bromohexyl) thiophene) (P3BrHT) and the post polymerization reaction to poly(6-(thiophen-3-yl)hexane-1-sulfonate) PTHS·X⁺ with tetrabutylammonium (X⁺ = TBA⁺), tetraethylammonium (X⁺ = TEA⁺) and tetramethylammonium (X⁺ = TMA⁺) as counter ions. Furthermore, the synthesis of the corresponding ammonium salts from dimethylsulfite are illustrated.

Chapter 4 is dealing with the influence of counter cations of the anionic conjugated polyelectrolyte on transconductance and response time in applications. Therefore, three different CPEs with different counter cations were prepared from the same precursor polymer. For this, a precursor polymer poly(3-(6-bromohexyl) thiophene) (P3BrHT) was converted via polymer analogous substitution of the bromine group by reacting with the respective tetraalkylammonium sulfite salts to PTHS·TBA⁺, PTHS·TEA⁺ and PTHS·TMA⁺, where TBA, TEA and TMA represent tetrabutyl, tetraethyl and tetramethyl ammonium cations respectively (Figure 3-2). The conversion was performed on the same precursor polymer, so that any influence of chain length (or molecular weight) can be neglected on comparison and thus any detected difference in performance of the different CPEs can be attributed to the change in cation size. UV-vis spectroscopy and spectroelectrochemistry showed that PTHS·TMA⁺ was the most aggregated of the three CPEs and the easiest to be oxidized and re-reduced. Furthermore, PTHS·TMA⁺ was not as soluble in aqueous solution as PTHS·TEA⁺ and PTHS·TBA⁺. Addition of the cross-linker (3-glycidyloxypropyl)trimethoxysilane (GOPS) (1 wt%) is a common way to stabilize the active layer in OECTs against dissolution in aqueous media, since PTHS·X⁺ CPEs are usually highly soluble in water. Independent of the CPE counter ion, similar trends for all three PTHS·X⁺ were observed in the absorption spectra due to cross-linking: The aggregation was decreased, which could be detected by a blue-shift of the maxima and the intensity reduction of the shoulder.

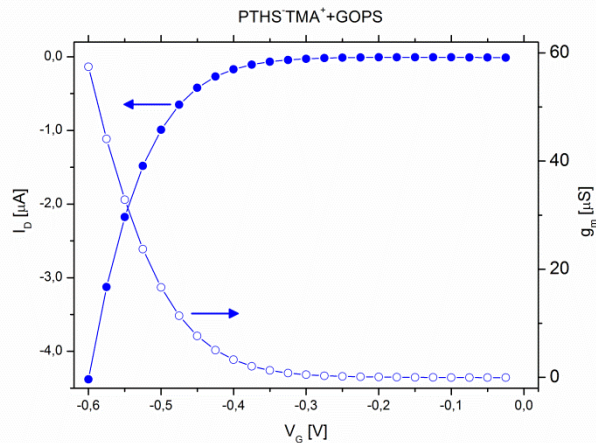


Figure 3-3: Transfer characteristics and transconductance (g_m) of a cross-linked on PTHSTMA⁺ based OECT measured at $V_D = -500$ mV.

As OECTs are electronic transducers, the ion uptake of the active layer is crucial for their performance. The ion uptake can be quantified by the measurement of the electrochemical capacitance. PTHSTMA⁺, here the CPE with the smallest counter ion, possessed the highest value with 82 Fcm^{-3} . All three CPEs showed oxidation by applying negative bias to the OECT. This led to an increase of the drain current and switched the device ON. Consequently, all tested CPEs operate in accumulation mode. A $0.1 \text{ M NaCl}_{\text{aq}}$ solution was used as electrolyte and an Ag/AgCl electrode as gate. The best performance was obtained for PTHSTMA⁺ based OECTs with a transconductance of $45.5 \mu\text{S}$, an I_D of $-350 \cdot 10^{-2} \mu\text{A}$, a response time of 0.2 seconds and an ON/OFF ratio of 250. The larger the counter ion is the lesser is the performance of device. Therefore, on comparison, PTHSTBA⁺ showed the worst performance of the tested CPEs. An addition of ethylene glycol as co-solvent led to an improvement of the performance of OECTs based on PTHSTBA⁺. As reason for that, the formation of fiber-like features was identified. The charge carrier mobilities of the CPEs were estimated from the volumetric capacitance values and the OECT performance. According to this, PTHSTMA⁺ possessed the highest hole mobility among the tested CPEs. This conformed to the densest π - π stacking and the most observed aggregation. In summary, chapter 4 identified that the counter ion in a CPE has a big influence on the properties and the performance in OECTs.

Up to now, the mechanism of the redox processes taking place in CPE based OECTs was still unclear, even though different suggestions have been made. The applied negative gate bias induces an oxidation of the CPE. The next step can be either ejection of counter ions or injection of electrolyte anions or both to obtain charge balance. To detect, which step is following what conditions, ion exchange and oxidation of PTHSTBA⁺ were closely studied in chapter 5. Therefore, a combination of spectroelectrochemical measurements and energy-dispersive X-ray

spectroscopy for elemental analysis (EDX) were used. The ion diffusion in a PTHS⁻TBA⁺ film was analyzed after immersion in different electrolytes. The films had to be cross-linked with GOPS to be stable in aqueous media. After a defined time, the film was removed from the electrolyte solution and rinsed with Millipore water. Some of the films were additionally biased, to examine, if bias has an influence on the ion diffusion, as well. The absorption spectra were recorded simultaneously to gain an insight into the created redox species. An example for a time-dependent spectroelectrochemical measurement of films, which were immersed for 120 minutes in different electrolytes, is shown in Figure 3-4a. Here, the oxidation of the films was recorded by application of 600 mV for 60 minutes, as well as the re-reduction over the duration of 60 minutes. The elements present in the films were determined by EDX. An EDX spectrum of a film, which was immersed 2 h in NaCl_{aq} solution without any applied bias, is shown as example in Figure 3-4b. However, EDX analysis exhibits some uncertainties, for which reason the atom % values could not be used as absolute values. Instead untreated films were used to determine the ratio of Si (component of GOPS) to S (part of PTHS⁻TBA⁺). As both elements are immobile, the ratio has to remain the same, independent from different treatments. Consequently, this ratio was used as reference to verify the correctness of the measured EDX values.

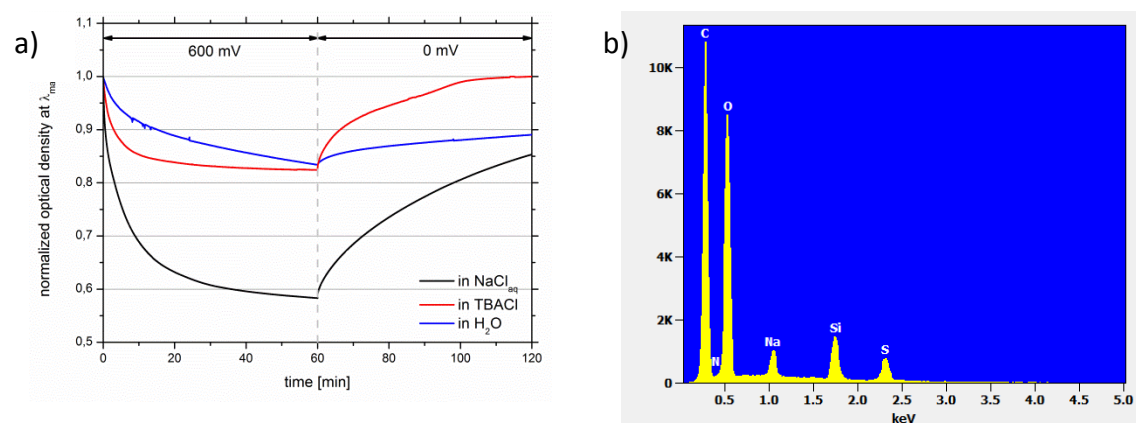


Figure 3-4: a) Time-dependent spectroelectrochemical absorption measurement of a drop-cast, cross-linked PTHS⁻TBA⁺ film at $\lambda_{\max,0}$. The value at $\lambda_{\max,0}$ is set as 1.0 and other values are normalized accordingly. The absorption was recorded for 120 minutes: In The first 60 minutes a voltage of 600 mV applied, followed by 60 minutes at a voltage set to 0 mV. b) Example of a obtained energy-dispersive X-ray spectrum, measured on a rectangular space of a cross-linked PTHS⁻TBA⁺ film (here: a film, which was immersed for 2 hours in 0.1 M NaCl_{aq} solution and subsequently rinsed with Millipore water).

Our investigations showed that ion exchange between a CPE film and an aqueous electrolyte solution occurred, as soon as they were brought in contact. In contrast to the common assumption, the ion exchange happened independent from the application of bias. As shown in chapter 4, counter ion exchange in a CPE can result in modification of its properties. As the ions of the electrolyte functions as new counter ions, the choice of the electrolyte modifies the kinetics and the degree of CPE oxidation. An optimized CPE-electrolyte combination can

therefore improve the performance of OECTs. According to our results, an injection of anions (here chloride) from the electrolyte into the CPE film can be precluded, as no electrolyte anion could be found within the volume of the film via EDX. To preserve electrical neutrality, in return the counter ions, here TBA^+ , had to diffuse into the electrolyte solution. On application of bias the determined electrolyte cation content inside the PTHSTBA^+ film as per EDX method did not change. Consequently, the ejection of counter ions due to oxidation (in this case the sodium ions of the electrolyte, which already diffused into the film) can be excluded, as well. As a result, we propose the formation of an electrical double layer in operating OECTs between the surface of the active film and the electrolyte as well as between the electrolyte and the electrode.

Improvement of the performance and stability of CPE based OECTs via blending and ion exchange (chapter 6)

The performance of OECTs can also be improved by blending a semiconducting CPE with a metallic CPE. PTHSTBA^+ was used as semiconducting CPE, since it already showed good performance in OECTs. The highly doped metallic PEDOT-S was used for blending. Both PTHSTBA^+ and PEDOT-S are soluble in water. Thus, the pristine blend would dissolve in aqueous solutions. Exchanging the counter ion of PEDOT-S (a proton) with dioctylammonium ($(\text{Oct})_2\text{NH}_2$) leads to a $\text{PEDOT-S}:(\text{Oct})_2\text{NH}_2$ complex. This is soluble in methanol and chloroform but not in water (Figure 3-5). At the same time the electronic conductivity remained unchanged.

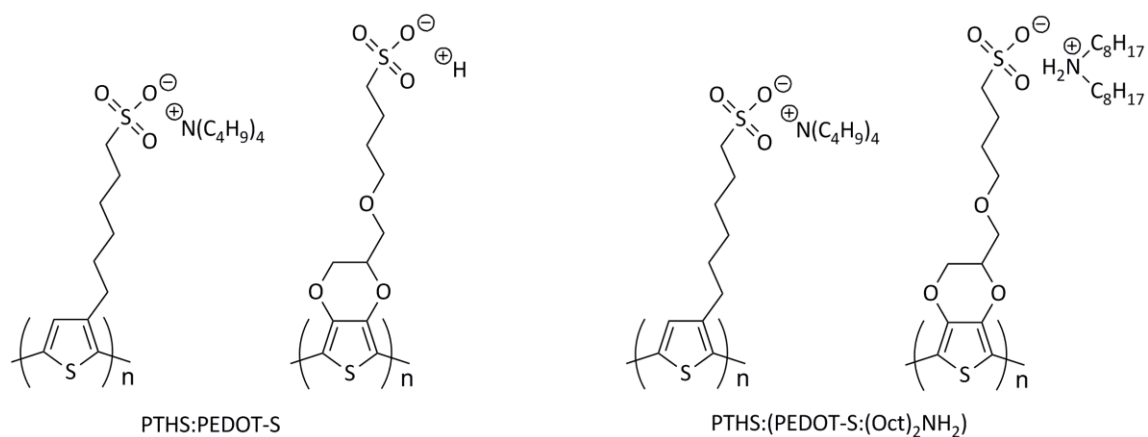


Figure 3-5: Chemical structures of the hydrophilic blend PTHS:PEDOT-S and the hydrophobic blend $\text{PTHS:(PEDOT-S:(Oct)}_2\text{NH}_2)$.

The combination of methanol soluble PTHSTBA^+ and $[\text{PEDOT-S}:(\text{Oct})_2\text{NH}_2]$ formed a blend, that was insoluble in water. Accordingly, cross-linking was not necessary for biological environment. To observe a homogeneous film of a blend, phase separation has to be prevented. Comparison of the absorption and emission spectra of pristine CPE films and the blended film during drying can give important information about the microstructure formation. In general, the emission

intensity of the CPE films decreases during drying because of solvent evaporation leading to an aggregation of the CPE backbones. PTHS⁻TBA⁺:PEDOT-S films prepared from water showed complete quenching of PTHS emission after drying, indicating a higher degree of aggregation. On the contrary, PTHS⁻TBA⁺:[PEDOT-S:(Oct)₂NH₂⁺] films from methanol showed a red shift of PTHS emission maximum without any quenching, that notified a change in the nature of aggregation. The difference between the two blends can be explained by the steric hindrance in the PTHS⁻TBA⁺:[PEDOT-S:(Oct)₂NH₂⁺] film due to the bulky (Oct)₂NH₂⁺ counter ion, which leads to a bigger distance between the backbones. Spectroelectrochemical investigations of the CPEs films showed that the electronic states built in PTHS⁻TBA⁺:PEDOT-S and PTHS⁻TBA⁺:[PEDOT-S:(Oct)₂NH₂⁺] films upon application of potential did not differ from each other.

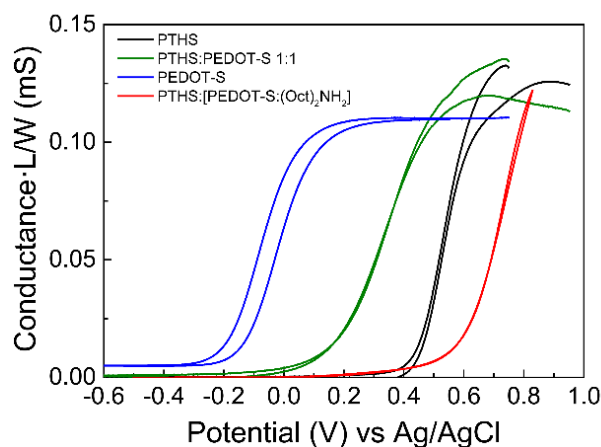


Figure 3-6: Conductance measurement spectra for pristine PTHS and pristine PEDOT-S films as well as for the blends PTHS⁻TBA⁺:PEDOT-S 1:1 and PTHS⁻TBA⁺:[PEDOT-S:(Oct)₂NH₂⁺] 1:1.

Conductance measurements illustrated that both blends are in a semiconducting form and can be used to fabricate accumulation mode organic electrochemical transistors (Figure 3-6). Whereas the threshold voltage of PTHS⁻TBA⁺:PEDOT-S lies between the ones for the pristine CPEs, the one of PTHS⁻TBA⁺:[PEDOT-S:(Oct)₂NH₂⁺] was at slightly higher voltage. Consequently, the threshold voltage can be modified by blending and ion exchange. The blends were furthermore tested as active materials in OECTs, which provided better performance with respect to OECTs fabricated using films of the pristine CPEs. OECTs based on PTHS⁻TBA⁺:[PEDOT-S:(Oct)₂NH₂⁺] achieved the highest maximum transconductance of 15.3 mS and short switching times of around 79 ms for ON and 11 ms for OFF. Due to the counter ion exchange, the stability upon fast pulsed cycles was increased compared to PTHS⁻TBA⁺:PEDOT-S based OECTs. PTHS⁻TBA⁺:[PEDOT-S:(Oct)₂NH₂⁺] based OECTs retained 88 % of the original ON current after 2·10³ ON/OFF cycles of 134 ms, whereas PTHS⁻TBA⁺:PEDOT-S based OECTs retained only 59 %. In conclusion, our results demonstrate that the optical properties and OECT performance can be

tuned due to blending two CPEs with semiconducting and metallic properties, respectively. Furthermore, the influence of counter ion exchange on the optoelectronic properties of CPE blends and the stability of their OECTs was presented.

Photonic probe for biomembrane organization based on CPE blend via tuning the stoichiometry of blending (chapter 7)

As described in chapter 1.2.2, CPEs can be used as photonic probes to study biomembrane organization. Their amphiphilic nature provides both a partly integration into the hydrophobic lipid bilayer as well as a processing form aqueous solution. So far, water-soluble CPEs were used to study biomembrane organization. Consequently, most previous reports focused on the examination of hydrophilic parts of cells or model membrane systems. We aimed at a blend of CPEs that can be incorporated into the hydrophobic core of the lipid bilayer to get insight into the local changes within the lipid packing in model membrane systems composed of DOPC, POPC, DPPC and cholesterol. Therefore, we investigated blends consisting of PEDOT-S and PTHS. To render the blend hydrophobic, dioctylammonium chloride ((Oct)₂NH₂Cl) was added. The sensitivity of the PEDOT-S backbone towards changes in the lipid bilayer as well as the emission properties of PTHS remained unchanged compared to the pristine materials by blending.

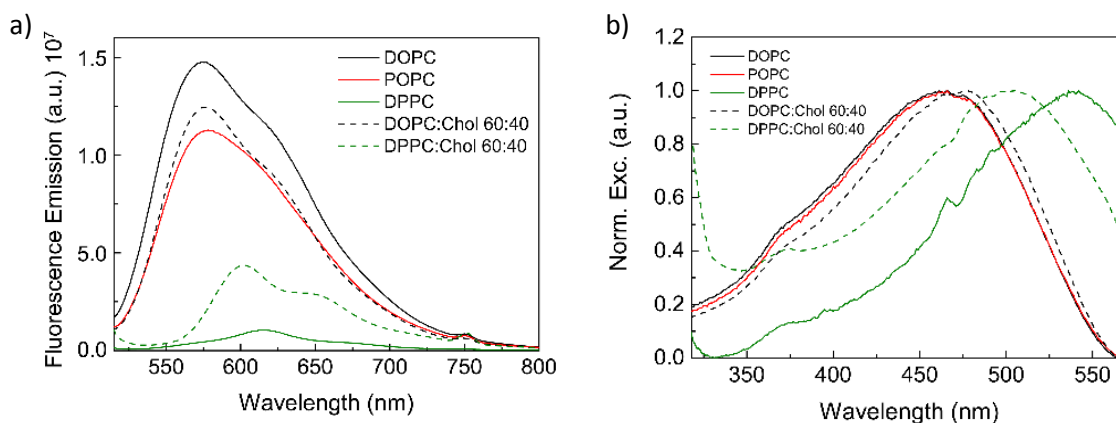


Figure 3-7: a) Fluorescence emission spectra and b) normalized excitation/absorption spectra of blend (PTHS:PEDOT-S 1:3):(Oct)₂NH₂ in liposomes of DOPC ($\lambda_{\max, em} = 577$ nm, $\lambda_{\max, ex} = 461$ nm), POPC, DPPC ($\lambda_{\max, em} = 614$ nm, $\lambda_{\max, ex} = 542$ nm) and compositions containing cholesterol (DOPC:Chol 60:40 and DPPC:Chol 60:40).

To verify the sensitivity of the blends the absorption and emission spectra in aqueous solution, chloroform and in DOPC-liposomes were recorded. Furthermore, different liposomes (DOPC, DPPC and POPC) and different DOPC:cholesterol and DPPC:cholesterol compositions were tested (Figure 3-7). Spectral shifts in the absorption spectra of the blends indicated changes in the physical states of the lipid bilayers. The emission spectra also varied by changing the lipids and cholesterol content. Thus, the (blends:(Oct)₂NH₂Cl) can be used for fluorescence imaging of

biomembranes. Testing different blend ratios, the blend PTHS:PEDOT-S:(Oct)₂NH₂ with a PTHS:PEDOT-S ratio of 1:3, showed the largest shifts in the absorption spectra at the lowest blend concentration and is thus the most suitable composition for photonic probes. Confocal microscopy experiments were used to examine the segregation behavior of the blend. The blend 1:3 was incorporated into giant unilamellar vesicles composed of DOPC/DPPC/cholesterol. As cholesterol shows a different affinity to phospholipids, L_{dis} and L_{ord} phases will be coexistent in this system. The hydrophobic blend possesses no preference for the L_{dis} or L_{ord} phase. Therefore, no partition of the probe into a specific phase occurred. The two coexisting phases were identified by the different emission behavior of the blend depending on the physical state of the lipid bilayer (Figure 3-8).

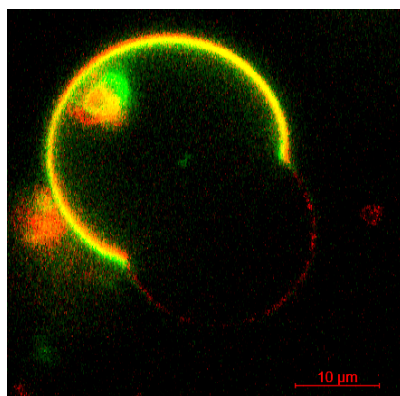


Figure 3-8: Confocal microscopy image of giant unilamellar vesicles (GUV). The vesicles are composed of DOPC:DPPC:Chol and were incorporated by the (PTHS:PEDOT-S 1:3):(Oct)₂NH₂ blend. The green-yellow region represents the L_{dis} phase (excitation wavelength: 488 nm), whereas the red region represents the L_{ord} phase (excitation wavelength: 555 nm).

Synthesis and characterization of n-type semiconductors for application as active layer in OECTs (chapter 8)

To date almost exclusively p-type semiconductor materials were studied as electro-active layers in OECTs. Fullerene and its derivatives are the standard n-type (electron acceptors) semiconductors for the usage in solar cells due to their high electron mobilities. Nevertheless, most of them have to be processed from toxic solvents, such as dichlorobenzene, because of their insufficient solubility in polar solvents. For an application in bioelectronic devices, materials should be processible from non-toxic solvents. Furthermore, it is advantageous, if the material swells in aqueous environment to improve the performance in OECTs. However, the material should not dissolve in water, as this would cause stability problems in the device. The development of new fullerene derivatives, that exhibit these requirements, is reported in chapter 8.

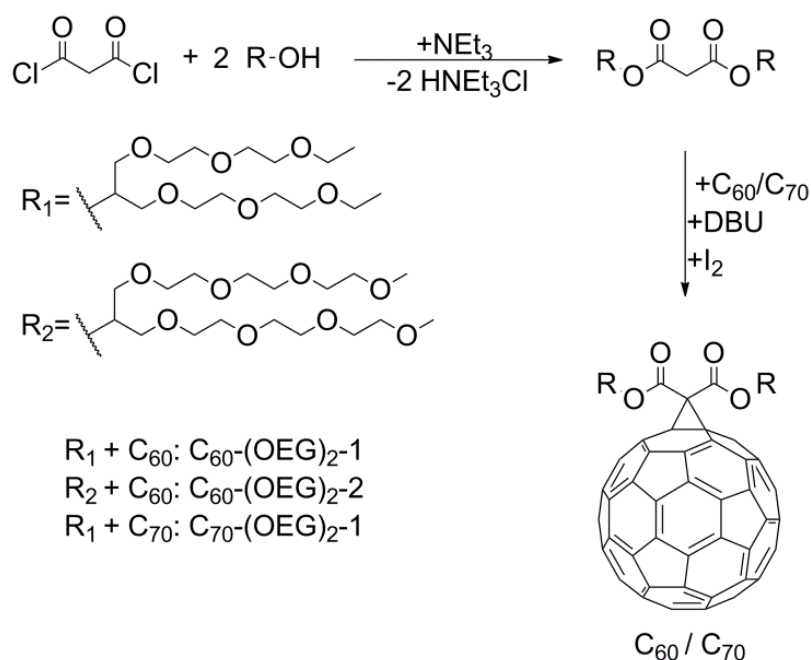


Figure 3-9: Schematics for the synthesis of the water compatible fullerene monoadducts.

Via Bingel-Hirsch reaction, swallow-tail oligo ethylene glycol groups were attached to C_{60} and C_{70} (Figure 3-9). The ratio of malonate to fullerene was optimized as 0.7:1 to achieve mainly monoadducts. In addition, the usage of iodine in combination with DBU as halogenating reagent instead of tetrabromomethane improved the yield. The newly synthesized fullerene derivatives showed a very high solubility in polar solvents, such as ethyl acetate and acetone, enabling an eco-friendly processing. The electron mobility was determined in bulk via space charge limited current method. The new fullerene derivatives exhibited electron mobilities up to $2.80 \cdot 10^{-2} \text{ cm}^2 \text{ V}^{-1} \text{ s}^{-1}$. This value is two orders of magnitude higher than for the reference material PC_{61}BM , which is the most used fullerene derivative. Correspondingly, in chapter 8 fullerene derivatives are highlighted, which are very promising candidates for bioelectronic applications.

Individual contributions to joint publications

The results of this thesis were obtained in cooperation with other groups and are published, submitted or prepared as manuscripts for submission as denoted below. In the following the individual contributions of all authors are summarized and specified.

Chapter 4

This work is published in *Macromolecular Chemistry and Physics* (2017, 1700374) under the title: "Smaller Counter Cation for Higher Transconductance in Anionic Conjugated Polyelectrolytes" by Martina M. Schmidt, Mohammed ElMahmoudy, George G. Malliaras, Sahika Inal, Mukundan Thelakkat.

I synthesized and characterized all polymers and prepared all films except of the ones for the QCM without the co-solvent EG. I performed and analyzed the UV-Vis/IR absorption and spectroelectrochemical measurements, as well as the cyclic voltammetric investigations. Furthermore, I performed and analyzed all transistor measurements, calculated the hole mobility and wrote the publication.

Mohammed ElMahmoudy prepared thin films for the QCM measurement without the co-solvent EG. Furthermore, he performed the QCM measurement of these films, analyzed them and wrote the corresponding part of the manuscript.

George G. Malliaras supervised the project.

Sahika Inal performed and analyzed the electrochemical impedance spectroscopy, corrected the manuscript and supervised the project.

Mukundan Thelakkat supervised the project and corrected the manuscript.

Chapter 5

This manuscript is ready for submission under the title:

"Conjugated polyelectrolytes in ionic solutions: mechanism of ion exchange and oxidation"

by Martina M. Schmidt, Beate Förster, Mukundan Thelakkat.

I synthesized and characterized the polymer and prepared all films. I performed and analyzed the spectroelectrochemical measurements. Furthermore, I measured the conductivity of the electrolytes, analyzed all EDX spectra and wrote the publication.

Beate Förster performed the EDX measurements and corrected the manuscript.

Mukundan Thelakkat supervised the project and corrected the manuscript.

Chapter 6

This work is published in *Chemistry of Materials* (2017, 29, 4293-4300) under the title:

“Conjugated Polyelectrolyte Blends for Highly Stable Accumulation Mode Electrochemical Transistors”

by Erica Zeglio, Martina M. Schmidt, Mukundan Thelakkat, Roger Gabrielsson, Niclas Solin, and Olle Inganäs.

I synthesized and characterized the polymer (GPC, MALDI-TOF, NMR), wrote the corresponding part and corrected the manuscript.

Erica Zeglio, Roger Gabrielsson, Niclas Solin performed the fluorescence and absorption spectroscopy measurements. Furthermore, they measured UV-vis spectroelectrochemistry and conductance of the single compounds as well as of the blends. They fabricated and characterized electrochemical transistors and wrote the manuscript.

Mukundan Thelakkat and Olle Inganäs supervised the project and corrected the manuscript.

Chapter 7

This work is published in *Chemistry Select* (2016, 1, 4340-4344) under the title:

“Conjugated Polyelectrolyte Blend as Photonic Probe of Biomembrane Organization”

by Erica Zeglio, Martina M. Schmidt, Mukundan Thelakkat, Roger Gabrielsson, Niclas Solin, and Olle Inganäs.

I synthesized and characterized the polymer (GPC, MALDI-TOF, NMR), wrote the corresponding part and corrected the manuscript.

Erica Zeglio, Roger Gabrielsson, Niclas Solin performed the spectroscopic, the fluorescence lifetime, the dynamic light scattering and the confocal microscopy measurements. Furthermore, they prepared the PTHS-complexes, characterized them spectroscopically and wrote the manuscript.

Mukundan Thelakkat and Olle Inganäs supervised the project and corrected the manuscript.

Chapter 8

This manuscript is ready for submission under the title:

“Eco-friendly processable fullerene derivatives with high electron mobility”

by Martina M. Schmidt, Chetan R. Singh, Mukundan Thelakkat.

The optimization of the synthesis for C_{60} -(OEG)₂-1, the UV-Vis spectra in THF of C_{60} -(OEG)₂-1, C_{60} -(OEG)₂-2 and PC₆₁BM and the cyclic voltammograms of C_{60} -(OEG)₂-1 and C_{60} -(OEG)₂-2 were already done in my master thesis. I synthesized C_{70} -(OEG)₂-1 and new material of C_{60} -(OEG)₂-1 and C_{60} -(OEG)₂-2, characterized the materials by means of ¹H-, ¹³C-NMR and MALDI-TOF spectroscopy and prepared all films. I measured and analyzed the optical properties of C_{70} -(OEG)₂-1 and the cyclic voltammograms of C_{70} -(OEG)₂-1 and PC₆₁BM. I determined the solubility and the thermal characteristics of all materials. I prepared and performed the SCLC measurements of all materials and measured and analyzed the film thicknesses as well as the film roughness by AFM. I wrote the manuscript.

Chetan R. Singh analyzed the SCLC data, wrote the corresponding part and corrected the manuscript.

Mukundan Thelakkat supervised the project and corrected the manuscript.

4 SMALLER COUNTER CATION FOR HIGHER TRANSCONDUCTANCE IN ANIONIC CONJUGATED POLYELECTROLYTES

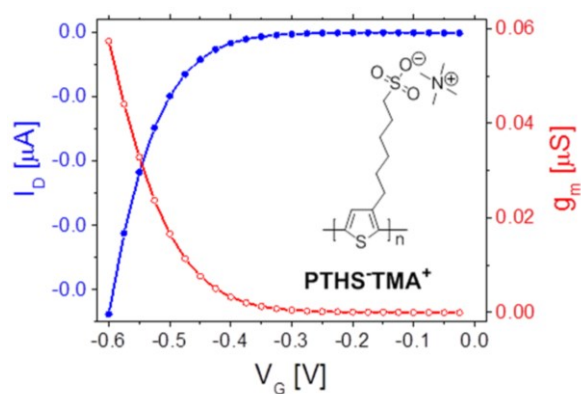
Martina M. Schmidt,^[a] Mohammed ElMahmoudy,^[b] George G. Malliaras,^[b] Sahika Inal,^{*[c]},
Mukundan Thelakkat^{*[a]}

[a] University of Bayreuth, Applied Functional Polymers, Bayreuth, 95440, Germany

[b] Department of Bioelectronics, Ecole Nationale Supérieure des Mines, CMP-EMSE, MOC,
Gardanne, 13541, France

[c] Biological and Environmental Science and Engineering, King Abdullah University of Science
and Technology (KAUST), Thuwal, 23955-6900, Kingdom of Saudi Arabia

*E-mail of corresponding authors: mukundan.thelakkat@uni-bayreuth.de,
sahika.inal@kaust.edu.sa



Published in *Macromol. Chem. Phys.* **2017**, 1700374

Abstract

Conjugated polyelectrolytes (CPEs) are a focus of research because they combine inherent electrical conductivity and the ability to interact with ions in aqueous solutions or biological systems. However, it is still not understood to what degree the counter ion in CPEs influences the properties of the CPE itself and the performance of electronic transducers. In order to investigate this, three different conjugated polyelectrolytes, poly(6-(thiophene-3-yl)hexane-1-sulfonate)s (PTHS⁻X⁺), are synthesized, which have the same polythiophene backbone but different X⁺ counter ions: the bulky tetrabutylammonium (TBA⁺), tetraethylammonium (TEA⁺), and the smallest tetramethylammonium (TMA⁺). At the interface with biological systems, thin CPE films have to be stable in an aqueous environment and should allow the inward and outward flow of ions from the electrolyte. Since the studied PTHS⁻X⁺ have different solubilities in water, the optical properties of pristine PTHS⁻X⁺ as well as of crosslinked PTHS⁻X⁺ via UV-vis absorption spectroscopy are investigated additionally. PTHS⁻TMA⁺ exhibits better aggregation, fast interdiffusion of ions, and fast recovery from the oxidized state. Additionally, spectroelectrochemical and cyclic voltammetric as well as electrochemical capacitance investigations show that PTHS⁻TMA⁺ can be oxidized to a higher degree. This leads to a better performance of PTHS⁻TMA⁺-based organic electrochemical transistors.

1. Introduction

Water-soluble conjugated/conducting polymers are very interesting for applications in biological systems. Heeger and co-workers obtained solubility of these polymers in water through implementation of ionic sidechains on the conjugated backbone.^[1] As ionic groups, either negatively charged sulfonates, carboxylates, phosphates or positively charged groups like tetraalkylammonium have been reported for the synthesis of conjugated polyelectrolytes (CPEs).^[1,2] In addition to the water compatibility, these CPEs are able to interact with ions or charged biological compounds, like DNA.^[3-5] Moreover, CPEs can be used to record electrically the changes in ionic atmosphere when integrated in organic electrochemical transistors (OECTs). In these devices, the current flow in a CPE film can be controlled by a gate voltage applied via an electrode immersed in an aqueous electrolyte in direct contact with the CPE film.^[6] CPEs are highly sensitive to the ion motion between the electrolyte and the polymer film, which strongly influences the performance of OECTs. Still the role of the used counter ion in CPEs is not completely understood regarding their influence on the properties of CPEs as well as the OECTs. It is generally assumed that the optical and electronic properties are controlled by the

conjugated backbone.^[7] For example, Yang et al. reported that cationic polyelectrolytes based on poly([(9,9-bis-(6'-N,N,N-trimethylammonium)-hexyl)fluorene] with different counter ions showed almost identical absorption spectra in solution. Nevertheless, they obtained different optical and electrical properties in film.^[8] On the contrary, McCullough et al. showed in carboxylated polythiophenes in aqueous solution that by choosing large counter cations the aggregation of the backbones due to π -stacking can be disrupted, whereas small counter cations promote aggregation of the polymers.^[9] Typically, high degree of π -stacking of the backbones is favorable for a lot of applications, since the charge transport mobility increases with the degree of aggregation/crystallization of the polymer chains.^[10] For polyelectrolytes with the same backbone but different counter ions, different ionization potentials (IPs) and electron affinities were reported by Nguyen and co-workers using ultraviolet photoelectron spectroscopy (UPS) studies.^[11,12]

Many of the reported CPEs were synthesized by oxidative methods in a noncontrolled fashion. However with poly(6-(thiophene-3-yl)hexane-1-sulfonate) tetrabutylammonium, we have recently reported a well-defined CPE exhibiting a high bulk charge transport mobility, which led to OECTs operating in accumulation mode with high transconductance.^[13,14] To further investigate electrochemical and optical properties of CPEs with the same backbone but different counterions, we synthesized three different poly(6-(thiophene-3-yl)hexane-1-sulfonate)s (PTHS⁻X⁺) with tetrabutylammonium (X⁺ = TBA⁺), tetraethylammonium (X⁺ = TEA⁺) and tetramethylammonium (X⁺ = TMA⁺) as counter ion. Via absorption measurement in solution and films, we examined the optical behavior in dependence of the counter cation sizes. As thin films have to be stable in aqueous environment for biological applications, we stabilized them with a cross-linker against dissolution and analyzed how the optical properties are influenced through cross-linking. Using spectroelectrochemistry, we investigated the redox behavior of the CPE films after crosslinking in order to understand the influence of interdiffusion of ions. Cyclic voltammetry (CV) gave information about the ionization potentials of the synthesized CPEs and the reversibility of the oxidation of the conjugated backbones. Via impedance spectroscopy, we determined the intrinsic wet capacitance of the CPE films before and after oxidation. A quartz crystal microbalance (QCM) was used to test the swelling capability in aqueous media, which enhance the drift mobility of ions in the film. All the PTHS⁻X⁺s were tested in OECTs to compare and elucidate the impact of the different counterions on device performance.

2. Results and Discussion

2.1. Synthesis and Solubility

In this work, we synthesized three different anionic PTHS X^+ varying in their counter cation size from tetrabutylammonium over tetraethylammonium to the smallest tetramethylammonium cation. All the CPEs were obtained from the precursor polymer, poly(3-(6-bromohexyl)-thiophene) (P3BrHT), whose synthesis was reported in a previous work.^[15] One third of a newly synthesized P3BrHT (size exclusion chromatography, M_n : 18 kg mol $^{-1}$, polydispersity index (PDI): 1.14) was converted to poly(6-(thiophene-3-yl)hexane-1-sulfonate) tetrabutylammonium (PTHSTBA $^+$),^[15] one third to poly(6-(thiophene-3-yl)hexane-1-sulfonate) tetraethylammonium (PTHSTEA $^+$), and the last third to poly(6-(thiophene-3-yl)hexane-1-sulfonate) tetramethylammonium (PTHSTMA $^+$) via polymer analogous substitution of the bromine group by reacting with the respective tetraalkylammonium sulfite salts. For all three compounds, the same P3BrHT was used with an average of 75 repeating units (calculated from matrix assisted laser desorption ionizations time-of-flight, MALDI-TOF) and a PDI of 1.14 (obtained by size exclusion chromatography). Thus, any detected difference in characteristics between PTHSTBA $^+$, PTHSTEA $^+$ and PTHSTMA $^+$ can be attributed to the change in cation size. Figure 4-1 shows a scheme of the synthesis.

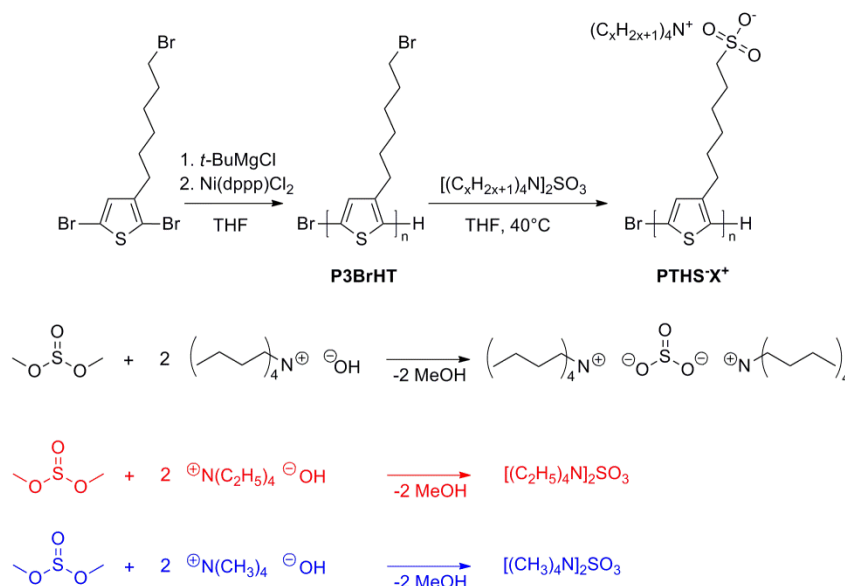


Figure 4-1: Scheme of Kumada catalyst transfer polycondensation for the synthesis of the precursor polymer, poly(3-(6-bromohexyl) thiophene) (P3BrHT) and its post polymerization reaction to obtain poly(6-(thiophene-3-yl)hexane-1-sulfonate) PTHS X^+ with tetrabutylammonium ($X^+ = \text{TBA}^+$), tetraethylammonium ($X^+ = \text{TEA}^+$) and tetramethylammonium ($X^+ = \text{TMA}^+$) as counter ions as well as the reactions to obtain the corresponding ammonium salts from dimethylsulfite.

PTHS⁻TBA⁺ and PTHS⁻TEA⁺ show very good solubility in water (2.5 wt % soluble), whereas PTHS⁻TMA⁺ is not very soluble (≈ 1 wt% solubility). TMA⁺ itself is known as a hydrophilic cation referring to the standard molar Gibbs energy of transfer.^[16] With increasing size of the alkyl chain, the hydrophobicity usually increases, which in turn should lead to a decrease of solubility in water. Otherwise, water molecules and counterions can diffuse between the hydrocarbon arms of TBA⁺ ions, whereas the small TMA⁺ ions cannot be penetrated.^[17] Thus, the attractive forces between the positively charged nitrogen of tetraalkylammonium and the negatively charged sulfonate group on the hexyl side chains should be the strongest for TMA⁺, as the center of the charge is less shielded due to bulky alkyl chains and diffusing water molecules. This leads to a decreased solubility of PTHS⁻TMA⁺ in water compared to the other two polyelectrolytes with bulkier tetraalkylammonium counter cations.

2.2. UV-Vis/IR Absorption in Aqueous Solution and Film

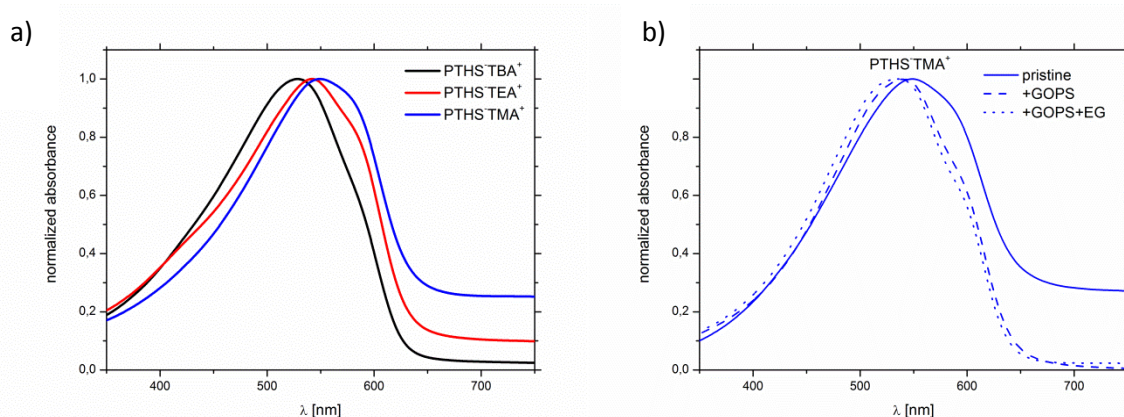


Figure 4-2: a) Normalized absorption of PTHS⁻TBA⁺, PTHS⁻TEA⁺ and PTHS⁻TMA⁺ in aqueous solution (concentration of $8.30 \cdot 10^{-7}$ mol L⁻¹) and b) in thin films spin coated on quartz substrates from aqueous solutions of PTHS⁻TMA⁺, PTHS⁻TMA⁺ with 1 wt% GOPS and PTHS⁻TMA⁺ with 1 wt% GOPS and 5 vol% EG. Comparable spectra for PTHS⁻TBA⁺ and PTHS⁻TEA⁺ films can be found in Figure 4-S2 in the Supporting Information.

To examine the influence of the counter ion on the optical properties, we performed UV-vis absorption measurements of the three synthesized polyelectrolytes in aqueous solution (Figure 4-2a). All the samples exhibit features of in situ doping (absorption in the range of 650 – 1100 nm) as obtained after synthesis. We observed a redshift of the absorption maximum for PTHS⁻TEA⁺ (λ_{\max} : 542 nm) and PTHS⁻TMA⁺ (λ_{\max} : 549 nm) in comparison to PTHS⁻TBA⁺ (λ_{\max} : 529 nm). Furthermore, the polyelectrolytes show a shoulder at around 580 nm, which is most pronounced for PTHS⁻TMA⁺. The normalized absorption spectra of thin films spin-coated from aqueous solution also feature the vibronic fine structure (mainly for PTHS⁻TEA⁺ and PTHS⁻TMA⁺) and the trend of the absorption maxima: PTHS⁻TBA⁺ (λ_{\max} : 499 nm) < PTHS⁻TEA⁺ (λ_{\max} : 540 nm) < PTHS⁻TMA⁺ (λ_{\max} : 549 nm) (Figure 4-S1, Supporting Information). For PTHS⁻TBA⁺, a distinct red-

shift of 30 nm of the λ_{\max} in solution (λ_{\max} : 529 nm) is obtained compared to in film (λ_{\max} : 499 nm).

The excitonic-vibronic coupling causing fine structure of absorption and emission, obtained in solution as well as in film, is complex for polymers with π - π -stacking.^[18] In polymer assemblies, intrachain through-bond interactions lead to J-aggregate behavior, whereas interchain Coulombic interactions lead to H-aggregate behavior. The photophysics of common emissive conjugated polymer films is determined by a competition between intrachain, J-favoring interactions and interchain, H-favoring interactions.^[19] TMA⁺ ions are less bulky than TEA⁺ and TBA⁺ ions. Consequently, the π - π -stacking of the hydrophobic polythiophene backbones in PTHS⁻TMA⁺ may be less hindered which leads to a stronger aggregation compared to PTHS⁻TEA⁺ and PTHS⁻TBA⁺. A redshift of the absorption maxima due to the exchange of the bulkier TBA⁺ ions to the less sterically hindered TMA⁺ ions was also reported by McCullough et al. for a 2,5-poly(thiophene-3-propionic acid)^[9] and by Hostnik et al. for an aqueous poly(thiophene-2-ylacetic acid) solution.^[20]

2.3. UV-Vis/IR Absorption of Crosslinked Polyelectrolyte Films

Since devices for biological applications have to be long-term stable in aqueous environment, we need to stabilize the highly water-soluble PTHS⁻X⁺ films with a crosslinker. Therefore, we added (3-glycidyloxypropyl)trimethoxysilane (GOPS) (1 wt%) as crosslinker to a solution of PTHS⁻X⁺ in deionized water (DI). Including GOPS in PEDOT:PSS dispersions is a common strategy to prevent the dissolution and delamination of films in an aqueous media.^[21-23] Moreover, as we have already shown in a previous work that ethylene glycol (EG) improved the OECT performance of a PTHS⁻TBA⁺, we also prepared films spin-coated from a solution containing 5 vol% EG.^[13] Unfortunately, the addition of additives may change the aggregation behavior of conjugated backbones. Since a larger volume of ordered conjugated polymer chains leads to a higher charge carrier mobility, the degree of aggregation is important for most applications.^[24-27] To evaluate the effect of the addition of GOPS and EG on the aggregation behavior of PTHS⁻X⁺, we compared the UV-vis absorption spectra of thin films containing GOPS and containing both GOPS and EG, with the ones of pristine PTHS⁻X⁺ films. In Figure 4-2b the absorption spectra for the PTHS⁻TMA⁺ films are shown as a typical example. The respective spectra for PTHS⁻TBA⁺ and PTHS⁻TEA⁺ can be found in Figure 4-S2 in the Supporting Information. By adding GOPS to the spin-coating solution, the absorption spectra of the films of all PTHS⁻X⁺ are blueshifted. PTHS⁻TBA⁺ is shifted by 45 nm, PTHS⁻TEA⁺ by 48 nm and PTHS⁻TMA⁺ only by 8 nm due to addition of the crosslinker. Still PTHS⁻TMA⁺ is redshifted in comparison to PTHS⁻TEA⁺ and PTHS⁻TBA⁺. A closer examination of the spectra for PTHS⁻TMA⁺ and PTHS⁻TEA⁺ containing GOPS reveals that there is still a tiny shoulder

visible around 600 nm. PTHS⁻TBA⁺ does not show a shoulder any more. The supplemental addition of EG does slightly shift the absorption maxima further in the blue region ($\Delta\lambda_{\text{max}}$: 6 - 15 nm).

The blueshift of the absorption spectra by adding GOPS indicates that the crosslinker changes the nature of the aggregation of the polythiophene backbones. In aqueous environment GOPS is forming methanol and (3-glycidyloxypropyl)trimethoxysilanol, which build at elevated temperature siloxane bonds with each other or with a methoxy group of another GOPS molecule during drying.^[28,29] In this way a crosslinked network is built. Furthermore, the epoxy group of GOPS is unstable in water and could react to a diol, which can interact with an acidic sulfonic group of polystyrene sulfonate (PSS) or in our case a sulfonate group on a hexyl side-chain of PTHS⁻X⁺.^[30,31] Due to the formed network and the hydrogen bonds to the polymer, the solubility of the film is decreased. Nevertheless, the aggregation of the polythiophene backbones may be simultaneously changed.

2.4. Spectroelectrochemical Measurements

To determine whether the hydrated ions interact with the conjugated backbone in our polyelectrolyte films, we proceeded with testing the electroactivity of the crosslinked films in presence of electrolytes.^[32] An electroactive material is able to record the influence of the ions in the surroundings on its electrical signal. Thus this material transduces ionic to electronic signals. For this, ions should be penetrating and drifting inside the thin film. By applying a varying bias (0 - 600 mV in steps of 100 mV) between the CPE film casted on indium tin oxide (ITO) substrate and a Pt-counter electrode, while both are immersed in a 0.1 M NaCl_{aq} electrolyte solution, oxidation of the polyelectrolyte is induced. These processes can be simultaneously monitored with UV-vis spectrometer as the charges formed on the polymer backbones lead to a structural and electronic distortion and consequently to a change in the spectra.^[33] Figure 4-3a shows the resulting plot for crosslinked PTHS⁻TMA⁺ as a typical example. Similar spectra for PTHS⁻TBA⁺ and PTHS⁻TEA⁺ are given in Figure 4-S3 a, c in the Supporting Information, respectively. To render the results even more comparable, the relative difference between the spectra achieved by applying a bias and the initial spectrum without applied bias (Δ_{Abs}) is also plotted (Figure 4-S3 b, d, f, Supporting Information).

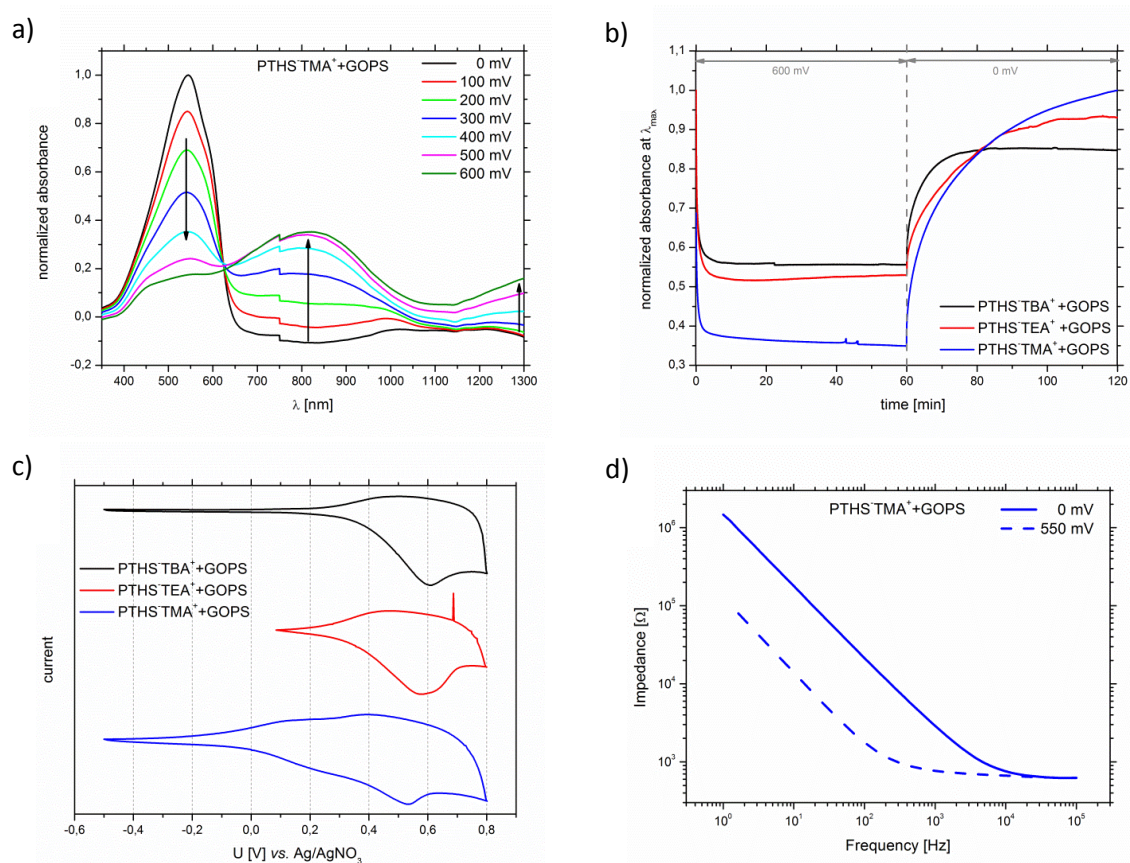


Figure 4-3: a) Normalized (with respect to λ_{\max} at 0 mV) spectra of a PTHS⁻TMA⁺ film (+ 1wt% GOPS) due to electrochemical oxidation (doping) by applying a varying bias from 0 to 600 mV in steps of 100 mV (Spectra of all CPE films containing GOPS can be found in Figure 4-S3, Supporting Information). b) Monitoring of change in absorption at the wavelength of the respective ground state maximum (PTHS⁻TBA⁺ at 482 nm, PTHS⁻TEA⁺ at 497 nm, and PTHS⁻TMA⁺ at 545 nm). For this measurement 600 mV was applied for one hour, followed by 0 mV for an additional hour for all the samples. c) Cyclic voltammogram of crosslinked PTHS⁻TBA⁺, PTHS⁻TEA⁺ and PTHS⁻TMA⁺ films cast on ITO substrates measured in DCM. d) Bode plot (impedance vs. frequency) of a thin crosslinked PTHS⁻TMA⁺ film recorded with and without 550 mV applied bias (The same plots for PTHS⁻TBA⁺ and PTHS⁻TEA⁺ films are shown in Figure 4-S4, Supporting Information).

For all crosslinked PTHS⁻X⁺ films, similar trends were observed. On increasing the applied bias, the absorption maxima of the films decrease and get slightly blueshifted. Furthermore, two additional bands appear, one between 650 and 1100 nm, and a second one starting at 1100 nm and extending beyond 1300 nm. Due to the absorption of the ITO substrate at higher wavelengths than 1300 nm, we were not able to measure this peak at higher wavelength range. When the applied bias was reversed stepwise back to 0 mV, the absorption at higher energies once more became dominant and the whole spectrum shifted back to the initial version at 0 mV (not shown). Thus, the two additional absorption bands due to oxidation at 650 and 1100 nm bleached. For each of the polyelectrolyte films, an isosbestic point exists, through which all their spectra pass through ($\lambda_{\text{isosbestic}}$: 584 nm for PTHS⁻TBA⁺, $\lambda_{\text{isosbestic}}$: 603 nm for PTHS⁻TEA⁺, $\lambda_{\text{isosbestic}}$: 625 nm for PTHS⁻TMA⁺). The appearance of clear isosbestic points are hints for the formation of a new species due to oxidation and also for the reversibility of the oxidation.^[34] For comparison,

the spectra obtained at 0 mV are normalized (to avoid inaccuracies due to possible thickness variations) and differential spectra for each applied voltage with respect to the respective normalized spectra are plotted in Figure 4-S3 in the Supporting Information. The easiness and degree of oxidation can be evaluated by comparing either the decrease in absorption maximum of the unbiased samples or the increase in radical cation absorption (650-1100 nm). If the differential spectra are compared at absorption maxima of the pristine samples ($\lambda = 500$ nm), it is obvious that PTHS⁻TMA⁺ favors the fastest oxidation. On the other hand, if the absorption maxima for the radical cations are considered, the difference in oxidizability between PTHS⁻TEA⁺ and PTHS⁻TMA⁺ is small. Anyhow, PTHS⁻TBA⁺ seems to get oxidized very slowly (Figure 4-S3, Supporting Information).

A similar behavior in spectroelectrochemical measurements is well-known for poly(3-hexylthiophene) (P3HT).^[33, 35] As the electronic and optical properties are mainly determined by the conjugated backbone,^[7] this is hardly surprising. The two simultaneously arising absorption bands, seen for all three polyelectrolyte films, represent the oxidized polythiophene backbone with polarons as charge carriers.^[33] This was demonstrated for P3HT experimentally as well as via quantum chemical calculations.^[33, 36] The conversion of the undoped sample into the oxidized species is denoted by the isosbestic point.^[33] As the polythiophene backbone is an electron donor, a positive bias has to be applied to obtain a change in the absorption spectrum. In contrast, poly(3,4-ethylenedioxythiophene) polystyrene sulfonate (PEDOT:PSS), which is a widespread material for bioelectronics, is a doped system. Thus, a negative bias (with respect to the reference electrode) has to be applied to induce dedoping of PEDOT:PSS and to observe a change in the absorption spectrum. Overall, bulk electrical oxidation was proven for all three polyelectrolytes by spectroelectrochemical measurements. All the films containing GOPS were stable in the aqueous electrolyte, even with applied bias. Furthermore, oxidation of the films was reversible and within the electrochemical window of aqueous solutions, which is important for bioelectronic applications utilizing devices such as OECTs.

To get a deeper insight in the electroactivity of the three polyelectrolytes and also in their stability over time, we applied 600 mV bias on thin films dipped in an electrolyte for one hour and examined the extent of oxidation by measuring the absorption at the wavelength of the respective ground state maximum (PTHSTBA⁺ at 482 nm, PTHSTEA⁺ at 497 nm and PTHSTMA⁺ at 545 nm, Figure 4-3b). All three polymers show immediately a decrease in absorption maxima under the applied bias. Most pronounced is the oxidation for PTHS⁻TMA⁺, for which absorption is reduced to 38 % of the initial value within 3 min and is decreasing further to 35 % over time. The absorption of PTHSTEA⁺ is reduced to 53 % and the one of PTHSTBA⁺ to 56 %. When we applied

0 mV, the ground state absorption started recovering. PTHS⁻TMA⁺ is the only one of the examined polyelectrolytes which exhibits a fast and efficient oxidation followed by recovering fully to its initial absorption maximum. PTHS⁻TEA⁺ reached 93 % of its initial absorption maximum, whereas PTHS⁻TBA⁺ only 85 %. For the recovery, as PTHS⁻TBA⁺ reached a plateau after around 20 min with no applied bias, PTHS⁻TEA⁺ and PTHS⁻TMA⁺ continue increasing till the measurement was ended after 60 min.

These results clearly indicate that in PTHS⁻TMA⁺ more thiophenes are oxidized than in PTHS⁻TEA⁺ or PTHS⁻TBA⁺ for the same applied voltage and duration of oxidation. The radical cations created by electrochemical oxidation seem to be stable over time to a certain degree, as the reduction at zero voltage was relatively slow. The maximum degree of oxidation of PTHS⁻TMA⁺ seems to be completed in about 10 min (reduction of absorption at 545 nm to 40%) and after that it continues monotonously during the whole 60 min, reaching 35% of the original absorption. Also the recovery was at a slow rate reaching 100% after 60 min. PTHS⁻TBA⁺, on the other hand, shows a fast recovery to reach a stable rereduction level at only about 85%. Thus, the degree of oxidation and its recovery are the best for PTHS⁻TMA⁺, which shows the most packed structure among all the discussed polyelectrolytes (see Figure 4-2).

2.5. Cyclic Voltammetry

To study the reversibility of the redox reactions and the electrochemical behavior of PTHS⁻X⁺, we performed cyclic voltammetry (CV) measurements. The polyelectrolyte films spin-coated on ITO served as working electrodes. Figure 4-3c shows the obtained cyclic voltammograms. PTHS⁻TBA⁺, PTHS⁻TEA⁺ and PTHS⁻TMA⁺ exhibit reversible oxidation behavior. Values calculated from the half-wave potential of the oxidation are often inappropriately referred to as highest occupied molecular orbital (HOMO). As suggested by Bredas, we are using the term ionization potential (IP) here.^[37] To calculate the IP values, ferrocene was used as standard and the influence of the solvent was taken into account.^[38,39] The half-wave potentials used for calculation are averages of several measurements to minimize the inaccuracy. Hereby, we obtained an IP of -5.52 eV for PTHS⁻TBA⁺, -5.50 eV for PTHS⁻TEA⁺ and -5.43 eV for PTHS⁻TMA⁺. The polyelectrolyte with the smallest counterion, PTHS⁻TMA⁺, is therefore relatively easier to be oxidized. IP values obtained from CV measurements should be taken with caution for their absolute values, since they give approximations based on calculations assuming the HOMO value of ferrocene system.^[37] It is interesting to note that Nguyen and co-workers reported for cationic polyelectrolytes with different counter anions the same trend for IP values as determined by UPS in solid state.^[11]

2.6. Electrochemical Impedance Spectroscopy (ESI)

The result of the ion uptake of a redox-active material could be quantified by the electrochemical capacitance.^[40] Since the ions are able to penetrate the films in aqueous media, we compared the volumetric capacitance as reported by Rivnay et al.^[41] We recorded the electrochemical impedance spectra of the films cast on gold substrates ($635 \times 635 \mu\text{m}^2$) in a frequency range of 1 Hz and 100 kHz. The spectra were acquired as the film was exposed to a DC voltage of 0 and 550 mV with respect to the reference electrode (Figure 4-3d and Figure 4-S4, Supporting Information). We modeled the data using an established equivalent circuit comprising serially connected impedance elements; the resistance of the electrolyte and the impedance of the polymer represented by a resistor and a capacitor, C , in parallel.^[42] As the films get doped with the applied bias, the impedance, below 1000 Hz decreases, with an increase in the extracted capacitance values (Figure 4-3d and Figure 4-S4, Supporting Information).^[43] The films can be assumed to have bulk doping, therefore, it is reasonable to assume a volumetric interaction of ions with the polymer. A clear trend in the obtained volumetric capacitances ($C^* = C/V$, V (volume)) for the three polyelectrolytes was recognized: By decreasing the size of counter ion on the polymer backbone, the C^* increases considerably (Table 4-1). The volumetric capacitance of PTHS⁻TEA⁺ at $V = 550$ mV (5 Fcm^{-3}) is approximately four times larger than for the most bulky PTHS⁻TBA⁺ (22 Fcm^{-3}), whereas for PTHS⁻TMA⁺, the CPE with the smallest counter ion, it is the highest (82 Fcm^{-3}). Taken together with the fast and efficient switching of the spectral properties under applied bias, PTHS⁻TMA⁺ constitutes a CPE having the highest potential for ion response.

Table 4-1: The OECT characteristics and materials figure of merit for the PTHS^X⁺ films studied in this work. Transconductance (g_m), drain current (I_D) at $V_G = -600$ mV and $V_D = -500$ mV, ON/OFF ratio and response time (τ_{ON}) at $V_G = -600$ mV and $V_D = -400$ mV. All the OECT parameters are averaged values obtained from two to five devices. All films contain GOPS (1 wt%). Also given is the volumetric capacitance (C^*) calculated at an offset potential versus Ag/AgCl of 550 mV, and the hole mobility (μ) calculated using Equation (1). Note that μ and C^* are extracted from single samples and under one biasing condition and might therefore be prone to error because of ion accumulation at the film/electrolyte interface and V_G dependent channel mobilities.

sample	OECT				C^* [F/cm ³]	μ [10 ⁻⁹ cm ² V ⁻¹ s ⁻¹]
	g_m [μ S] ^{a)}	I_D [10 ⁻² μ A] ^{a)}	$I_D^{a)}/I_{D,0}$	τ_{ON} [s] ^{b)}		
PTHS ^{TBA} ⁺	0.13	-2.56	3.72	3.3	5	8.18
PTHS ^{TEA} ⁺	2.16	-14.50	87.50	0.8	22	8.21
PTHS ^{TMA} ⁺	45.50	-350	250	0.2	82	267
PTHS ^{TBA} ⁺ +EG	2.30	-28.10	19	1.4	15	288
PTHS ^{TEA} ⁺ +EG	1.16	-8.79	170	0.8	13	53.7
PTHS ^{TMA} ⁺ +EG	36.9	-276	523	0.4	-	-

a) Average at $V_G = -600$ mV and $V_D = -500$ mV; b) At $V_D = -400$ mV, for a step of $V_G = 0$ mV to $V_G = -600$ mV.

2.7. Swelling Capability

To a large volumetric capacitance, the capability of a film to take up water and swell also contributes.^[41] We, therefore, examined the swelling capacity of the CPEs using QCM. Figure 4-S5 in the Supporting Information shows the changes in QCM signals (immediate drop in oscillation frequency (f) and increase in dissipation (D)) for the quartz crystals coated with the polymers as the films are exposed to DI water and NaCl solution. This change in f accompanied with an increase in dissipation D with the inflow of water/NaCl solution is translated into an increase in the mass of the film, i.e., swelling due to uptake of water/hydrated ions. We treated our data with Sauerbrey model which directly correlates the change in f to swelling (see the Experimental Section).^[44] When we calculate the swelling percentages, we see that for PTHS^{TMA}⁺, PTHS^{TEA}⁺, PTHS^{TBA}⁺ is 2 %, 2 %, 3 % in DI water, and 3.4 %, 3.5 %, 6.3 % in NaCl, respectively, as shown in Table 4-S1 in the Supporting Information. With the addition of EG, swelling of the three polymers does not seem to be affected. Previous studies have shown that swelling of OECT materials is correlated with ion mobility and/or OECT performance.^[45] Our current findings demonstrate that the CPEs swell less than PEDOT-based materials, presumably due to the lack of a polyionic phase. Although swelling is limited, the capacitance measured at the oxidation potential is higher for PTHS^{TBA}⁺ than for PEDOT:PSS, indicating the ease of ion access to the conjugated backbone in the former.^[43]

2.8. Performance in OECTs

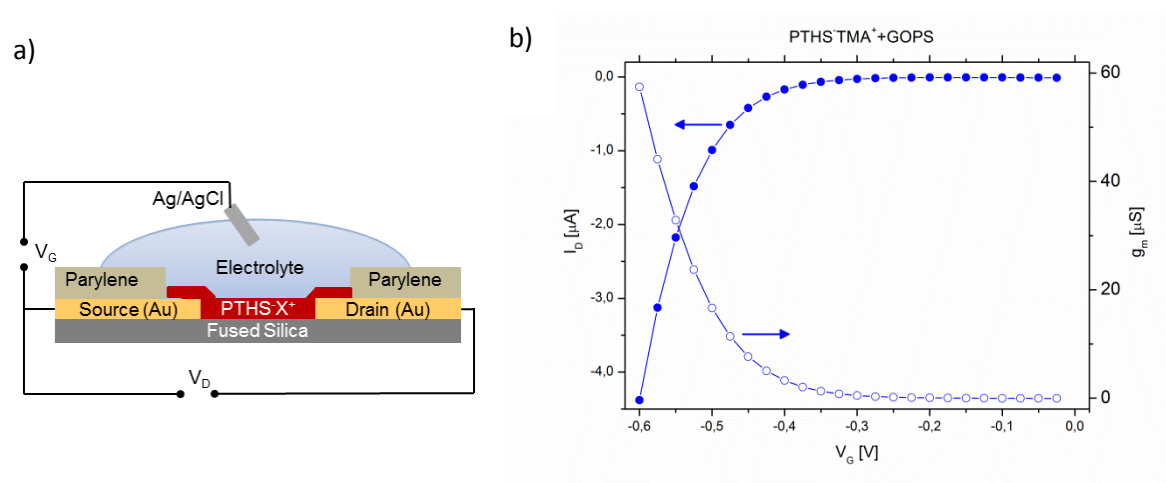


Figure 4-4: a) Cross-sectional schematic of an OECT. b) Transfer characteristics and corresponding transconductance (g_m) of a crosslinked PTHSTMA⁺-based device at $V_D = -500$ mV. Output and transfer characteristics for all CPEs are given in Figure 4-S6 – S9 in the Supporting Information.

OECTs are electronic transducers that also enable studies of mixed (ionic and electronic) transport of redox-active films. The counterion effect on mixed transport could be finally studied using the CPEs in the channel of OECTs. A cross-sectional schematic of the used structure is shown in Figure 4-4a. The channel length was 10 μm and the width 100 μm . We prepared OECTs from six different solutions: PTHSTBA⁺, PTHSTEA⁺ and PTHSTMA⁺ containing GOPS as cross-linker as well as the same CPE solutions containing EG as the cosolvent. For all solutions, the same spin-coating conditions were used, resulting in thin layers of 10 - 20 nm. A series of drain (V_D) and gate voltage steps (V_G) were applied at room temperature, while recording the resulting drain current (I_D). The transfer characteristic for such an OECT is shown in Figure 4-4b as a typical example. All the output characteristics are shown in Figure 4-S6, Supporting Information, devices without EG and Figure 4-S8, Supporting Information, devices with EG. The transfer characteristics and corresponding transconductance of PTHSTBA⁺ and PTHSTEA⁺ devices are also shown in Figure 4-S7, Supporting Information, without EG and Figure 4-S9, Supporting Information, with EG. Upon applying a negative voltage at the gate electrode, the current between the source and the drain electrode increases, showing that the channel is p-type doped (Figure 4-4b). The negative bias triggers the doping of the polymer via oxidation (along with possible ejection of the counter cation and/or injection of the Cl⁻ of the electrolyte), which increases the current flowing in the channel and switches the device ON.^[46] Since we use an aqueous electrolyte, the gate potentials to be applied are limited due to the possible electrolysis (at 1.23 eV at pH 0) and a lack of stability of the oxidized CPE in water.^[47] Such accumulation mode transistors are in fact attractive for sensing applications as they consume low power.^[13]

When defining the performance of OECTs, an important parameter is the transconductance ($g_m = \frac{\partial I_D}{\partial V_G}$), quantifying the magnitude of a change in I_D as a small V_G is applied at the gate. Table 4-1 summarizes the OECT characteristics and the crucial thin film parameters for our CPEs. Comparing the three polymers of similar thicknesses, we see that when PTHS⁻TMA⁺ is in the channel, the device exhibits the best performance compared to other films: highest values of g_m ($\approx 45.5 \mu\text{S}$), I_D ($-350 \cdot 10^{-2} \mu\text{A}$) and ON/OFF (250) with the fastest switching speed (0.2 s). These results are in good agreement with the observed rate of oxidation and its reversibility in spectroelectrochemical (SEC) measurements.

Devices with EG treated samples showed in general higher ON/OFF ratios than their respective devices without EG. Addition of EG improves the performance of PTHS⁻TBA⁺ based devices (g : $2.30 \mu\text{S}$, I_D : $-28.1 \cdot 10^{-2} \mu\text{A}$). This improvement with EG is similar to that reported in a previous work.^[13] In the earlier report, fiber-like features were observed in atomic force microscopy (AFM) images of the EG-treated films, whereas the films without EG exhibited no such features.^[13] In contrary, PTHS⁻TEA⁺ (g : $1.16 \mu\text{S}$, I_D : $-8.79 \cdot 10^{-2} \mu\text{A}$) and PTHS⁻TMA⁺ (g : $36.9 \mu\text{S}$, I_D : $-276 \cdot 10^{-2} \mu\text{A}$) based devices perform worse when containing EG compared to the ones without. However, PTHS⁻TMA⁺ is the best performing CPE among the three polymers independent of the cosolvent additive.

In order to determine the temporal response of the devices, I_D was recorded while the voltage is pulsed at the gate electrode. The pulses were 15 s long with amplitude of -600 mV and applied with an interval of 45 s. The ON response time (τ_{ON}) is defined as the time required to reach 90 % of the maximal I_D of the resp. pulse.^[46] PTHS⁻TMA⁺ shows the fastest response with 0.2 s, followed by PTHS⁻TEA⁺ and PTHS⁻TBA⁺ which have a τ_{ON} of 3.8 and 3.3 s, respectively. Repeating the pulses several times, we noticed that temporal response stays the same for each applied pulse (not shown). However, the current does not reach the maximum value obtained for the first pulse. Here, PTHS⁻TMA⁺ shows the best stability, while PTHS⁻TEA⁺ and PTHS⁻TBA⁺ degrade with time. Moreover, as with steady state characteristics, EG improves the response time of the PTHS⁻TBA⁺-based devices. For the case of PTHS⁻TEA⁺ and PTHS⁻TMA⁺, on the other hand, there was almost no difference in the response time, induced by the cosolvent. As mentioned above, the accumulation mode transistors are switched ON by doping the polymer in the channel due to application of a positive (n-type, reduction) or like in our case, negative (p-type, oxidation) gate bias.^[48] Negative gate bias can induce the oxidation of a polyelectrolyte followed by either ejection of counter ions (here TBA⁺, TEA⁺ and TMA⁺) or by injection of electrolyte anions (here chloride anions) or both to have charge balance.^[13,46] As TMA⁺ is the smallest and less sterically hindered counter ion among the polymers tested, its ejection might be much easier than the

bulky TBA⁺ cation. This could hint the fastest temporal response and stability of TMA. Response time and the stability of the OECT might be related to the mobility of ions inside the polymer film, which is governed by the swelling behavior. Our results, however, do not show any trend between the two, presumably due to the response times not ranging widely. In addition to the C*, the charge carrier mobility (μ) is another material related parameter governing the g and can be determined using the following equation for OECT^[41]

$$g = \frac{W \cdot d}{L} \cdot \mu \cdot C^* \cdot (V_T - V_G) \quad (1)$$

where W is the channel width, d is the film thickness, L is the length of the channel, and V_T is the geometry-independent threshold voltage.^[41] When C^* values extracted from electrochemical impedance spectra are plugged into this equation, we find that the hole mobility of PTHS⁻TMA⁺ ($267 \cdot 10^{-9} \text{ cm}^2 \text{V}^{-1} \text{s}^{-1}$) is orders of magnitude higher than the other two films (for PTHS⁻TBA⁺, μ : $8.18 \cdot 10^{-9} \text{ cm}^2 \text{V}^{-1} \text{s}^{-1}$; and for PTHS⁻TEA⁺, μ : $8.21 \cdot 10^{-9} \text{ cm}^2 \text{V}^{-1} \text{s}^{-1}$). Although, these values are just rough approximations calculated at one V_G and using a C^* extracted from one impedance plot, the trend is clear and correlates with the aggregation behavior of the polymers revealed by UV-vis absorption measurements: as PTHS⁻TMA⁺ shows the most aggregation and with that the densest π - π stacking, it is expected to have a higher hole mobility than the less aggregated PTHS⁻TEA⁺ and PTHS⁻TBA⁺. The mobility values for PTHS⁻X⁺ may be less than for neutral polythiophenes, if the aggregation is hindered due to the incorporation of charged units on side chains.^[49-51] Moreover, the addition of crosslinker disturbs the aggregation of the conjugated backbones. This also can lead to a decrease of electronic coupling and consequently to lower electronic charge mobility. Garcia and Nguyen obtained a similar effect by adding polyethylene glycol (PEG) to an anionic CPE.^[51] A drop in electrical conductivity due to addition of GOPS is well known for PEDOT:PSS, as well.^[23,29,42,52]

3. Conclusion

In conclusion, we showed that the selection of counter ion in CPEs plays an important role in determining the thin film characteristics and OECT performance. We synthesized three different CPEs from the same precursor polymer which differ only in the size of counter ions. The used counter ions varied in size from the bulky tetrabutylammonium, over tetraethylammonium to the smallest tetramethylammonium ion. According to UV-vis absorption studies in aqueous solution as well as in thin films, the CPE with the smallest counter ion showed the highest degree of aggregation. Crosslinking of the materials with GOPS hindered the aggregation of the conjugated backbones independent of the used counter cation. Spectroelectrochemical

investigations revealed that the CPE with the smallest counterion can be oxidized to a higher degree than the CPEs with bulkier counter ions. As evidenced by CV and electrochemical impedance spectroscopy measurements, the CPE with the smallest counter ion was able to convert more dopant ions to electrical charges. These results has a direct implication on the performance of an OECT utilizing the CPE in the channel, as the CPE with the smallest counter ion led to best performing devices.

4. Experimental Section

The salts tetra-n-butyl, tetraethyl and tetramethyl ammonium sulfite were prepared by adding one equivalent dimethyl sulfite to a solution of two equivalents of tetra-n-butyl, resp. tetraethyl, resp. tetramethyl ammonium hydroxide in methanol. All other chemicals were received from commercial suppliers. The synthesized polyelectrolytes were analyzed via $^1\text{H-NMR}$ using a Bruker Avance 250 spectrometer at 300 MHz. For calibration of the spectra the respective solvent signal was used. Matrix assisted laser desorption ionizations spectroscopy with time-of-flight detection mass spectroscopy (MALDI-TOF MS) of the precursor polymer P3BrHT was measured on a Bruker Reflex III in linear mode. Trans-2-[3-(4-tert-butylphenyl)-2-methyl-2-propenylidene]malononitrile (DCTB) was used as matrix and a matrix to PTHS ratio of 1000:1.

Size exclusion chromatography of P3BrHT was performed utilizing a Waters 515 HPLC pump with stabilized THF as the eluent at a flow rate of 0.5 mL/min. Into a column setup consisting of a guard column (Varian, 50 × 0.758 cm, ResiPore gel, particle size 3 μm) and two separation columns (Varian, 300 × 0.758 cm, ResiPore gel, particle size 3 μm) 20 μL of a P3BrHT solution (concentration of approximately 1 mg/mL) was injected. With a Waters 2489 tunable UV detector at 254 nm the polymer size distribution was monitored. For calibration Polystyrene was used as external and 1,2-dichlorobenzene as an internal standard.

4.1 Synthesis

The syntheses of the precursor polymer P3BrHT and PTHSTBA⁺ are already published.^[15] The molecular weight of P3BrHT was analyzed by MALDI-TOF MS ($M_n = 18.5 \text{ kg mol}^{-1}$, $M_w = 18.9 \text{ kg mol}^{-1}$, average 75 repeating units) and Size Exclusion Chromatography: $M_n = 18.2 \text{ kg mol}^{-1}$, $M_w = 20.8 \text{ kg mol}^{-1}$, PDI: 1.14).

PTHSTEA⁺ was prepared according to the procedure reported for PTHSTBA⁺.^[15] Instead of tetra-n-butyl ammonium sulfite tetraethyl ammonium sulfite (0.83 mol L⁻¹ in MeOH, 11 mL, 9.13 mmol) was used. NMR: δ_{H} (300 MHz; DMSO-d₆) 1.06-1.20 (12 H, t, N⁺(-CH₂-CH₃)₄), 1.30-1.47 (4 H, m, CH₂-CH₂-CH₂-CH₂-CH₂-CH₂-S), 1.50-1.75 (4 H, m, CH₂-CH₂-CH₂-CH₂-CH₂-CH₂-S), 2.37-2.48

(2 H, m, CH₂-CH₂-CH₂-CH₂-CH₂-S), 2.69-2.90 (2 H, m, CH₂-CH₂-CH₂-CH₂-CH₂-S), 3.12-3.27 (8 H, q, N⁺(-CH₂-CH₃)₄), 7.14-7.26 (1 H, s, H_{arom}).

PTHSTMA⁺ was also prepared according to the procedure reported for PTHSTBA⁺[15] using a solution of 0.14 g of poly(3-(6-bromohexyl)-thiophene) (0.008 mmol) in 38 mL dry THF. Instead of tetra-n-butyl ammonium sulfite tetramethyl ammonium sulfite (1.29 mol L⁻¹ in MeOH, 6 mL, 7.72 mmol) was added. NMR: δ_H (300 MHz d-THF/D₂O: 2/1) 1.30-1.46 (4 H, m, CH₂-CH₂-CH₂-CH₂-CH₂-S), 1.55-1.69 (4 H, m, CH₂-CH₂-CH₂-CH₂-CH₂-S), 2.63-2.85 (4 H, m, CH₂-CH₂-CH₂-CH₂-CH₂-S), 3.07-3.19 (12 H, s, N⁺(-CH₃)₄), 6.95-7.07 (1 H, s, H_{arom}).

4.2 Absorption Measurements

The polyelectrolyte films were prepared from 2.5 wt% solutions of PTHSTBA⁺ and PTHSTEA⁺, and 1 wt% solution of PTHSTMA⁺ in ultrapure water (Milli-Q). Before spin-coating the solutions on cleaned quartz substrates, the solutions were filtered using polyamide syringe filters. For the cross-linked films a solution of 1 wt% polyelectrolyte in ultrapure water (Milli-Q) was prepared and 1 wt% GOPS was added. For the films containing EG 5 vol% of this solvent was added. After filtration and spin-coating of the solutions on quartz substrates, the films were annealed at 90 °C for 1.5 h.

The films for spectroelectrochemical measurements were prepared like the ones for absorption measurements but on ITO substrates. Spectroelectrochemical measurements were performed in a 1 cm quartz cuvette containing 0.1 M NaCl_{aq} and using a platinum wire as counter electrode. The film and the platinum wire were connected to a source meter to apply bias. Every bias was applied for seven minutes, consisting of five minutes waiting time and two minutes for recording the spectra. The bias was changed by steps of 100 mV. For the time dependent measurements, the extent of oxidation was recorded by measuring the absorption at the wavelength of the respective ground state maximum. First, a bias of 600 mV was applied for one hour. Afterwards, the bias was removed and the associated changes in the spectra were recorded for one hour. All absorption spectra were recorded using a Jasco V670 spectrophotometer.

4.3 Cyclic Voltammetry

The cyclic voltammetry measurements were performed using a standard three electrode assembly under nitrogen with a scanning rate of 100 mV s⁻¹. The assembly was connected to a potentiostat model 263A from EG&G Princeton Applied Research. The measurements were performed in a 0.1 M tetra-butylammonium hexafluorophosphate solution in dichloromethane. A platinum wire in a 0.1 M tetra-butylammonium hexafluorophosphate solution in dichloromethane served as counter electrode, whereas an Ag wire in a 0.1 M AgNO₃ solution in

acetonitrile was used as reference electrode. The working electrode was the polyelectrolyte film spin-coated on an ITO substrate. The measurements were calibrated with ferrocene/ferrocenium as external standard. Considering the solvent effects the IP values were calculated as already published.^[38]

4.4 Electrochemical Impedance Spectroscopy

Electrochemical Impedance Spectroscopy (EIS) was performed in aqueous NaCl solution (0.1 M) using an impedance spectrometer (potentiostat/galvanostat, Metrohm Autolab B.V.) with a three electrode configuration. The polymer-coated gold electrode ($4.03 \cdot 10^{-3} \text{ cm}^2$) was the working electrode, a Pt mesh was the counter, and Ag/AgCl is used as a standard reference electrode. EIS was performed over a range of 1 Hz- 100 kHz—with an AC 10 mV sine wave, and a DC offset of 550 mV and 0 V (the potential on the working electrode with respect to the reference). In order to extract capacitance (C) and volumetric capacitance (C^*) the spectra of doped films (DC offset=at 550 mV) were fit to an (RC) equivalent circuit using NOVA software.

4.5 QCM

The swelling of the thin polymer films was studied using QCM-D (Q-Sense, from Biolin Scientific). The polymer solutions were spun cast on clean plasma activated gold-coated Q-sensors. They were kept under vacuum overnight to ensure complete drying of the film. Filtered DI water and afterwards aqueous NaCl solution (0.1 M) were flown over the samples at 24 °C at a flow rate of 50–100 $\mu\text{L} \cdot \text{min}^{-1}$ controlled by a peristaltic pump. The adsorbed mass (Δm) was estimated from Δf using the Sauerbrey equation $\Delta m = -C \frac{\Delta f_n}{n}$ where C is the mass sensitivity constant (17.7 $\text{ng} \cdot \text{cm}^{-2} \text{ Hz}$ at $f = 5 \text{ MHz}$) and Δf_n is the change in resonance frequency at n th overtone.^[44] The 3rd, 5th, and 7th overtones were used for the calculations. Given the initial thickness of the dry films, the water and NaCl uptake could be estimated. The error was due to variation in the measurement of the films thickness.

4.6 OECT Performance

OECT devices were prepared as described previously, fabricated photo lithographically using a parylene-C lift-off process.^[13] The patterned channels of the transistors had a width of 100 μm and a length of 10 μm . 1 wt% CPE was dissolved in deionized water and 1 wt% GOPS was added. Films containing EG had 5 vol% of the co-solvent. The films were spin-coated at 1500 rpm for 30 sec. Afterward, the substrates were annealed at 90 °C for 1.5 h. Thickness measurements of the polyelectrolyte films were performed using a Dektak profilometer. All measurements were

performed using an Ag/AgCl wire (Warner Instruments) as the gate electrode and NaCl solution (0.1 M) as the electrolyte. The steady-state measurements of the OECT (output and transfer curves) and the pulsed gate experiments were performed using a Keithley 2612A with customized LabVIEW software.

Supporting Information

Supporting Information is available from the Wiley Online Library or from the author.

Acknowledgements

The authors acknowledge Anna Maria Pappa for providing OECTs. Financial support from Deutsche Forschungsgemeinschaft (DFG) (GRK 1640) is kindly acknowledged. M. M. S. acknowledges also the support from Elite Study program, Macromolecular Science at the University of Bayreuth.

References

- [1] A. O. Patil, Y. Ikenoue, N. Basescu, N. Colaneri, J. Chen, F. Wudl, A. J. Heeger, *Synth. Met.* **1987**, *20*, 151.
- [2] M. R. Pinto, K. S. Schanze, *Synthesis* **2002**, *9*, 1293.
- [3] L. Chen, D. W. Mcbranch, H.-L. Wang, R. Helgeson, F. Wudl, D. G. Whitten, *Proc. Natl. Acad. Sci. USA* **1999**, *96*, 12287.
- [4] H.-A. Ho, M. Boissinot, M. G. Bergeron, G. Corbeil, K. Doré, D. Boudreau, M. Leclerc, *Angew. Chem. Int. Ed.* **2002**, *41*, 1548.
- [5] H. A. Ho, A. Najari, M. Leclerc, *Acc. Chem. Res.* **2008**, *41*, 168.
- [6] H. S. White, G. P. Kittlesen, M. S. Wrighton, *J. Am. Chem. Soc.* **1984**, *106*, 5375.
- [7] W. Lee, J. H. Seo, H. Y. Woo, *Polymer* **2013**, *54*, 5104.
- [8] R. Yang, H. Wu, Y. Cao, G. C. Bazan, *J. Am. Chem. Soc.* **2006**, *128*, 14422.
- [9] R. D. McCullough, P. C. Ewbank, R. S. Loewe, *J. Am. Chem. Soc.* **1997**, *119*, 633.
- [10] C. R. Singh, G. Gupta, R. Lohwasser, S. Engmann, J. Balko, M. Thelakkat, T. Thurn-Albrecht, H. Hoppe, *J. Polym. Sci. Part B Polym. Phys.* **2013**, *51*, 943.
- [11] J. H. Seo, T.-Q. Nguyen, *J. Am. Chem. Soc.* **2008**, *130*, 10042.
- [12] J. H. Seo, Y. Jin, J. Z. Brzezinski, B. Walker, T. Q. Nguyen, *ChemPhysChem* **2009**, *10*, 1023.
- [13] S. Inal, J. Rivnay, P. Leleux, M. Ferro, M. Ramuz, J. C. Brendel, M. M. Schmidt, M. Thelakkat, G. G. Malliaras, *Adv. Mater.* **2014**, *26*, 7450.
- [14] J. C. Brendel, M. M. Schmidt, G. Hagen, R. Moos, M. Thelakkat, *Chem. Mater.* **2014**, *26*, 1992.
- [15] E. Zeglio, M. M. Schmidt, M. Thelakkat, R. Gabrielsson, N. Solin, O. Inganäs, *ChemistrySelect* **2016**, *1*, 4340.
- [16] Y. Marcus, *J. Solution Chem.* **2008**, *37*, 1071.
- [17] D. Bhowmik, N. Malikova, G. Mériguet, O. Bernard, J. Teixeira, P. Turq, *Phys. Chem. Chem. Phys.* **2014**, *16*, 13447.
- [18] R. H. Lohwasser, M. Thelakkat, *Macromolecules* **2010**, *43*, 7611.
- [19] F. C. Spano, C. Silva, *Annu. Rev. Phys. Chem.* **2014**, *65*, 477.
- [20] G. Hostnik, M. Bončina, C. Dolce, G. Mériguet, A.-L. Rollet, J. Cerar, *Phys. Chem. Chem. Phys.* **2016**, *18*, 25036.
- [21] S. Zhang, P. Kumar, A. S. Nouas, L. Fontaine, H. Tang, F. Cicoira, *APL Mater.* **2015**, *3*, 14911.
- [22] M. Sessolo, D. Khodagholy, J. Rivnay, F. Maddalena, M. Gleyzes, E. Steidl, B. Buisson, G. G. Malliaras, *Adv. Mater.* **2013**, *25*, 2135.

- [23] M. ElMahmoudy, S. Inal, A. Charrier, I. Uguz, G. G. Malliaras, S. Sanaur, *Macromol. Mater. Eng.* **2017**, *302*, 1600497.
- [24] H. Sirringhaus, P. J. Brown, R. H. Friend, M. M. Nielsen, K. Bechgaard, B. M. W. Langeveld-Voss, a. J. H. Spiering, R. a. J. Janssen, E. W. Meijer, P. Herwig, D. M. de Leeuw, *Nature* **1999**, *401*, 685.
- [25] V. Coropceanu, J. Cornil, D. A. da Silva Filho, Y. Olivier, R. Silbey, J.-L. Bredas, *Chem. Rev.* **2007**, *107*, 926.
- [26] J. Gierschner, Y.-S. Huang, B. Van Averbeke, J. Cornil, R. H. Friend, D. Beljonne, *J. Chem. Phys.* **2009**, *130*, 44105.
- [27] C. Scharsich, R. H. Lohwasser, M. Sommer, U. Asawapirom, U. Scherf, M. Thelakkat, D. Neher, A. Köhler, *J. Polym. Sci. Part B Polym. Phys.* **2012**, *50*, 442.
- [28] A. K. Y. Wong, U. J. Krull, *Anal. Bioanal. Chem.* **2005**, *383*, 187.
- [29] O. Berezhetska, B. Liberelle, G. De Crescenzo, F. Cicoira, *J. Mater. Chem. B* **2015**, 5087.
- [30] S. Wu, W. Cui, N. Aghdassi, T. Song, S. Duhm, S. T. Lee, B. Sun, *Adv. Funct. Mater.* **2016**, *26*, 5035.
- [31] W. Cui, S. Wu, F. Chen, Z. Xia, Y. Li, X. H. Zhang, T. Song, S. T. Lee, B. Sun, *ACS Nano* **2016**, *10*, 9411.
- [32] C. M. Pacheco-Moreno, M. Schreck, A. D. Scaccabarozzi, P. Bourgun, G. Wantz, M. M. Stevens, O. J. Dautel, N. Stingelin, *Adv. Mater.* **2017**, *29*, 1604446.
- [33] C. Enengl, S. Enengl, S. Pluczyk, M. Havlicek, M. Lapkowski, H. Neugebauer, E. Ehrenfreund, *ChemPhysChem* **2016**, *17*, 3836.
- [34] W. Kaim, J. Fiedler, *Chem. Soc. Rev.* **2009**, *38*, 3373.
- [35] R. Hu, H. Ni, Z. Wang, Y. Liu, H. Liu, X. Yang, J. Cheng, *Chem. Phys.* **2016**, *476*, 29.
- [36] S. Stafström, J. L. Bredas, *Phys. Rev. B* **1988**, *38*, 4180.
- [37] J.-L. Bredas, *Mater. Horiz.* **2014**, *1*, 17.
- [38] K. Gräf, M. A. Rahim, S. Dasb, M. Thelakkat, *Dyes Pigm.* **2013**, *99*, 1101.
- [39] I. Noviadri, K. N. Brown, D. S. Fleming, P. T. Gulyas, P. A. Lay, A. F. Masters, L. Phillips, *J. Phys. Chem. B* **1999**, *103*, 6713.
- [40] C. M. Proctor, J. Rivnay, G. G. Malliaras, *J. Polym. Sci. Part B Polym. Phys.* **2016**, *54*, 1433.
- [41] J. Rivnay, P. Leleux, M. Ferro, M. Sessolo, A. Williamson, D. A. Koutsouras, D. Khodagholy, M. Ramuz, X. Strakosas, R. M. Owens, C. Benar, J.-M. Badier, C. Bernard, G. G. Malliaras, *Sci. Adv.* **2015**, *1*, 1400251.
- [42] Y. Zhang, S. Inal, C.-Y. Hsia, M. Ferro, M. Ferro, S. Daniel, R. M. Owens, *Adv. Funct. Mater.* **2016**, *26*, 7304.

- [43] A. Giovannitti, D.-T. Sbircea, S. Inal, C. B. Nielsen, E. Bandiello, D. A. Hanifi, M. Sessolo, G. G. Malliaras, I. McCulloch, J. Rivnay, *Proc. Natl. Acad. Sci. USA* **2016**, *113*, 12017.
- [44] R. Schumacher, G. Borges, K. K. Kanazawa, *Surf. Sci.* **1985**, *163*, L621.
- [45] S. Inal, J. Rivnay, A. I. Hofmann, I. Uguz, M. Mumtaz, D. Katsigiannopoulos, C. Brochon, E. Cloutet, G. Hadziioannou, G. G. Malliaras, *J. Polym. Sci. Part B Polym. Phys.* **2016**, *54*, 147.
- [46] E. Zeglio, M. Vagin, C. Musumeci, F. N. Ajjan, R. Gabrielsson, X. T. Trinh, N. T. Son, A. Maziz, N. Solin, O. Inganäs, *Chem. Mater.* **2015**, *27*, 6385.
- [47] D. M. De Leeuw, M. M. J. Simenon, A. R. Brown, R. E. F. Einerhand, *Synth. Met.* **1997**, *87*, 53.
- [48] A. Giovannitti, C. B. Nielsen, D.-T. Sbircea, S. Inal, M. Donahue, M. R. Niazi, D. A. Hanifi, A. Amassian, G. G. Malliaras, J. Rivnay, I. McCulloch, *Nat. Commun.* **2016**, *7*, 1.
- [49] G. K. V. V. Thalluri, J.-C. Bolsée, A. Gadisa, M. Parchine, T. Boonen, J. D'Haen, A. E. Boyukbayram, J. Vandenbergh, T. J. Cleij, L. Lutsen, D. Vanderzande, J. Manca, *Sol. Energy Mater. Sol. Cells* **2011**, *95*, 3262.
- [50] D. Tordera, M. Kuik, Z. D. Rengert, E. Bandiello, H. J. Bolink, G. C. Bazan, T.-Q. Nguyen, *J. Am. Chem. Soc.* **2014**, *136*, 8500.
- [51] A. Garcia, T.-Q. Nguyen, *J. Phys. Chem. C* **2008**, *112*, 7054.
- [52] X. Strakosas, M. Bongo, R. M. Owens, *J. Appl. Polym. Sci.* **2015**, *132*, 41735.

Supporting Information

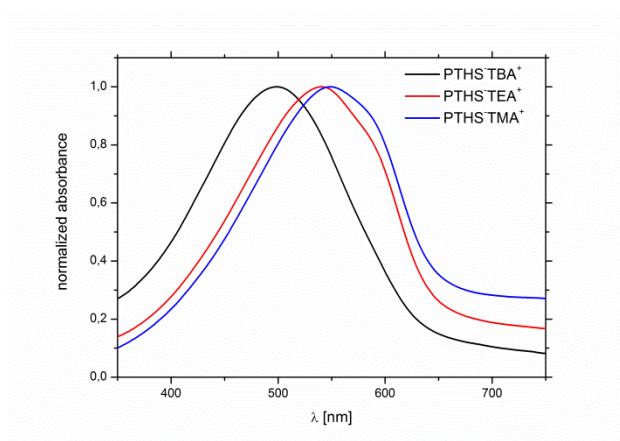


Figure 4-S1: Normalized absorption of thin films spin coated on quartz substrates from aqueous solutions of PTHS⁻ TBA⁺, PTHS⁻TEA⁺ and PTHS⁻TMA⁺.

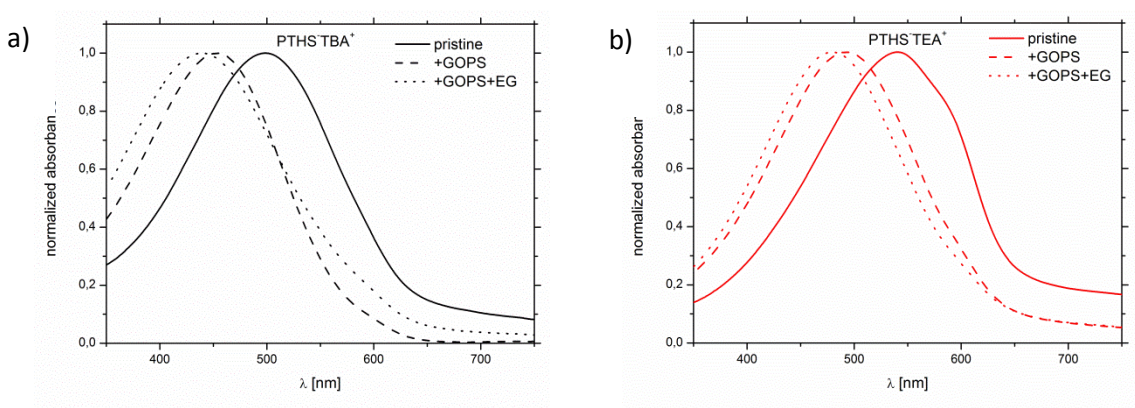


Figure 4-S2: Normalized absorption of thin films spin coated on quartz substrates from aqueous solutions of pristine PTHS-X, with 1 wt% GOPS and with 1 wt% GOPS and 5 vol% EG for a) PTHS⁻TBA⁺ and b) for PTHS⁻TEA⁺.

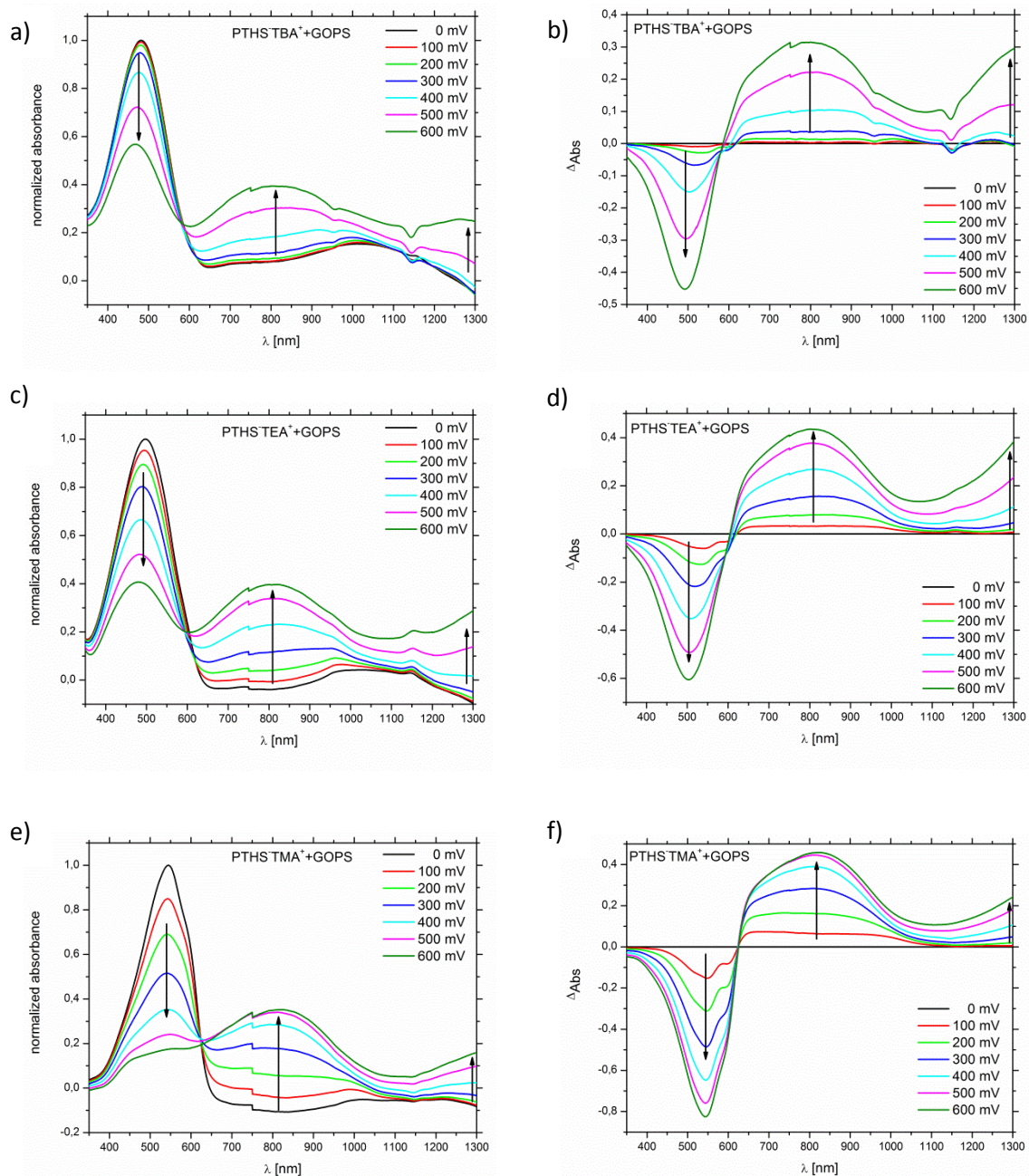


Figure 4-S3: a), c), e) Normalized spectral changes and b), d), f) relative difference between the spectra recorded with bias (0 mV to 600 mV in steps of 100 mV) and the initial spectrum without bias of a PTHSTBA⁺ (a and b), a PTHSTEA⁺ (c and d) and a PTHSTMA⁺ (e and f) film containing GOPS.

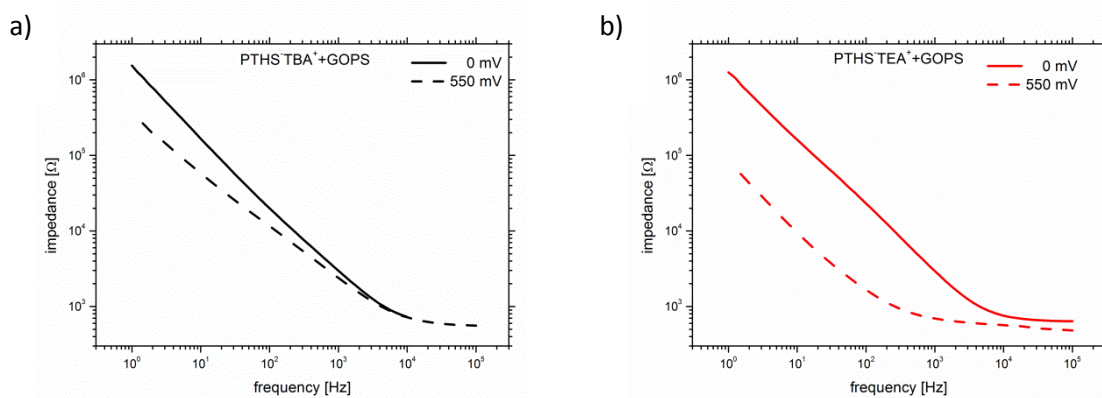


Figure 4-S4: Impedance measurements of thin cross-linked a) PTHS⁻TBA⁺ and b) PTHS⁻TEA⁺ film with 0 and 550 mV applied bias against the reference electrode.

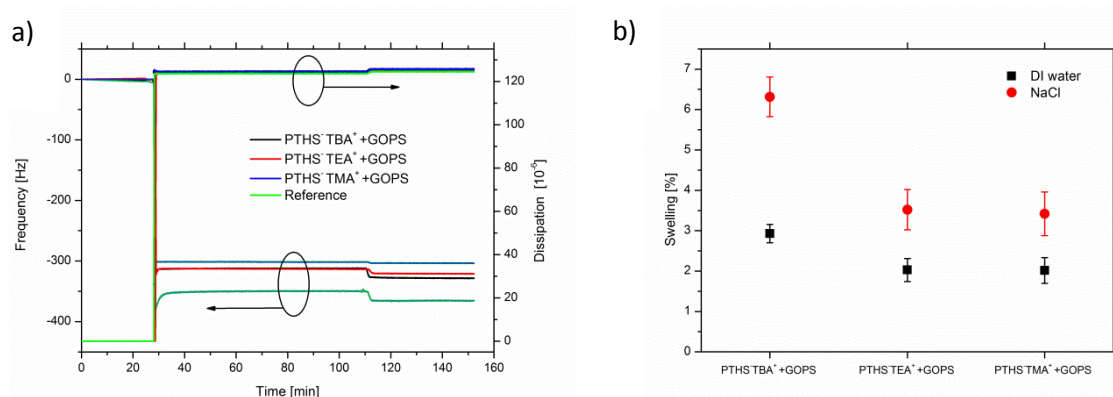


Figure 4-S5: a) 5th overtone frequency and dissipation curves of cross-linked PTHS⁻TBA⁺, PTHS⁻TEA⁺, and PTHS⁻TMA⁺ films, as well as of a pristine reference sensor using QCM-D, and b) swelling percentage of cross-linked PTHS⁻TBA⁺, PTHS⁻TEA⁺, and PTHS⁻TMA⁺ in both deionized water (in black) and NaCl (in red).

Table 4-S1: Summary of the change in thickness (Δd) and corresponding swelling values in deionized (DI) water and NaCl, with standard deviation based on three different thickness measurements.

Material	Initial thickness (d) [nm]	Δd (Di water) [nm]	Δd (NaCl) [nm]	Swelling (DI water) [%]	Swelling (NaCl) [%]
PTHS ⁻ TBA ⁺	16.7 ± 1.3	0.5 ± 0.22	1.05 ± 0.4	2.9 ± 0.2	6.3 ± 0.5
PTHS ⁻ TEA ⁺	18.3 ± 2.4	0.36 ± 0.06	0.6 ± 0.2	2 ± 0.3	3.5 ± 0.5
PTHS ⁻ TMA ⁺	66 ± 10.7	1.3 ± 0.7	2.2 ± 0.4	2 ± 0.3	3.4 ± 0.5
PTHS ⁻ TBA ⁺ + EG	42.2 ± 5.6	2.2 ± 1.2	2.2 ± 1.3	4.6 ± 1.7	5.2 ± 0.6
PTHS ⁻ TEA ⁺ + EG	79.3 ± 57.6	2.6 ± 1.5	3 ± 1.6	5.8 ± 2.5	6 ± 3.4
PTHS ⁻ TMA ⁺ + EG	144, 7 ± 11,6	2,9 ± 1,6	3,1 ± 1,6	2,3 ± 0,5	2,1 ± 0,2

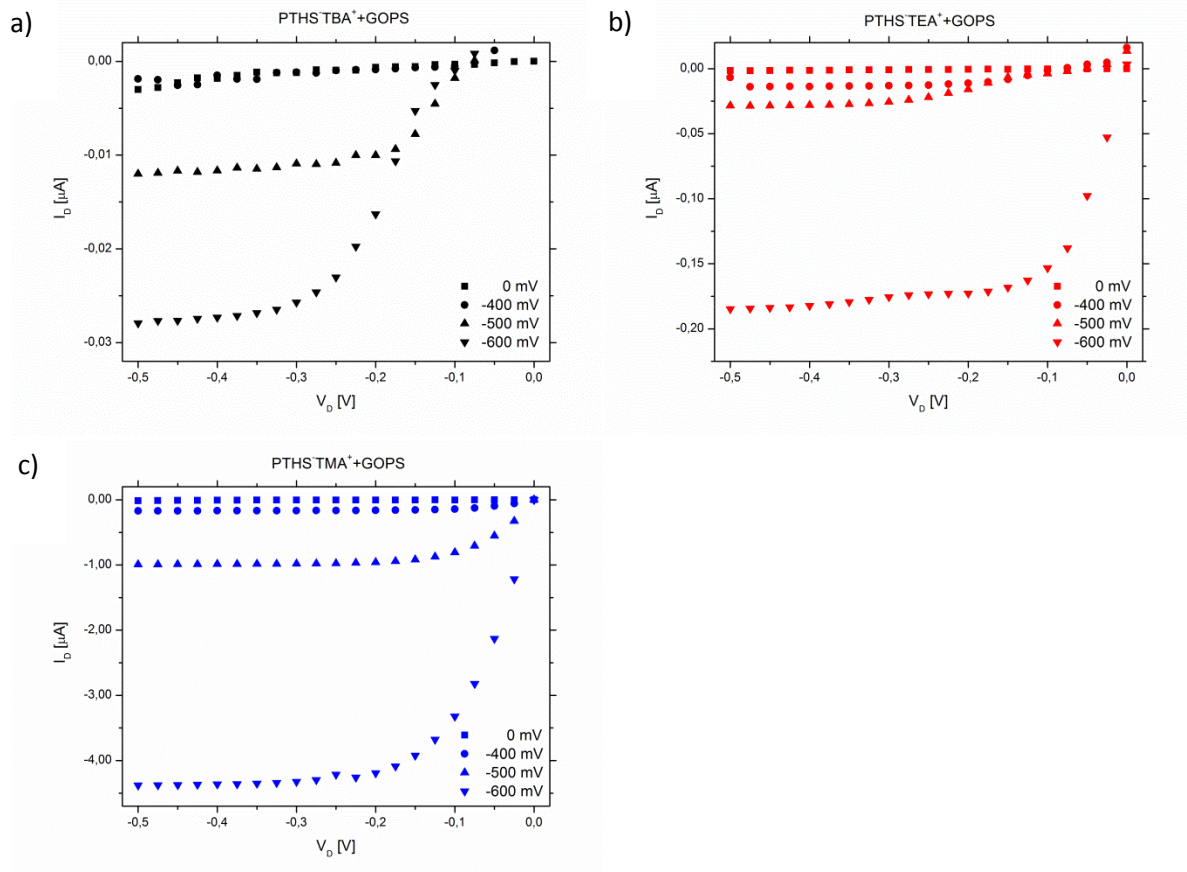


Figure 4-S6: Output characteristics of cross-linked PTHS⁻TBA⁺ (a), PTHS⁻TEA⁺ (b), and PTHS⁻TMA⁺ (c) based device with V_G of 0 mV, 400 mV, 500 mV and 600 mV.

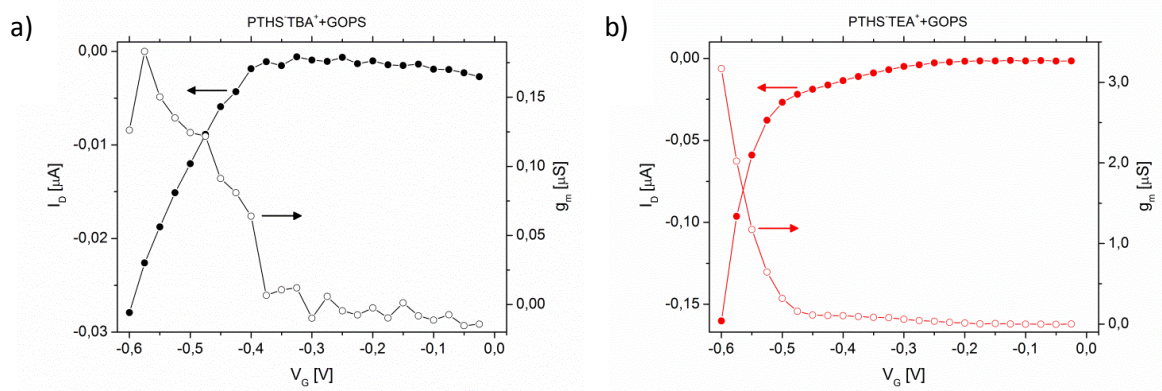


Figure 4-S7: Transfer characteristics and corresponding transconductance of a cross-linked PTHS⁻TBA⁺ (a) and PTHS⁻TEA⁺ (b) based device at $V_D = -500$ mV.

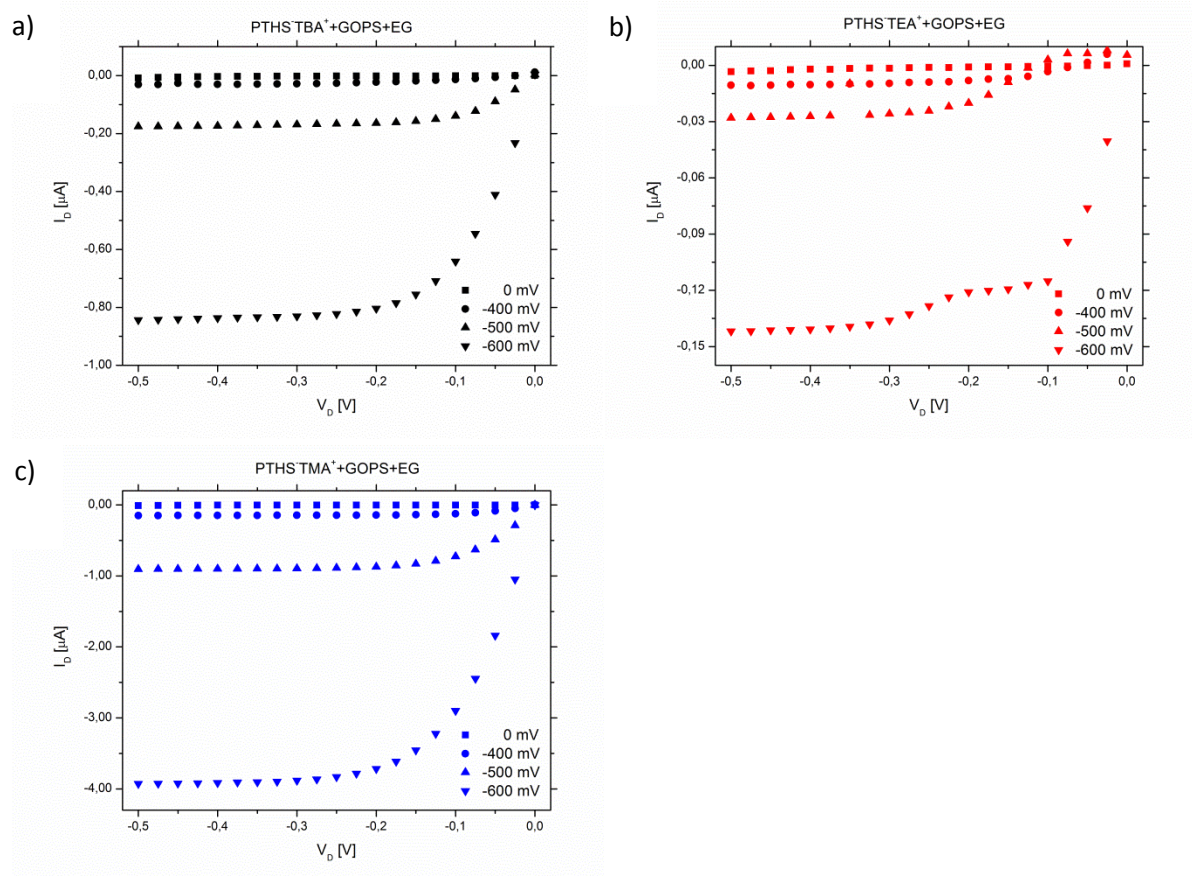


Figure 4-S8: Output characteristics of cross-linked PTHS^{TBA}⁺ (a), PTHS^{TEA}⁺ (b), and PTHS^{TMA}⁺ (c) based devices prepared with EG containing solutions, measured at V_G of 0 mV, 400 mV, 500 mV and 600 mV.

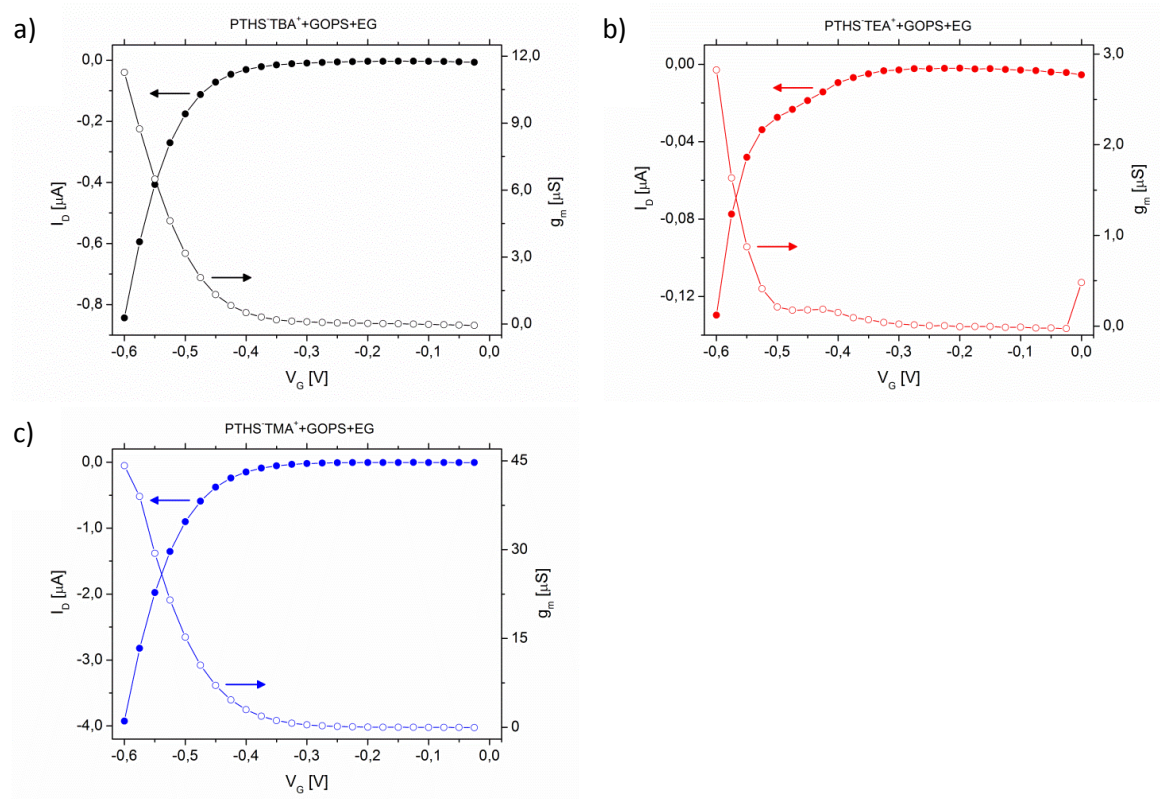


Figure 4-S9: Transfer characteristics and corresponding transconductance of cross-linked PTHS⁻TBA⁺ (a), PTHS⁻TEA⁺ (b), and PTHS⁻TMA⁺ (c) based devices prepared with EG containing solutions, measured at $V_D = -500$ mV.

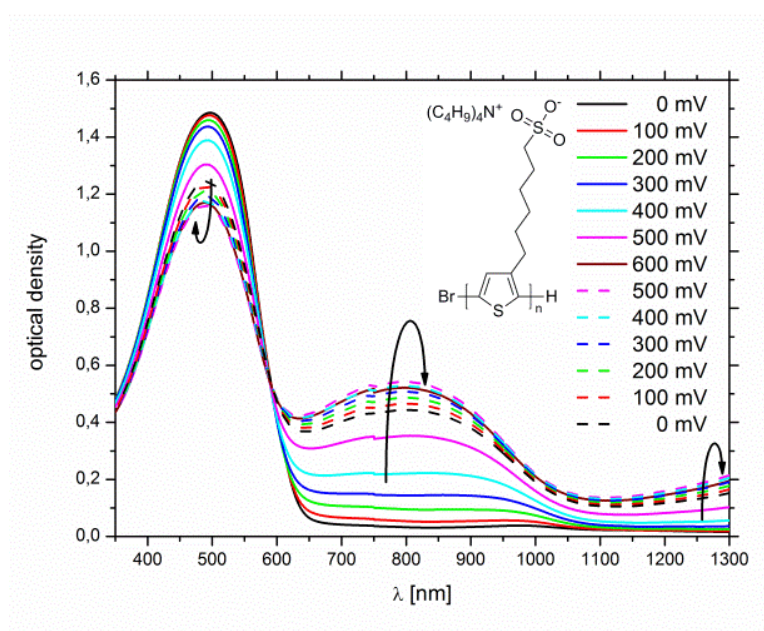
5 CONJUGATED POLYELECTROLYTES BIASED IN AQUEOUS ELECTROLYTES: MECHANISM OF ION EXCHANGE AND OXIDATION

Martina M. Schmidt,^[a] Beate Förster,^[b] Mukundan Thelakkat^{[a,b]*}

[a] University of Bayreuth, Applied Functional Polymers, Macromolecular Chemistry I, Bayreuth, 95440, Germany

[b] Bavarian Polymer Institute (BPI) Bayreuth, 95440, Germany

*E-mail of corresponding author: mukundan.thelakkat@uni-bayreuth.de



Prepared for submission

Abstract

Not all processes taking place in electrolyte biased conjugated polyelectrolytes (CPEs) are understood. Electronic and ionic processes CPEs in contact with aqueous electrolytes and with an applied voltage are interesting for applications in bioelectronics. Here, we show that ion exchange between CPEs having bulky tetraalkylammonium cations and a NaCl-electrolyte solution happens within minutes and independent of voltage application. Furthermore, the composition of ions inside the CPE film is not changing during oxidation processes for a long duration from 5 to 120 minutes. However, using spectroelectrochemical measurements, we detected a dependency of the degree and kinetics of the polyelectrolyte oxidation on the nature of electrolyte as well as on the film thickness. Based on energy-dispersive X-ray spectroscopy for elemental analysis (EDX), we demonstrated that no additional anions of the electrolyte solution are diffusing into the film to oxidize it. The required charge neutralization during partial oxidation of the polymer chain requires the ejection of cations (or insertion of anions); both of which could not be detected by the methods of study here, suggesting that cation ejection from bulk or anion insertion into bulk is perhaps not necessary if the charges accumulate at the electrolyte interface. The fundamental knowledge presented here about redox processes, ion diffusion mechanism and the influence of the electrolyte will pioneer the design of optimized material-electrolyte combinations for bioelectronic devices.

1. Introduction

Conjugated polyelectrolytes (CPEs) are interesting materials for bioelectronic devices. Beside the water-compatibility, CPEs are able to interact with chemical and biological compounds.^[1-3] Still not all processes happening in CPEs are understood. The knowledge of redox process mechanisms in contact with aqueous electrolyte solutions pioneers the design of materials, which can perfectly meet the respective requirements e.g. in bioelectronic applications. For example, the influence of ion diffusion into and out of the polymer film during switching on (oxidation) and switching-off (reduction) of the electrolyte-biased transistor (OECT) determines the rate of charge transport and therefore the transconductance in such a device. An oxidation of the anionic CPE (under applied potential as in an accumulation mode OECT) can be accompanied by the expulsion of a cation into the electrolyte or movement of the anion into the film or a combination of the two. Wudl, Heeger et al. studied anionic poly(3-alkyl thiophene sulfonates) films having Li⁺ and Na⁺ counter-cations and confirm that during charge injection into the conjugated backbone (self-doping), counter cations are ejected into the surrounding solution

to keep the electro neutrality of the film.^[4,5] This voltage controlled cation exchange was proved using cyclic voltammetry measurements in combination with determination of the ion composition in the electrolyte. Similarly Reynolds et al. observed cation ejection in copolymers of polypyrrole and poly(pyrrole propanesulfonate) containing potassium cations on oxidation of the backbone. This was confirmed by quartz crystal microbalance experiments.^[5] Canavesi et al. were the first to propose that in an anionic polyelectrolyte, simultaneous to the ejection of counter cations, anions of the electrolyte are injected in the polyelectrolyte film. This finding was supported by IR analysis and by mismatch of the experimental and the theoretically calculated mass change in relationship to the applied voltage.^[6] However, most of these fundamental studies regarding the self-doping (oxidation) and ion-diffusion in electrolytes carried out earlier involve conjugated polymers and polyelectrolytes obtained by an uncontrolled electrochemical polymerization of monomers in presence of conducting salts. This may cause the incorporation of unwanted ions/salts in these insoluble films during the polymerization step itself. Moreover, in general the mechanism of ion diffusion and exchange also depends on the solvation and size of the concerned ions, both in the polymer film as well as in the electrolyte. In recent publications based on Bernard model of ion diffusion and charge transport in OECT, it has also been suggested that anions diffuse into the polymer film for charge neutralization.^[7]

Based on the above facts, we aimed at studying the cation exchange processes in an anionic CPE in contact with an electrolyte with and without bias. For this, we used a well-soluble anionic conjugated polyelectrolyte [poly(6-(thiophen-3-yl)hexane-1-sulfonate) tetra butyl ammonium (PTHSTBA⁺)] prepared from a precursor polymer obtained by controlled catalyst transfer polymerization. In order to make sure that the anionic CPE is not itself washed away during the experiments, we cross-linked them in films. Using spectroelectrochemical methods (SEC) in combination with elemental analysis performed by energy-dispersive X-ray spectroscopy (EDX), we address the questions; 1) when and under which conditions cation exchange between an anionic polyelectrolyte film and an aqueous electrolyte solution takes place, 2) what is the influence of the applied voltage on ion exchange and 3) if the chosen electrolyte influences the redox processes in CPE films and to what extent. Here we present fundamental information regarding ion diffusion taking place in anionic CPE films in contact with different electrolytes with and without additional bias, so that the influence of ions on the doping of a CPE can be better understood.

2. Results

2.1. Film preparation

Poly(6-(thiophen-3-yl)hexane-1-sulfonate) tetra butyl ammonium (PTHSTBA⁺) is a promising candidate for bioelectronic applications. It exhibits an excellent hole mobility and was already used as p-type channel material in high transconductance accumulation mode electrochemical transistors.^[7,8] Furthermore, a blend of PTHSTBA⁺ and poly(3,4-ethylenedioxythiophene) (PEDOT-S) successfully served as photonic probe to directly visualize membrane organization.^[9] As bioelectronic devices have to be stable in aqueous environment, we added the cross-linker (3-glycidyloxypropyl)trimethoxysilane (GOPS) to a solution of PTHSTBA⁺ before film preparation. The molar ratio of PTHSTBA⁺ monomer to GOPS is selected as 1:2. This is common practice in bioelectronics to prevent the dissolution and delamination of films in aqueous media.^[10–12]

2.2. Spectroelectrochemical investigations

The solution was drop-cast or spin-coated on ITO substrates and served as working electrode in the SEC setup. Together with a Pt-counter electrode it was immersed in a quartz cuvette containing aqueous electrolyte solution or Millipore water. Then a voltage was applied and the CPE starts getting oxidized. The oxidized form leads to structural and electronic changes, which could be monitored by UV-Vis-NIR absorption studies. We applied voltages in steps of 100 mV, starting from 0 mV to 600 mV and back to 0 mV, henceforth referred to as “stepwise cycle”. To avoid electrolysis of the used aqueous 0.1 M NaCl solution, 600 mV was chosen as the maximum bias. To give the system time to equilibrate, every voltage step was applied for five minutes before the absorption was detected between 350 and 1300 nm (Figure 5-1a). Similar absorption curves in Millipore water and 0.1 M TBACl_{aq} are showed in Figure 5-S1. Due to application of voltage, the ground state absorption maximum at 497 nm ($\lambda_{\max,0}$) decreases, whereas two bands representing the oxidized species appear (between 650 and 1100 nm as well as around 1300 nm). By increasing the voltage, these two bands increase, while the absorption at $\lambda_{\max,0}$ further decreases. On the reverse cycle, reduction of the voltage leads to an increase at $\lambda_{\max,0}$ and a decrease of the oxidized species. A clear isosbestic point at 590 nm reflects the reversibility of the occurring processes and the interconversion of the neutral and oxidized species. It is important to note that even a low degree of oxidation of CPE already changes the $\lambda_{\max,0}$ drastically. Therefore, the percentage of reduction of $\lambda_{\max,0}$ does not give directly the amount of oxidation of CPE.

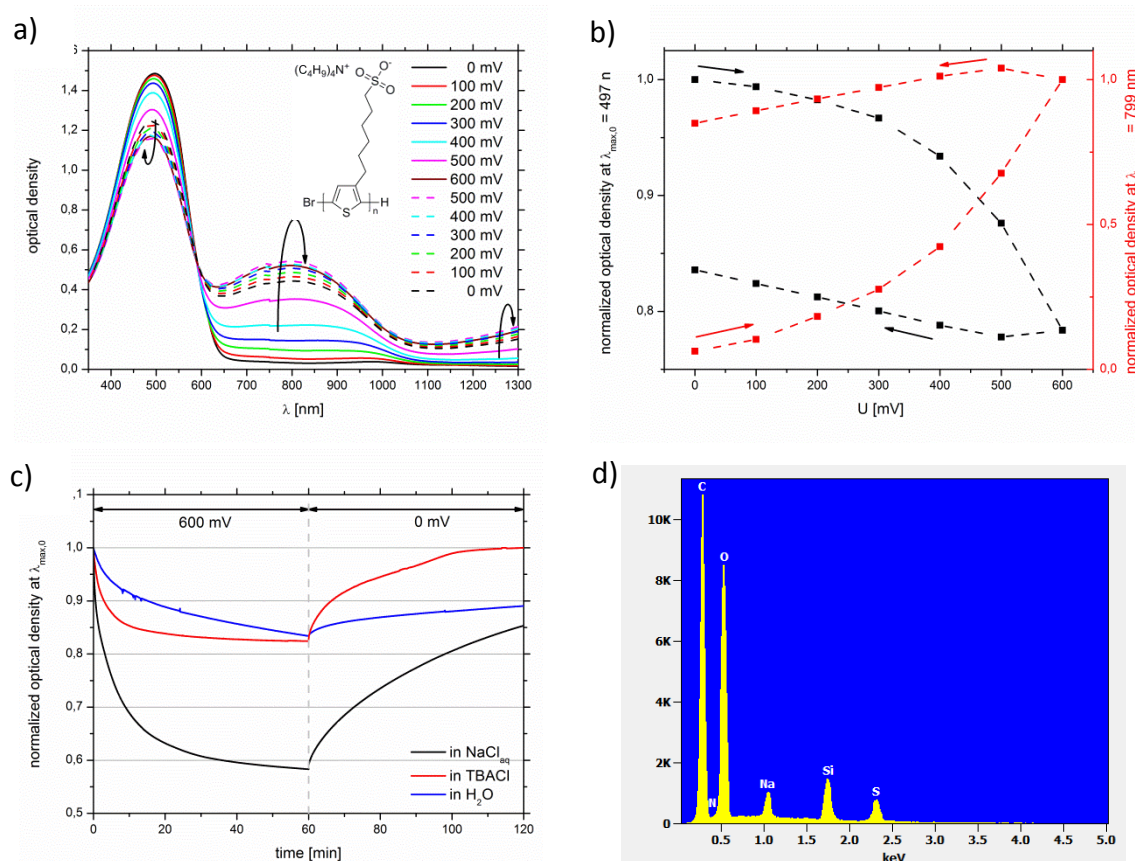


Figure 5-1: Spectroelectrochemical studies showing absorption of a drop-cast, cross-linked PTHS-TBA⁺ film as a function of applied voltage in NaCl_{aq} solution. a) Spectra from 350 to 1300 nm and chemical structure of PTHS-TBA⁺, b) relative optical density at $\lambda_{\max,0}$ (black curve) and $\lambda_{\max,ox}$ (red curve) against applied voltage (0 to 600 mV and back), c) time-dependent absorption measurement at $\lambda_{\max,0}$. The value at $\lambda_{\max,0}$ is normalized and other values are shown relative to this. After 60 minutes at 600 mV, the voltage was set to 0 mV and the absorption recorded for further 60 minutes to observe the recovery. d) Energy-dispersive X-ray spectrum measured on a rectangular space of film 7.

In Figure 5-1b the development of the absorption at $\lambda_{\max,0}$ (black curve) as well as at $\lambda_{\max,ox}$ (red curve) is plotted against the applied voltage. The relative values are normalized with respect to the initial maximum at $\lambda_{\max,0}$ or at $\lambda_{\max,ox}$ (799 nm). In both curves, the oxidation (0 mV to 600 mV) is faster than the re-reduction (600 mV to 0 mV). The re-reduction is even retarded in regard to the decrease of voltage. At $\lambda_{\max,0}$ as well as at $\lambda_{\max,ox}$ the absorption does not recover to the initial value. Hence, we assume that the oxidized state in PTHS-TBA⁺ is stable over time.

To investigate the stability of the oxidized form, the absorption changes against time were recorded. Here, we concentrated on the changes at $\lambda_{\max,0}$, as this wavelength peak can be easily determined even at 0 mV and the changes at $\lambda_{\max,0}$ and $\lambda_{\max,ox}$ are reciprocal to each other. A voltage of 600 mV was applied and the absorption measurement at $\lambda_{\max,0}$ was started simultaneously (Figure 5-1c). After 60 minutes, the voltage was set at 0 mV and the recovery of the absorption was monitored. To be able to compare the degree of oxidation, we normalized the values with respect to the initial absorption value at 0 mV. In aqueous NaCl solution, as soon

as voltage was applied, the absorption decreases rapidly. After about 20 minutes it decelerates, reaching a value of 58 % with respect to the initial absorption. 60 minutes after the voltage was removed, the absorption recovered to a value of 85 % of the initial value. To ascertain if the used 0.1 M NaCl_{aq} solution influences the redox processes, the time-dependent measurement was repeated in Millipore water as well as in 0.1 M aqueous tetra butyl ammonium chloride solution (Figure 5-1c). In Millipore water, the oxidation of PTHSTBA⁺ was very slow. After 60 minutes, only 15 % were oxidized. The re-reduction is also slower than that observed in NaCl_{aq}. After 60 minutes, the absorption recovered to 89 %. In 0.1 M TBACl_{aq} solution, the oxidation happened faster than in Millipore water and reached a plateau at 82 % after around 20 minutes. This value did not differ much from the one in Millipore water. In TBACl_{aq} the re-reduction is slower than the oxidation process. However, the absorption recovered completely to its initial value. To obtain a whole picture of the processes and kinetics, we determined the conductivity of the aqueous solutions. Purified water showed a conductivity of 0.001 mS/cm, 0.1 M TBACl_{aq} of 6.42 mS/cm and 0.1 M NaCl_{aq} of 9.85 mS/cm. As Millipore water is less conductive, the redox reactions of PTHSTBA⁺ films in purified water are very slow. Though, the conductivity of TBACl_{aq} and NaCl_{aq} are in the same range, the degree and kinetics of the redox processes differ. Hence, the nature of the used electrolyte influences the rate of redox processes, especially how fast the recovery is. To monitor if the absorption is changing when immersed in NaCl_{aq}, the absorption at $\lambda_{\max,0}$ was detected for two hours without application of voltage (Figure 5-S2). As no change in absorption occurred, it can be concluded that NaCl_{aq} does not influence the electronic absorption.

Furthermore, the influence of the film thickness on oxidizability and kinetics was examined by time-dependent absorption measurements of drop-cast (around 1200 nm) and spin-coated (around 40 nm) films. Here NaCl_{aq} as well as Millipore water was used as medium (Figure 5-S3). In both solutions, the thinner films respond faster to the applied voltage than the thicker ones. The thin film measured in NaCl_{aq} was oxidized to a saturation value of $\lambda_{\max,0}$ (absorption decay up to 55%) after a few minutes. In contrast, the drop-cast film did not reach a saturated oxidation level even after 60 minutes. This results in a slightly different degree of oxidation: while the 40 nm thin film reached a value of 55 % of original absorption, the drop-cast reached 58 % of the $\lambda_{\max,0}$. 60 minutes after removal of the voltage both films recovered to a value of 85 % of original optical density, but with different rates. In Millipore water similar trends were observed regarding the film thickness. As Millipore water exhibits a negligible conductivity, the recovery of the film absorption was monitored for 190 minutes instead of 60 minutes. Nevertheless, the absorption of both films did not recover completely. The spin-coated film flattens off at about

92 % after around 60 minutes, whereas the drop-cast one needed much longer. Thus, independent of the used electrolyte, the film thickness has an influence on the degree and kinetics of the redox processes.

Based on this result, the time-dependent spectroelectrochemical measurement was repeated in 0.1 M TBACl_{aq} and 0.1 M NaCl_{aq} solutions, using the same film (700-1000 nm) to exclude film thickness effects (Figure 5-S4). As the oxidation was completely reversible in TBACl_{aq} and as the cations of the electrolyte solution are chemically identical to the ones in the polyelectrolyte, the measurement in this electrolyte was done first. Afterwards, the film was rinsed with purified water and the measurement was repeated in 0.1 M NaCl_{aq}. As seen before on different films, the redox processes proceeded to a higher degree and at a faster rate in NaCl_{aq} than in TBACl_{aq} solution. As the conductivities of NaCl_{aq} and TBACl_{aq} are comparable and thickness effects are excluded, the difference in swelling and ion diffusion may be the reasons for the differences in the redox processes.

2.3. EDX measurements

Table 5-1: Results of energy-dispersive X-ray spectroscopy for elemental analysis (EDX) on cross-linked PTHS⁻TBA⁺ films after different treatment given in atom %. The atom % errors are listed in Table 5-S1. Representative EDX spectra of the films are shown in Figure 5-S5.

number of film	film treatment	atom %							ratio	
		C	N	O	Na	Si	S	Cl	Si:S	Na: $\frac{S}{2}$
Batch A										
1	5 min immersed in NaCl _{aq}	39.5	2.3	42.3	2.1	8.3	5.6	0	1.5	0.7
2	5 min 600 mV in NaCl _{aq}	39.3	2.3	42.6	2.0	8.2	5.5	0	1.5	0.7
3	10 min immersed in NaCl _{aq}	38.8	2.1	42.8	2.3	8.3	5.8	0	1.4	0.8
4	10 min 600 mV in NaCl _{aq}	38.7	2.2	42.9	2.2	8.3	5.7	0	1.4	0.8
Batch B										
5	1 h immersed in NaCl _{aq}	38.2	2.0	42.6	2.6	7.8	7.0	0	1.1	0.7
6	1 h 600 mV in NaCl _{aq}	38.4	1.8	41.9	3.0	7.6	7.4	0	1.0	0.8
7	2 h immersed in NaCl _{aq}	38.0	1.8	42.3	3.0	7.8	7.1	0	1.1	0.9
8	1h 600 mV, 1h 0 mV in NaCl _{aq}	37.5	1.9	42.0	3.0	8.1	7.4	0	1.1	0.8
9	stepwise cycle in NaCl _{aq}	38.7	1.9	41.6	2.8	7.7	7.2	0	1.1	0.8

To get more insight how the electrolyte solution is influencing the redox processes, we treated cross-linked PTHS⁻TBA⁺ films in different ways, rinsed them with Millipore water to remove any NaCl crystals physisorbed to the surface and measured EDX. The experiments were conducted in

two different batches, A and B for practical reasons of measurement. All the films were immersed in 0.1 M NaCl_{aq} and some of them were additionally biased; Films **1, 3, 5 and 7** were immersed in NaCl solution for 5, 10, 60 and 120 minutes respectively. Films **2, 4 and 6** were additionally biased continuously with a voltage of 600 mV during the time of immersion in NaCl electrolyte. Additionally, films **8 and 9** were biased differently. For example, film **8** (unlike film **6**) was not directly removed after biasing at 600 mV for 60 minutes, but the voltage was set at 0 mV for additional 60 minutes to understand the ion diffusion during de-doping process. Thus, the treatment of film **8** corresponds to the same conditions as used for time-dependent SEC measurements. Film **9** was subjected to the stepwise bias cycle as described earlier in chapter 5-2.2. As the electron-beam is of high-energetic nature and the films consist of lightweight elements, they were easily permeated. To eliminate signals of the ITO substrate, we used drop-cast films and measured rectangular spaces. Some single point measurements served to ensure that all elements are considered, which are present in the volume of the film. Table 5-1 gives the average values in atom percentage for each element detected in the films. The error of the atom% values can be found in Table 5-S1. The X-rays emitted from nitrogen atoms can excite carbon or oxygen atoms and thus not all emitted x-rays of nitrogen are detected. Thus, the atom % values for carbon and oxygen are overestimated by the measurement technique. As EDX analysis was performed in low vacuum, some additional oxygen atoms can get absorbed on the surface of the samples. Hence, the obtained atom % value of oxygen is higher than the real value in the sample.

To eliminate the described uncertainties, untreated samples were measured in both batches to determine the real Si:S ratio present in the samples and to use it as a reference in all measurements. Even though the molar ratio of PTHSTBA⁺ monomer to GOPS is selected as 1:2 (which corresponds to a Si:S ratio of 1:1), the measured ratios are 1:1.6 and 1:1.2 for the batches A and B. This can happen due to non-completion of cross-linking and thus washing away of some of the GOPS molecules. The ratio of Si atoms in GOPS to the sulfur atoms in PTHSTBA⁺ verify the correctness of the obtained values, as this ratio cannot change in one batch due to the different treatments. Comparing the films prepared from batch A, the experimentally determined ratio is not changing. This is also the case for the films prepared from batch B. In all films treated with NaCl_{aq} (samples **1-9**), sodium was detected. A measure for ion exchange is the ratio of the sodium (coming from NaCl_{aq}) to the sulfur atoms (1 S from hexylside chain and 1 S from thiophene ring of the CPE). For each film, which was in contact with NaCl_{aq} (films **1 to 9**), the same Na: $\frac{S}{2}$ ratio of around 0.8 was obtained. This was independent of the immersion time (5 minutes, 10 minutes, one hour or two hours) and also of the application of bias. The small

variations of the ratios are in the range of the measurement errors, which can be found in table S1. According to this ratio, 80 % of the TBA counter ions in the films were exchanged with sodium ions of the electrolyte. As the Na: $\frac{S}{2}$ ratio is not changing over longer time scale, the ion exchange can be considered to be completed within just 5 minutes immersion in aqueous NaCl solution.

As both, sodium and sulfur, showed clear signals in the EDX-spectroscopy without interferences, we consider the both values to be very accurate. In the aqueous NaCl solution the ions will be dissociated and hydrated, because of the low concentration (0.1 M). In comparison to the sterical demanding tetra butyl ammonium ion, in which the positive charged nitrogen is not easily accessible, sodium ions are more electropositive and are more likely to build up an ionic bond. Thus, the small sodium ions will diffuse inside the polyelectrolyte films to take over the stabilization of the negative charged side chain sulfonate from the tetra butyl ammonium ions, which will simultaneously diffuse in the aqueous solution and be hydrated by water molecules to maintain charge neutralization.

Chloride ions were found in none of the films **1** to **9**. To make sure that this is the case for the whole volume or thickness of the film, different spots were measured on the films **1** to **4** and film **8** as typical cases. The resulting spectra exhibited only signals for In L α 1 and Sn L α 1, indicating that the ITO surface was reached by the electron beam and thus the complete thickness of the film was considered (Figure 5-S6). Nevertheless, no chloride signal was achieved.

3. Discussion

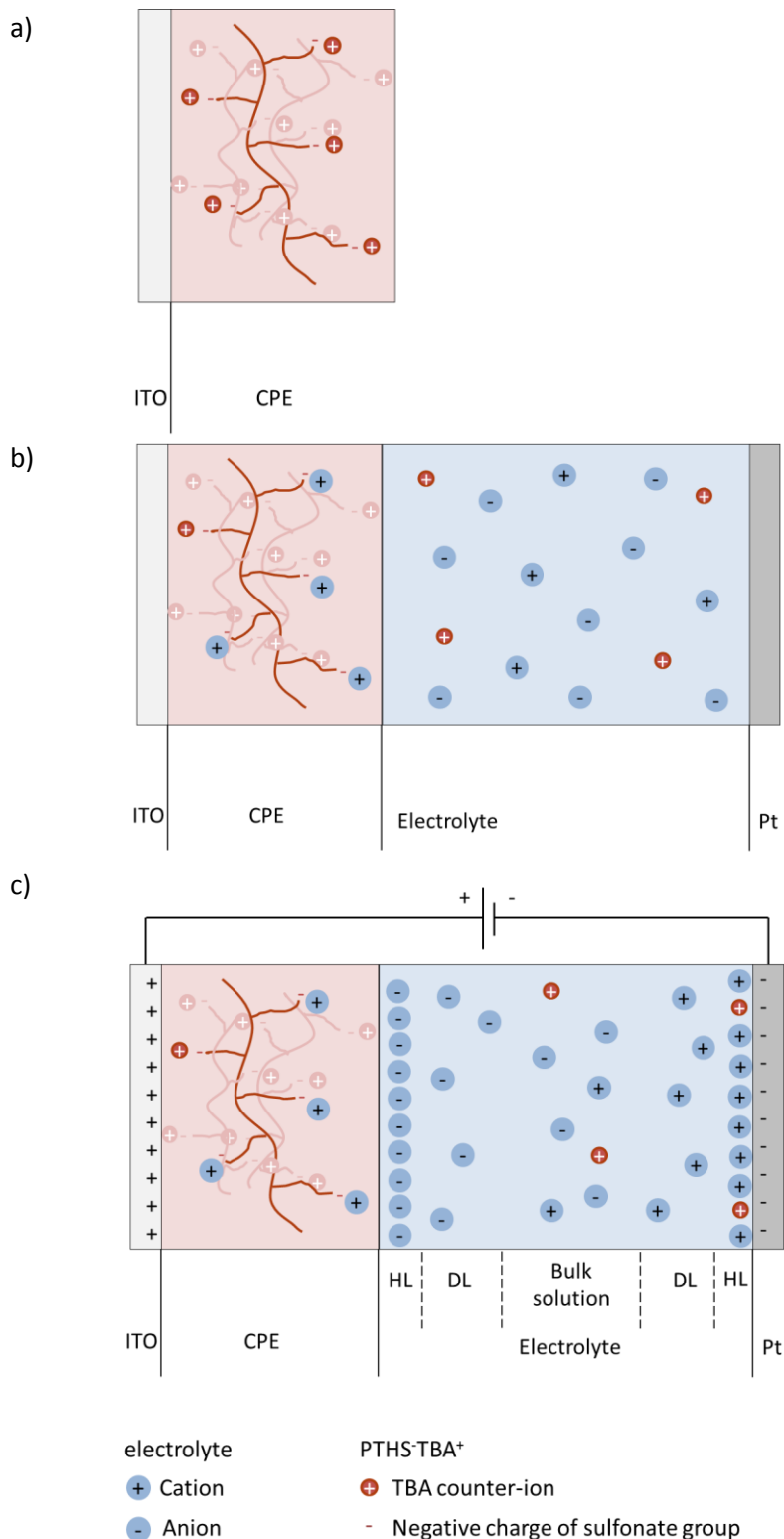


Figure 5-2: Schematic of the successive running processes in a (a) PTHS-TBA⁺ film (b) immersed in electrolyte solution and (c) with applied voltage.

Based on the SEC and EDX results we propose the following mechanism for the successive steps happening in an electrolyte-biased CPE film as shown schematically in Figure 5-2. To simplify the

schematic, the hydration shells of the ions in aqueous solution are not shown. In the untreated film (a), the negative charged sidechains of the anionic polyelectrolyte are compensated by TBA counter ions. As soon as the PTHS⁻TBA⁺ film is immersed in an electrolyte solution, TBA counter ions are exchanged with the cations of the electrolyte (b). This proceeds independent of the application of voltage. According to the EDX results around 80 % of the counter ions are exchanged after 5 minutes immersion in electrolyte. As soon as voltage is applied between the ITO substrate and a Pt-counter electrode, the Cl⁻ anions of the electrolyte migrate to the surface of the PTHS⁻TBA⁺ film, due to the positive charge accumulation in the underneath ITO substrate. However, the absence of Cl⁻ ions within the films clearly indicate that the charge neutralization of partially oxidized CPE is achieved by partial ejection of counter cations (TBA⁺ or Na⁺) and not by infiltration of Cl⁻ ions. The cations in the electrolyte are attracted by the negatively charged Pt-electrode. These processes result in an electrical double layer (EDL) between the surface of the PTHS⁻TBA⁺ film and the electrolyte solution as well as between the Pt-electrode and the electrolyte (c). As per the Stern's Model, the EDL consists of Helmholtz layers (HL) and diffuse layers (DL).^[13] HLs are compact monolayers of ions built at interfaces. DLs are resulting of the attractive forces on the ions, which lead to zones with accumulated cations resp. anions. Ions, which are too far away from the interfaces to be affected, are stocked inside the bulk solution. EDLs operate as capacitors with remarkable high capacitances per area at the interfaces.^[13,14] This leads to low operational voltages of e.g. organic field effect transistors, which is necessary for the usage in bioelectronic systems.^[14,15] In thicker PTHS⁻TBA⁺ films the construction of an EDL at the interface to the electrolyte needs more time. This was seen in SEC, where the redox processes were much slower for thicker than for thinner films. Apart from the film thickness, the kinetics depend on the used electrolyte. Sodium ions can diffuse much faster than the bulky tetra butyl ammonium ions leading to a faster buildup of EDL. In Millipore water the conductivity is negligible and correspondingly the EDL is built very slowly and the redox processes need more time. In addition, the oxidizability of the film depends on the used electrolyte solution, as the counter ions of the CPE film are exchanged with the cations in the electrolyte. The SEC investigations revealed a much higher relative intensity ratio of the absorption at $\lambda_{\max,0}$ and the absorption at $\lambda_{\max,ox}$ when oxidized in NaCl_{aq} than in TBACl_{aq} or Millipore water. The ion exchange between the PTHS⁻TBA⁺ film and the electrolyte probably leads to a change in the doping level and also in the stability and kinetics of the oxidized species. It is already known that polyelectrolytes with either sodium or tetra butyl ammonium counter ions differ in their electrical conductivity.^[16] Mai et al. proposed based on absorption and GIWAXS results that the reason is a higher doping efficiency and a better crystallinity for small counter ions like sodium

compared to the bulky tetra butyl ammonium.^[16] When immersed in $TBACl_{aq}$ the TBA counter ions of the film can only be exchanged by the chemically identical tetra butyl ammonium ions of the electrolyte resulting in no change in the doping level and a completely recovering redox-process. We assume, that in purified water some tetra butyl ammonium counter ions will diffuse out of the film caused by concentration gradient. This leads to a change in the doping level, as well. As a result the absorption in purified water did not recover completely.

Reynolds et al. suggested based on quartz crystal microbalance experiments that in conducting pyrrole polyelectrolytes counter cations are ejected upon oxidation into the surrounding electrolyte and will diffuse back into the film upon reduction.^[5] Canavesi et al. proceed with this question and checked also with QCM the relationship between mass change of a polythiophene based polyelectrolyte upon oxidation and the applied charge. A linear behavior was obtained, but the mass change was lower than expected. Supported by IR analysis, it was proposed that beyond the ejection of counter cations, anions of the electrolyte are injected in the polyelectrolyte film simultaneously. The counter cation flux into the electrolyte was claimed to be the same for different counter cations independently of their size and the concentration of ions in the surrounding electrolyte.^[6] The reported mass change upon application of voltage could be an effect of the HL, built on the CPE surface. As it is a surface effect the mass expected from Canavesi et al. should not be reached. The with IR spectroscopy detected anion could be attached to the surface instead of diffused inside the film. With EDX we were able to clearly show that no anions of the electrolyte are diffusing into the film. As the content of sodium cations from the electrolyte is not changing inside the films independent of the previous treatment, we suggest that no bulk effect occurs and the detected mass changes are obtained due to attached HL.

4. Conclusion

In conclusion, we showed via SEC and EDX investigations that an exchange of ions between an anionic polyelectrolyte film and an electrolyte solution takes place as soon as both are in contact. Contrary to the general acceptance, no application of voltage is needed to indicate the exchange. We assume that instead of a bulk effect, electrical double layers are built between the surface of the film and the electrolyte solution as well as between the counter-electrode and the electrolyte. This is reinforced by the detected constant composition of ions in oxidized and recovered CPE films. The degree and kinetics of the anionic polyelectrolyte oxidation depends on the used electrolyte. As bulky counter ions of the polyelectrolyte film are exchanged by smaller, mobile ions from the electrolyte, the oxidation will proceed faster and to a higher degree. We

also showed that the film thickness plays an important role for the oxidation kinetics. Since it is known for organic electrochemical transistors that the response time and the transconductance are dependent of the used film thickness, the effect of the film thickness on the redox processes in polyelectrolyte films should be further investigated. With a clear insight into the redox processes and the influence of the electrolyte solution, we are able to design materials and electrolyte biased devices with optimized response times and transfer characteristics.

Experimental section

Synthesis:

The synthesis of PTHSTBA⁺ is already published.^[9] The molecular weight of the precursor polymer P3BrHT was analyzed by MALDI-TOF MS ($M_n = 18.5$ kg/mol, $M_w = 18.9$ kg/mol, average 75 repeating units) and Size Exclusion Chromatography ($M_n = 18.2$ kg/mol, $M_w = 20.8$ kg/mol, PDI: 1.14).

Film preparation:

The used films were prepared from a solution of 1 wt% PTHSTBA⁺ in purified water. To access films, which are stable in aqueous media, 1 wt% of GOPS as cross-linker was added. After the solutions were filtered, they were drop-casted resp. spin-coated on cleaned and plasma-etched ITO slides. The films were annealed at 90 °C for 1.5 h.

Spectroelectrochemical measurements:

Spectroelectrochemical measurements were performed in a 1 cm quartz cuvette containing 0.1 M NaCl_{aq}, 0.1 M TBACl_{aq} resp. purified water. A platinum wire was used as counter electrode. The on ITO prepared film and the platinum wire were connected to a source meter to apply voltage.

For the “stepwise cycle” every voltage was applied for seven minutes, consisting of five minutes waiting time and two minutes for recording the spectra. The voltage was changed by steps of 100 mV to a maximal voltage of 600 mV. Afterwards, the voltage was reduced till 0 mV also in steps of 100 mV.

For the spectroelectrochemical measurements against time, the progress of the oxidation was recorded by measuring the absorption at the wavelength of the respective ground state maximum. First, a voltage of 600 mV was applied for one hour. Afterwards it was removed and the change was recorded once more for one hour or even longer.

All absorption spectra were recorded using a Jasco V670 spectrophotometer.

Conductivity of electrolyte solutions:

The conductivity of the used electrolyte solutions and the purified water were measured with a conductivity meter CDM230 from MeterLab, which was calibrated using a KCl standard.

EDX/WDX:

The uncoated samples were investigated under low vacuum conditions in a FEI Quanta FEG SEM using a 100mm² UltraDry detector (SDD) from Thermo Fisher Scientific for EDS. To avoid charging, the chamber pressure was set to 100 Pa water vapor. To measure light elements an acceleration voltage of 5 kV was used, keeping the interaction volume of the electron beam in the range of film thickness, thus no signal from the underlying ITO layer was seen.

Corresponding Author

E-mail: mukundan.thelakkat@uni-bayreuth.de

Acknowledgements

Financial support from DFG (GRK 1640) is kindly acknowledged. Martina M. Schmidt acknowledges the support from Elite Study program, Macromolecular Science at the University of Bayreuth and GRK1640.

References

- [1] L. Chen, D. W. Mcbranch, H.-L. Wang, R. Helgeson, F. Wudl, D. G. Whitten, *PNAS* **1999**, *96*, 12287.
- [2] H.-A. Ho, M. Boissinot, M. G. Bergeron, G. Corbeil, K. Doré, D. Boudreau, M. Leclerc, *Angew. Chem. Int. Ed.* **2002**, *41*, 1548.
- [3] H. A. Ho, A. Najari, M. Leclerc, *Acc. Chem. Res.* **2008**, *41*, 168.
- [4] A. O. Patil, Y. Ikenoue, N. Basescu, N. Colaneri, J. Chen, F. Wudl, A. J. Heeger, *Synth. Met.* **1987**, *20*, 151.
- [5] J. R. Reynolds, N. S. Sundaresan, M. Pomerantz, S. Basak, C. K. Baker, *J. Electroanal. Chem.* **1988**, *250*, 355.
- [6] G. Zotti, S. Zecchin, G. Schiavon, A. Berlin, G. Pagani, A. Canavesi, *Chem. Mater.* **1997**, *9*, 2940.
- [7] S. Inal, J. Rivnay, P. Leleux, M. Ferro, M. Ramuz, J. C. Brendel, M. M. Schmidt, M. Thelakkat, G. G. Malliaras, *Adv. Mater.* **2014**, *26*, 7450.
- [8] J. C. Brendel, M. M. Schmidt, G. Hagen, R. Moos, M. Thelakkat, *Chem. Mater.* **2014**, *26*, 1992.
- [9] E. Zeglio, M. M. Schmidt, M. Thelakkat, R. Gabrielsson, N. Solin, O. Inganäs, *ChemistrySelect* **2016**, *1*, 4340.
- [10] S. Zhang, P. Kumar, A. S. Nouas, L. Fontaine, H. Tang, F. Cicoira, *APL Mater.* **2015**, *3*, 14911.
- [11] M. Sessolo, D. Khodagholy, J. Rivnay, F. Maddalena, M. Gleyzes, E. Steidl, B. Buisson, G. G. Malliaras, *Adv. Mater.* **2013**, *25*, 2135.
- [12] D. Martin, G. Malliaras, *ChemElectroChem* **2016**, *3*, 686.
- [13] O. Stern, *Zeitschrift für Elektrochemie* **1924**, *30*, 508.
- [14] L. Herlogsson, X. Crispin, N. D. N. D. Robinson, M. Sandberg, O.-J. O. J. Hagel, G. Gustafsson, M. Berggren, *Adv. Mater.* **2007**, *19*, 97.
- [15] O. Larsson, E. Said, M. Berggren, X. Crispin, *Adv. Funct. Mater.* **2009**, *19*, 3334.
- [16] C. Mai, R. A. Schlitz, G. M. Su, D. Spitzer, X. Wang, S. L. Fronk, D. G. Cahill, M. L. Chabinyc, G. C. Bazan, *J. Am. Chem. Soc.* **2014**, *136*, 13478.

Supporting Information

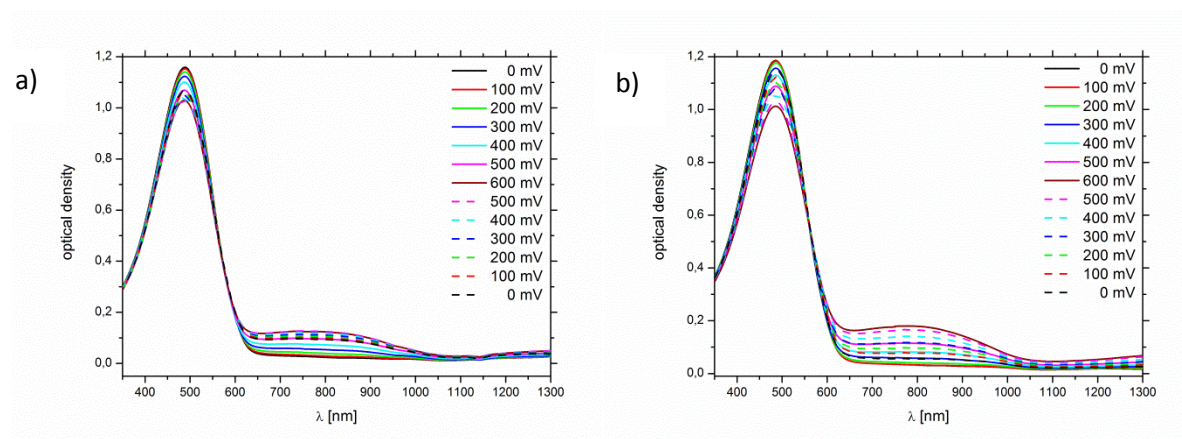


Figure 5-S1: Spectroelectrochemical absorption of drop-cast, cross-linked PTHS-TBA⁺ films as a function of applied voltage measured a) in Millipore water and b) in 0.1 M TBACl_{aq} solution.

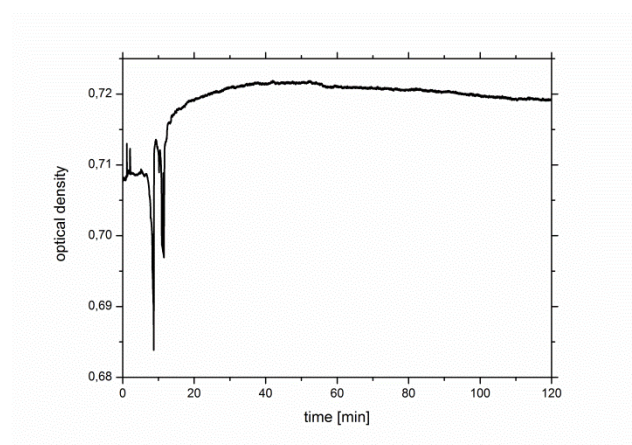


Figure 5-S2: Optical density at $\lambda_{\max,0}$ of a drop-casted, cross-linked PTHS-TBA film immersed in 0.1 M NaCl_{aq} with no current applied against the time.

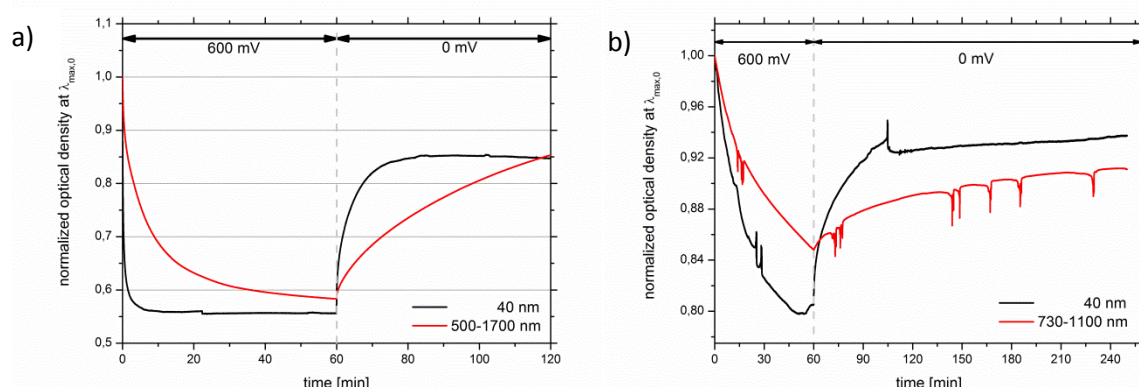


Figure 5-S3: Time-dependent absorption measurement at $\lambda_{\max,0}$ in a) 0.1 M NaCl_{aq} and b) in H₂O of PTHS-TBA films with different thickness. The values are normalized with respect to the maximal ground state absorption. After 60 minutes at 600 mV, the current was removed and the absorption was recorded further.

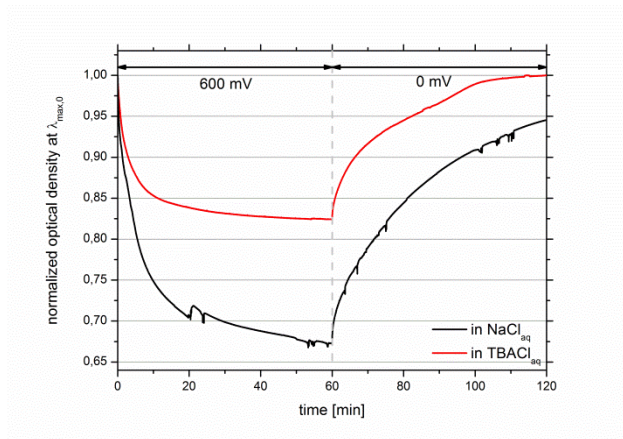
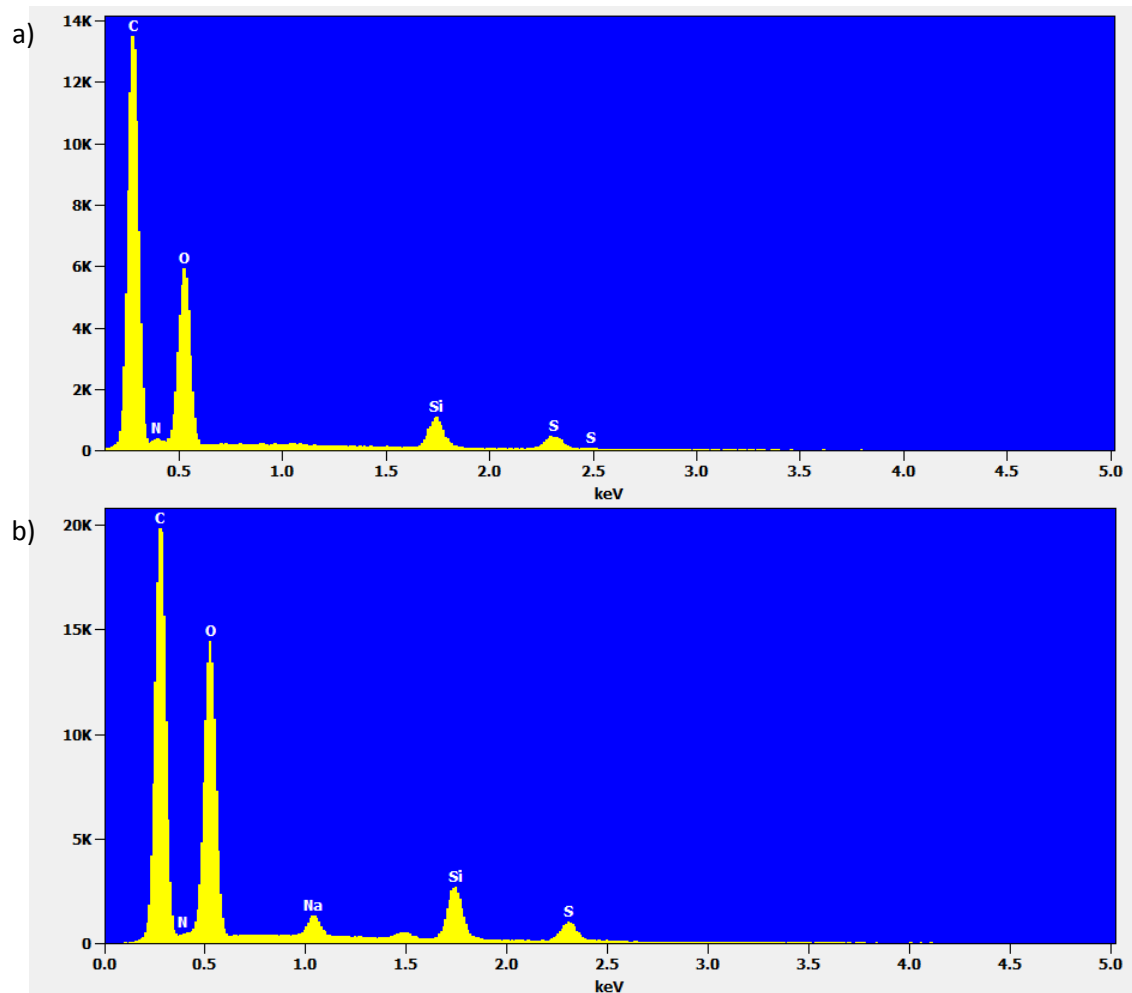
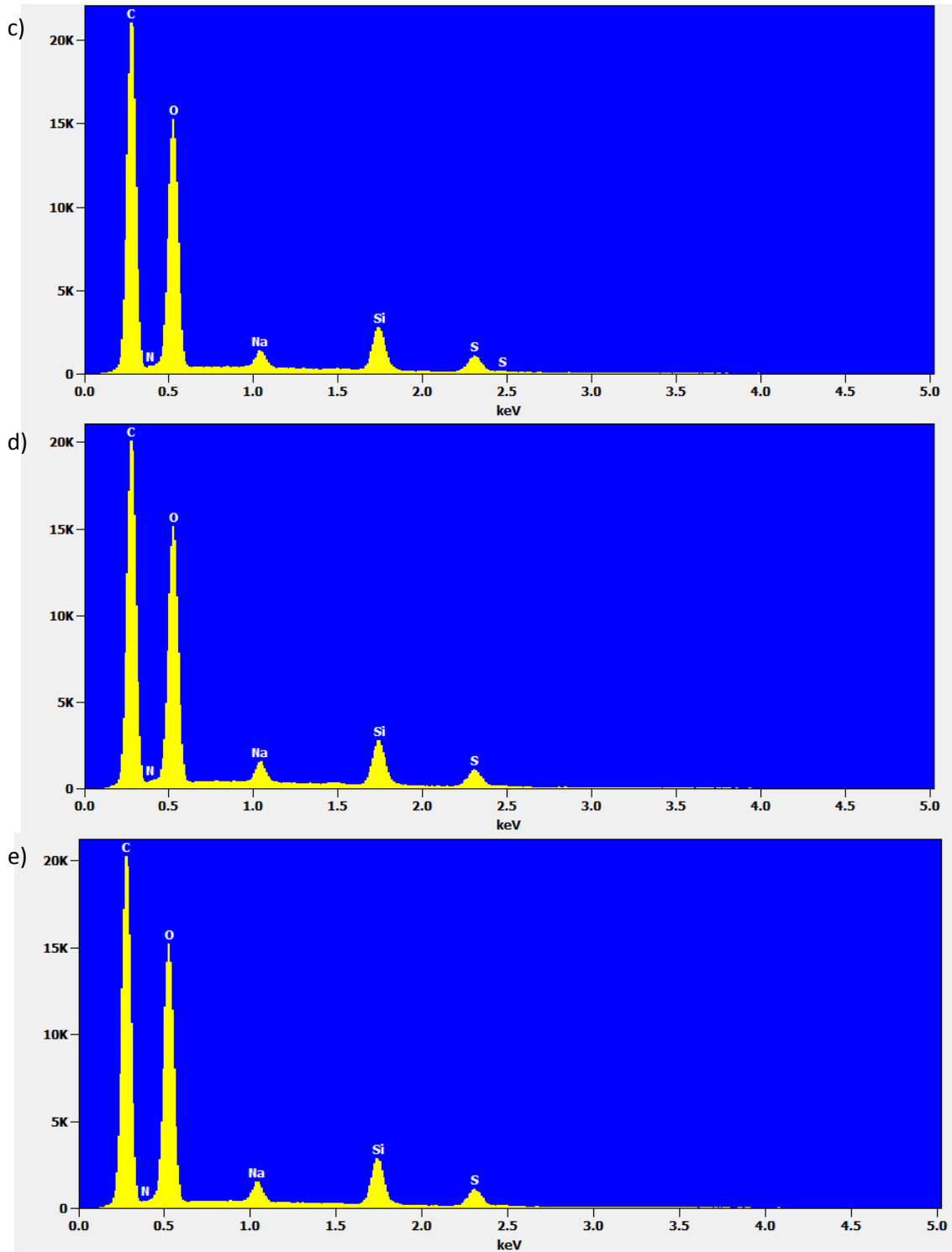
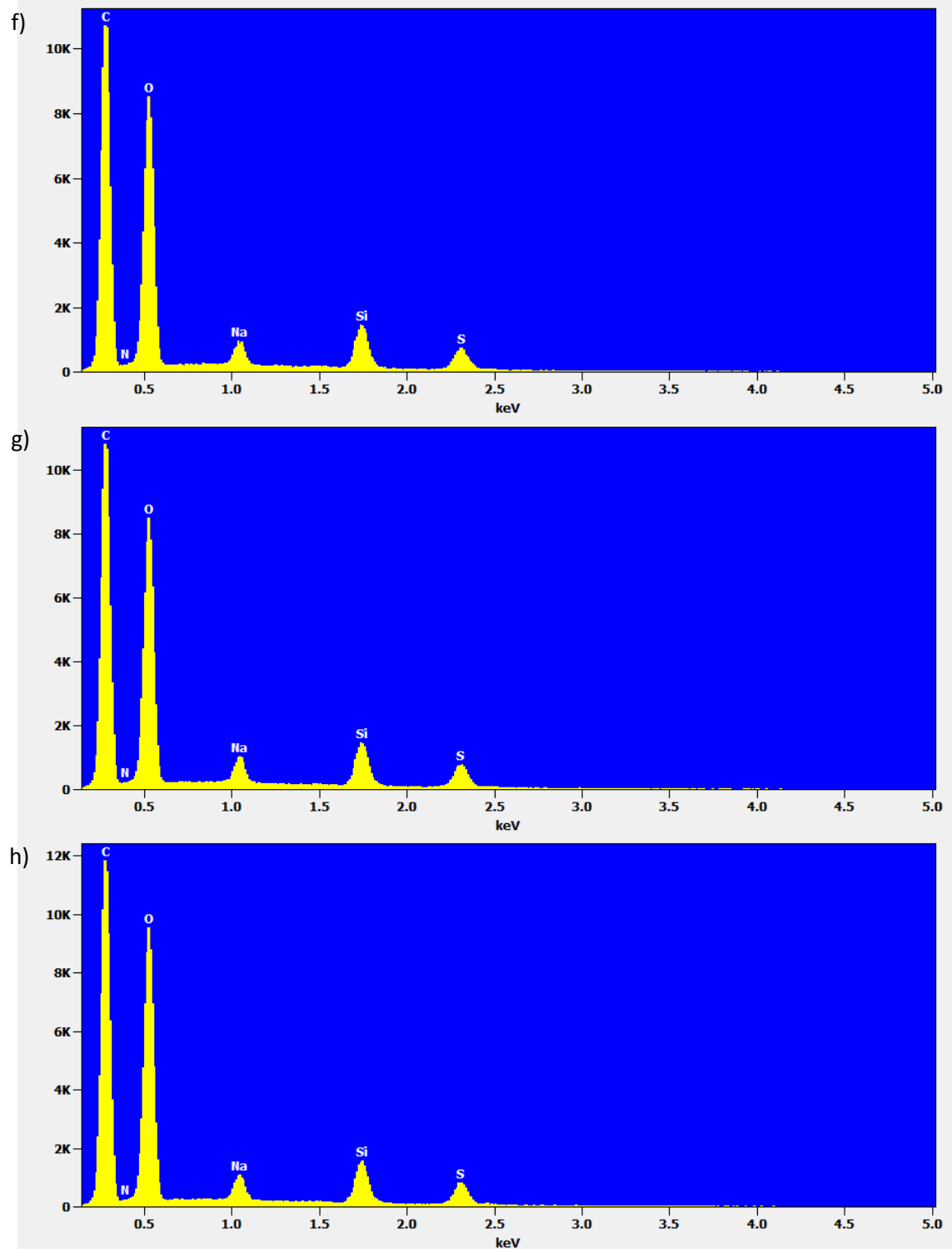


Figure 5-S4: Time-dependent absorption measurement at $\lambda_{\max,0}$ in 0.1 M NaCl_{aq} and in H_2O of the same PTHS-TBA film. The values are normalized with respect to the maximal ground state absorption. After 60 minutes at 600 mV, the current was removed and the absorption was recorded for further 60 minutes.



Conjugated polyelectrolytes biased in aqueous electrolytes:
mechanism of ion exchange and oxidation





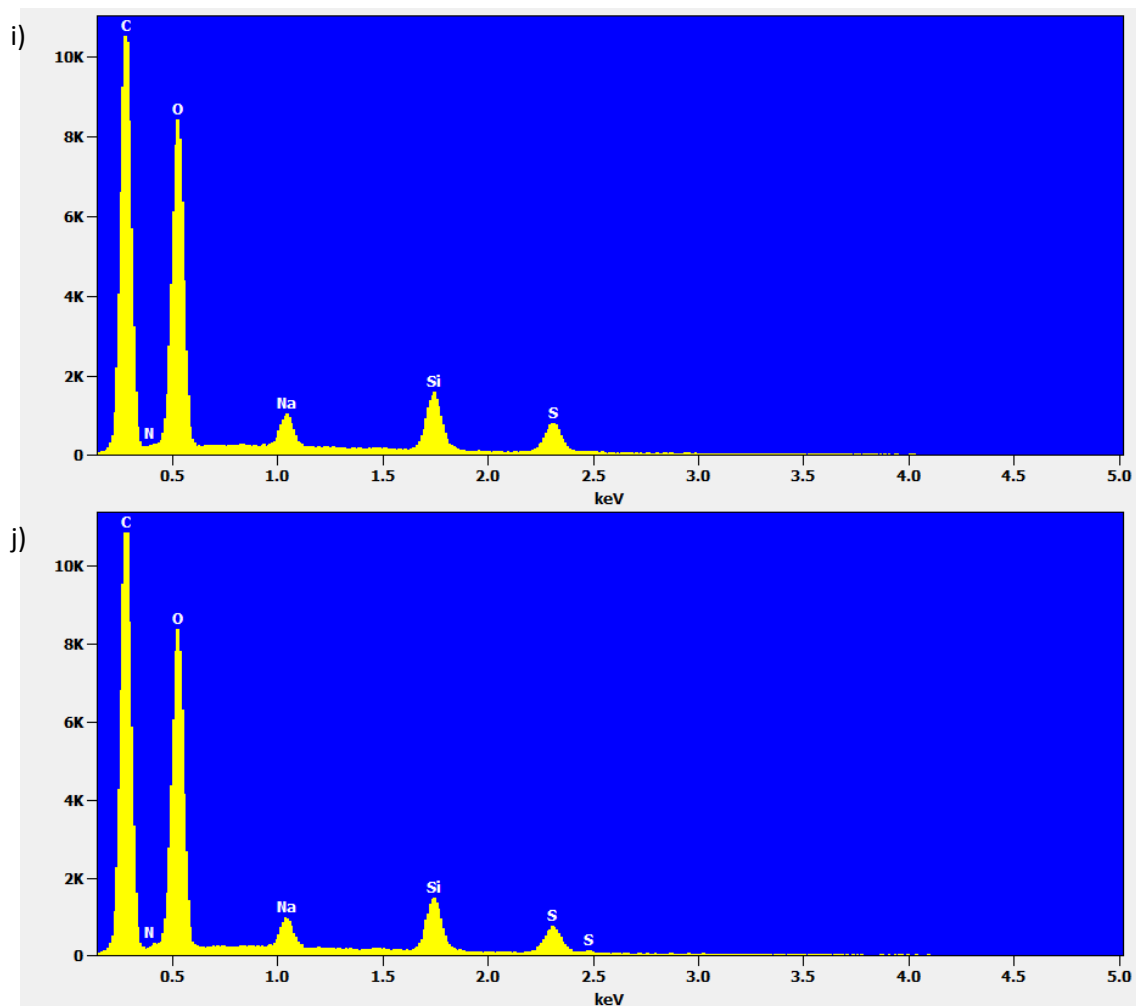
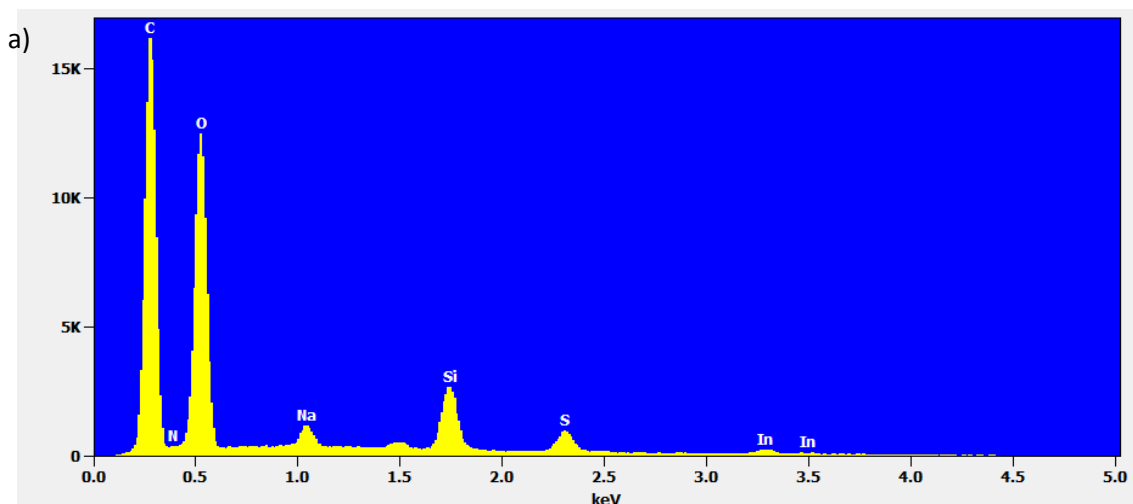
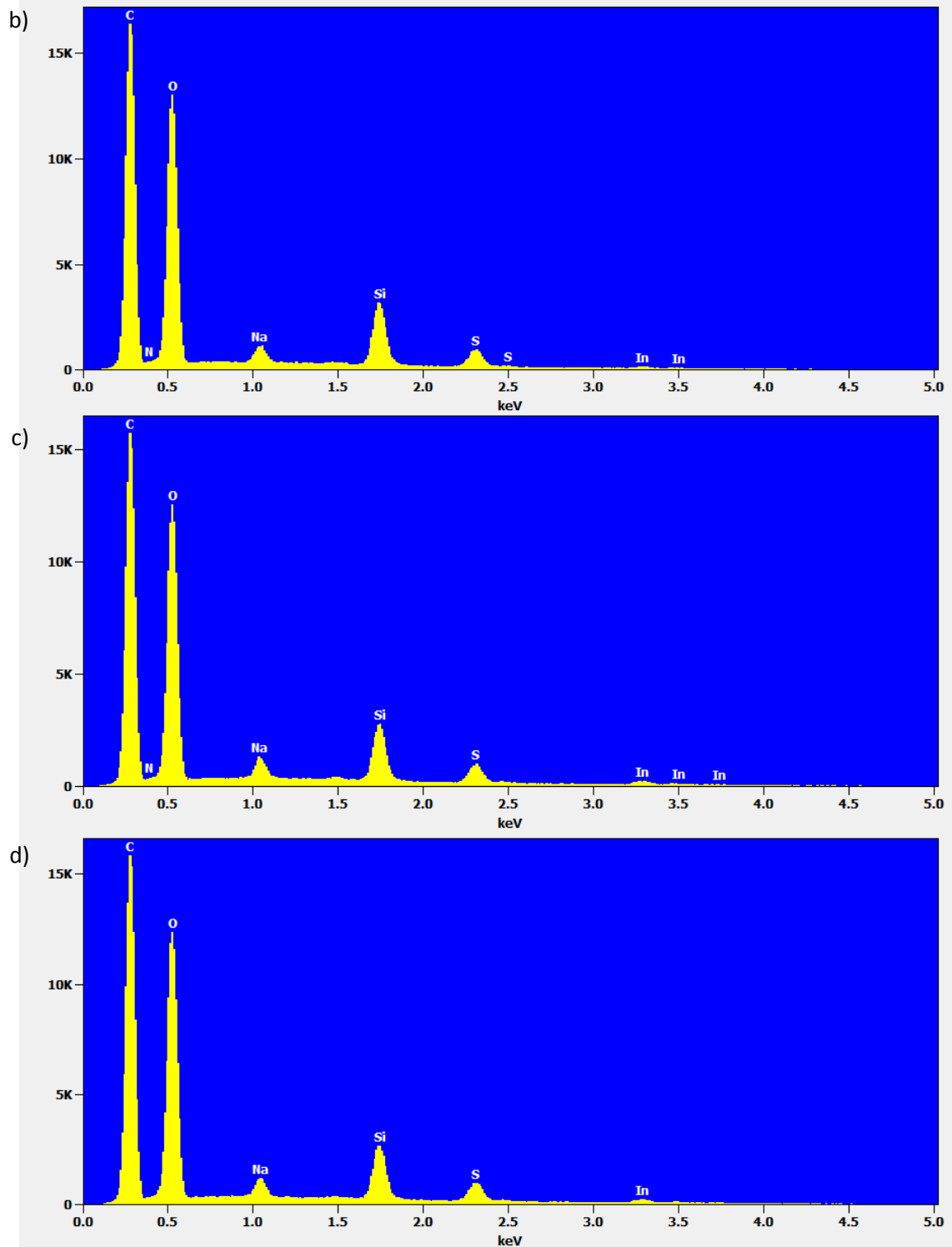


Figure 5-S5: Representative EDX spectra measured on a rectangular space of a) an untreated film, b) film 1, c) film 2, d) film 3, e) film 4, f) film 5, g) film 6, h) film 7, i) film 8 and j) film 9.





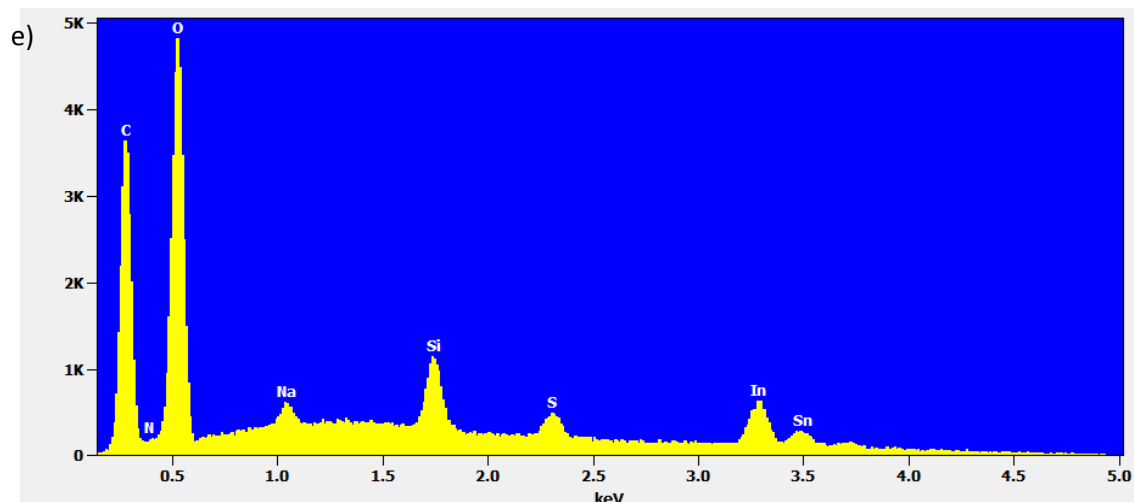


Figure 5-S6: EDX spectra measured on a spot of film a) 1, b) 2, c) 3, d) 4 and e) 8.

Table 5-S1: Results of EDX measurement on cross-linked PTHS⁻TBA⁺ films after different treatment given in atom %. The listed atom % error values represent the standard derivation of $\pm 2\sigma$.

number of film	film treatment	atom %							atom % error					
		C	N	O	Na	Si	S	Cl	C	N	O	Na	Si	S
Batch A														
	untreated reference	44.6	3.7	39.7	-	7.3	4.7	0.0	0.4	0.7	0.5		0.1	0.2
1	5 min immersed in NaCl _{aq}	39.5	2.3	42.3	2.1	8.3	5.6	0.0	0.4	0.6	0.5	0.1	0.1	0.2
2	5 min 600 mV in NaCl _{aq}	39.3	2.3	42.6	2.0	8.2	5.5	0.0	0.4	0.6	0.5	0.1	0.1	0.2
3	10 min immersed in NaCl _{aq}	38.8	2.1	42.8	2.3	8.3	5.8	0.0	0.4	0.6	0.5	0.1	0.1	0.2
4	10 min 600 mV in NaCl _{aq}	38.7	2.2	42.9	2.2	8.3	5.7	0.0	0.4	0.6	0.6	0.1	0.1	0.2
Batch B														
	untreated reference	48.6	4.0	35.9	-	6.2	5.2	0.0	0.5	0.9	0.6		0.1	0.2
5	1 h immersed in NaCl _{aq}	38.2	2.0	42.6	2.6	7.8	7.0	0.0	0.4	0.8	0.6	0.1	0.2	0.2
6	1 h 600 mV in NaCl _{aq}	38.4	1.8	41.9	3.0	7.6	7.4	0.0	0.4	0.8	0.6	0.1	0.2	0.3
7	2 h immersed in NaCl _{aq}	38.0	1.8	42.3	3.0	7.8	7.1	0.0	0.4	0.8	0.6	0.1	0.1	0.2
8	1h 600 mV, 1h 0 mV in NaCl _{aq}	37.5	1.9	42.0	3.0	8.1	7.4	0.0	0.4	0.7	0.6	0.1	0.2	0.3
9	stepwise cycle in NaCl _{aq}	38.7	1.9	41.6	2.8	7.7	7.2	0.0	0.4	0.8	0.6	0.1	0.2	0.2

6 CONJUGATED POLYELECTROLYTE BLENDS FOR HIGHLY STABLE ACCUMULATION MODE ELECTROCHEMICAL TRANSISTORS

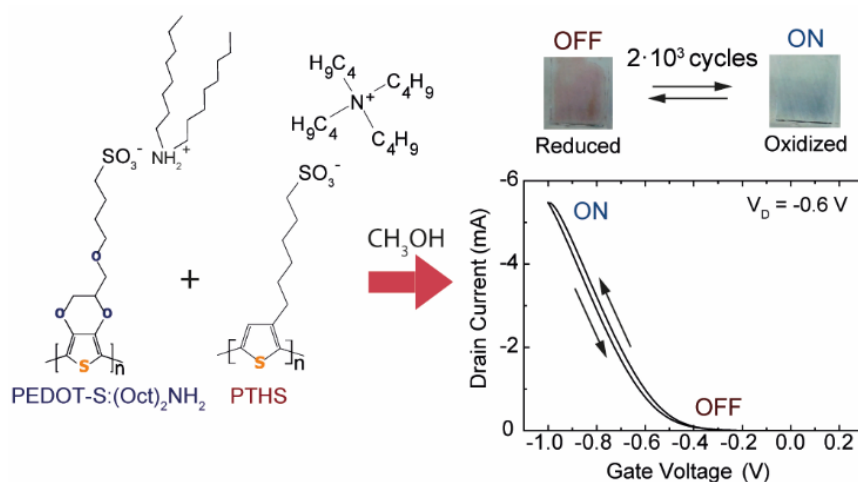
Erica Zeglio,^[a] Martina M. Schmidt,^[b] Mukundan Thelakkat,^[b] Roger Gabrielsson,^[c] Niclas Solin,^[a]
and Olle Inganäs*^[a]

[a] Biomolecular and Organic Electronics, Department of Physics Chemistry and Biology,
Linköping University, SE-58183, Linköping, Sweden

[b] Macromolecular Chemistry I—Applied Functional Polymers, University of Bayreuth,
Universitätsstrasse 30, 95440 Bayreuth, Germany

[c] Chemistry, Department of Science and Technology, Linköping University, Campus Norrköping,
S-60174 Norrköping, Sweden

*E-mail of corresponding author: oling@ifm.liu.se



Published in *Chem. Mater.* **2017**, *29*, 4293–4300

Abstract

Counterion exchange has been introduced as a method to modify properties of anionic conjugated polyelectrolyte (CPE) blends. Blending of two self-doped CPEs having metallic and semiconducting behavior has been achieved from two different solvents, by exchanging the counterion of the metallic component. Different blending conditions lead to films exhibiting different optical properties, depending on the aggregation states of the CPEs. Conductance responses for the blends showed the opportunity to tune threshold voltage of the films both by blending and counterion exchange. Therefore, the blends have been exploited for the fabrication of accumulation mode organic electrochemical transistors. These devices exhibit short switching times and high transconductance, up to 15.3 mS, as well as high stability upon fast pulsed cycles, retaining 88% of the drain currents after $2 \cdot 10^3$ cycles.

Introduction

Conjugated polyelectrolytes (CPEs) are organic materials possessing a conjugated polymeric backbone and charged side groups. Their electronic structure is analogous to the one of conjugated polymers (CPs), and they are, therefore, electronic conductors. Contrary to CPs, their ionic functionalities ensure them solubility in polar solvents and water compatibility for bioapplications. The unique optical and electronic properties of CPs have been successfully exploited for the production of a wide range of optoelectronic devices.^{1,2} In addition, CPEs have recently been introduced as active materials for the fabrication of organic electrochemical transistors (OECTs).³ Introduced for the first time in 1984, OECTs combine electronic transport in the polymeric network with ionic transport from the polymer to the electrolyte and vice versa.⁴ Their working mechanism is thus dependent on the ability of ions from the electrolyte to penetrate into the active material and shift the equilibria of the redox active species toward the conductive (ON) or non-conductive (OFF) state. Because of their ability to act as an interface between ionic and electronic transport, OECTs have been exploited for bioelectronic applications, such as the realization of biological sensors.⁵ Moreover, the processability and stability of CPEs under ambient conditions render OECTs suitable devices for low-cost printed electronic applications.⁶ OECTs can operate in two different modes depending on the redox status of the active material in its pristine state. Depletion-mode devices are ON at zero gate bias, and can be switched OFF via application of positive gate biases. Most of the devices produced so far work in depletion mode, as they comprise films from the highly conducting polymeric dispersion poly(3,4-ethylenedioxythiophene):poly(styrenesulfonate) (PEDOT:PSS) as

active material. In contrast, accumulation mode OECTs comprise a semiconductor species, with low conductivity in its pristine state. Therefore, the devices are, by default, in an OFF state, and can be turned ON upon application of a gate bias. Accumulation-mode devices have attracted a great interest, because of their low power consumption and their relevance in sensing applications, where “switching ON” events are beneficial for ease of detection. The majority of the accumulation mode OECTs reported so far possesses CPs as active materials.⁷⁻⁹ Thiophene-based CPs have been recently exploited for the production of accumulation-mode OECTs exhibiting transconductance of 20 mS and cycling stability under ambient conditions up to 700 cycles.^{10,11} Semiconducting CPEs have been recently introduced as promising materials for accumulation mode OECTs. Their optoelectronic properties combined with useful properties (such as self-doping ability and electrolyte-like behavior) provided by the hydrophilic side groups render them suitable for sensing and bioelectronics applications. However, the resulting devices could not match the high performances achieved by CPs counterparts. In our previous work, we demonstrated that blending of a semiconducting and a metallic CPE can be used as a strategy to tune OECTs operation mode and produce devices that possess enhanced properties, with respect to devices prepared from the corresponding pure materials.¹² Moreover, we have recently proved that counterion exchange of a metallic CPE is an effective method to enhance devices operation and stability.¹³ In this work we, therefore, aim to combine the two self-assembly strategies (blending and counterion exchange) to produce high-performance devices operating in pure accumulation mode. The semiconducting tetrabutylammonium poly(6-(thiophene-3-yl)hexane-1-sulfonate) (abbreviated as PTHS) has been chosen for this study, because of its high hole mobility.¹⁴ Herein, we report that blending with the metallic poly(4-(2,3-dihydrothieno[3,4-b]-[1,4]dioxin-2-yl-methoxy)-1-butanefulfonic acid) (abbreviated as PEDOT-S) from aqueous solution leads to films possessing threshold voltage between the two pure components and improved device characteristics. However, negative effects have been observed in device stability over cycling, with respect to a pure PTHS device. This can be due to the poorer stability of PEDOT-S, with respect to PTHS.¹³ Therefore, PEDOT-S properties have been modified by counterion exchange with a selected alkylammonium salt. PEDOT-S:(Oct)₂NH₂ has previously been shown to be soluble in organic solvents (such as methanol or chloroform) while preserving electronic conductivity, which is desirable for organic electronics applications.¹⁵ Therefore, PTHS:[PEDOT-S:(Oct)₂NH₂] blend could be processed from methanol to form thin films, exhibiting an increase in conductance at higher potentials, with respect of the pure components.¹³ Accumulation-mode OECTs possessing PTHS:[PEDOT-S:(Oct)₂NH₂] as active material do not only show better performance, with respect to PTHS:PEDOT-S blend, but also

high stability upon cycling, retaining >88% of the original ON currents after $2 \cdot 10^3$ cycles, which, to the best of our knowledge, is the best value reported so far for accumulation-mode OECTs. Spectroscopic studies have been performed on the drying films to investigate microstructure effects of blending in different conditions. Instead, ultraviolet-visible light (UV-vis) spectroelectrochemistry and conductance measurements have been exploited to understand changes in the electronic properties of the films, which are responsible for device operation.

Experimental section

Materials. Poly(4-(2,3-dihydrothieno-(3,4-b)-(1,4)dioxin-2-yl-me-thoxy)-1-butanefulfonic acid, sodium salt), referenced hereafter as PEDOT-S (average 16 repeating units, $M_w = 5500$ g/mol),^{16,17} and tetrabutylammonium poly(6-(thiophen-3-yl)hexane-1-sulfonate), referenced hereafter as PTHS, were synthesized according to previously reported procedures.^{14,18,19} PTHS precursor polymer, poly(3-(6-bromohexyl)-thiophene) (P3BrHT), has $M_n = 18480$ g/mol, corresponding to an average of 75 repeating units, as determined by matrix-assisted laser desorption ionization time-of-flight detection mass spectroscopy (MALDI-TOF MS). PEDOT-S:(Oct)₂NH₂ was produced, starting from PEDOT-S, according to the method developed by Inganäs et al.¹⁵ Zonyl FS-300 (DuPont) was used as an additive (0.05% with respect to the total polyelectrolytes concentration) to improve uniformity of the films deposited from water solution. All of the other chemicals were purchased from Sigma-Aldrich and used as received.

Molecular Weight Characterization. The molecular weight characterization was performed on the precursor polymer P3BrHT. For size exclusion chromatography (SEC) measurements, a Waters 515 HPLC pump with stabilized THF as the eluent at a flow rate of 0.5 mL/min was used. Twenty microliters (20 μ L) of the P3BrHT solution with a concentration of ~ 1 mg/mL was injected into a column setup, which consists of a guard column (Varian, 50 cm \times 0.758 cm, ResiPore gel, particle size = 3 μ m) and two separation columns (Varian, 300 \times 0.758 cm, ResiPore gel, particle size = 3 μ m). The polymer size distribution of the P3BrHT was monitored with a Waters Model 2489 tunable UV detector at 254 nm resulting in $M_n = 18184$ g/mol, $M_w = 20784$ g/mol and PDI: 1.14. Polystyrene was used as an external standard and 1,2-dichlorobenzene was used as an internal standard for molecular weight calibration. MALDI-TOF MS measurement for P3BrHT was performed on a Bruker Reflex III in linear mode, using trans-2-[3-(4-tert-butylphenyl)-2-methyl-2-propenylidene]malononitrile (DCTB) as the matrix and a matrix:P3BrHT ratio of 1000:1, and resulting in $M_n = 18480$ g/mol and $M_w = 18894$ g/mol.

Fluorescence Measurements. Fluorescence spectra of samples in solution (0.01 g/L for blends and 0.00613 g/L for PTHS) and spin-coated films (10 g/L PTHS and 8.14 g/L PTHS:PEDOT-S (1:1) at

800 rpm from water, and 0.613 g/L PTHS and 1 g/L PTHS:[PEDOT-S:(Oct)₂NH₂] (1:1) at 600 rpm from methanol) were acquired with a Horiba Jobin Yvon Fluoromax 4 spectrofluorometer. Luminescence measurements of the drying films were acquired using a customized setup, consisting of a laser with a wavelength of $\lambda = 450$ nm. The measurements were performed on drying films of drop-cast polyelectrolyte solutions on top of glass slides. These were placed on a black substrate, to avoid the reflection of light. All of the glass substrates were cleaned by rinsing with Milli-Q water and then washing with an H₂O:H₂O₂:NH₃ (5:1:1) solution for 10 min at 85°C.

Absorption of drying films. Absorption measurements of drying films were performed using a tungsten-halogen lamp as light source. The samples were deposited on glass slides positioned on a reflective substrate. An optical fiber was used both to illuminate the sample and to transmit the incoming signal to the detector. Samples deposition was performed as previously described for luminescence measurements.

Uv-vis Spectroelectrochemistry. An Autolab PGStat 10 (EchoChemie, The Netherlands) connected to a three-electrode setup was used to perform electrochemical measurements. The setup was made of an Ag/AgCl reference electrode and a platinum wire as a counter electrode. The working electrode consisted of an indium tin oxide (ITO)-coated glass, on top of which was casted a solution of polyelectrolyte/polyelectrolyte blend. All glass substrates were cleaned first by rinsing with Milli-Q water and then by washing with a solution of H₂O:H₂O₂:NH₃ (5:1:1) for 10 minutes at 85°C prior to polyelectrolyte deposition. 1,1-Butyl-3-methylimidazoliumtetrafluoroborate (BMIMBF₄) ionic liquid was used as an electrolyte. The measurements were carried out *in situ*, using a quartz cuvette equipped with a sealed cap as electrochemical cell. Absorption spectra of the films at each voltage were acquired using a spectrophotometer (Lambda 950, PerkinElmer).

Conductance Measurements. Solutions of PTHS:PEDOT-S 1:1 (8.14 g/L), PTHS (5 g/L), and PTHS:[PEDOT-S:(Oct)₂NH₂] 1:1 (1 g/L) were spin-coated (400 rpm) on top of a two-terminal interdigitated microelectrode array (IDMA) on glass (MicruX Technologies), which were used as working electrodes one and two. Prior to deposition, substrates were cleaned by sonication first in water and then in acetone for 10 minutes. Ag/AgCl was used as the reference electrode and a Pt wire as the counter electrode. All the electrodes were then connected to an Autolab type III bipotentiostat system (Autolab, EcoChemie, The Netherlands) and to each other through an ionic liquid electrolyte solution (BMIMBF₄). Cyclic voltammetry (CV) measurements were performed while retaining a bias of -0.05 V between the two working electrodes, and a scan rate of 0.01 V/s.

Fabrication and Characterization of Electrochemical Transistors. PTHS and blend films were prepared by spin coating on IDMA (10 g/L for PTHS, 8.14 g/L for PTHS:PEDOT-S 1:1, and 1 g/L PTHS:[PEDOT-S:(Oct)₂NH₂] 1:1 at 400 rpm), having a channel length $L = 20 \mu\text{m}$ and width $W = 1125 \mu\text{m}$. The two terminals were used as drain and source contacts. Poly-2-hydroxyethyl methacrylate (PHEMA) network in BMIMBF₄ ionic liquid was placed on top of the polyelectrolyte film and used as solid polymer-in-salt electrolyte. The solid polymer electrolyte was prepared as previously described by Inganäs and co-workers.¹² A PEDOT:PSS film was casted on top of the electrolyte membrane and constituted the gate (see Scheme 6-S3 in the Supporting Information). Silver paste was used to improve the contact at the gate. A Keithley 4200 parameter analyzer was used for the electrical characterization of all the devices. All the measurements were performed at room temperature in air. A Dektak Profilometer has been used to evaluate film thicknesses, which were 133 nm for PTHS, 102 nm for PTHS:PEDOT-S, and 112 nm PTHS:[PEDOT-S:(Oct)₂NH₂].

Results and discussion

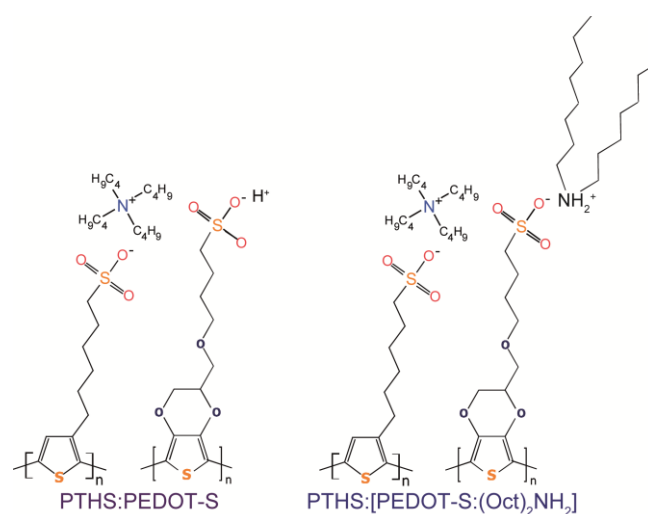


Figure 6-1: Chemical structure of the CPEs composing PTHS:PEDOT-S 1:1 blend and PTHS:[PEDOT-S:(Oct)₂NH₂] 1:1 blend.

The two conjugated polyelectrolytes chosen for this study (PTHS and PEDOT-S, see Figure 6-1) possess sulfonate groups in side chains, which are covalently attached to their backbones. The negative charges can stabilize positive charges formed in the backbone upon oxidation, rendering the materials both p-type and self-doped. The last definition is derived from the fact that no external species is required to provide counterions for the charges formed in the CPEs backbone upon oxidation. The main difference between the two CPEs resides in their ability to conduct in their pristine form: PTHS is a semiconductor, while PEDOT-S is a metallic conductor. This dissimilarity is due to the different electronic structure, deriving from the 3,4-ethylenedioxy

moiety in PEDOT-S backbone, where the two oxygens are able to stabilize positive charges by their electron-donating properties.²⁰ The nature of the counterions plays a critical role in CPEs solubility: PTHS is soluble both in methanol and water, PEDOT-S is soluble only in water, while PEDOT-S:(Oct)₂NH₂ is soluble in less-polar solvents such as methanol and chloroform. Therefore, blending with PTHS can be accomplished in water for PEDOT-S and in methanol for PEDOT-S:(Oct)₂NH₂.

Spectroscopic investigation of samples in solution has been performed in order to evaluate effects of blending on CPEs conformation in different solvents (see Figure 6-S1 and Figure 6-S2 in the Supporting Information). No changes can be detected in PTHS absorption and emission maxima upon blending from water or methanol, indicating that the presence of PEDOT-S has no effect on PTHS conformation in solution. Changes in PTHS emission and absorption maxima have been recorded as a function of chosen solvent. In particular, PTHS samples in water exhibit red-shifted maxima, with respect to methanol, attributable to a larger degree of aggregation in the highly polar solvent (Figure 6-S2).¹⁹ PEDOT-S exhibit a broad absorption under all conditions, because of doping. Casting the solutions to form a thin film is a required step for device fabrication. Absorption measurements of spin-coated films of the blends show shifts in opposite directions for the PTHS maximum, depending on the blending conditions (Figure 6-2a). This can be rationalized as the result of different CPEs aggregation states. Fluorescence spectra of PTHS:PEDOT-S films obtained from aqueous solutions exhibit a blue shift and quenching of the PTHS emission maximum, attributable to a close contact between the two CPEs in film form (Figure 6-2b). Surprisingly, no quenching is observed for PTHS:[PEDOT-S:(Oct)₂NH₂] films obtained from methanol, probably because of reduced aggregation of CPEs chains in the presence of bulky dioctylammonium counterions.²¹

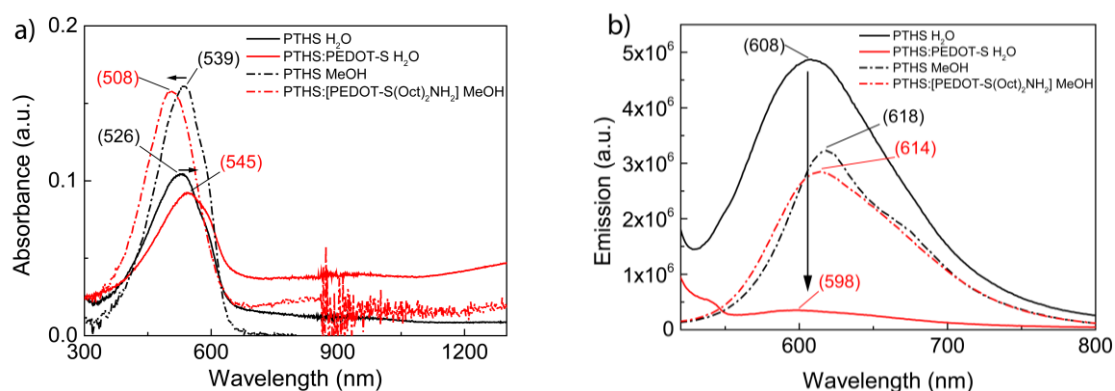


Figure 6-2: (a) Absorption and (b) fluorescence spectra of spin-coated films of PTHS (black, solid trace, 10 g/L) and PTHS:PEDOT-S 1:1 (red, solid trace, 8.14 g/L) from aqueous solution, and PTHS (black, dot-dashed trace, 0.613 g/L) and PTHS:[PEDOT-S:(Oct)₂NH₂] 1:1 (red, dot-dashed trace, 1 g/L) from methanol. Excitation wavelength: 450 nm for samples in methanol and 500 nm for samples in water.

Spectroscopic studies on the drying processes have been performed to gain insight on changes in CPEs aggregation during film formation. The samples have been deposited on a substrate and dried under ambient conditions while luminescence and absorption spectra have been recorded (see Scheme 6-S1 in the Supporting Information).

Absorption spectra of drying films of PTHS cast from a methanol solution reveal a red shift of $\Delta\lambda_{\text{abs}} = +60$ nm of absorption maximum (Figure 6-S3a in the Supporting Information). Emission spectra have been also acquired, showing a red shift of emission maxima to $\Delta\lambda_{\text{em}} = +55$ nm (Figure 6-S3b in the Supporting Information). In contrast, when PTHS is deposited from water solution, small changes ($\Delta\lambda_{\text{abs}} = +9$ nm) are observed in the absorption maximum, while emission data show no shifts in emission maximum from the wet to the dried film (Figure 6-S4 in the Supporting Information). However, changes in the fine structure of the emission spectra can be observed for films deposited from water solution. In order to relate these changes with modifications in the physical state of PTHS, the drying process has been monitored in three different experiments, employing different starting concentrations of PTHS in water. Absorption spectra show a relative increase of a red-shifted shoulder while drying for all the observed concentrations (Figure 6-S4 and Figure 6-S5 in the Supporting Information). Emission spectra of wet films show differences in positions of vibrational shoulder (blue or red-shifted), depending on concentration of starting solution (see Figure 6-3a, as well as Figure 6-S4b and Figure 6-S6 in the Supporting Information). A decrease in intensity and a red shift are observed for dried films at increased concentrations, probably due to higher aggregation of PTHS chains (Figure 6-3b). Generally, concentration-dependent absorption and emission properties were reported for conjugated polyelectrolytes.²²

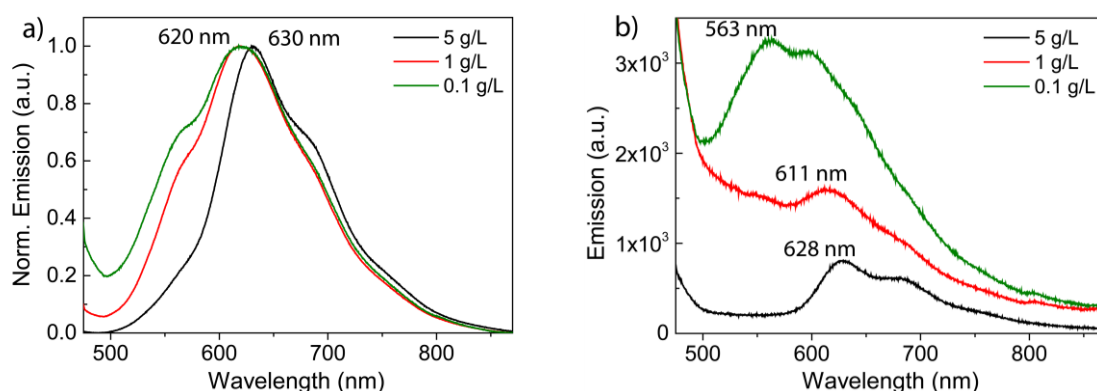


Figure 6-3: Normalized luminescence spectra of PTHS (a) wet and (b) dried films deposited from water solutions having the following concentrations: 5 g/L (black), 1 g/L (red), and 0.1 g/L (green). Excitation wavelength = 450 nm.

Drying films of PTHS:PEDOT-S deposited from water solution show small changes in absorption spectra (see Figure 6-4, as well as Figure 6-S7a in the Supporting Information). Absorption

measurements acquired for drying films of PTHS:[PEDOT-S:(Oct)₂NH₂] from the methanol solution exhibit a red shift of $\Delta\lambda_{\text{abs}} = +44$ nm from the wet form to the dried form, which is smaller, with respect to pure PTHS (see Figure 6-4a, as well as Figure 6-S8a in the Supporting Information). Complete quenching of PTHS emission is observed when PTHS:PEDOT-S films are in the dried form, as previously observed for spin-coated films (see Figure 6-4b, as well as Figure 6-S7b in the Supporting Information). Emission spectra of PTHS:[PEDOT-S:(Oct)₂NH₂] show a red shift of PTHS maximum from the wet state to the dried state, and no quenching of PTHS emission (see Figure 6-4b, as well as Figure 6-S8b in the Supporting Information).

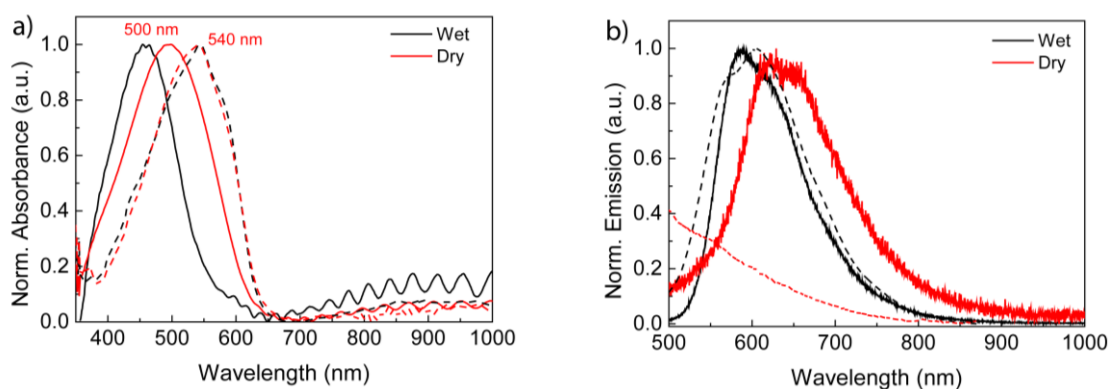


Figure 6-4: Normalized (a) absorbance and (b) luminescence spectra wet (black) and dried (red) films of PTHS:PEDOT-S 1:1 (dash, 1.63 g/L) from the water solution, and PTHS:[PEDOT-S:(Oct)₂NH₂] 1:1 (solid, 1 g/L) from the methanol solution. Excitation wavelength = 450 nm.

In order to understand whether quenching of PTHS emission in PTHS:PEDOT-S films is related to CPEs aggregation, the drying process has been followed for three different concentrations of PTHS:PEDOT-S in water (see Figure 6-5, as well as Figure 6-S9 and Figure 6-S10 in the Supporting Information). No spectral changes have been recorded for the absorption maximum, while emission data of wet films show a pronounced blue-shifted shoulder for PTHS:PEDOT-S 1.63 g/L to 0.163 g/L (Figure 6-5a). Emission of dried films show a disappearance of PTHS emission maximum for higher concentration of casted solutions of the blend (Figure 6-5b). Data, therefore, confirm that PTHS and PEDOT-S chains shall be in a high aggregation state to lead to quenching of the PTHS emission.²³

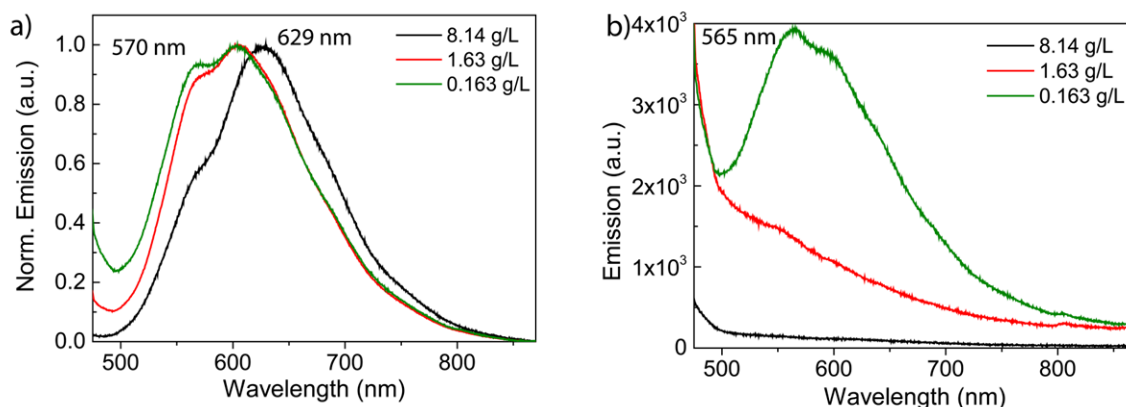


Figure 6-5: Normalized luminescence spectra of PTHS:PEDOT-S (a) wet and (b) dried films deposited from water solutions having the following concentrations: 8.14 g/L (black), 1.63 g/L (red) and 0.163 g/L (green). Excitation wavelength = 450 nm.

UV-vis spectroelectrochemistry is a useful tool to investigate the states formed upon oxidation, both in pristine CPEs as well as their blends. Pure PTHS films show oxidation above $E = 0.3$ V (vs Ag/AgCl), demonstrated by the appearance of a band at $\lambda = 787$ nm and a rise in intensity at $\lambda > 1100$ nm, together with decrease of intensity of the neutral polyelectrolyte at $\lambda = 520$ nm (Figure 6-6). An isosbestic point can be found at $\lambda = 622$ nm, indicating interconversion among the two species.

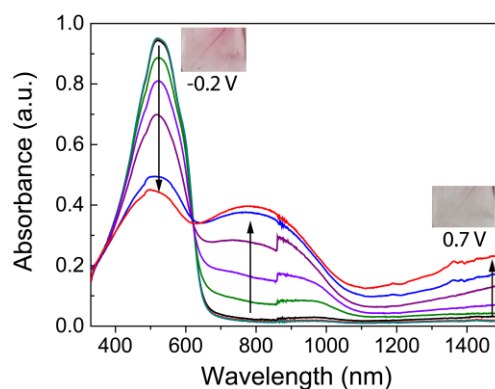


Figure 6-6: UV-vis spectroelectrochemistry of PTHS film (5 g/L) acquired from $E = -0.2$ V to $E = 0.7$ V in steps of 0.1 V. Inset show photographs of the films in the reduced (-0.2 V) and oxidized (0.7 V) state.

Investigation of PTHS:PEDOT-S 1:1 films show that, at $E = -0.5$ V, the absorption spectra are dominated by a maximum at $\lambda = 551$ nm, because of PTHS in its neutral form, and a shoulder at $\lambda \sim 670$ nm, attributable to neutral PEDOT-S (Figure 6-7). Increase of the potential to $E = 0.2$ V results in a decrease of the PEDOT-S shoulder and the formation of a band at $\lambda \sim 1000$ nm, together with an increase in intensity at $\lambda > 1100$ nm, due to PEDOT-S oxidation to both polaron and bipolaron states (an isosbestic point is found at $\lambda = 790$ nm). Further increases in potential lead to an interconversion of PTHS to its oxidized state (isosbestic point at $\lambda = 622$ nm). In this

case, the increased intensity at $\lambda > 1100$ nm is due to the PEDOT-S bipolaron contribution. Similar changes have been recorded for PTHS:[PEDOT-S:(Oct)₂NH₂] 1:1, demonstrating that the electronic states formed in the CPEs upon oxidation are unaffected by counterion exchange (see Figure 6-S11 and Scheme 6-S2 in the Supporting Information).

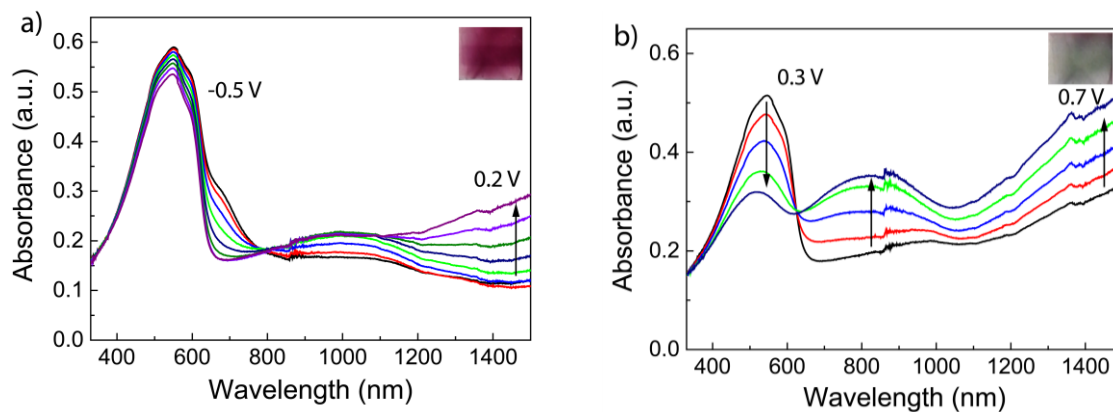


Figure 6-7: UV-vis spectroelectrochemistry of PTHS:PEDOT-S 1:1 film (5 g/L) acquired from (a) -0.5 V to 0.2 V, and (b) from 0.3 V to 0.7 V. Insets show photographs of the films in (a) the reduced state (-0.6 V) and (b) the oxidized state (0.7 V).

A four-terminal electrochemical setup has been exploited to investigate changes in films conductance as a function of the applied potential.¹² Measurements have been carried out by applying a small potential difference (-0.05 V) between two working electrodes, which have been connected by means of a CPE film. All samples show an increase of conductance at higher potentials, because of CPEs interconversion to their oxidized (conducting) states (Figure 6-8). In our previous work, we showed that, at 0 V, PEDOT-S is already present in a conducting form.¹² Data acquired for pure PTHS show that it is oxidized at higher potentials, in accordance with spectroelectrochemical data. This difference is due to the chemical and electronic structure of PTHS and PEDOT-S, as well as doping conditions. Hysteresis from the forward scan to the reverse scan acquired for PTHS is very small, demonstrating high reversibility of PTHS redox processes. Conductance measurements acquired for the blends show no or little hysteresis. PTHS:PEDOT-S 1:1 exhibit a rise in conductance at intermediate values between pure PTHS and PEDOT-S, while exchange of the PEDOT-S counterion leads to an increase of oxidation voltage at higher values.

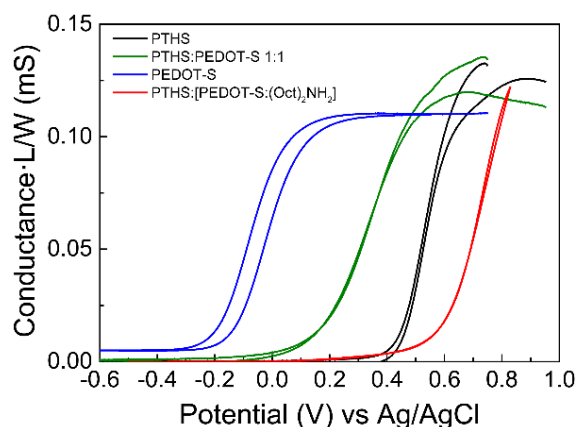


Figure 6-8: Conductance measurements acquired for films of PTHS (black), PEDOT-S (blue), PTHS:PEDOT-S 1:1 (green) and PTHS:[PEDOT-S:(Oct)₂NH₂] 1:1 (red). The length:width ratio of the channels was L/W = 0.018.

Overall, the data demonstrate that the threshold voltage of CPEs can be tuned both by blending and counterion exchange. As the blends show an increase in conductance above $E = 0$ V, they can be exploited to produce accumulation mode organic electrochemical transistors (OECTs, Scheme 6-S3). Output characteristics have been acquired at each gate bias step (V_G). The drain current (I_D) has been measured for negative drain voltage (V_D) sweeps, while the source has been grounded. As expected, the blends work mainly in accumulation mode (see Figure 6-9a and b). Transfer curves have been acquired by monitoring the drain current I_D for V_G sweeps at constant V_D . The last parameter has been chosen by the best match of the switching ability and stability of the devices. The transfer curve acquired for PTHS shows that devices operate from $V_G = -0.2$ V to $V_G = -0.8$ V (see Figure 6-S12 in the Supporting Information).

As anticipated from conductance measurements, the PTHS:PEDOT-S 1:1 transfer curve is shifted toward more positive V_G , while PTHS:[PEDOT-S:(Oct)₂NH₂] 1:1 transfer curve exhibit a shift in the opposite direction (Figure 6-9c and d). Transconductance ($g_m = \delta I_D / \delta V_G \frac{\delta I_D}{\delta V_G}$) has been calculated for all the devices to evaluate their signal amplification ability. Devices made with the blends as active materials exhibit higher g_m , with respect to pure PTHS devices. A maximum of $g_m = 15.3$ mS has been obtained for PTHS:[PEDOT-S:(Oct)₂NH₂] 1:1 devices, comparable with previously published values obtained for depletion-mode OECTs having PEDOT-S as active material. All devices show good $I_{on/off}$ ratio, up to $8.8 \cdot 10^4$. A summary of the data can be found in Table 6-1.

Table 6-1: Summary of device characteristics.

active material	g_m (mS)		$I_{ON/OFF}$		τ_{ON} (ms)	τ_{OFF} (ms)
	max	avg	max	avg		
PTHS	12.2	9.4±1.7	$3.1 \cdot 10^4$	$(1.3 \pm 1.0) \cdot 10^4$	428±237	62±30
PTHS:PEDOT-S 1:1	13.7	11.4±2.1	$8.8 \cdot 10^4$	$(2.0 \pm 3.0) \cdot 10^4$	91±48	16±13
PTHS:[PEDOT-S:(Oct) ₂ NH ₂] 1:1	15.3	13.1±1.9	$4.4 \cdot 10^4$	$(2.6 \pm 1.9) \cdot 10^4$	79±22	11±8

Transient responses have been acquired to evaluate the kinetics of device switching: square-wave gate voltages have been applied, while the drain currents have been recorded as a function of time. All produced devices exhibit switching behavior (see Figure 6-S13 in the Supporting Information, as well as Figure 6-9e and f), and switching times in the millisecond range. ON and OFF times have been defined as the time required to achieve the 90% and the 10% of the ON and OFF states, respectively. Devices having blends as active materials show shorter switching times, if compared with pure PTHS and previously reported PEDOT-S data (see Figure 6-10),¹² indicating that blending has a positive effect on the transport ability of the films. Counterion exchange leads to even shorter switching times ($\tau_{ON} = 79 \pm 22$ ms, $\tau_{OFF} = 11 \pm 8$ ms).

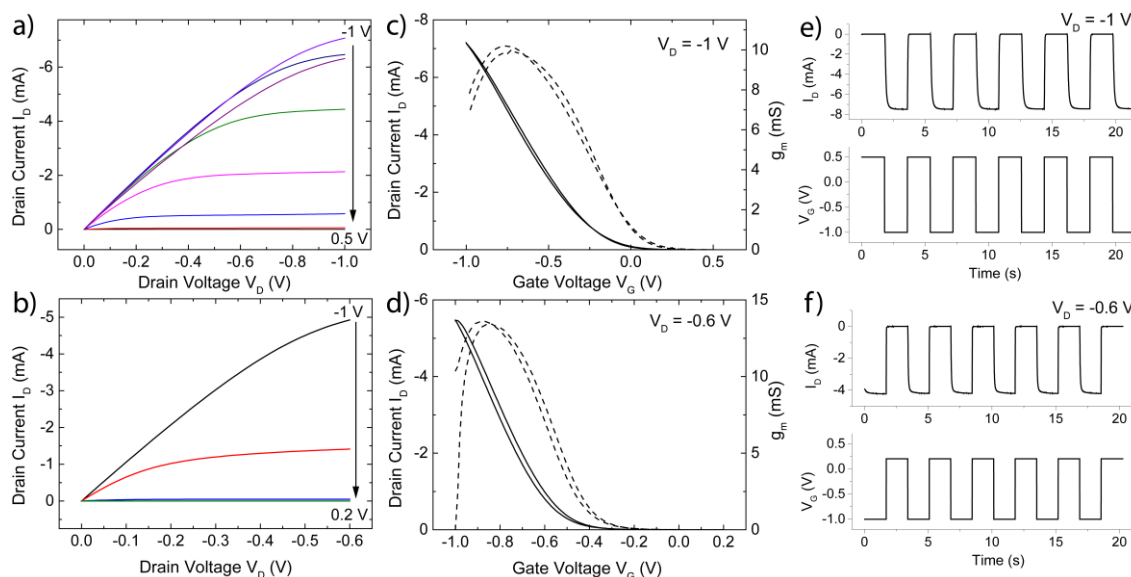


Figure 6-9: Representative (a, b) output, (c, d) transfer, and (e, f) switching characteristics of devices having PTHS:PEDOT-S 1:1 as active material (panels (a), (c), and (e)), and PTHS:[PEDOT-S:(Oct)₂NH₂] 1:1 as active material (panels (b), (d), and (f)). Transfer and switching characteristics have been acquired at constant drain bias of $V_D = -1$ V for PTHS:PEDOT-S, and $V_D = -0.6$ V for PTHS:[PEDOT-S:(Oct)₂NH₂] 1:1.

To evaluate the limits of devices operation over cycling, stability tests have been performed by monitoring I_D for square wave gate voltages at fixed V_D over the shortest possible ON/OFF cycling times. PTHS devices retain 90% of the original drain currents after $2 \cdot 10^3$ cycles (see

Figure 6-S14a in the Supporting Information). PTHS:PEDOT-S devices exhibit lower stability, retaining only 59% of initial I_D after $2 \cdot 10^3$ cycles (Figure 6-S14b in the Supporting Information). Therefore, the measurements indicate that blending PTHS with PEDOT-S has a detrimental effect on devices stability over cycling. PTHS:[PEDOT-S:(Oct)₂NH₂] devices show comparable cycling stability, with respect to pure PTHS devices, and preserves 88% of the initial I_D after $2 \cdot 10^3$ cycles (Figure 6-11a). Therefore, the data indicate that blending conditions are of high importance in device stability upon cycling. Stability over long switching times has also been considered, by operating the devices for slow ON/OFF switches of 7.8 s. In this operation regime, PTHS devices show the best performance, retaining 78% of I_D after 60 min (Figure 6-S15a in the Supporting Information). PTHS:PEDOT-S devices show limited stability over time, retaining only 4.9% of the starting I_D after 30 min (Figure 6-S15b in the Supporting Information). Instead, PTHS:[PEDOT-S:(Oct)₂NH₂] devices exhibit intermediate stability, preserving 32% of the starting I_D after 60 min of operation, and demonstrating the limits of OECTs operation over time.

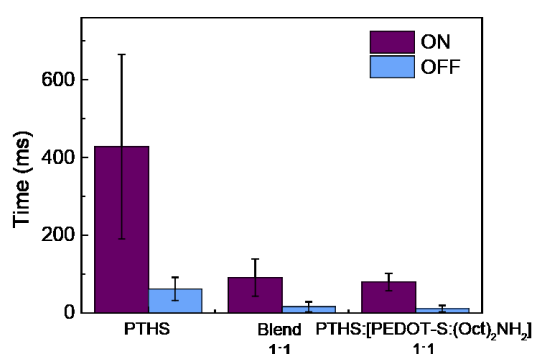


Figure 6-10: Switching times for PTHS, PTHS:PEDOT-S 1:1, and PTHS:[PEDOT-S:(Oct)₂NH₂] 1:1.

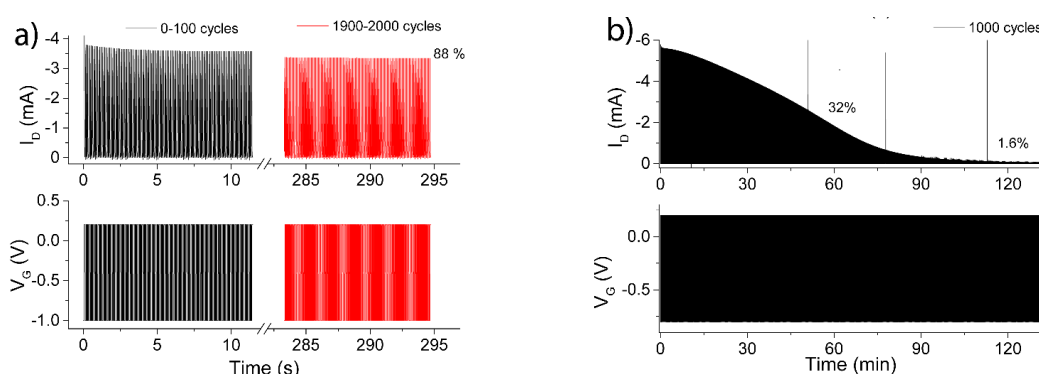


Figure 6-11: (a) Stability upon fast switching cycles for PTHS:[PEDOT-S:(Oct)₂NH₂] acquired for ON/OFF cycles of 134 ms. (b) Stability upon time for PTHS:[PEDOT-S:(Oct)₂NH₂] acquired for ON/OFF cycles of 7.8 s. In both cases, the drain current (I_D) has been measured for drain bias of $V_D = -0.6$ V, and gate voltage (V_G) switches (a) from $V_G = 0.2$ V to $V_G = -1$ V and (b) from $V_G = 0.2$ V to $V_G = -0.8$ V.

In conclusion, counterion exchange has been introduced as a method to produce CPEs blends from different solvents, leading to films and devices with desired properties. Changes in blend

microstructure were investigated by spectroscopic methods, revealing differences in aggregation state of CPEs, depending on blending conditions. No changes were observed in the nature of the states formed in the blends upon oxidation. However, conductance measurements demonstrated that blending PTHS with PEDOT-S having different counterions produces opposite effects in the threshold voltage of the blend. Films of the blends have been successfully used for the fabrication of accumulation mode OECTs exhibiting higher performance with respect of devices made with the pure components. PTHS:[PEDOT-S(Oct)₂NH₂] blend enabled the production of devices displaying high stability upon cycling. The results highlight the importance of use self-assembly strategies to tune materials from solution, leading to the production of devices with the stability needed for practical applications.

Associated content

Supporting Information

Optical properties of PTHS and PTHS:[PEDOT-S:(Oct)₂NH₂] 1:1 in methanol solution; absorption and emission spectra of PTHS while drying; absorption and emission spectra of PTHS:PEDOT-S 1:1 and PTHS:[PEDOT-S:(Oct)₂NH] 1:1 while drying; UV-vis spectroelectrochemistry of PTHS:[PEDOT-S:(Oct)₂NH₂] 1:1 films; schematic representation of OECT; characteristics of OECTs having PTHS as active material; stability measurements.

Acknowledgment

We would like to acknowledge the Marie Curie network “Renaissance” founded by the People FP7 Program, and the Knut and Alice Wallenberg foundation through a Wallenberg Scholar grant to O.I., and the Swedish Strategic Research Foundation through the project SiOS. Mukundan Thelakkat and Martina Schmidt acknowledge DFG (GRK 1640) for the financial support. Martina Schmidt acknowledges support from Elite Study programme, Macromolecular Science at the University of Bayreuth.

Abbreviations

PEDOT-S, poly(4-(2,3-dihydrothieno-(1,4)dioxin-2-yl-methoxy)-1-butanefulfonic acid); PTHS, tetrabutylammonium poly(6-(thiophen-3-yl)hexane-1-sulfonate); (Oct)₂NH₂Cl, dioctylammonium chloride; MeOH, methanol.

References

- (1) Duarte, A.; Pu, K.-Y.; Liu, B.; Bazan, G. C. Recent Advances in Conjugated Polyelectrolytes for Emerging Optoelectronic Applications. *Chem. Mater.* **2011**, *23*, 501-515.
- (2) Lee, W.; Seo, J. H.; Woo, H. Y. Conjugated polyelectrolytes: A new class of semiconducting material for organic electronic devices. *Polymer* **2013**, *54*, 5104-5121.
- (3) Inal, S.; Rivnay, J.; Leleux, P.; Ferro, M.; Ramuz, M.; Brendel, J. C.; Schmidt, M. M.; Thelakkat, M.; Malliaras, G. G. A High Transconductance Accumulation Mode Electrochemical Transistor. *Adv. Mater.* **2014**, *26*, 7450-7455.
- (4) White, H. S.; Kittlesen, G. P.; Wrighton, M. S. Chemical derivatization of an array of three gold microelectrodes with polypyrrole: fabrication of a molecule-based transistor. *J. Am. Chem. Soc.* **1984**, *106*, 5375-5377.
- (5) Strakosas, X.; Bongo, M.; Owens, R. M. The organic electrochemical transistor for biological applications. *J. Appl. Polym. Sci.* **2015**, *132*, 41735.
- (6) Kawahara, J.; Ersman, P. A.; Kato, K.; Berggren, M. Fast-Switching Printed Organic Electrochemical Transistors Including Electronic Vias Through Plastic and Paper Substrates. *IEEE Trans. Electron Devices* **2013**, *60*, 2052-2056.
- (7) Panzer, M. J.; Frisbie, C. D. Polymer Electrolyte-Gated Organic Field-Effect Transistors: Low-Voltage, High-Current Switches for Organic Electronics and Testbeds for Probing Electrical Transport at High Charge Carrier Density. *J. Am. Chem. Soc.* **2007**, *129*, 6599-6607.
- (8) Yuen, J. D.; Dhoot, A. S.; Namdas, E. B.; Coates, N. E.; Heeney, M.; McCulloch, I.; Moses, D.; Heeger, A. J. Electrochemical Doping in Electrolyte-Gated Polymer Transistors. *J. Am. Chem. Soc.* **2007**, *129*, 14367-14371.
- (9) Laiho, A.; Herlogsson, L.; Forchheimer, R.; Crispin, X.; Berggren, M. Controlling the dimensionality of charge transport in organic thin-film transistors. *Proc. Natl. Acad. Sci. U.S.A.* **2011**, *108*, 15069-15073.
- (10) Nielsen, C. B.; Giovannitti, A.; Sbircea, D.-T.; Bandiello, E.; Niazi, M. R.; Hanifi, D. A.; Sessolo, M.; Amassian, A.; Malliaras, G. G.; Rivnay, J.; McCulloch, I. Molecular Design of Semiconducting Polymers for High-Performance Organic Electrochemical Transistors. *J. Am. Chem. Soc.* **2016**, *138*, 10252-10259.
- (11) Giovannitti, A.; Sbircea, D.-T.; Inal, S.; Nielsen, C. B.; Bandiello, E.; Hanifi, D. A.; Sessolo, M.; Malliaras, G. G.; McCulloch, I.; Rivnay, J. Controlling the mode of operation of organic transistors through side-chain engineering. *Proc. Natl. Acad. Sci. U.S.A.* **2016**, *113*, 12017-12022.

- (12) Zeglio, E.; Vagin, M.; Musumeci, C.; Ajjan, F. N.; Gabrielsson, R.; Trinh, X. T.; Son, N. T.; Maziz, A.; Solin, N.; Inganäs, O. Conjugated Polyelectrolyte Blends for Electrochromic and Electrochemical Transistor Devices. *Chem. Mater.* **2015**, *27*, 6385-6393.
- (13) Erica Zeglio, J. E., Roger Gabrielsson, Niclas Solin, and Olle Inganäs* Highly Stable Conjugated Polyelectrolytes for Water-based Hybrid Mode Electrochemical Transistors. *Adv. Mater.* **2017**, <http://dx.doi.org/10.1002/adma.201605787>.
- (14) Brendel, J. C.; Schmidt, M. M.; Hagen, G.; Moos, R.; Thelakkat, M. Controlled Synthesis of Water-Soluble Conjugated Polyelectrolytes Leading to Excellent Hole Transport Mobility. *Chem. Mater.* **2014**, *26*, 1992-1998.
- (15) Johansson, P. K.; Julleson, D.; Elfving, A.; Liin, S. I.; Musumeci, C.; Zeglio, E.; Elinder, F.; Solin, N.; Inganäs, O. Electronic polymers in lipid membranes. *Sci. Rep.* **2015**, *5*, 11242.
- (16) Elfving, A.; Backlund, F. G.; Musumeci, C.; Inganäs, O.; Solin, N. Protein nanowires with conductive properties. *J. Mater. Chem. C* **2015**, *3*, 6499-6504.
- (17) Persson, K. M.; Karlsson, R.; Svennersten, K.; Löffler, S.; Jager, E. W. H.; Richter-Dahlfors, A.; Konradsson, P.; Berggren, M. Electronic Control of Cell Detachment Using a Self-Doped Conducting Polymer. *Adv. Mater.* **2011**, *23*, 4403-4408.
- (18) Karlsson, R. H.; Herland, A.; Hamed, M.; Wiggenius, J. A.; Åslund, A.; Liu, X.; Fahlman, M.; Inganäs, O.; Konradsson, P. Iron-Catalyzed Polymerization of Alkoxysulfonate-Functionalized 3,4-Ethylenedioxythiophene Gives Water-Soluble Poly(3,4-ethylenedioxythiophene) of High Conductivity. *Chem. Mater.* **2009**, *21*, 1815-1821.
- (19) Zeglio, E.; Schmidt, M. M.; Thelakkat, M.; Gabrielsson, R.; Solin, N.; Inganäs, O. Conjugated Polyelectrolyte Blend as Photonic Probe of Biomembrane Organization. *ChemistrySelect* **2016**, *1*, 4340-4344.
- (20) Burkhardt, S. E.; Rodríguez-Calero, G. G.; Lowe, M. A.; Kiya, Y.; Hennig, R. G.; Abruña, H. D. Theoretical and Electrochemical Analysis of Poly(3,4-alkylenedioxythiophenes): Electron-Donating Effects and Onset of p-Doped Conductivity. *J. Phys. Chem. C* **2010**, *114*, 16776-16784.
- (21) Setayesh, S.; Grimsdale, A. C.; Weil, T.; Enkelmann, V.; Müllen, K.; Meghdadi, F.; List, E. J. W.; Leising, G. Polyfluorenes with Polyphenylene Dendron Side Chains: Toward Non-Aggregating, Light-Emitting Polymers. *J. Am. Chem. Soc.* **2001**, *123*, 946-953.
- (22) Garcia, A.; Nguyen, T.-Q. Effect of Aggregation on the Optical and Charge Transport Properties of an Anionic Conjugated Polyelectrolyte. *J. Phys. Chem. C* **2008**, *112*, 7054-7061.

- (23) Brown, P. J.; Thomas, D. S.; Köhler, A.; Wilson, J. S.; Kim, J.-S.; Ramsdale, C. M.; Siringhaus, H.; Friend, R. H. Effect of interchain interactions on the absorption and emission of poly(3-hexylthiophene). *Phys. Rev. B* **2003**, 67, 064203.

Supporting information

Table of contents

1	Optical properties of PTHS and PTHS:[PEDOT-S:(Oct) ₂ NH ₂] 1:1 in solution	142
2	Setup for absorption measurements of drying films	143
3	Absorption and emission spectra of PTHS while drying	143
4	Absorption and emission spectra of PTHS:PEDOT-S 1:1 and PTHS:[PEDOT-S:(Oct) ₂ NH ₂] 1:1 while drying	145
5	UV-vis spectroelectrochemistry of PTHS:[PEDOT-S:(Oct) ₂ NH ₂] 1:1 films	146
6	Schematic representation of OECT	147
7	Characteristics of OECTs having PTHS as active material	147
8	Stability measurements	148

1 Optical properties of PTHS and PTHS:[PEDOT-S:(Oct)₂NH₂] 1:1 in solution

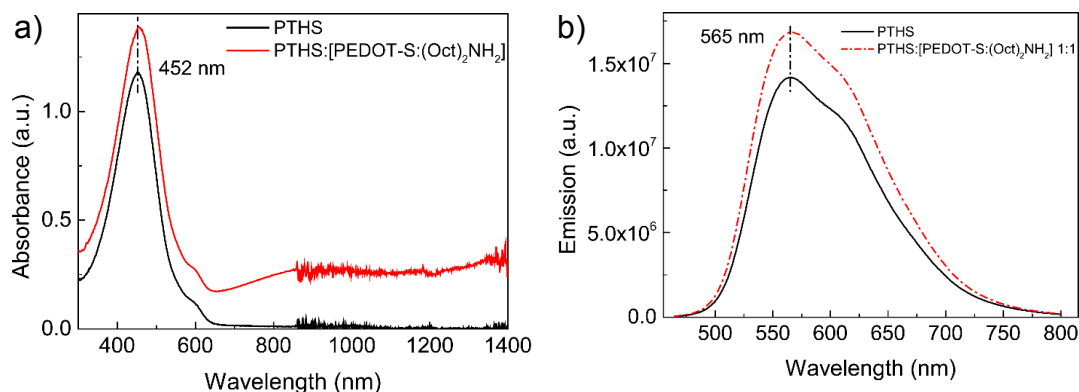


Figure 6-S1: a) Absorption spectra of methanol solutions of PTHS (0.0613 g/L, black) and PTHS:[PEDOT-S:(Oct)₂NH₂] 1:1 (0.1 g/L, red). b) Emission spectra of methanol solutions of PTHS (0.00613 g/L, black) and PTHS:[PEDOT-S:(Oct)₂NH₂] 1:1 (0.01 g/L, red). Excitation wavelength: 450 nm.

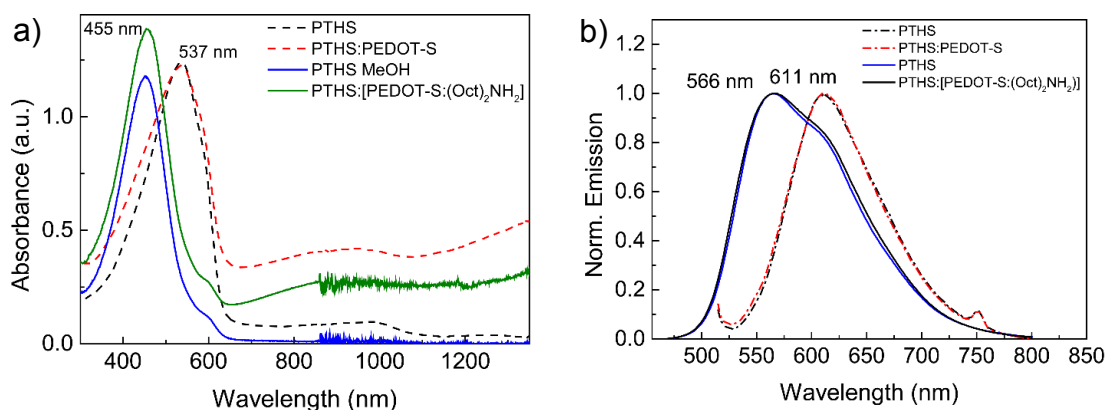
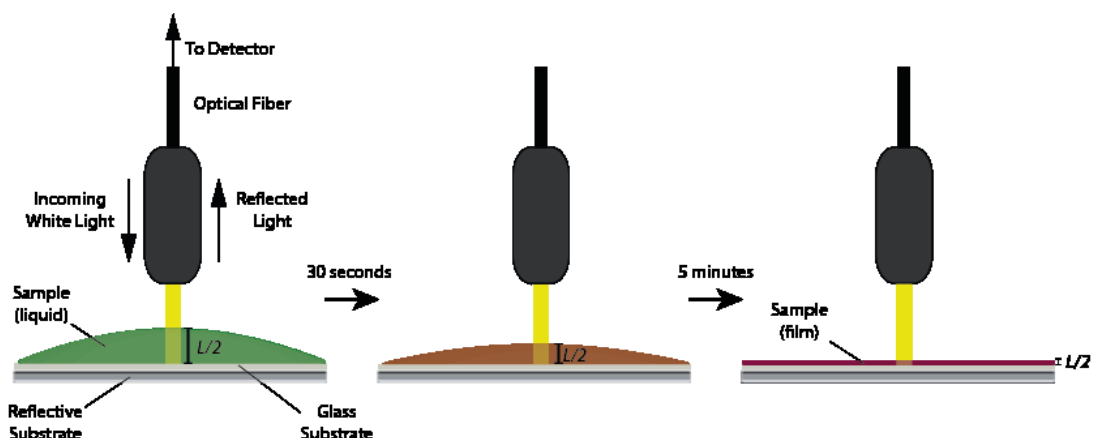


Figure 6-S2: a) Absorption and b) normalized emission spectra of PTHS and PTHS:[PEDOT-S:(Oct)₂NH₂] 1:1 dissolved in methanol (solid), and PTHS and PTHS:PEDOT-S 1:1 dissolved in water (dashed). PTHS concentration was 0.0613 g/L for absorption and 0.00613 g/L for emission, while PTHS:PEDOT-S and PTHS:[PEDOT-S:(Oct)₂NH₂] concentrations were 0.1 g/L for absorption and 0.01 g/L for emission. Excitation wavelength: 450 nm for samples in methanol and 500 nm for samples in water.

2 Setup for absorption measurements of drying films



Scheme 6-S1: Schematic representation of the setup used to record absorption spectra of drying films. The liquid sample has been deposited on top of a glass substrate mounted on a reflective substrate (a mirror). Then the sample has been left to dry for 5 minutes, meanwhile the absorption data have been collected. The absorbance of the sample decreased with time according to the Beer-Lambert law $A = \epsilon c L$, where A is the absorbance, ϵ and c are the molar attenuation coefficient and the concentration of the absorbing specie, respectively, and L is the pathlength. The local concentration and the pathlength are expected to change in an inversely proportional fashion, however, the second effect is more pronounced and leads to a decrease in absorbance while measuring.

3 Absorption and emission spectra of PTHS while drying

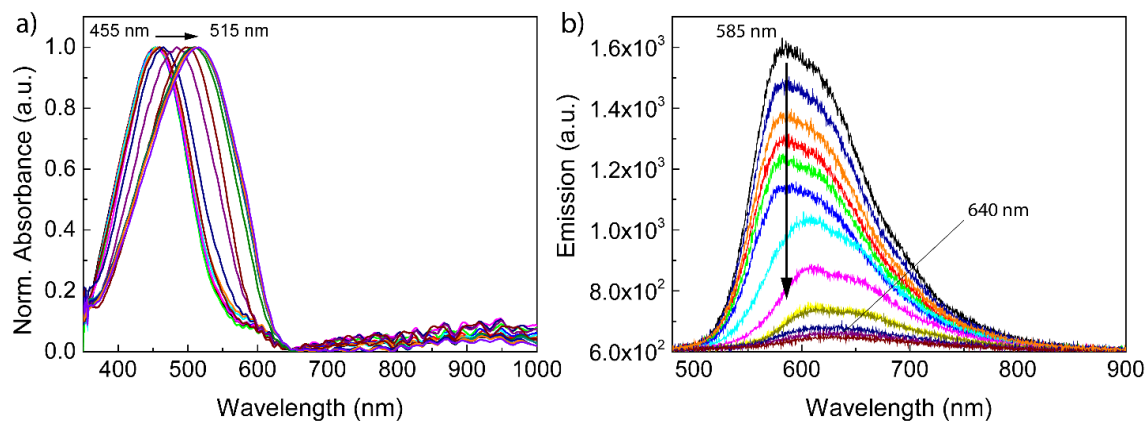


Figure 6-S3: a) Normalized absorption and b) luminescence spectra of PTHS films while drying from methanol solution (0.613 g/L). Excitation wavelength: 450 nm.

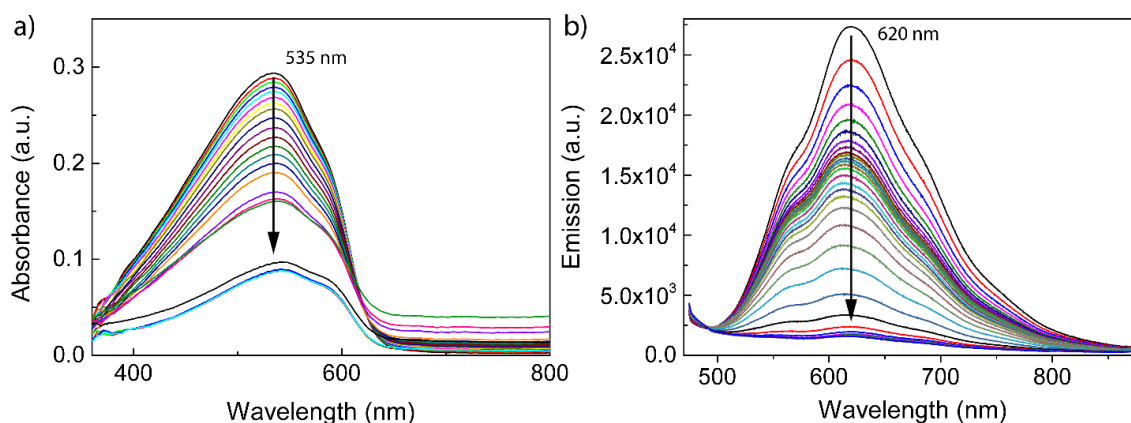


Figure 6-S4: a) Absorption and b) luminescence spectra of PTHS films while drying from water solution (1 g/L). Excitation wavelength: 450 nm.

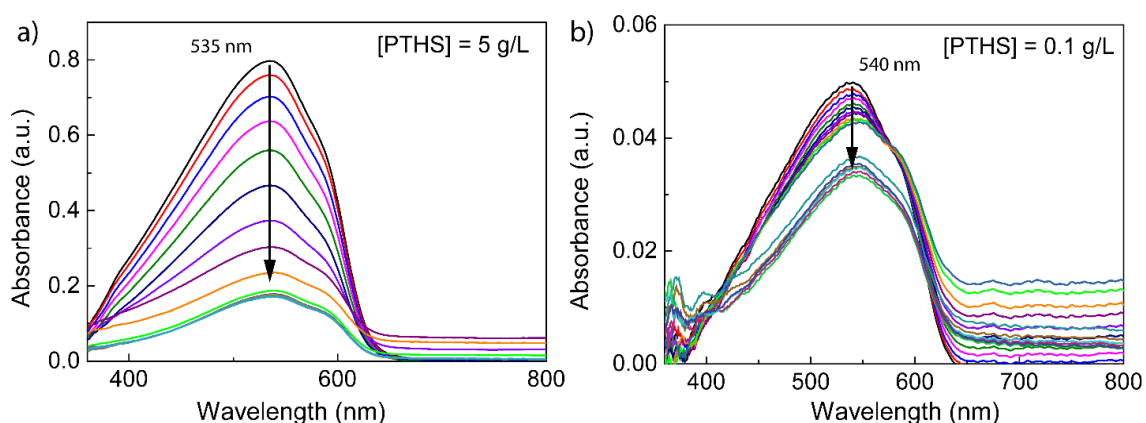


Figure 6-S5: Absorption spectra of PTHS while drying from water solutions having the following concentrations: a) 5 g/L and b) 0.1 g/L.

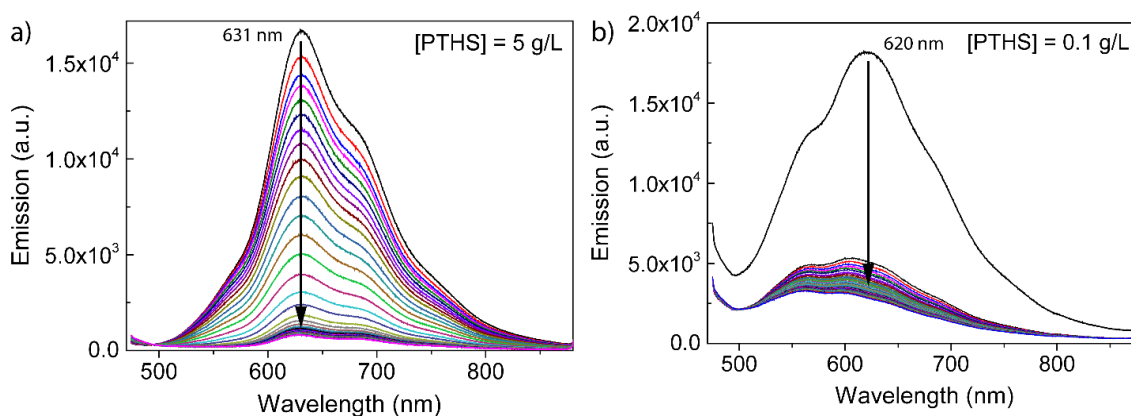


Figure 6-S6: Luminescence spectra of PTHS while drying from water solutions having the following concentrations: a) 5 g/L and b) 0.1 g/L. Excitation wavelength: 450 nm.

4 Absorption and emission spectra of PTHS:PEDOT-S 1:1 and PTHS:[PEDOT-S:(Oct)₂NH₂] 1:1 while drying

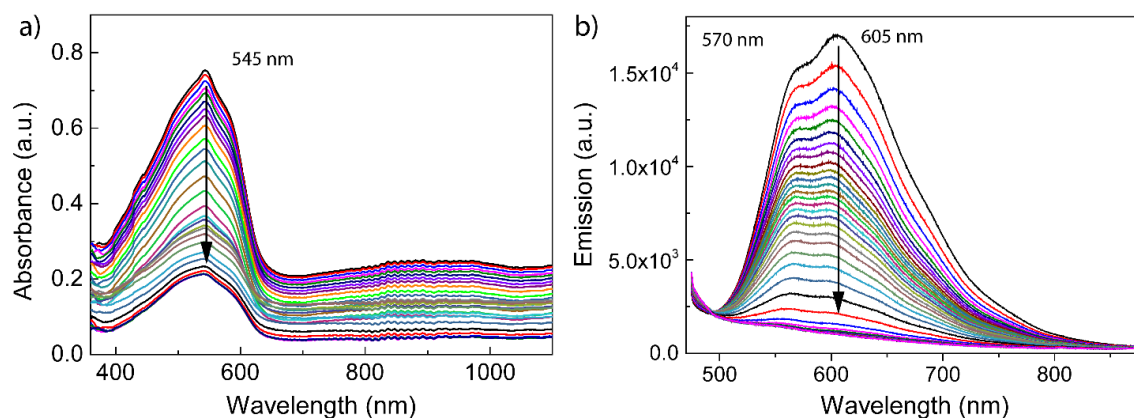


Figure 6-S7: a) Absorption and b) luminescence spectra of PTHS:PEDOT-S 1:1 films while drying from water solution (1.63 g/L). Excitation wavelength: 450 nm.

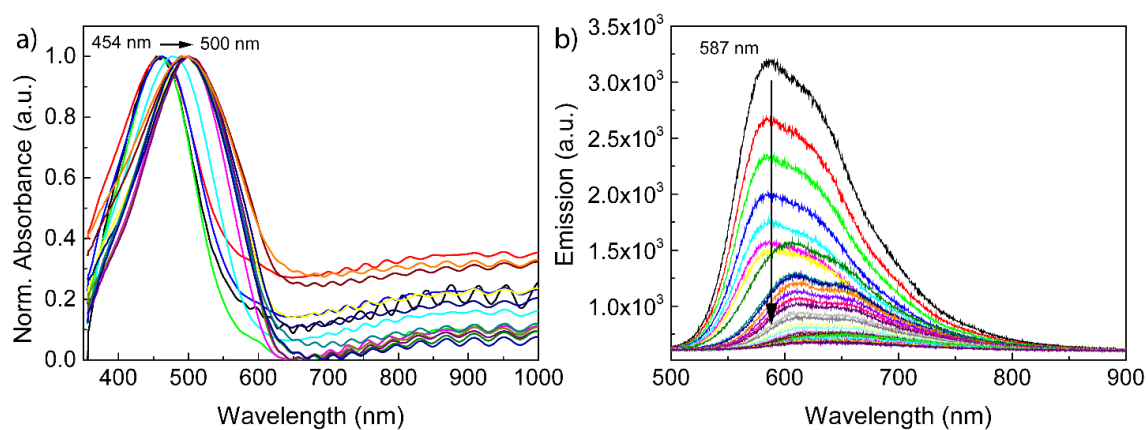


Figure 6-S8: a) Absorption and b) luminescence spectra of PTHS:[PEDOT-S:(Oct)₂NH₂] 1:1 films while drying from methanol solution (1 g/L). Excitation wavelength: 450 nm.

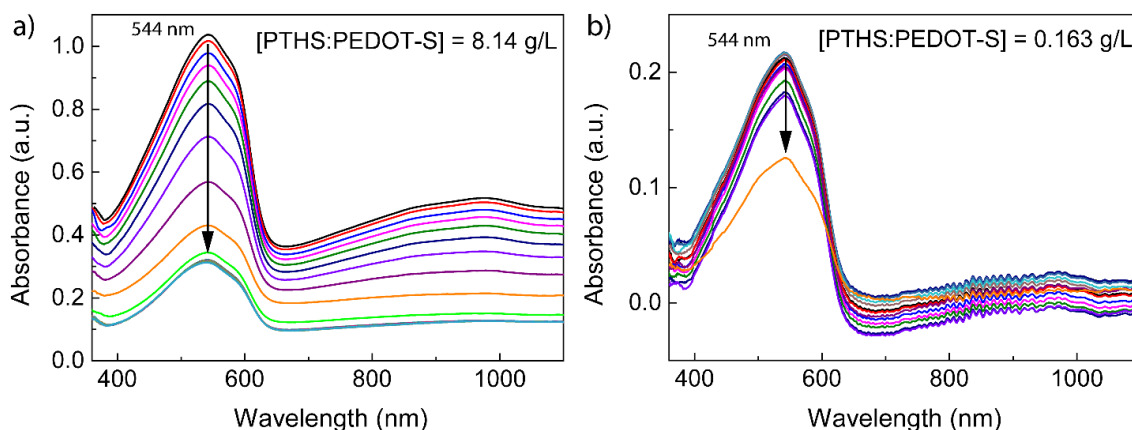


Figure 6-S9: Absorption spectra of PTHS:PEDOT-S 1:1 films while drying from water solutions having the following concentrations: a) 8.14 g/L and b) 0.163 g/L.

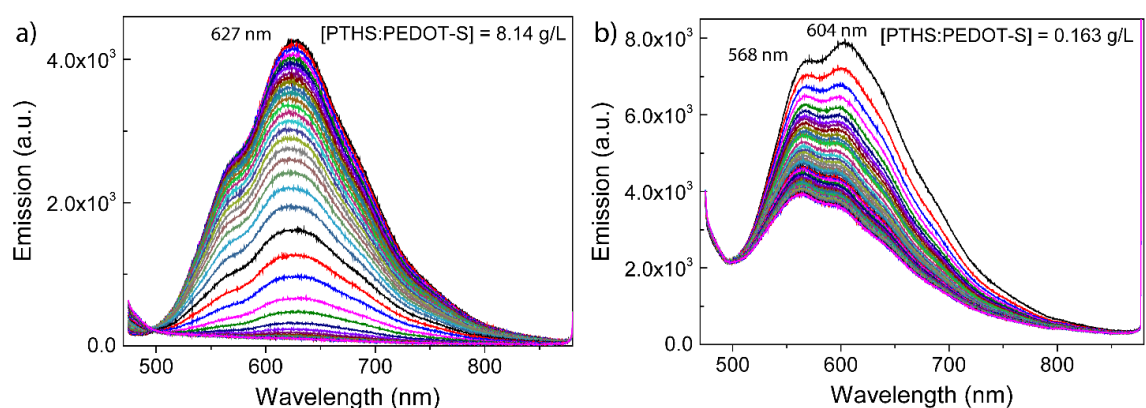


Figure 6-S10: Luminescence spectra of PTHS:PEDOT-S 1:1 films while drying from water solutions having the following concentrations: a) 8.14 g/L and b) 0.163 g/L. Excitation wavelength: 450 nm.

5 UV-vis spectroelectrochemistry of PTHS:[PEDOT-S:(Oct)₂NH₂] 1:1 films

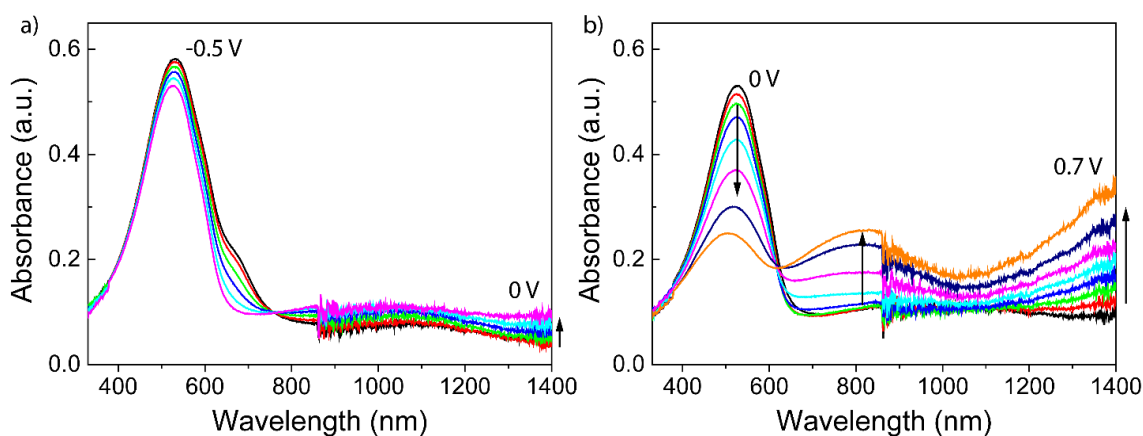
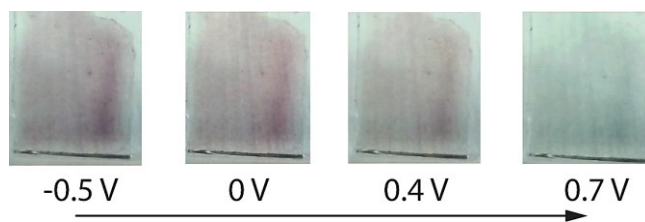
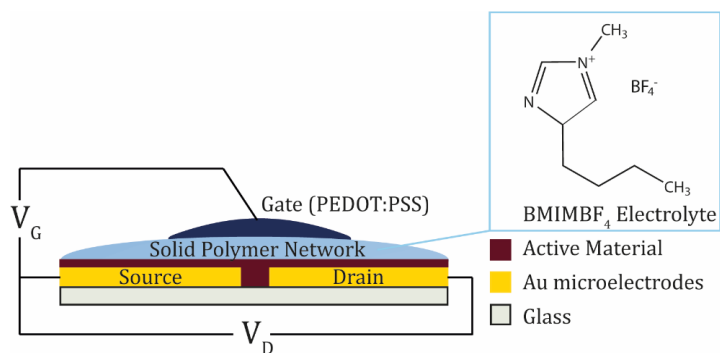


Figure 6-S11: UV-vis spectroelectrochemistry of PTHS:[PEDOT-S:(Oct)₂NH₂] 1:1 film (1 g/L) acquired from a) -0.5 V to 0 V, and b) from 0 V to 0.7 V vs Ag/AgCl reference electrode.



Scheme 6-S2: Changes in color observed for PTHS:[PEDOT-S:(Oct)2NH2] 1:1 film (1 g/L) from -0.5 V to 0.7 V vs Ag/AgCl reference electrode.

6 Schematic representation of OECT



Scheme 6-S3: Schematic representation of the fabricated organic electrochemical transistor devices.

7 Characteristics of OECTs having PTHS as active material

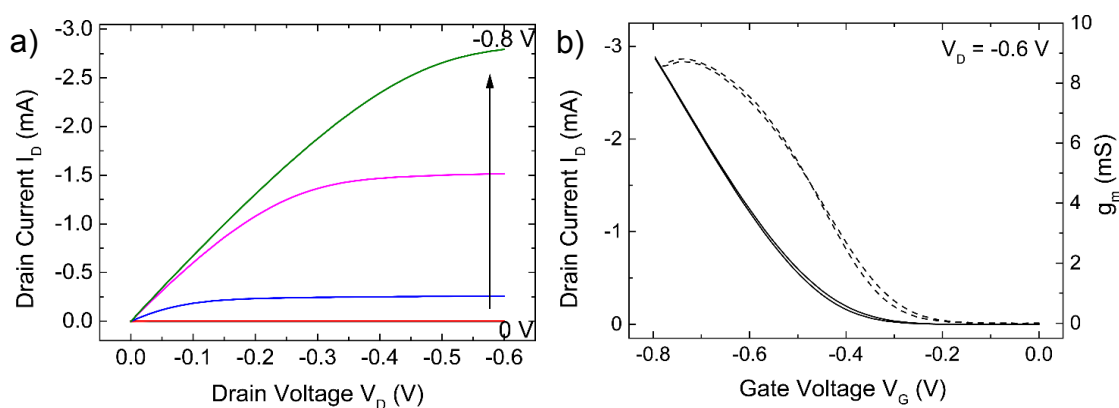


Figure 6-S12: Representative a) output characteristics and b) transfer characteristics of device made with PTHS as active material. Output curves (a) have been acquired for gate voltage (V_G) steps of 0.2 V. Transfer curves have been acquired for gate voltage sweeps from 0. to -0.8 V and vice versa, keeping a constant drain voltage of -0.6 V.

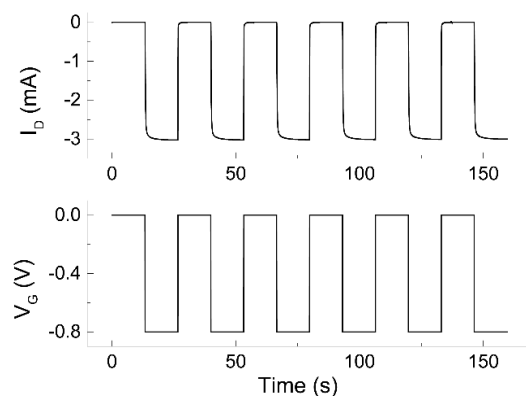


Figure 6-S13: Switching characteristics for devices having PTHS as active material, acquired for V_G switching from $V_G = 0$ V to $V_G = -0.8$ V, and constant $V_D = -0.6$ V.

8 Stability measurements

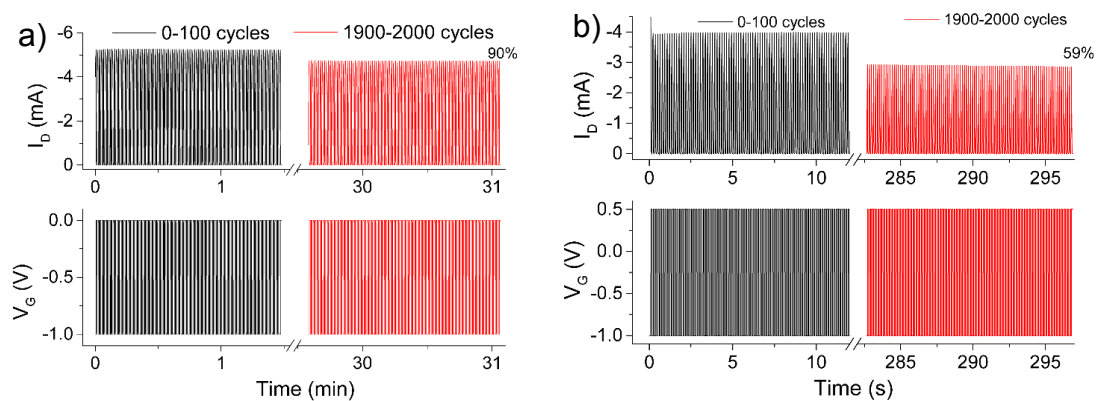


Figure 6-S14: a) Stability test over cycling for PTHS for V_G switching from $V_G = 0$ V to $V_G = -0.8$ V, constant $V_D = -0.6$ V, and ON/OFF cycles of 890 ms. b) Stability test over cycling for PTHS:PEDOT-S 1:1 devices for V_G switching from $V_G = 0.5$ V to $V_G = -1$ V, constant $V_D = -1.0$ V, and ON/OFF cycles of 150 ms.

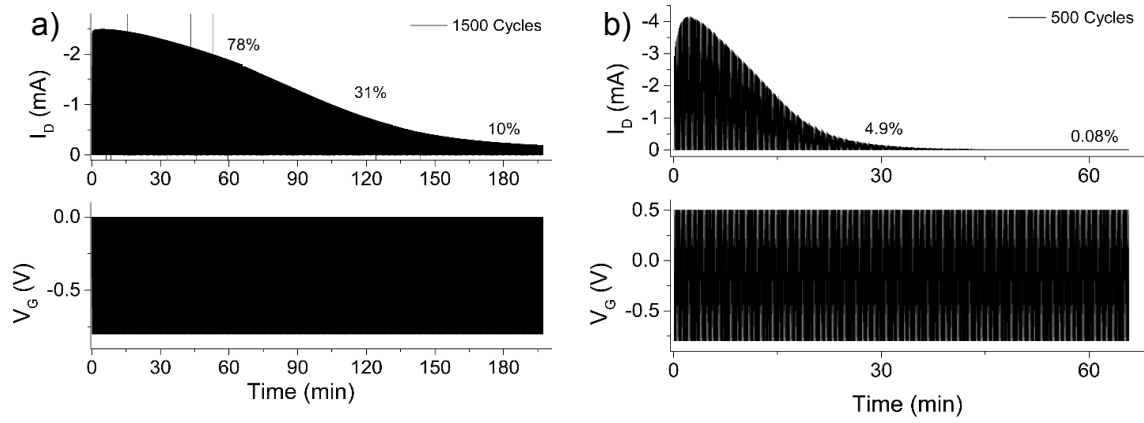


Figure 6-S15: Long time stability over cycling for a) PTHS for V_G switching from $V_G = 0$ V to $V_G = -0.8$ V, at constant $V_D = -0.6$ V, and b) PTHS:PEDOT-S 1:1 devices for V_G switching from $V_G = 0.5$ V to $V_G = -0.8$ V, at constant $V_D = -1.0$ V. The ON/OFF cycles were 7.8 s.

7 CONJUGATED POLYELECTROLYTE BLEND AS PHOTONIC PROBE OF BIOMEMBRANE ORGANIZATION

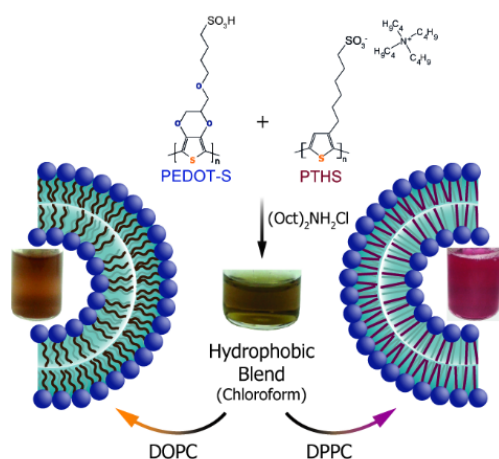
Erica Zeglio,^[a] Martina M. Schmidt,^[b] Mukundan Thelakkat,^[b] Roger Gabrielsson,^[c] Niclas Solin,^[a]
and Olle Inganäs*^[a]

[a] Department of Physics, Chemistry and Biology, Linköping University, SE-581 83 Linköping,
Sweden

[b] Macromolecular Chemistry I—Applied Functional Polymers, University of Bayreuth,
Universitätsstrasse 30, 95440 Bayreuth, Germany

[c] Department of Science and Technology, Linköping University, Campus Norrköping, S-60174
Norrköping, Sweden

*E-mail of corresponding author: oling@ifm.liu.se



Published in *ChemistrySelect* **2016**, *1*, 4340-4344

Abstract

In the following report, a conjugated polyelectrolyte (CPE) blend has been introduced for the first time as a fluorescent probe of membrane organization. Insertion of the blend into the lipid double layer has been rendered possible through formation of a hydrophobic complex by counterion exchange. Changes in membrane physical state from liquid-disordered (L_{dis}) to liquid-ordered (L_{ord}), and to solid-ordered (S_{ord}) result in red shifts of blend excitation (up to $\Delta\lambda_{ex}=+90$ nm) and emission (up to $\Delta\lambda_{em}=+37$ nm) maxima attributable to backbone planarization of CPEs. We found that blend stoichiometry can be adjusted to attain the best interplay among single polyelectrolytes properties, such as sensitivity and luminescence. The resulting probes therefore allow a bimodal detection of membrane physical state: changes in absorption permit a direct visualization of membrane organization, while variations in emission spectra demonstrate that CPE-blends are promising probes that can be used for imaging applications.

Paper

Fluorescent conjugated polyelectrolytes (CPEs) have been extensively used for both in vivo and in vitro bioimaging, as well as sensing applications.^[1] The attractive properties of CPEs, such as water solubility, low cytotoxicity, facile bioconjugation, aggregation dependent fluorescence, and photostability render them exceptional candidates for applications involving biological systems.^[2] The polar nature of the CPEs, however, precludes studies on the hydrophobic membrane core. As a result, previous studies have been focused exclusively on the hydrophilic areas of cells and/or model membrane systems. Local changes in lipid packing in biological membranes have been subject to intense investigation due to their importance in protein function, membrane signaling and virus trafficking.^[3] However, the mechanisms involved in those processes are still to a large extent unclear. One way to explore the role of lipid organization in membrane dynamics is to develop new environment sensitive membrane probes for fluorescence microscopy.^[4] Polarity sensitive probes, such as Laurdan, have so far been extensively employed,^[5] but their shortcomings limit their use as general probes. Conjugated oligomers in form of oligothiophenes have been recently introduced by Dal Molin et al. as mechanosensitive membrane probes,^[6] producing shifts in excitation upon changes in lipid packing. Fluorescence resonance energy transfer (FRET) could then be used for certain probes as a strategy to transcribe excitation shifts to emission shifts.^[7] Only two examples have been reported so far where CPEs are used as a detection tool for lipid organization,^[8] but in both cases the CPEs have been used in their hydrophilic form. In our previous work, we used a self-doped CPE (Poly(4-(2,3-dihydrothieno-(3,4-b)-(1,4)dioxin-2-yl)-me-thoxy)-1-butanefulfonic acid, PEDOT-

S), in combination with positively charged ammonium salts (such as dioctylammonium chloride, $(\text{Oct})_2\text{NH}_2\text{Cl}$), to produce hydrophobic complexes preserving certain polyelectrolyte properties, such as the metallic conductivity.^[9] However, PEDOT-S is not a good candidate as a membrane probe, since it is not fluorescent. Poly(6-(thiophen-3-yl)hexane-1-sulfonate) PTHS, conversely, has a backbone constituted by thiophene units and it is highly luminescent.^[10] However, as we will demonstrate, PTHS is not suitable as a membrane probe either, as its complexes exhibit very little sensitivity to changes in membrane organization. Herein, we report that blending of the two CPEs (Figure 7-1) from water solution is a viable strategy to produce new materials able to efficiently sense and report changes in membrane environment through changes in their backbone conformation. To best of our knowledge, this is the first time that CPEs sensitivity has been exploited to produce an internalized bimodal probe for biomembranes organization. Blend complexation with a chosen ammonium salt has been used to produce hydrophobic complexes of the blend that can then be transferred to the hydrophobic lipid bilayer of liposomes, while preserving the sensitivity desired for practical applications.

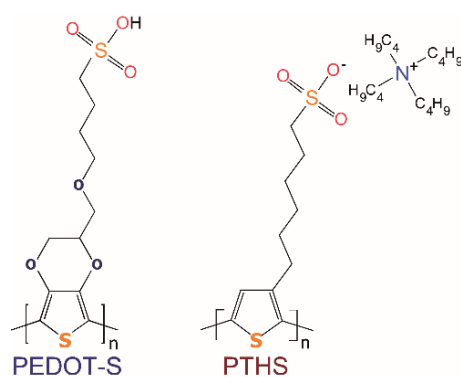


Figure 7-1: Chemical structure of the two conjugated polyelectrolytes used in this work.

The structural differences between the two polyelectrolytes give rise to different behavior toward interaction with oppositely charged surfactants. In our previous study, where we investigated the combination of PEDOT-S with ammonium salts,^[9] we found that addition of an excess of $(\text{Oct})_2\text{NH}_2\text{Cl}$ to PEDOT-S resulted in the formation of a precipitate. In contrast, addition of an excess of $(\text{Oct})_2\text{NH}_2\text{Cl}$ to PTHS leads to formation of a water soluble complex (i.e. no precipitate is formed, Figure 7-S2 and Figure 7-S3). In order to produce an hydrophobic PTHS:ammonium salt complex that would show hydrophobic properties (i.e. precipitate from water) trioctylammonium chloride ($(\text{Oct})_3\text{NHCl}$) was used. The orange complex solution turned into a red precipitate upon heating (Scheme 7-S1), which upon isolation could be dissolved in hydrophobic solvents such as chloroform (Figure 7-S4 and Figure 7-S5). In order to test the sensitivity of the PTHS: $(\text{Oct})_3\text{NH}$ complex toward lipid packing, liposomes composed of different

lipid species have been prepared. The chosen lipids were 1,2-dihexadecanoyl-*sn*-glycero-3-phosphocholine (DPPC), 1-palmitoyl-2-oleoyl-*sn*-glycero-3-phosphocholine (POPC), and 1,2-dioleoyl-*sn*-glycero-3-phosphocholine (DOPC), having a different number of unsaturated C-C bonds in the alkyl chains (none, one and two, respectively). This structural difference gives rise to different physical states of the lipids with respect to temperature, described by a parameter called the “phase transition temperature” T_m . POPC and DOPC have a T_m of -2°C and -17°C , respectively, and are consequently found in a fluid liquid disordered (L_{dis}) state at room temperature. DPPC has a T_m of 41°C , and accordingly it is in a more densely packed gel solid ordered (S_{ord}) state at room temperature.^[11] Increase of temperature above T_m leads to a phase transition from S_{ord} to L_{dis} state. Moreover, binary mixtures of phospholipids with cholesterol (Chol) lead to the formation of a liquid ordered (L_{ord}) phase, which has intermediate properties with respect to the S_{ord} and L_{dis} phases.^[12]

By comparing emission and excitation spectra for liposomes containing PTHS:(Oct)₃NH prepared from lipids in either the S_{ord} or L_{dis} state at 25°C , we were able to assess the suitability of PTHS:(Oct)₃NH as a probe for the lipid physical state. Spectroscopic investigation of such liposomes revealed small red shifts both in emission ($\Delta\lambda_{\text{em}}=+11$ nm) and excitation ($\Delta\lambda_{\text{ex}}=+10$ nm) for the complex in DPPC, with respect to DOPC and POPC liposomes (Figure 7-S6). These results reveal opposite spectral shifts with respect to the ones occurring for polarity sensitive probes.^[13] This suggests a different working mechanism for CPEs, which can be rationalized as the occurrence of backbone planarization (increase of conjugation length) in the more stiff S_{ord} phase rather than dipolar relaxation.^[6a] Changes in lipid phase with temperature have also been investigated for DPPC liposomes (Figure 7-S7). Excitation and emission spectra have been recorded at 55, 35 and 25°C . Results show a red shift in excitation of $\Delta\lambda_{\text{ex}}=+27$ nm for spectra acquired below the T_m , and no changes in emission maximum, indicating that the phase transition lead only to an increase in PTHS ground state planarity.^[14] Control experiments have been carried out using DOPC liposomes at the same conditions, in order to investigate whether the shifts may originate from thermochromic phenomena (Figure 7-S8). A shift of $\Delta\lambda_{\text{ex}}=+14$ nm is observed, indicating that thermochromism indeed play an important role. Therefore, even though the PTHS:(Oct)₃NH complex is highly fluorescent, its low sensitivity render it unable to efficiently probe changes in lipid packing.

PTHS has been mixed with PEDOT-S in a 1:1 ratio (based on monomer concentration), to produce a polyelectrolyte blend, hereafter abbreviated as blend 1:1. Even though spectroscopic data indicate no specific interaction among the two polyelectrolytes in water solution (Figure 7-S9 and Figure 7-S10), the fine mixture of the two species deeply influences their behavior in

presence of surfactants (Figure 7-S11). Addition of an excess of $(\text{Oct})_3\text{NHCl}$ to the CPEs blend 1:1 results in formation of a complex possessing high water solubility. Replacement of $(\text{Oct})_3\text{NHCl}$ with $(\text{Oct})_2\text{NH}_2\text{Cl}$ lead instead to full complex precipitation upon heating. The purple blend(1:1): $(\text{Oct})_2\text{NH}_2\text{Cl}$ pellet could then be dissolved in chloroform, leading to a green solution (Figure 7-S12 and Figure 7-S13).

Incorporation of the blend(1:1): $(\text{Oct})_2\text{NH}_2$ complex into DOPC liposomes results in changes in both absorption and emission (summarized in Figure 7-2), demonstrating an unique sensitivity of the blend and related hydrophobic complex toward changes in surrounding environment.

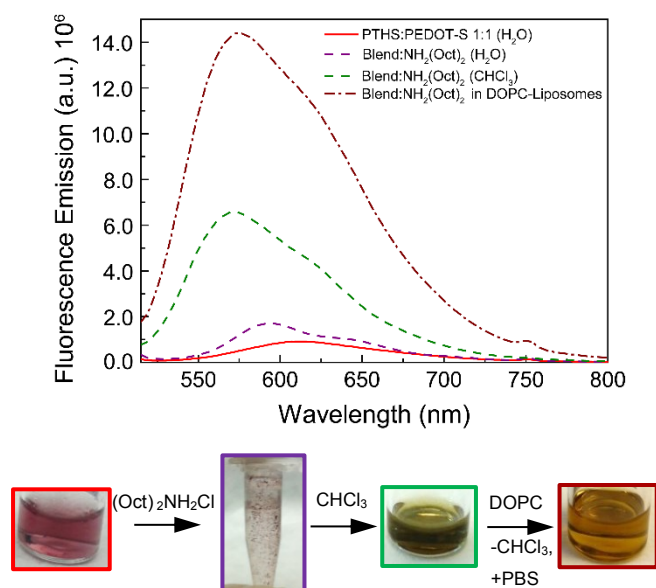


Figure 7-2: Fluorescence spectra and scheme reporting PTHS:PEDOT-S 1:1 (red) and blend(1:1): $(\text{Oct})_2\text{NH}_2$ complex (purple) in water solution, dissolution of complex in chloroform (green) and embedding into DOPC liposomes (wine). Blend concentration was 0.01 g/L in all the measurements, while DOPC concentration was 0.1 g/L.

Tests of the effects of blend stoichiometry on the sensitivity to lipid phase showed that a range of compositions are suitable for application as a probe (Table 7-S1), but the composition PTHS:PEDOT-S 1:3 produced the largest shifts in wavelength at the lowest concentration (see below, Figure 7-6 for further discussion). Blend(1:3): $(\text{Oct})_2\text{NH}_2$ sensitivity has then been tested toward different liposomes compositions. As expected, emission spectra of blend(1:3): $(\text{Oct})_2\text{NH}_2$ in DOPC and POPC liposomes at room temperature (L_{dis} phase) exhibit the same maxima, at $\lambda_{\text{max,em}}=577$ nm and $\lambda_{\text{max,ex}}=461$ nm. When blend(1:3): $(\text{Oct})_2\text{NH}_2$ is introduced in DPPC liposomes (S_{ord} phase) a red shift in emission of $\Delta\lambda_{\text{em}}=+37$ nm and excitation of $\Delta\lambda_{\text{exc}}=+79$ nm are observed (Figure 7-3, a and b). Those results are consistent with an increase in conjugation length of PTHS backbone, due to planarization effects that influence both the ground and the excited states. Fluorescence quenching and the formation of a vibrational shoulder at ~ 670 nm indicate a higher interchain π - π interaction among the two polyelectrolytes and increase of

blend(1:3):(Oct)₂NH₂ crystallinity in the most packed S_{ord} state.^[15] The blend(1:3):(Oct)₂NH₂ has then been added to liposomes composed of binary mixtures of DPPC and cholesterol (20% and 40%), where blue shifts of $\Delta\lambda_{em}=-13$ nm and $\Delta\lambda_{exc}=-40$ nm were observed, due to the S_{ord}→L_{ord} transition (Figure 7-3, c and d).^[16]

Increase of cholesterol content from 0% to 40% also causes an increase in both emission and excitation intensities that can be attributed to a lower CPEs proximity in the less packed L_{ord} state. Similar experiments carried out with DOPC:Chol mixtures lead to no shift in emission and a small changes in excitation spectra ($\Delta\lambda_{exc}=+11$ nm) upon cholesterol addition, coupled with a decrease of signal intensity (Figure 3, e and f). Shifts of $\Delta\lambda_{em}=+24$ nm and $\Delta\lambda_{exc}=+25$ nm are also found for DPPC:Chol (60:40) with respect to DOPC:Chol (60:40), as well as a decrease in signal intensity and enhancement of a vibrational shoulder for the DPPC:Chol system (Figure 3, a and b), meaning that blend(1:3):(Oct)₂NH₂ is also sensitive to different L_{ord} phases, resulting from the difference in affinity of cholesterol for different phospholipids.^[12]

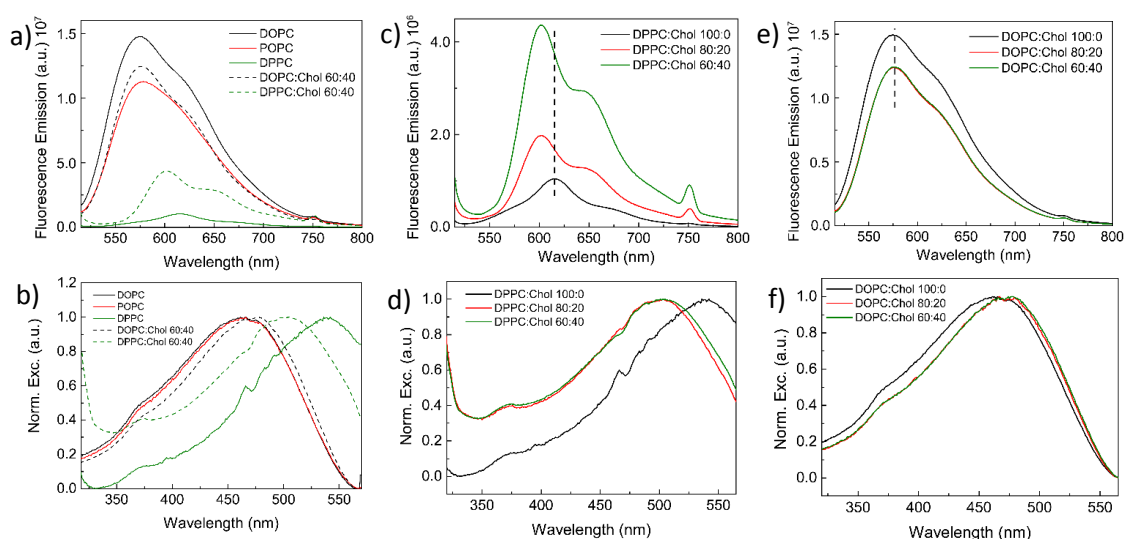


Figure 7-3: Emission (a) and normalized excitation (b) spectra of blend(1:3):(Oct)₂NH₂ in liposomes composed of DOPC ($\lambda_{max,em}=577$ nm and $\lambda_{max,ex}=461$ nm), POPC, DPPC ($\lambda_{max,em}=614$ nm and $\lambda_{max,ex}=542$ nm), DOPC:Chol 60:40, and DPPC:Chol 60:40. Emission (c) and normalized excitation (d) spectra of blend(1:3):(Oct)₂NH₂ in liposomes composed of binary mixtures of DPPC:Chol 100:0, DPPC:Chol 80:20, and DPPC:Chol 60:40 ($\lambda_{max,em}=601$ nm and $\lambda_{max,ex}=503$ nm). Emission (e) and normalized excitation (f) spectra of blend(1:3):(Oct)₂NH₂ in liposomes composed of binary mixtures of DOPC:Chol 100:0, DOPC:Chol 80:20, and DOPC:Chol 60:40 ($\lambda_{max,em}=577$ nm and $\lambda_{max,ex}=466$ nm) at 25°C. Blend 1:3 concentration was 0.01 g/L, while the total lipid concentration was 0.1 g/L.

The spectral changes resulting from difference in temperature for blend(1:3):(Oct)₂NH₂ added to DPPC phospholipids are in agreement with spectral changes resulting from differences in composition (Figure 7-4): at 55°C (L_{dis} phase) absorption and emission maxima are found at $\lambda_{em}=585$ nm and $\lambda_{ex}=450$ nm. Cooling the sample below the phase transition temperature results in red shifts of $\Delta\lambda_{em}=+31$ nm and changes in shape of the emission band, due to the L_{dis}→S_{ord} transition. Moreover, shift in excitation of $\Delta\lambda_{ex}=+90$ nm allows a direct visualization of

membrane state (Figure 7-5). Control experiments with liposomes made of DOPC phospholipids reveal small variations in excitation and emission intensities, and very small changes in excitation wavelength ($\Delta\lambda_{\text{ex}}=+7$ nm), confirming that thermochromic effects are negligible (Figure 7-S14). In order to confirm that blend hydrophobicity is essential to provide the desired sensitivity, aliquots of water solutions of the polyelectrolyte blend have been added to solutions of pre-formed liposomes with no inserted blends. Fluorescence spectra of the hydrophilic blend shows a shift from $\lambda_{\text{max,DPPC}}=605$ nm, when added to DPPC liposomes, to $\lambda_{\text{max,DOPC}}=570$ nm, when added to DOPC liposomes, but no emission fine structures (Figure 7-S15). Moreover, recording of blend emission spectra of samples where the hydrophilic blend is added to DPPC liposomes, below and above the phase transition temperature, does not lead to any spectral shift. The data indicates that, even though a certain degree of polyelectrolytes intercalation into the zwitterionic phospholipids is achieved,^[17] full embedding of the hydrophobic blend into the double layer is necessary for an efficient report of lipid organization (Figure 7-S16).

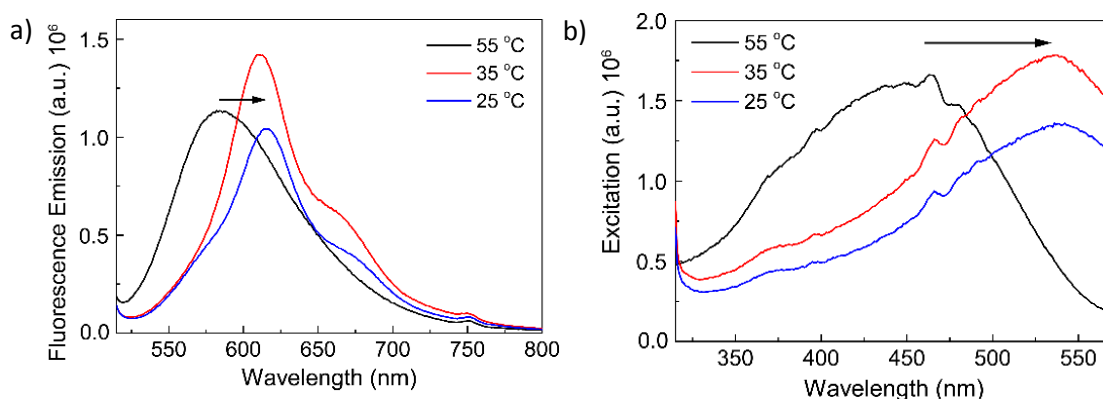


Figure 7-4: Emission (a) and excitation (b) spectra of blend(1:3):(Oct)₂NH₂ complex (blend concentration 0.01 g/L) in DPPC liposomes at 55°C, 35°C and 25°C. Blend 1:3 concentration was 0.01 g/L, while the total lipid concentration was 0.1 g/L.

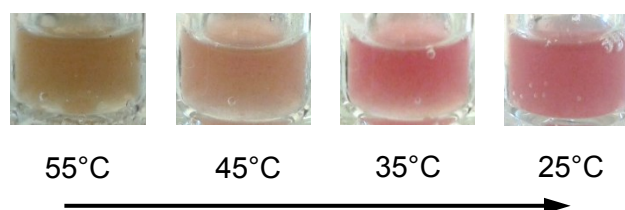


Figure 7-5: Solutions of blend(1:3):(Oct)₂NH₂ complex in DPPC liposomes at different temperatures. Blend 1:3 concentration was 0.1 g/L, while the total lipid concentration was 1 g/L.

Fluorescence depth quenching experiments have been performed to study whether changes in lipid organization and composition affect the position of the probe into the lipid bilayer.^[7] DOXYL-PC phospholipids, having a quencher covalently bonded at two different positions (5 and

14) of the lipid tails, have been used to label DOPC and DPPC vesicles. Afterwards, parallax analysis has then been used to estimate the average position of the probe from the bilayer center (Table 7-S3, Figure 7-S17 and Figure 7-S18).^[7, 18] Results show an average distance of 6.3 Å in both DPPC and DOPC L_{dis} phases, and 6.2 Å for DPPC in S_{ord} phase, indicating essentially no repositioning of the blend upon changes in lipid organization.

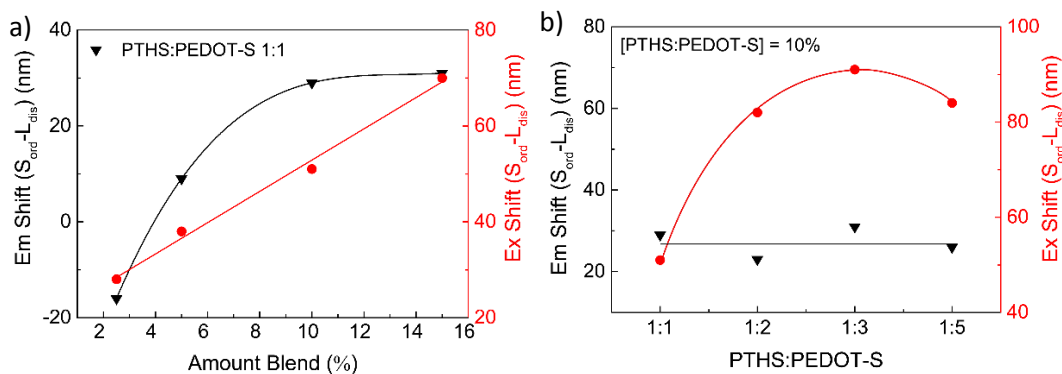


Figure 7-6: Emission (black) and excitation shifts (red) of the blend:(Oct)₂NH₂ complex for the $L_{dis} \rightarrow S_{ord}$ transition in DPPC liposomes as function of a) mole fraction of the blend(1:1):(Oct)₂NH₂ complex at constant stoichiometry, and b) PTHS:PEDOT-S stoichiometry at constant molar fraction (10%).

Effects related to changes in PTHS:PEDOT-S:(Oct)₂NH₂ blend 1:1 molar fraction (with respect to total lipid concentration, Table 7-S2) and blend stoichiometry have also been considered. Emission and excitation shifts due to the $L_{dis} \rightarrow S_{ord}$ transition have therefore been evaluated for DPPC liposomes at increasing molar fraction of blend(1:1):(Oct)₂NH₂ (Figure 7-6, a): data shows increased emission and excitation shifts (up to $\Delta\lambda_{em}=+31$ nm and $\Delta\lambda_{ex}=+74$ nm) for higher blend(1:1):(Oct)₂NH₂ amounts. On the other hand, changes in blend stoichiometry, while keeping the total blend molar fraction constant (10%) show that increase of PEDOT-S content in the blend leads to higher excitation shifts, while emission shifts remain somewhat constant (Figure 7-6, b). Results point out toward the importance of fine tuning of blend stoichiometry, which allow the use of lower amounts of probe, while retaining high luminescence and sensitivity. Observation of emission and excitation spectra from the blend(1:3):(Oct)₂NH₂ at the above described conditions also highlight the importance of PEDOT-S presence in the blend (Figure 7-S19 and Figure 7-S20). Spectra acquired in the L_{dis} state show similar absorption and emission maxima as for PTHS:(Oct)₃NH complex in the same phase, and none or little sensitivity to changes in molar fraction/stoichiometry of the blend, indicating that in this state PEDOT-S has no or little influence on the PTHS backbone conformation. Contrarily, in the S_{ord} state, large red shifts in excitation spectra and an interchange between a blue shifted and a red shifted shoulder in emission are found at higher molar fraction/PEDOT-S content. Those results show that PEDOT-S conformational changes determine the highly sensitivity to changes in membrane organization.

Close proximity with a highly luminescent polyelectrolyte, such as PTHS, allow to report those changes through shifts in excitation and emission. Dynamic light scattering (DLS) and confocal microscopy experiments have been performed to validate vesicles formation. Data show that blend(1:3):(Oct)₂NH₂ inclusion does not lead to liposomes rupture and/or lipid segregation (Figure 7-S21 and Figure 7-S22). Moreover, confocal images of giant unilamellar vesicles (GUV) composed of DOPC/DPPC/chol confirmed that blend(1:3):(Oct)₂NH₂ do not segregate preferentially in L_{dis} or in L_{ord} phase. Different emissive behavior of the blend allows recognition of the two different phases according to the above described emission characteristics (Figure 7-S23). The produced probe therefore proved to have extraordinary sensitivity toward changes in lipid packing, which can be exploited for practical applications. Moreover, previous studies involving the introduction of hydrophobic PEDOT-S complexes into the membrane of *Xenopus oocytes* suggest that integration into living cell membranes is possible. Therefore, the blend probe is a promising candidate for the study of lateral heterogeneity in biological lipid membranes.

Supporting Information

PTHS synthesis, experimental details, PTHS complexes characterization, characterization of liposomes containing PTHS:(Oct)₃NH, formation and characterization of PTHS:PEDOT-S complexes, characterization of blend(1:3):(Oct)₂NH₂ in DOPC liposomes, blend interaction with preformed liposomes in water, depth quenching experiments, spectroscopic characterization of increased blend content and stoichiometry, dynamic light scattering, confocal images of LMV and GUV.

Acknowledgements

We would like to acknowledge the Marie Curie network “Renaissance” founded by the People FP7 Program, and the Knut and Alice Wallenberg foundation through a Wallenberg Scholar grant to O.I. for financial support. Mukundan Thelakkat and Martina Schmidt acknowledge DFG (GRK 1640) for the financial support. We gratefully acknowledge Camilla Sandén for useful discussions on liposomes preparation and characterization. Martina Schmidt acknowledges support from Elite Study programme, Macromolecular Science at the University of Bayreuth.

Keywords: Conjugated Polyelectrolytes • Fluorescent Probes • Liposomes • Membrane Probes • Polyelectrolytes blend

References

- [1] a) K.-Y. Pu, B. Liu, *Adv. Funct. Mater.* **2011**, *21*, 3408-3423; b) G. Feng, D. Ding, B. Liu, *Nanoscale* **2012**, *4*, 6150-6165; c) K. P. R. Nilsson, A. Herland, P. Hammarström, O. Inganäs, *Biochemistry* **2005**, *44*, 3718-3724.
- [2] K. Magnusson, H. Appelqvist, A. Cieślak-Pobuda, J. Wiggenius, T. Karlsson, M. J. Łos, B. Kågedal, J. Jonasson, K. P. R. Nilsson, *Cytometry Part A* **2015**, *87*, 262-272.
- [3] K. Simons, M. J. Gerl, *Nat. Rev. Mol. Cell Biol.* **2010**, *11*, 688-699.
- [4] M. Carquin, L. D'Auria, H. Pollet, E. R. Bongarzone, D. Tyteca, *Prog. Lipid Res.* **2016**, *62*, 1-24.
- [5] E. Sezgin, T. Sadowski, K. Simons, *Langmuir* **2014**, *30*, 8160-8166.
- [6] a) D. A. Doval, M. D. Molin, S. Ward, A. Fin, N. Sakai, S. Matile, *Chem. Sci.* **2014**, *5*, 2819-2825; b) M. Dal Molin, S. Matile, *Org. Biomol. Chem.* **2013**, *11*, 1952-1957.
- [7] M. Dal Molin, Q. Veroleto, A. Colom, R. Letrun, E. Derivery, M. Gonzalez-Gaitan, E. Vauthey, A. Roux, N. Sakai, S. Matile, *J. Am. Chem. Soc.* **2015**, *137*, 568-571.
- [8] a) Z. Kahveci, M. J. Martínez-Tomé, R. Mallavia, C. R. Mateo, *Biomacromolecules* **2013**, *14*, 1990-1998; b) J. E. Houston, M. Kraft, U. Scherf, R. C. Evans, *Phys. Chem. Chem. Phys.* **2016**.
- [9] P. K. Johansson, D. Julleson, A. Elfving, S. I. Liin, C. Musumeci, E. Zeglio, F. Elinder, N. Solin, O. Inganäs, *Sci. Rep.* **2015**, *5*, 11242.
- [10] J. C. Brendel, M. M. Schmidt, G. Hagen, R. Moos, M. Thelakkat, *Chem. Mater.* **2014**, *26*, 1992-1998.
- [11] L. Picas, F. Rico, S. Scheuring, *Biophys. J.* **2012**, *102*, L01-L03.
- [12] T. P. W. McMullen, R. N. A. H. Lewis, R. N. McElhane, *Curr. Opin. Colloid Interface Sci.* **2004**, *8*, 459-468.
- [13] S. Sanchez, M. Tricerri, G. Gunther, E. Gratton, *Modern Research and Educational Topics in Microscopy (Formatex)* **2007**, *2*, 1007-1014.
- [14] Y. Sun, Y. Li, Y. Li, F. Ma, *Comput. Mater. Sci.* **2007**, *39*, 673-677.
- [15] F. J. M. Hoeben, P. Jonkheijm, E. W. Meijer, A. P. H. J. Schenning, *Chem. Rev.* **2005**, *105*, 1491-1546.
- [16] M. B. Sankaram, T. E. Thompson, *Proc. Natl. Acad. Sci. U. S. A.* **1991**, *88*, 8686-8690.
- [17] A. T. Ngo, G. Cosa, *Langmuir* **2010**, *26*, 6746-6754.
- [18] a) A. Chattopadhyay, E. London, *Biochemistry* **1987**, *26*, 39-45; b) M. Kondo, M. Mehiri, S. L. Regen, *J. Am. Chem. Soc.* **2008**, *130*, 13771-13777.

Supporting Information

Table of contents

1	Materials and methods	161
1.1	Synthesis of the precursor polymer poly(3-(6-bromohexyl)-thiophene)	161
1.1.1	SEC and MALDI-ToF analysis of the precursor polymer poly(3-(6-bromohexyl)-thiophene).....	162
1.2	Synthesis of poly(6-(thiophen-3-yl)hexane-1-sulfonate) PTHS.....	162
1.3	Spectroscopic measurements.....	162
1.4	Fluorescence lifetime measurements.....	163
1.5	Dynamic light scattering measurements	163
1.6	Confocal microscopy measurements.....	163
1.7	Blend preparation	163
1.8	Preparation of trioctylammonium complexes	164
1.9	Preparation of dioctylammonium complexes.....	164
2	Vesicles preparation.....	165
2.1	Preparation of PTHS:(Oct) ₃ NH and blend:(Oct) ₂ NH ₂ lipid vesicles	165
3	Giant unilamellar vesicles (GUV) preparation by gentle hydration	166
4	Characterization of PTHS complexes	167
4.1	Characterization of PTHS:(Oct) ₂ NH ₂ and PTHS:(Oct) ₃ NH complexes.....	167
5	Characterization of liposomes containing PTHS:(Oct) ₃ NH complexes.....	169
6	Formation and characterization of PTHS:PEDOT-S complexes.....	170
7	Characterization of blend(1:3):(Oct) ₂ NH ₂ complex in DOPC liposomes	173
8	Liposomes interaction with blend from water solution	173
9	Depth quenching experiments.....	174
10	Effects related to increase of blend content and stoichiometry	177
11	Dynamic Light Scattering Experiments	179
12	Confocal images of LMV.....	180
13	Confocal images of GUV.....	180
	Supporting References.....	181

1 Materials and methods

Poly(4-(2,3-dihydrothieno-(3,4-b)-(1,4)dioxin-2-yl-methoxy)-1-butanefulfonic acid, sodium salt) PEDOT-S (3-16 repeating units, maximum $M_w=4899.2$ g/mol, from MALDI-TOF mass spectrum)^[1] was synthesized as previously reported.^[2] Tetrabutylammonium Poly(6-(thiophen-3-yl)hexane-1-sulfonate) PTHS was synthesized as described below.^[3] Chloroform solutions of 1,2-dioleoyl-*sn*-glycero-3-phosphocholine (DOPC), 1-palmitoyl-2-oleoyl-*sn*-glycero-3-phosphocholine (POPC) and 1,2-dihexadecanoyl-*sn*-glycero-3-phosphocholine (DPPC), and of the probes 16:0-5 Doxyl PC (1-palmitoyl-2-stearoyl-(5-doxyl)-*sn*-glycero-3-phosphocholine) and 16:0-14 Doxyl PC (1-palmitoyl-2-stearoyl-(14-doxyl)-*sn*-glycero-3-phosphocholine) were purchased from Avanti Polar Lipids, Inc. (Alabaster, Alabama, USA). Dioctylamine 98%, trioctylamine 98% and phosphate buffered saline (PBS) tablets were purchased from Sigma Aldrich AB. All the other chemicals were purchased from Sigma Aldrich AB and used as received.

1.1 Synthesis of the precursor polymer poly(3-(6-bromohexyl)-thiophene)

2,5-Dibromo-3-(6-bromohexyl)thiophene (1.86 g, 4.59 mmol) was added to a dried 250 mL flask. With a LiCl solution ($c=0.5$ mol/L) in THF the concentration was set to 0.5 mol/L. Tert-butylmagnesium chloride ((1.24 mol/L in THF, 3.33 mL, 4.13 mmol) was added dropwise. After 24 h the concentration was reduced to 0.1 mol/L and a suspension of 1,3-bis(diphenylphosphino)propan-nickel-(II)chlorid (0.025 g, 0.046 mmol) in THF was added. After 1 h the polymerization was quenched by adding 2 mL of 16 % aqueous HCl. The solution was concentrated. After precipitation of the polymer in methanol, it was purified via Soxhlet extraction with methanol. SEC: M_n : 18184 g/mol, M_w : 20784 g/mol, PDI: 1.14. MALDI-ToF MS: M_n : 18480 g/mol, M_w : 18894 g/mol, PDI: 1.02. NMR: δ_H (300 MHz; $CDCl_3$) 1.39-1.47 (4 H, m), 1.64-1.68 (2 H, q, CH₂), 1.78-1.85 (2 H, q, -CH₂-CH₂-Br), 2.73-2.78 (2 H, t, CH₂), 3.36 (2 H, CH₂-Br), 6.91 (1 H, s, H_{arom}).

1.1.1 SEC and MALDI-ToF analysis of the precursor polymer poly(3-(6-bromohexyl)-thiophene)

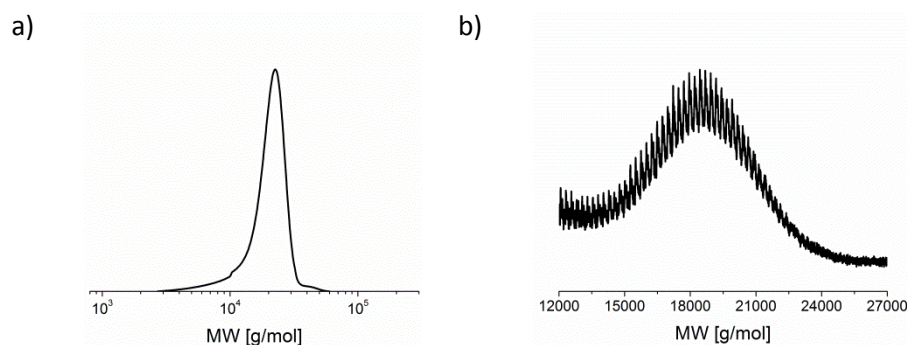


Figure 7-S1: a) SEC trace and b) MALDI-ToF analysis of the precursor polymer poly(3-(6-bromohexyl)-thiophene). For the calibration of the SEC polystyrene was used as external standard.

1.2 Synthesis of poly(6-(thiophen-3-yl)hexane-1-sulfonate) PTHS

Poly(3-(6-bromohexyl)-thiophene) (0.15 g, 0.008 mmol) was added in a dried 100 mL flask and solved in dry THF (40.5 mL). The mixture was degassed by a constant argon stream for 30 minutes. After the addition of tetra-*n*-butyl ammonium sulfite (0.93 mol/L in MeOH, 6 mL, 5.58 mmol), the reaction mixture was heated to 40 °C and stirred overnight. Water was added. The polymer was purified via dialysis against ultrapure water (Milli-Q) and freeze-drying. NMR: δ_{H} (300 MHz; d-THF/D₂O: 2/1) 0.86-0.96 (12 H, t, N⁺(-CH₂-CH₂-CH₂-CH₃)₄), 1.25-1.41 (8 H, dt, N⁺(-CH₂-CH₂-CH₂-CH₃)₄), 1.35-1.48 (4 H, m, CH₂-CH₂-CH₂-CH₂-CH₂-S), 1.52-1.67 (8 H, m, N⁺(-CH₂-CH₂-CH₂-CH₃)₄), 1.67-1.80 (4 H, m, CH₂-CH₂-CH₂-CH₂-CH₂-S), 2.63-2.88 (4 H, m, CH₂-CH₂-CH₂-CH₂-CH₂-S), 3.10-3.25 (8 H, m, N⁺(-CH₂-CH₂-CH₂-CH₃)₄), 6.98-7.08 (1 H, s, H_{arom}).

1.3 Spectroscopic measurements

UV-Vis absorption measurements of the samples in solution were performed with an Autolab PGStat 10 (EchoChemie, The Netherlands). Fluorescence and excitation measurements were performed with a Horiba Jobin Yvon Fluoromax 4 spectrofluorometer equipped with a magnetic stirrer and a thermostat. In all the experiments involving changes in temperature, the solutions were stirred for 20 minutes after the correct temperature was reached to allow sample equilibration. Slit sizes for emission measurements were 5 nm and 6 nm for the incoming and emitted light, respectively, and 2 nm and 3 nm for excitation measurements.

1.4 Fluorescence lifetime measurements

Fluorescence lifetime data were collected with a time-correlated single photon counting spectrometer (Mini- τ , Edinburgh Instruments) equipped with a laser of $\lambda = 500$ nm. A longpass filter was used in order to absorb the scattered light above 540 nm and a gray filter having absorbance 0.1 was used to attenuate the intensity of the incoming laser light.

1.5 Dynamic light scattering measurements

Correlation curves of the pure liposomes and liposomes containing blend 1:3 were acquired using an ALV/DLS/SLS-5022, compact goniometer system (ALV-GmbH, Germany), equipped with a HeNe laser ($\lambda=532$ nm, power=22 mW) as a light source, and two avalanche photo diodes (Perkin Elmer, Canada) working in cross auto correlation mode. The temperature of the surrounding toluene bath was kept constant at 22°C or 55°C with the help of a thermostat. All the samples were left to equilibrate at the desired temperature for at least 20 minutes prior measurements. The lipids concentration was 0.1 g/L in all cases, while the blend 1:3 concentration was 0.01 g/L. All the liposomes have been prepared as reported in the lipid vesicles preparation section. The scattered light was collected at 90° from the incoming laser beam. The CONTIN analysis was used to extrapolate the hydrodynamic radius (R_h). Data were calculated from the average of 5 measurements of 30 seconds each.

1.6 Confocal microscopy measurements

Large multilamellar vesicles (LMV) and giant unilamellar vesicles (GUV) were observed through a 100x objective on an inverted Zeiss LSM 700 confocal microscope (Carl Zeiss Microscopy GmbH, Germany). The observation chamber was constituted of a cover slip and a polydimethylsiloxane (PDMS) well (1 cm x 1 cm wide and 2 mm high). Glass cover slips were cleaned prior use with soap and with a solution of deionized $H_2O:H_2O_2:NH_3$ 5:1:1 at 85°C for 10 minutes. The signal was analyzed using a Zeiss Zen confocal software (Carl Zeiss Microscopy GmbH, Germany).

1.7 Blend preparation

The two polyelectrolytes were dissolved in water separately to produce single PTHS and PEDOT-S solutions having concentration of 5 g/L. Aliquots of stock solutions were therefore mixed

together to produce final water solutions of the blends (1 g/L) having the following monomer concentrations:

Table 7-S1: Monomers concentration related to blend stoichiometries.

Blend Stoichiometry	PTHS monomers concentration	PEDOT-S monomers concentration
PTHS:PEDOT-S 1:1	0.613 g/L, 1.26 mM	0.387 g/L, 1.26 mM
PTHS:PEDOT-S 1:2	0.443 g/L, 0.91 mM	0.557 g/L, 1.82 mM
PTHS:PEDOT-S 1:3	0.347 g/L, 0.71 mM	0.653 g/L, 2.13 mM
PTHS:PEDOT-S 1:5	0.242 g/L, 0.49 mM	0.758 g/L, 2.47 mM

1.8 Preparation of trioctylammonium complexes

109 μL of trioctylammonium chloride ($(\text{Oct})_3\text{NHCl}$) were added to 9.891 mL of HCl 0.1 mM and sonicated to form a colloidal dispersion. 200 μL of PTHS:PEDOT-S 1:1 blend 1g/L or 200 μL of PTHS 1g/L were mixed with 1.3 mL of $(\text{Oct})_3\text{NHCl}$ dispersion. The mixture was heated in an oil bath at $\sim 80^\circ\text{C}$. PTHS complexation leads to complete precipitation of PTHS: $(\text{Oct})_3\text{NH}$ after 48 hours, while blend complexation led only to partial complex precipitation after 72 hours. Heating for several days did not lead to further precipitation. The PTHS: $(\text{Oct})_3\text{NH}$ precipitate was vortexed and then sonicated for 5 min. As the precipitate remained attached to the cuvette walls, the supernatant (containing the liquid excess of $(\text{Oct})_3\text{NHCl}$) was discarded and the solid phase was then washed with HCl 0.1 mM for three times. The resulting pellet was blow-dried with N_2 for 20 minutes to complete removal of the solvent and dissolved in 200 μL of chloroform, producing a yellow solution.

1.9 Preparation of dioctylammonium complexes

An excess solution of dioctylammonium chloride ($(\text{Oct})_2\text{NH}_2\text{Cl}$) in HCl 0.1 mM was prepared (2.5 mM). $(\text{Oct})_2\text{NH}_2\text{Cl}$ was in a solid state at room temperature, therefore heating in a water bath at $\sim 50^\circ\text{C}$ for few minutes was necessary to allow compound withdrawal. The mixture was sonicated to allow $(\text{Oct})_2\text{NH}_2\text{Cl}$ solubilization and the pH was adjusted to $\text{pH} \sim 4$ by adding aliquots of HCl 0.1 M. The solution was filtered through a 0.2 μm PVDF filter. 200 μL of PTHS:PEDOT-S blend 1g/L or 200 μL of PTHS 1g/L were mixed with 1.3 mL of the previously prepared $(\text{Oct})_2\text{NH}_2\text{Cl}$ solution. The mixture was heated in an oil bath at $\sim 80^\circ\text{C}$. While for PTHS the solution turned from purple to orange upon complexation, the blend: $(\text{Oct})_2\text{NH}_2$ complex was heated until

full precipitation occurred, leaving a clear supernatant solution. The dispersion was vortexed and sonicated for 5 min then, after centrifugation at 10000 g for 10 min, the supernatant was discarded. The remaining precipitate was then washed with HCl 0.1 mM. The above process was repeated for three times to remove all the excess of dioctylammonium salt. The resulting pellet was blow-dried with N₂ for 20 minutes to remove the solvent and dissolved in 200 µL of chloroform, producing a green solution.

2 Vesicles preparation

2.1 Preparation of PTHS:(Oct)₃NH and blend:(Oct)₂NH₂ lipid vesicles

To incorporate the PTHS:(Oct)₃NH and blend:(Oct)₂NH₂ complexes into liposomes lipid bilayers, 0.2 mL of PTHS:(Oct)₃NH or blend:(Oct)₂NH₂ chloroform solutions (1 g/L) were added to 0.8 mL of lipid (DOPC, POPC or DPPC) 5 g/L in chloroform to achieve final blend concentration of 0.1 g/L and total lipid concentration of 1 g/L.

For experiments involving different molar fraction of the blend, blend 1:1 (1 g/L) was added to reach the following final concentrations:

Table 7-S2: Monomer concentrations of blend 1:1 and single components for different molar fractions of blend 1:1.

Molar fraction of the blend (%)	Blend 1:1 concentration (g/L)	DPPC concentration (g/L)	PTHS monomer concentration (mM)	PEDOT-S monomer concentration (mM)	DPPC concentration (mM)
2.5	0.025	1	0.031	0.031	1.36
5	0.05	1	0.063	0.063	1.36
10	0.1	1	0.126	0.126	1.36
15	0.15	1	0.189	0.189	1.36

The solvent was evaporated using a N₂ flow first, and then vacuum for 20 minutes. A red lipid cake remained at the bottom of the vial. 2 mL of PBS buffer solution (10 mM, pH 7.4), previously filtrated through a 0.2 µm PVDF filter, were added to the lipid cake leading to a final lipid concentration of 1 g/L and PTHS/blend concentration of 0.1 g/L. The cake was allowed to hydrate for 10 minutes. The solution was then stirred for 60 minutes and sonicated for 5 minutes to let the material detach from the walls. The solution was then extruded through a 0.4 µm pore size polycarbonate membrane (Avanti Polar Lipids, Inc) using a Mini-Extruder device (Lipofast Basic, Milmedtek AB) for 25 cycles. For confocal measurements on LMV, 20 µL of non-extruded liposomes solutions (1 g/L total lipid concentration, 0.1 g/L blend 1:3 concentration)

were added to 80 μL of agarose solution (50% w/v) in PBS buffer (10 mM).^[4] The images were acquired using two excitation wavelengths: 405 nm or 555 nm. Detection wavelengths were 405-490 nm (green, in the picture) for excitation at 405 nm, and 600-700 nm for excitation at 555 nm (red, in the picture), respectively.

3 Giant unilamellar vesicles (GUV) preparation by gentle hydration

Giant unilamellar vesicles (GUV) were prepared by the method of Akashi and co.^[5] Stock chloroform solutions containing DOPC (4.5 g/L), DPPC (4.5 g/L), cholesterol (1.18 g/L), blend 1:3 (1 g/L), and POPG (1 g/L) were prepared. POPG has been added during the preparation because charged phospholipids are needed for the preparation of GUV by this method.^[6] The solution was placed in a 10 mL round bottom flask and dried at 45°C with a rotary evaporator until a uniform dried film was formed at the bottom of the flask. Last traces of organic solvent were removed by placing the flask in vacuum for 6 hours. The lipid film was then hydrated with water-saturated nitrogen for 15 minutes. An aqueous sucrose solution (0.1 M) containing KCl (0.1 M) was purged with N_2 for 10 minutes and gently added to the flask (5 mL). The flask was sealed under N_2 and incubated at 37°C overnight to allow GUV formation. For confocal images of GUV the samples were prepared by mixing 20 μL of previously prepared GUV solution with 80 μL of glucose (0.1 M) and KCl (0.1 M) solution as an external media. The difference in density between the glucose external media and sucrose contained inside the vesicles (internal media) was used to allow the vesicles to settle down at the bottom of the chamber.^[5] The images were acquired using two excitation wavelengths: 488 nm or 555 nm. In the first case detection wavelengths were settled between 500-555 nm (green, in the picture), while in the second case between 600-700 nm (red, in the picture).

4 Characterization of PTHS complexes

4.1 Characterization of PTHS:(Oct)₂NH₂ and PTHS:(Oct)₃NH complexes

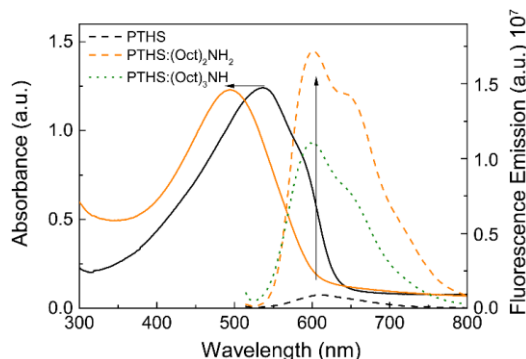


Figure 7-S2: Absorption (solid) and fluorescence (dashed) spectra of PTHS (black) and PTHS:(Oct)₂NH₂ complex (orange) in water solution. Blue shift is observed in the absorption band from 536 nm to 495 nm ($\Delta\lambda_{\text{abs}} = -41$ nm). Moreover, the emission intensity ($\lambda_{\text{max}} = 603$ nm) increases and a vibrational shoulder appears at $\lambda \sim 650$ nm. Those changes have been related to a breakage of polyelectrolyte aggregates, due to intercalation of hydrophobic surfactant alkyl chains among PTHS backbones,^[7] and/or reduction of the polarity of the surrounding media.^[8] The complex shows high water solubility. Fluorescence spectra of PTHS:(Oct)₃NH complex (dashed, green): acquisition of the absorption spectra was not possible due to scattering from the (Oct)₃NHCl dispersion. Increase in PTHS fluorescence intensity is also observed upon interaction with (Oct)₃NHCl. However, the complex precipitates over time, due to an increase in hydrophobicity of surfactant chains. PTHS concentration was 0.0613 g/L for absorption spectra and 0.00613 g/L for emission experiments.

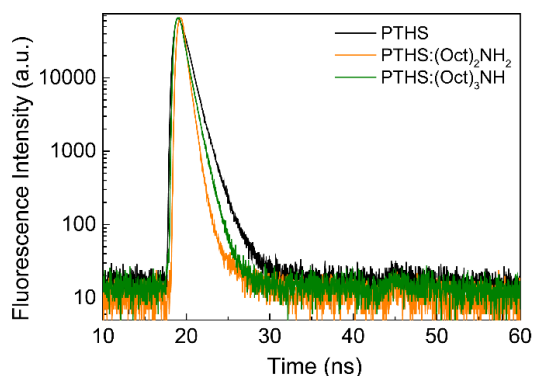
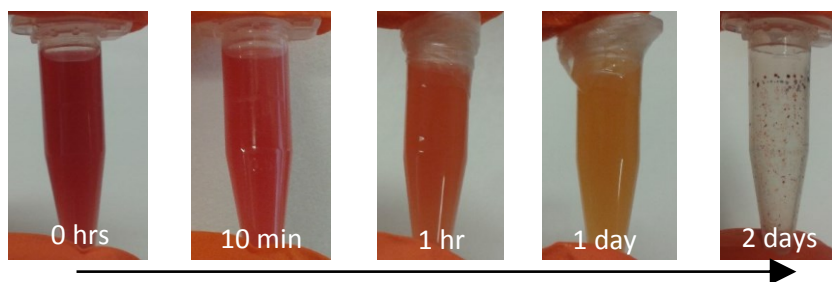


Figure 7-S3: Fluorescence lifetime of PTHS (black), PTHS:(Oct)₂NH₂ (orange) and PTHS:(Oct)₃NH (green) in water solution. Results confirm complete breakage of PTHS aggregates in presence of (Oct)₂NH₂Cl, which allows more interactions with surrounding solvent and increase of decay paths. Interaction with (Oct)₃NHCl however leads to new forms of aggregates, which have a lifetime in between the one observed for pure PTHS and PTHS:(Oct)₂NH₂ complex. PTHS concentration was 0.00613 g/L for all experiments.



Scheme 7-S1: From left to right: formation and consequent precipitation of PTHS:(Oct)₃NH complex at 80°C over time.

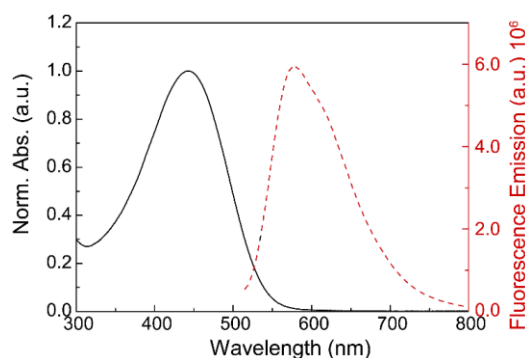


Figure 7-S4: Normalized absorption (left) and fluorescence (right) spectra of PTHS:(Oct)₃NH complex in chloroform. Both the absorption and fluorescence bands are considerably blue shifted (to 443 nm, and 577 nm, respectively) with respect to the measurements acquired from the complex in water solution ($\Delta\lambda_{\text{abs}}=-91$ nm and $\Delta\lambda_{\text{em}}=-26$ nm), due to decrease in conjugation length upon complex dissolution in a good solvent. PTHS concentration was 0.0613 g/L for absorption (inserted picture) and 0.00613 g/L for emission data.

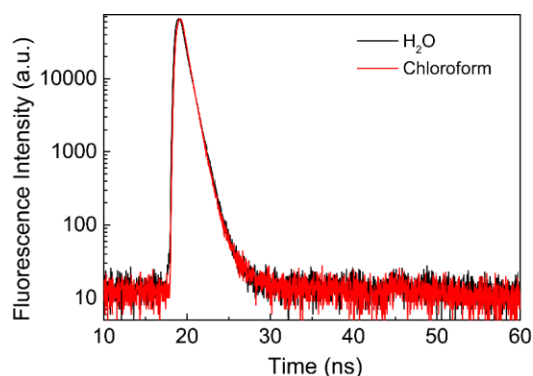


Figure 7-S5: Fluorescence lifetime of PTHS:(Oct)₃NH complex in water (black) and chloroform (red). Results indicate no change in decay paths upon change of solvent. PTHS concentration was 0.00613 g/L.

5 Characterization of liposomes containing PTHS:(Oct)₃NH complexes

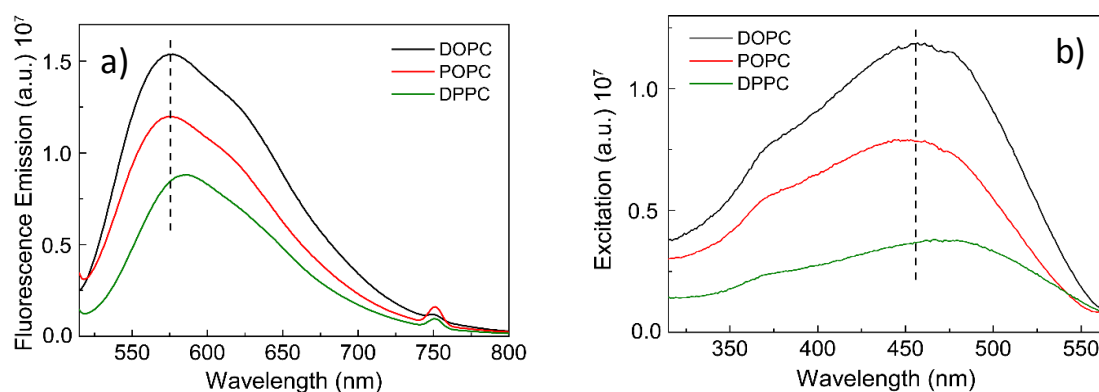


Figure 7-S6: a) Fluorescence spectra and b) excitation spectra of PTHS:(Oct)₃NH complex embedded in liposomes double layer made of phospholipids in L_{dis} phase (λ_{em} =575 nm, λ_{ex} =457 nm): DOPC (black) and POPC (red), and in S_{ord} phase: DPPC (green, (λ_{em} =586 nm, λ_{ex} =467 nm). All the spectra have been acquired at 25°C. PTHS concentration was 0.01 g/L, while lipid concentration was 0.1 g/L.

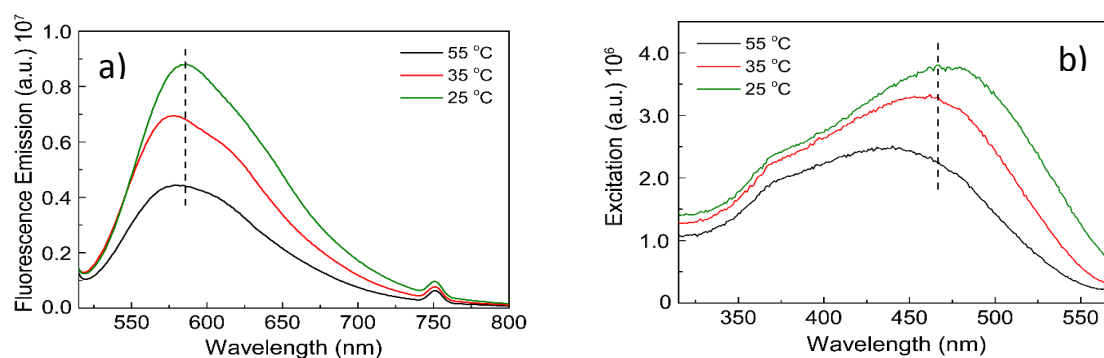


Figure 7-S7: a) Fluorescence spectra and b) excitation spectra of DPPC liposomes containing PTHS:(Oct)₃NH complex recorded above the phase transition temperature (L_{dis} phase, λ_{em} =580 nm, λ_{ex} =440 nm), at 55°C (black), and below (S_{ord} phase), at 35°C (red) and 25°C (green, λ_{em} =586 nm, λ_{ex} =467 nm). PTHS concentration was 0.01 g/L, while lipid concentration was 0.1 g/L.

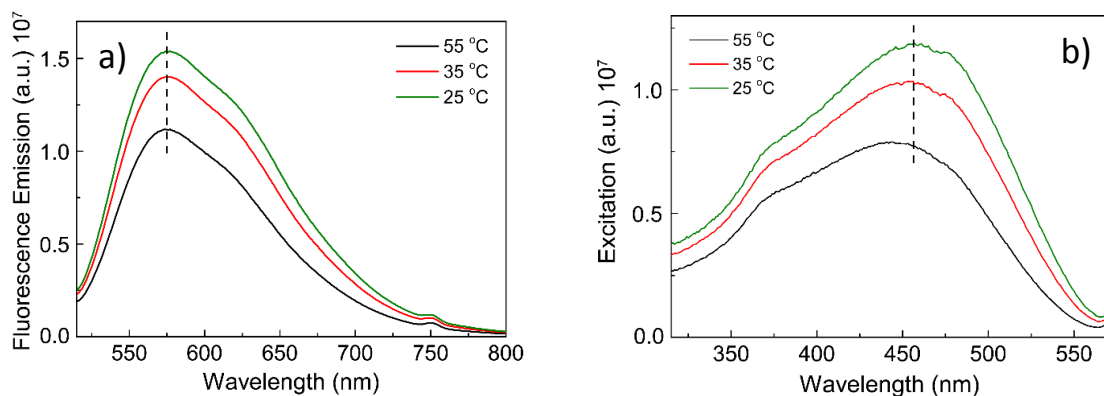


Figure 7-58: a) Fluorescence spectra and b) excitation spectra of DOPC liposomes containing PTHS:(Oct)₃NH complex recorded at 55°C (black, λ_{em} =577 nm, λ_{ex} =441 nm), 35°C (red) and 25°C (green, λ_{em} =577 nm, λ_{ex} =455 nm). The liposomes share the same phase (Ldis phase) at all the recorded temperatures. PTHS concentration was 0.01 g/L, while lipid concentration was 0.1 g/L.

6 Formation and characterization of PTHS:PEDOT-S complexes

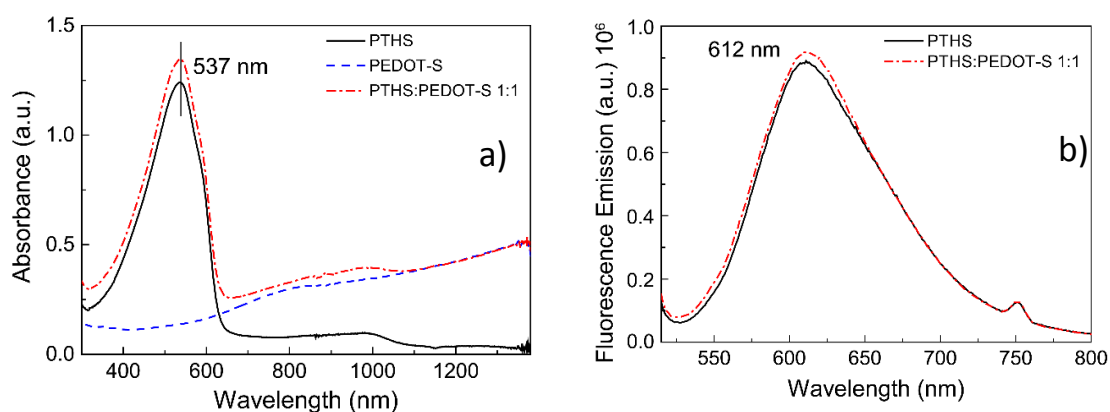


Figure 7-59: a) Absorption spectra of PTHS (black, solid), PEDOT-S (blue, dashed) and PTHS:PEDOT-S blend 1:1 (red, dot-dash) in water solution. PTHS concentration was 0.0613 g/L, PEDOT-S concentration was 0.0387 g/L, and PTHS:PEDOT-S blend 1:1 concentration 0.1 g/L. b) Fluorescence spectra of PTHS (black, solid) and PTHS:PEDOT-S 1:1 blend (red, dot-dash) in water solution. PTHS concentration was 0.00613 g/L, and PTHS:PEDOT-S blend 1:1 concentration 0.01 g/L. Spectroscopic data indicate no specific interaction among the two polyelectrolytes in a diluted regime.

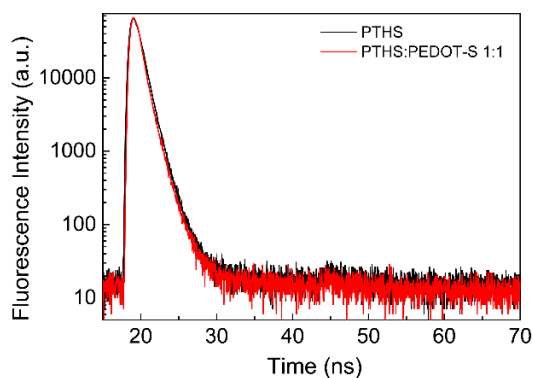


Figure 7-S10: Fluorescence lifetime of PTHS (black) and PTHS:PEDOT-S 1:1 blend (red) confirming spectroscopic data. PTHS concentration was 0.00613 g/L, and blend 1:1 concentration 0.01 g/L.

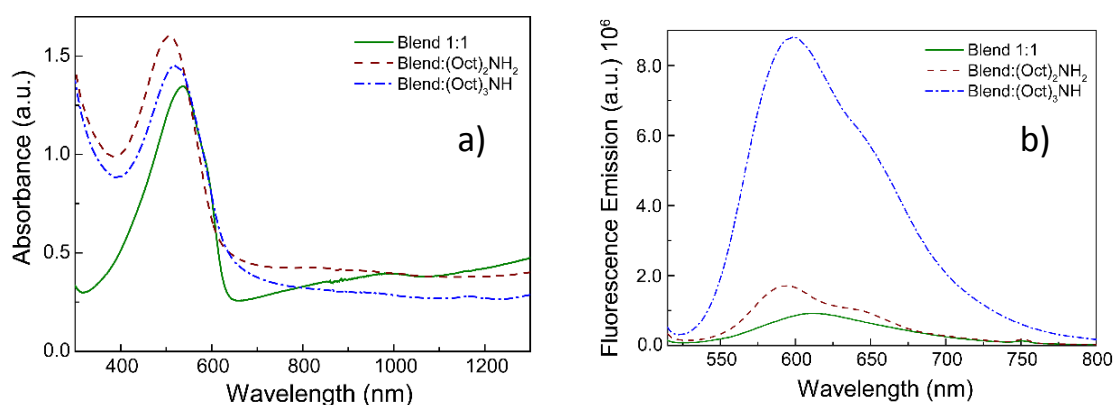


Figure 7-S11: a) Absorption spectra of blend 1:1 in water (green, solid, λ_{\max} =537 nm), blend(1:1):(Oct)₂NH₂ in water before precipitation (wine, dashed, λ_{\max} =506 nm), and blend(1:1):(Oct)₃NH (blue, dash-dot, λ_{\max} =519 nm). Blue shift of PTHS band is observed from blend 1:1 in water, to blend(1:1):(Oct)₃NH, and to blend(1:1):(Oct)₂NH₂, indicating a progressive decrease of PTHS conjugation length. b) Fluorescence spectra of blend 1:1 in water (green, solid), blend(1:1):(Oct)₂NH₂ 1:1 in water before precipitation (wine, dashed), and blend(1:1):(Oct)₃NH (blue, dash-dot). Formation of complex with (Oct)₂NH₂Cl lead to a blue shift of PTHS emission band from 610 to 595 nm, and formation of a vibrational shoulder at 640 nm. Complexation with (Oct)₃NHCl, instead, lead to both a blue shift to 599 nm and increase of emission intensity due to CPEs solubilization. The data indicate a clear difference in behavior of pristine PTHS and of PTHS in presence of PEDOT-S, probably due to undifferentiated self-doping from the sulfonate groups of the CPEs, which lead to co-precipitation in presence of (Oct)₂NH₂Cl.^[9] Blend 1:1 concentration was 0.1 g/L for absorption and 0.01 g/L for emission spectra.

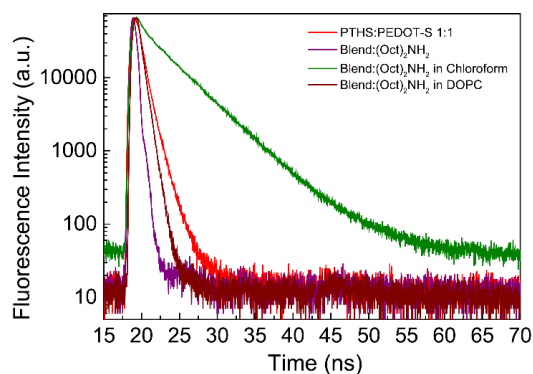


Figure 7-S12: Fluorescence lifetime of PTHS:PEDOT-S 1:1 (red) and blend(1:1):(Oct)₂NH₂ complex (purple) in water solution, of the complex in chloroform (green) and into DOPC liposomes (wine). Long lifetime of the complex in chloroform can be due to complete dissolution of the hydrophobic blend(1:1):(Oct)₂NH₂ complex in a good solvent.^[7] Conversely, shorter lifetime for the complex of the blend in water and into DOPC membrane double layer is probably due to increase of rate of decay of excited states in embedded environments. Blend 1:1 concentration was 0.01 g/L in all the measurements.

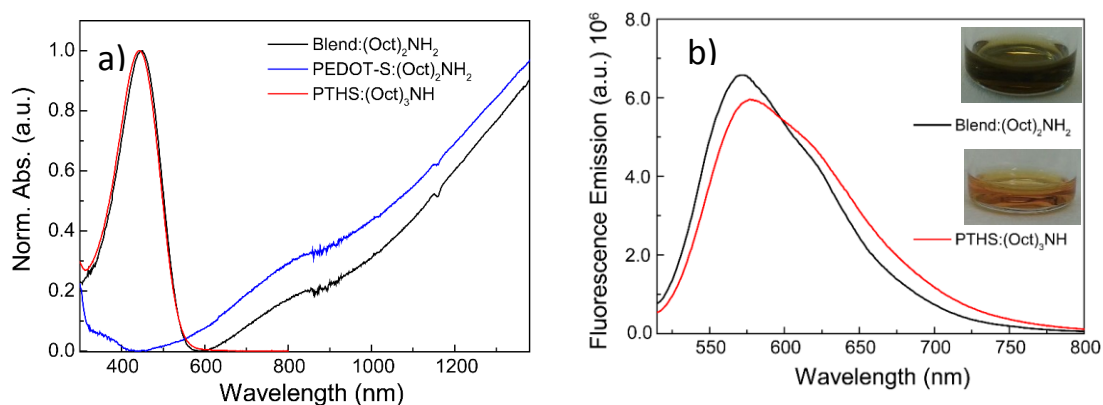


Figure 7-S13: a) Normalized absorption spectra for blend(1:1):(Oct)₂NH₂ complex (black, λ_{abs} = 449 nm), PEDOT-S:(Oct)₂NH₂ complex (blue) and PTHS:(Oct)₂NH₂ complex (red) in chloroform. PTHS concentration was 0.0613 g/L, PEDOT-S concentration was 0.0387 g/L, and blend 1:1 concentration 0.1 g/L. b) Fluorescence spectra of blend(1:1):(Oct)₂NH₂ complex (black, λ_{em} = 571 nm) and PTHS:(Oct)₂NH₂ complex (red) in chloroform. No substantial changes have been observed in absorption spectra, while a small blue shift is observed in blend emission and decrease of vibrational shoulder, probably due to a decrease of PTHS chains organization in presence of PEDOT-S. PTHS concentration was 0.00613 g/L, and blend 1:1 concentration 0.01 g/L.

7 Characterization of blend(1:3):(Oct)₂NH₂ complex in DOPC liposomes

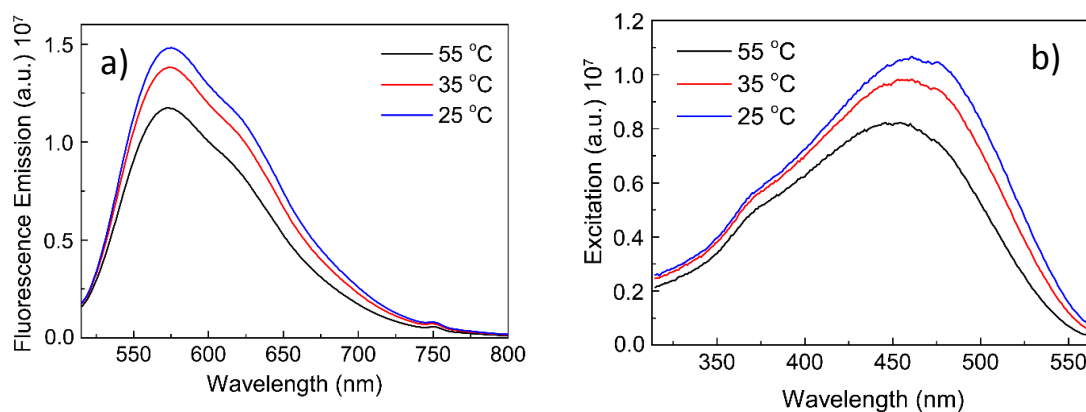


Figure 7-S14: Emission (a) and excitation (b) spectra of blend(1:3):(Oct)₂NH₂ complex in DOPC liposomes (L_{dis} phase) at 55°C (black), 35°C (red) and 25°C (blue). The small observed changes are related to thermochromism. The blend concentration was 0.01 g/L, while the total lipid concentration was 0.1 g/L.

8 Liposomes interaction with blend from water solution

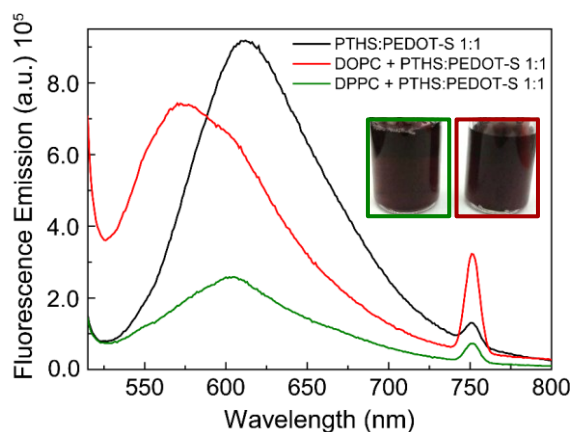


Figure 7-S15: Emission spectra of PTHS:PEDOT-S 1:1 in water (0.01 g/L, black), or added to DOPC liposomes (red) and DPPC liposomes (green). Pristine liposomes were formed by extrusion through 400 nm pore size filter. The process was followed by addition of polyelectrolyte blend 1:1 (1 g/L) aliquot to reach a final blend concentration of 0.1 g/L. The samples were then diluted to reach a final blend 1:1 concentration of 0.01 g/L and a total lipid concentration of 0.1 g/L. Despite what previously observed for same concentration of the blend 1:1 added from chloroform solution, in this case the color differences were undiscernible through the naked eye.

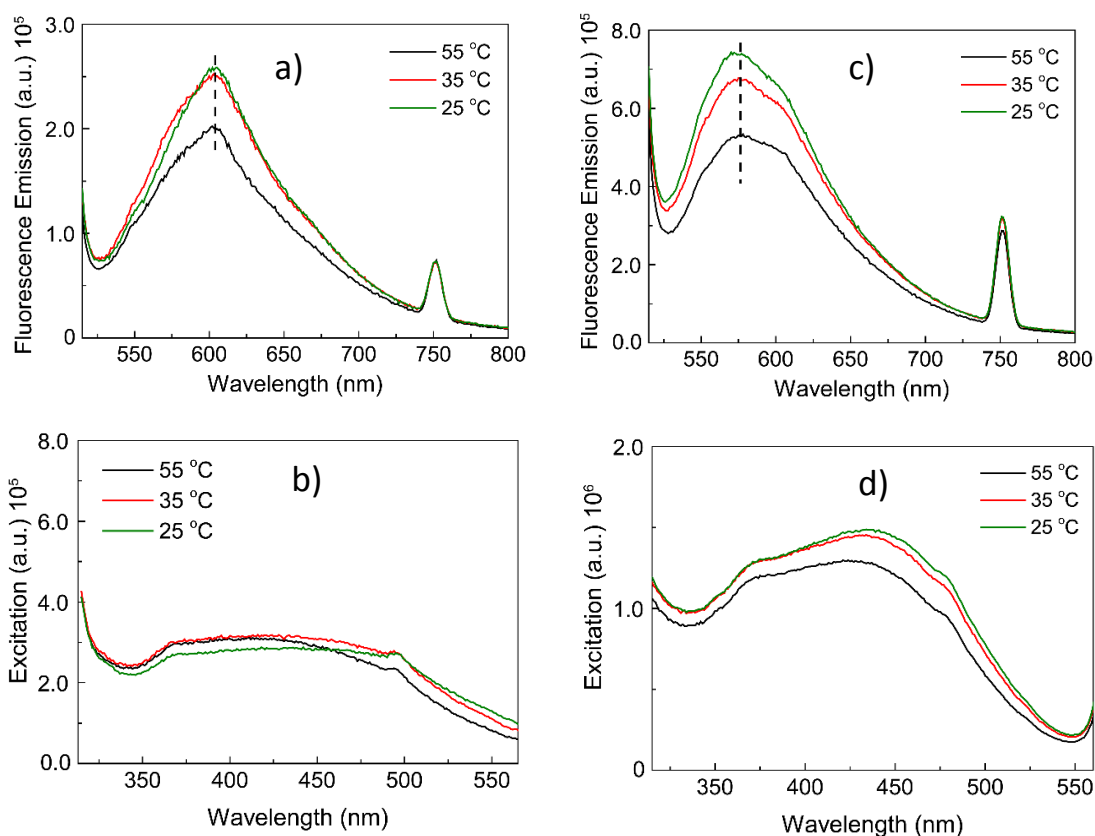


Figure 7-S16: Emission and excitation spectra of blend 1:1 added to DPPC liposomes (a, b) and DOPC liposomes (c, d) solutions at 55°C (black), 35°C (red), and 25°C (green). The blend concentration was 0.01 g/L, while the total lipid concentration was 0.1 g/L. No changes in excitation and emission maxima were detected.

9 Depth quenching experiments

A lipid cake was prepared by evaporating a chloroform solution of DPPC (5 g/L, 40 μ L), blend(1:3):(Oct)₂NH₂ complex (0.5 g/L, 40 μ L) and the DOXYL-labeled phospholipid (5-DOXYL or 14-DOXYL, 10% mol/mol). The dried cake was then hydrated for 10 minutes with 2 mL of PBS buffer solution (10 mM, pH 7.4). The solution was then stirred for 60 minutes and sonicated for 5 minutes to let the material detach from the walls. LUVs were prepared by extrusion through a 0.2 μ m pore size polycarbonate membrane (Avanti Polar Lipids, Inc) using a Mini-Extruder device (Lipofast Basic, Milmedtek AB) for 25 cycles. Analogous procedure was followed to prepare DOPC-DOXYL labeled liposomes.

The parallax analysis was applied in order to estimate the distance of the fluorophore from the bilayer center.^[10] The following equation was used for this purpose:

$$z_{1f} = \left(-\frac{1}{\pi C} \ln \frac{F_1}{F_2} - L_{21}^2 \right) / 2L_{21}$$

Where z_{1f} is defined as the distance (\AA) between 5-DOXYL and the fluorophore.

C is the concentration of molecules of quencher per unit area: considering a surface area of 70 \AA^2 for each lipid, $C = \text{mol fraction of quencher} / 70 \text{ \AA}^2$.

F_1 and F_2 are the fluorescence intensities at a certain wavelength for the quencher 1 and 2.

L_{21} is the distance difference (\AA) between quencher 1 and 2, which is 9.2 \AA .^[11]

Then, the following equation can be used to estimate the distance between the fluorophore and the bilayer center (z_{cf}):

$$z_{cf} = z_{1f} + L_{c1}$$

Where L_{c1} is the distance between 5-DOXYL and the bilayer center.

z_{cf} data are summarized in the following table:

Table 7-S3: Estimated distances (z_{cf}) between the probe (blend(1:3):(Oct)₂NH₂ complex) and the bilayer center for liposomes made of DOPC and DPPC lipids, at 25°C and 55°C. The blend concentration was 0.01 g/L, while the total lipid concentration was 0.1 g/L.

Liposomes Composition	z_{cf} (\AA) 25°C	z_{cf} (\AA) 55°C
DOPC	6.3	6.3
DPPC	6.2	6.3

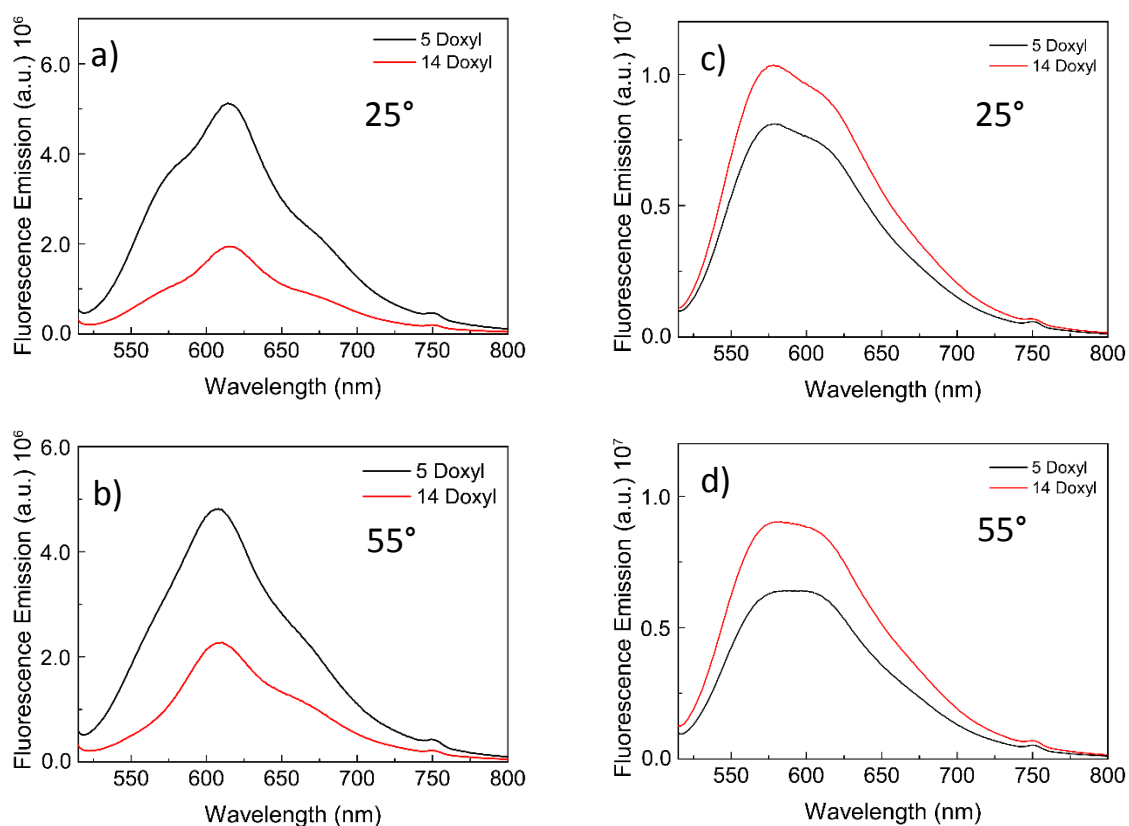


Figure 7-S17: Fluorescence spectra of blend(1:3):(Oct)₂NH₂ in DPPC liposomes containing 5-DOXYL PC (black) and 14-DOXYL PC (red) at 25°C a) and 55°C b). Fluorescence spectra of blend(1:3):(Oct)₂NH₂ in DOPC liposomes containing 5-DOXYL PC (black) and 14-DOXYL PC (red) at 25°C c) and 55°C d).

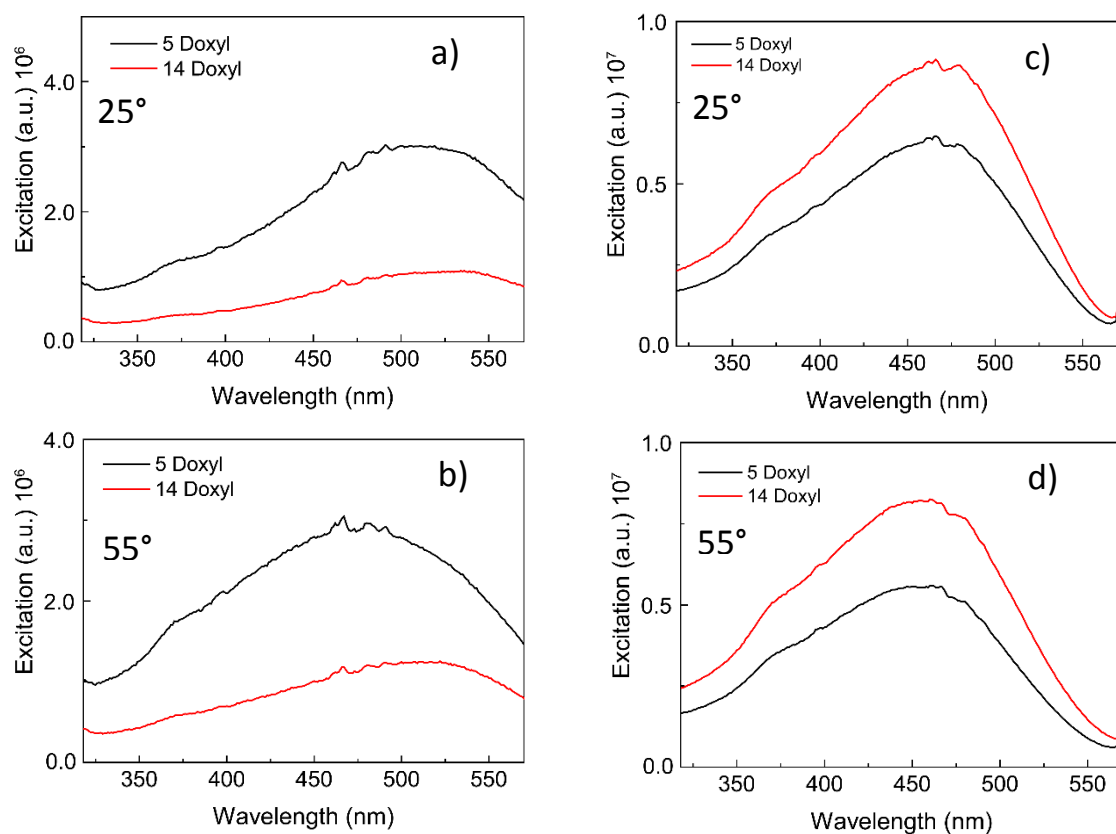


Figure 7-S18: Excitation spectra of blend(1:3):(Oct)₂NH₂ in DPPC liposomes containing 5-DOXYL PC (black) and 14-DOXYL PC (red) at 25°C a) and 55°C b). Fluorescence spectra of blend(1:3):(Oct)₂NH₂ in DOPC liposomes containing 5-DOXYL PC (black) and 14-DOXYL PC (red) at 25°C c) and 55°C d).

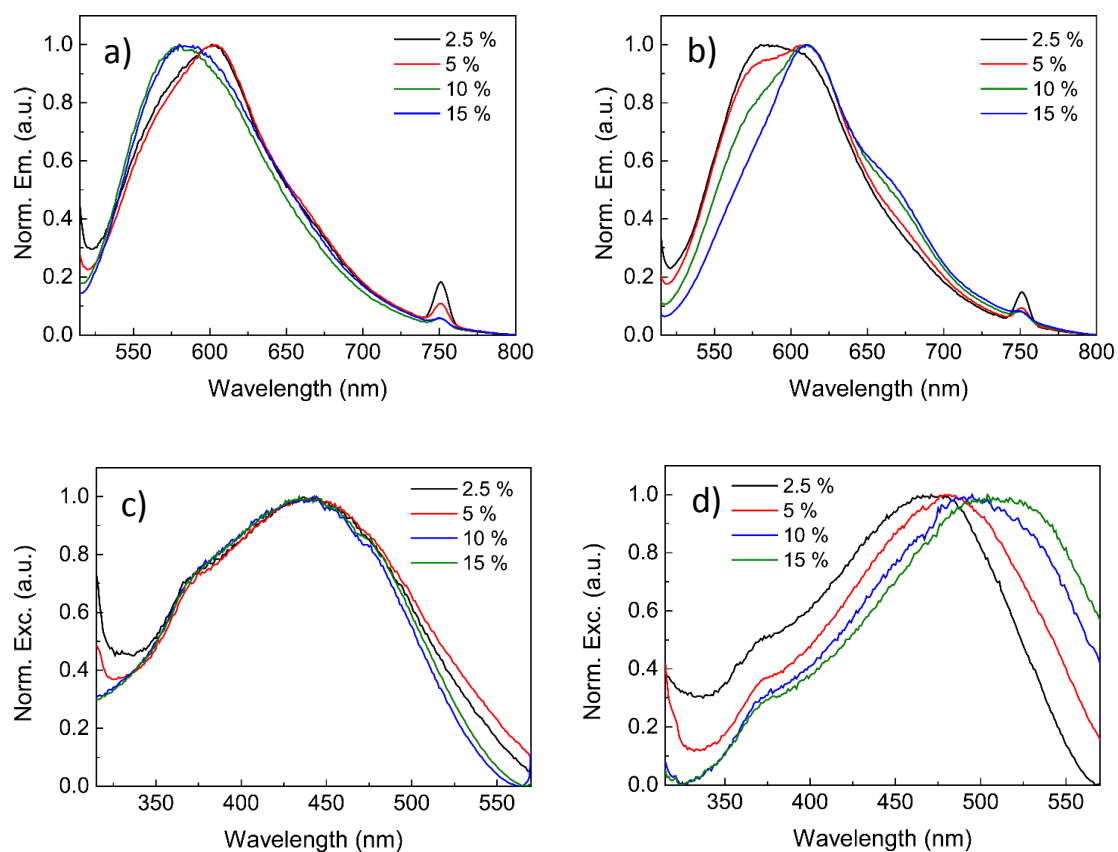
10 Effects related to increase of blend content and stoichiometry


Figure 7-S19: Emission spectra of blend(1:1):(Oct)₂NH₂ in DPPC liposomes at increased blend concentrations (with respect to total lipid concentration) at a) 55°C and b) 25°C. Excitation spectra of blend(1:1):(Oct)₂NH₂ in DPPC liposomes at increased blend concentrations at c) 55°C and d) 25°C. Lipid concentration was 0.1 g/L for all the liposomes preparations.

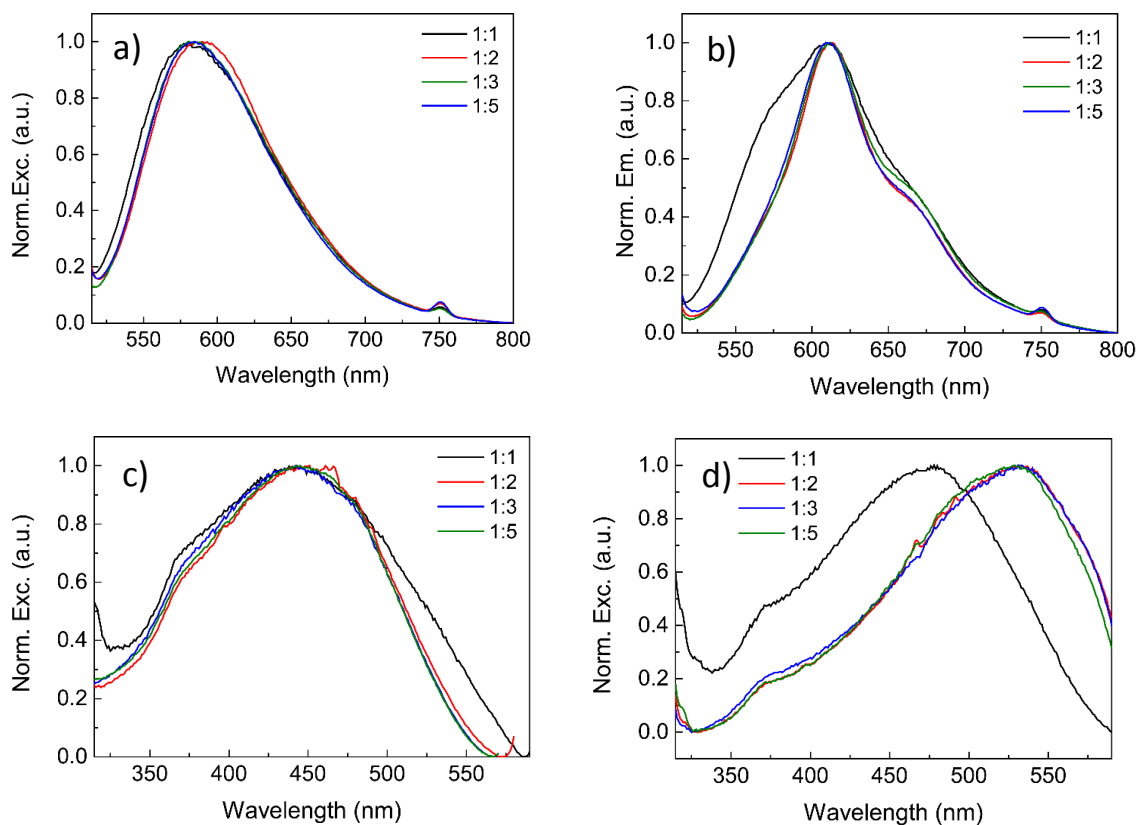


Figure 7-S20: Emission spectra of blend: $(\text{Oct})_2\text{NH}_2$ (10% molar fraction) for different PTHS:PEDOT-S ratios at a) 55°C and b) 25°C, and excitation spectra of blend: $(\text{Oct})_2\text{NH}_2$ for different PTHS:PEDOT-S ratios at c) 55°C and d) 25°C. Lipid concentration was 0.1 g/L for all the liposomes preparations.

11 Dynamic Light Scattering Experiments

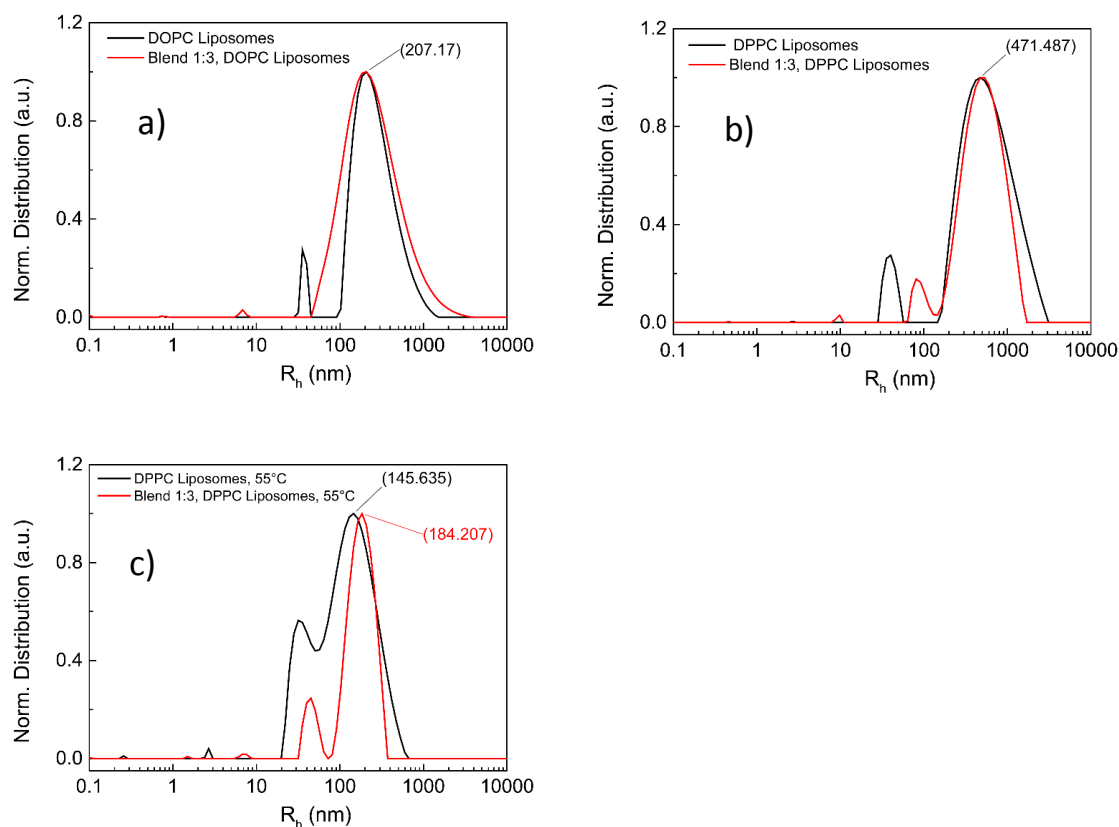


Figure 7-S21: Dynamic Light Scattering (DLS) size distribution data obtained at $\theta = 90^\circ$ of a) pristine DOPC liposomes (black) and DOPC liposomes containing blend(1:3):(Oct)₂NH₂ (red) recorded at 22°C, b) pristine DPPC liposomes (black) and DPPC liposomes containing blend(1:3):(Oct)₂NH₂ (red) recorded at 22°C, c) pristine DPPC liposomes (black) and DPPC liposomes containing blend(1:3):(Oct)₂NH₂ (red) recorded above the phase transition temperature (55°C). Blend concentration was 0.01 g/L, while lipid concentration was 0.1 g/L in all cases.

The incorporation of blend(1:3):(Oct)₂NH₂ into liposomes double layer may cause changes in size distribution or rupture of the liposomes.^[12] Dynamic light scattering (DLS) has been used to compare the hydrodynamic radius (R_h) of liposomes containing blend(1:3):(Oct)₂NH₂ with the one of pristine liposomes. Data recorded at 22°C show no differences in the mean peak position for blend(1:3):(Oct)₂NH₂-DOPC liposomes if compared to pristine liposomes. Also in the case of DPPC liposomes, incorporation blend(1:3):(Oct)₂NH₂ did not lead to any size change. In general DPPC liposomes show a higher hydrodynamic radius, due to aggregation below the phase transition temperature. Increase of temperature above the phase transition temperature causes a decrease of size distribution, due to vesicles disaggregation.^[13] Blend(1:3):(Oct)₂NH₂-DPPC liposomes showed a decrease of size as for pristine DPPC liposomes. A higher propensity to preserve the original size is also found, probably due to a stabilizing effect of the probe once the liposomes are formed.

12 Confocal images of LMV

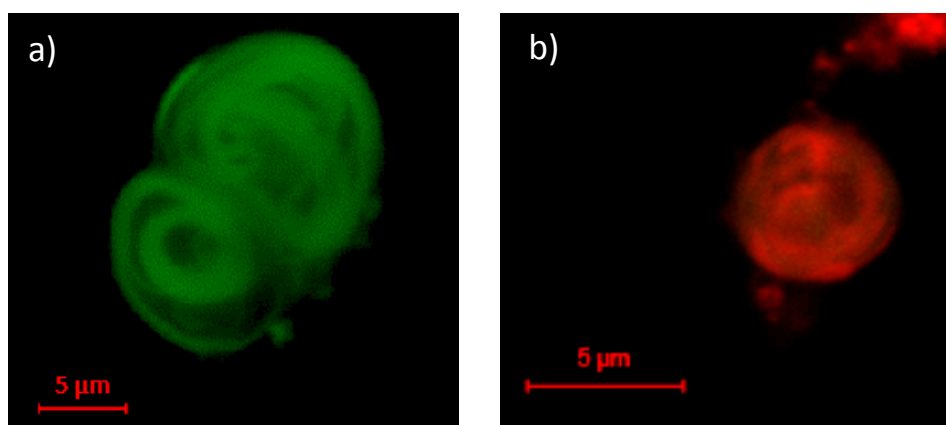


Figure 7-S22: Confocal microscopy images of large multilamellar vesicles (LMV) composed of a) DOPC:blend(1:3):(Oct)₂NH₂ (lipid:blend, 10:1) and b) DPPC:blend(1:3):(Oct)₂NH₂ (lipid:blend, 10:1). Detection wavelengths were 405-490 nm (green, in the picture) for excitation at 405 nm, and 600-700 nm for excitation at 555 nm (red, in the picture), respectively.

13 Confocal images of GUV

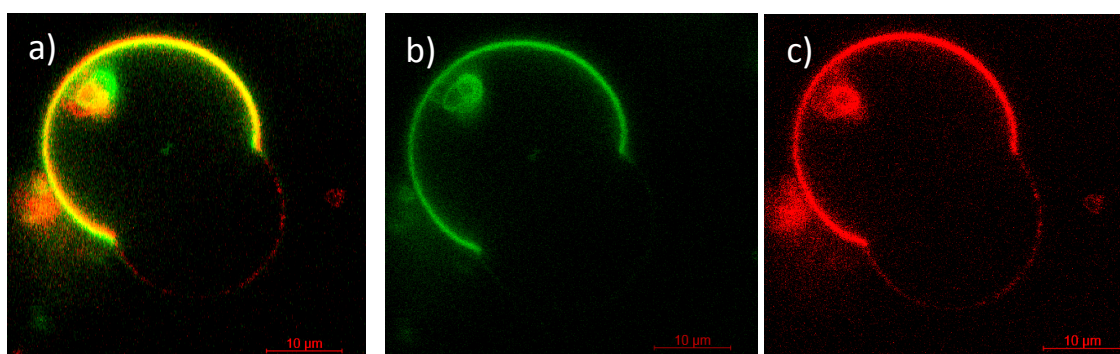


Figure 7-S23: Confocal microscopy image of giant unilamellar vesicles (GUV) composed of DOPC:DPPC:Chol, containing 10% PG. The vesicles were prepared by gentle hydration. GUV were labeled with blend(1:3):(Oct)₂NH₂ (10%, with respect to total lipid concentration). Green and red colors have been used to differentiate between signal acquired at $\lambda=500-555$ nm (green) and $\lambda=600-755$ nm (red). In image a) both the green and red channels are active, while in b) and c) are single-channel images, where the green and red channels have been highlighted, respectively. The image show coexistence between two phases: one that display emission both in the green and in the red, and one that show emission only in the red. The two domains can be identified on the base of emission spectra of blend(1:3):(Oct)₂NH₂ in different lipid phases. The green-red phase can be attributed to a DOPC rich L_{dis} phase, where blend(1:3):(Oct)₂NH₂ has an emission maximum at $\lambda=577$ nm and strong emission also at $\lambda<555$ nm. The red phase corresponds to a DPPC and cholesterol rich L_{ord} domain, where blend(1:3):(Oct)₂NH₂ has an emission maximum at $\lambda=601$ nm and no emission at $\lambda<555$ nm. The low emission intensity of the probe in L_{ord} domain, with respect to the L_{dis} domain, is attributed to the difference in emission intensity of the probe in the two phases (around one order of magnitude), as highlighted by emission data acquired for single-phase vesicles. About the shape of the GUV, a change in curvature is observed at the boundary of L_{dis} and L_{ord} domains. This behavior has been previously observed for GUV made of DOPC:sphingomyelin:chol by Bacia et al., which attribute the effect to the particular cholesterol structure.^[14]

Supporting References

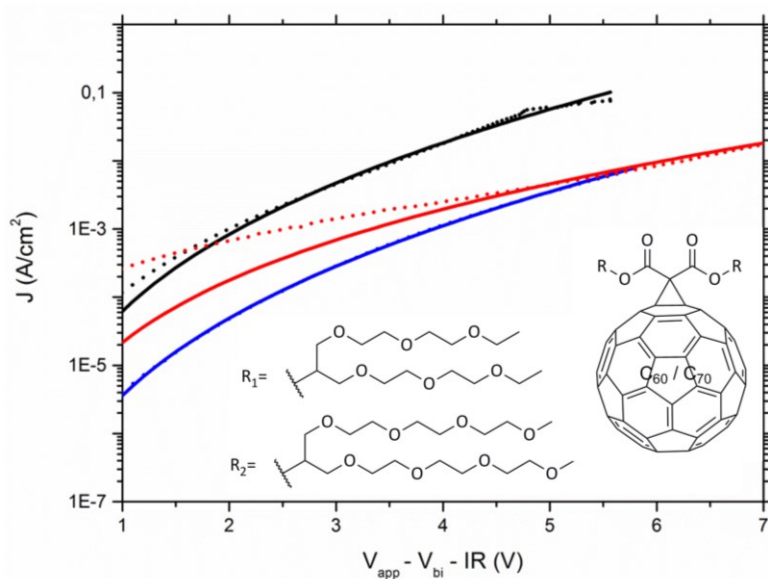
- [1] A. Elfving, F. G. Backlund, C. Musumeci, O. Ingnas, N. Solin, *J. Mater. Chem. C* **2015**, *3*, 6499-6504.
- [2] R. H. Karlsson, A. Herland, M. Hamed, J. A. Wiggenius, A. Åslund, X. Liu, M. Fahlman, O. Ingnäs, P. Konradsson, *Chem.Mater.* **2009**, *21*, 1815-1821.
- [3] J. C. Brendel, M. M. Schmidt, G. Hagen, R. Moos, M. Thelakkat, *Chem.Mater.* **2014**, *26*, 1992-1998.
- [4] R. B. Lira, J. Steinkühler, R. L. Knorr, R. Dimova, K. A. Riske, *Sci. Rep.* **2016**, *6*, 25254.
- [5] K. Akashi, H. Miyata, H. Itoh, K. Kinoshita, *Biophys. J.* **1996**, *71*, 3242-3250.
- [6] a) Matthew C. Blosser, Jordan B. Starr, Cameron W. Turtle, J. Ashcraft, Sarah L. Keller *Biophys. J.* **2013**, *104*, 2629-2638; b) J. Zhao, J. Wu, F. A. Heberle, T. T. Mills, P. Klawitter, G. Huang, G. Costanza, G. W. Feigenson, *Biochim. Biophys. Acta, Biomembr.* **2007**, *1768*, 2764-2776.
- [7] H. D. Burrows, M. Knaapila, S. M. Fonseca, T. Costa, in *Conjugated Polyelectrolytes*, Wiley-VCH Verlag GmbH & Co. KGaA, **2012**, pp. 127-167.
- [8] M. Laurenti, J. Rubio-Retama, F. Garcia-Blanco, E. López-Cabarcos, *Langmuir* **2008**, *24*, 13321-13327.
- [9] E. Zeglio, M. Vagin, C. Musumeci, F. N. Ajjan, R. Gabrielsson, X. T. Trinh, N. T. Son, A. Maziz, N. Solin, O. Ingnäs, *Chem.Mater.* **2015**, *27*, 6385-6393.
- [10] a) M. Dal Molin, Q. Verolet, A. Colom, R. Letrun, E. Derivery, M. Gonzalez-Gaitan, E. Vauthey, A. Roux, N. Sakai, S. Matile, *J. Am. Chem. Soc.* **2015**, *137*, 568-571; b) M. Kondo, M. Mehiri, S. L. Regen, *J. Am. Chem. Soc.* **2008**, *130*, 13771-13777.
- [11] A. S. Ladokhin, *Biochim. Biophys. Acta, Biomembr.* **2014**, *1838*, 2289-2295.
- [12] M. Johnsson, K. Edwards, *Biophys. J.* **2003**, *85*, 3839-3847.
- [13] M. Wong, T. E. Thompson, *Biochemistry* **1982**, *21*, 4133-4139.
- [14] K. Bacia, P. Schwille, T. Kurzchalia, *Proc. Natl. Acad. Sci. U. S. A.* **2005**, *102*, 3272-3277.

8 ECO-FRIENDLY PROCESSABLE FULLERENE DERIVATIVES WITH HIGH ELECTRON MOBILITY

Martina M. Schmidt, Chetan R. Singh, Mukundan Thelakkat*

Applied Functional Polymers, Macromolecular Chemistry I, University of Bayreuth, 95440
Bayreuth, Germany

*E-mail of corresponding author: mukundan.thelakkat@uni-bayreuth.de



Prepared for submission

Abstract

Fullerene derivatives are commonly used in electronic and optical devices at laboratory scale by processing from chlorinated solvents. However, this is a limitation for industrial production processes by printing or coating on a large area scale. One reason which limits their processability at large scale is their low solubility in common non-toxic solvents such as ethyl acetate and acetone. Here we show the synthesis and characterization of three new fullerene monoadducts which show such a high solubility and therefore they are processable from these eco-friendly solvents. To achieve this, we attached a malonate with different swallow-tail oligo ethylene glycol groups to C₆₀ as well as C₇₀ via Bingel-Hirsch reaction and optimized both the malonate/fullerene ratio and the halogenating reagent to obtain high yield of the monoadducts. To check if these new fullerene derivatives meet the requirements for electronic and optical devices, the electron affinities were determined via cyclic voltammetry and the bulk electron mobilities by the space charge limited current method. While the electron affinities were comparable with the most commonly used phenyl-C61-butyric acid methyl ester (PC₆₁BM), the mobilities of one of our materials were two orders of magnitude higher than PC₆₁BM.

1. Introduction

Through its unique electrochemical characteristics, fullerenes and their derivatives are very interesting for a lot of different applications. The most common and promising usage is as n-type material in electronic and optical devices because of high electron mobilities up to $11 \text{ cm}^2 \text{ V}^{-1} \text{ s}^{-1}$ in transistors and due to its capability to form a highly stable anion.^[1-3] However, fullerenes and their derivatives cannot be processed from usual industrial solvents such as ethyl acetate and this impedes industrial production processes of devices involving these materials. One reason is their low solubility in environmental benign solvents like acetone or ethyl acetate.

To address this problem, we synthesized new fullerene derivatives, and quantified their solubility and charge transport properties compared to the commonly used PCBM. They showed improved solubility in environment friendly, non-chlorinated solvents. For the synthesis, first of all, malonic acid diesters with swallow-tail oligo ethylene glycol side chains were synthesized and afterwards attached to C₆₀ and C₇₀ *via* Bingel-Hirsch reaction. We selected OEG substituents, since Hummelen et al. have shown that the relative permittivities of fullerene derivatives can be enhanced up to a value of six by functionalization with triethylene glycol side chains.^[4,5] Two swallow-tail oligo ethylene glycol side chains differing in their lengths were used. To preserve the unique electronic characteristics of fullerenes, the addition reaction to C₆₀ and C₇₀ was aimed at monoadducts. After optimizing the reaction conditions, the optical characteristics, thermal

stability, electron affinity as well as charge carrier mobility were investigated. In this work, PC₆₁BM served as a reference material.

2. Results and Discussion

2.1. Synthesis of OEG substituted fullerenes

The synthesis schema for obtaining the three oligoethylene glycol (OEG) substituted fullerene derivatives, C₆₀-(OEG)₂-1, C₆₀-(OEG)₂-2 and C₇₀-(OEG)₂-1, is shown in Figure 8-1. In a first step, the malonic acid diesters with swallow-tail oligo ethylene glycol side chains were synthesized via esterification of malonyl dichloride in the presence of triethylamine. The Bingel-Hirsch reaction was used to attach the malonic acid diesters to C₆₀ and C₇₀ cores.^[6,7] Usually mono- and multiadducts are formed during cyclopropanation reaction of fullerenes and multi-adducts drastically change the electronic properties of fullerene.^[8]

First, we optimized the reaction conditions for the synthesis of C₆₀-(OEG)₂-1 to improve the yield of monoadduct. Afterwards, the optimized conditions were used for the synthesis of the fullerene derivatives C₆₀-(OEG)₂-2 and C₇₀-(OEG)₂-1.

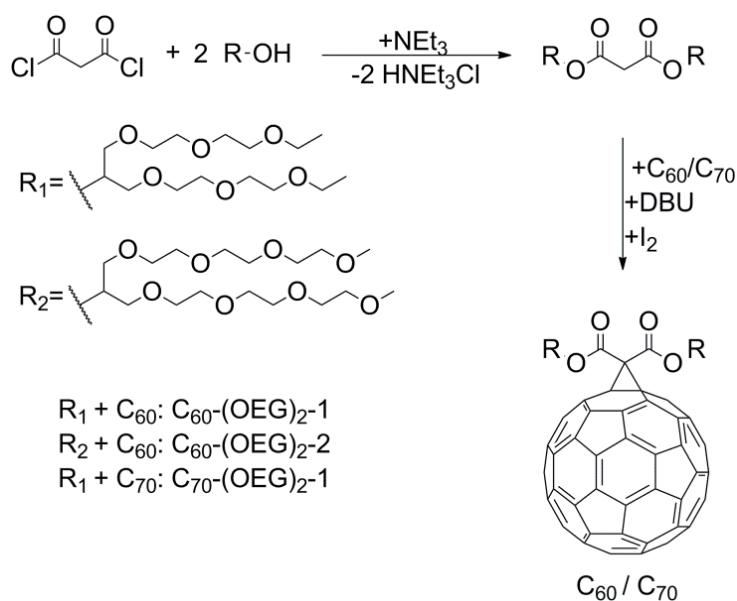


Figure 8-1: Synthesis schema of C₆₀-(OEG)₂-1, C₆₀-(OEG)₂-2 and C₇₀-(OEG)₂-1.

We synthesized the fullerene derivative C₆₀-(OEG)₂-1 either using tetrabromomethane or iodine as halogenating reagent, since they are the most commonly used for Bingel-Hirsch reactions. The ratio of higher addition products can be evaluated via the integrals of the protons located at the two tertiary carbon atoms of the attached OEG group in ¹H-NMR spectroscopy. For an isolated monoadduct the two protons at the tertiary carbon atoms are represented by a quintet in ¹H-NMR spectrum (5.50 ppm), whereas multiadducts show further signals in the region of 4.90 and

5.80 ppm (Figure 8-S1). From the integrals of these signals, the ratio of monoadduct in the crude reaction product can be determined. Monoadducts were observed both with tetrabromomethane as well as with iodine reagents. Also higher addition products were detected via ^1H -NMR spectroscopy. An essential difference appeared in the ratio of higher addition products. The amount of higher addition products was less using iodine instead of tetrabromomethane as reagent. As iodine favors monoaddition in Bingel-Hirsch reactions, further reactions were carried out using exclusively iodine as halogenating reagent.

A further important factor for the synthesis of monoadducts is the ratio of C_{60} to malonate. While the ratio of the other reagents to malonate was kept constant, the ratio C_{60} /malonate was changed from 1.0:0.7 to 1.0:1.0 and to 1.0:1.2. For example, for $\text{C}_{60}^-(\text{OEG})_2-1$, the highest yield of monoadduct (55 %) could be reached using the ratio of 1:0.7, even though the malonate was used in less amounts than required stoichiometrically. In this way, the bisadduct was produced only in small amounts and it was removed by column chromatography. Thus, pure monoadduct could be isolated easily. In contrast, several column chromatographic steps were necessary to isolate pure monoadduct when a C_{60} /malonate ratio of 1:1.0 was used. Here the yield was reduced to 43 % due to formation of multiadducts. In general, separation of different fullerene adducts is very difficult due to their similar elution properties. The monoadduct could not be isolated using a C_{60} /malonate ratio of 1:1.2, because a multitude of different higher adducts were obtained.

The further fullerene derivatives, $\text{C}_{60}^-(\text{OEG})_2-2$ and $\text{C}_{70}^-(\text{OEG})_2-1$ also were synthesized with the optimized reaction conditions: C_{60} /malonate ratio of 1:0.7 and iodine as halogenating reagent. $\text{C}_{60}^-(\text{OEG})_2-2$ and $\text{C}_{70}^-(\text{OEG})_2-1$ were isolated with yields of 67 % and 32 %, respectively. Beyond ^1H - and ^{13}C - NMR spectroscopy, matrix-assisted laser desorption/ionization-time of flight-mass spectrometry (MALDI-TOF MS, Figure 8-S2) was used to verify the successful isolation of the monoadducts.

2.2. Optical characteristics

The UV-vis absorption spectra of $\text{C}_{60}^-(\text{OEG})_2-1$, $\text{C}_{60}^-(\text{OEG})_2-2$, $\text{C}_{70}^-(\text{OEG})_2-1$ and PC_{61}BM dissolved in tetrahydrofuran ($c = 1 \cdot 10^{-5} \text{ mol} \cdot \text{L}^{-1}$) are compared in Figure 8-S3a with that of PC_{61}BM . Whereas the C_{60} based fullerene derivatives showed comparable absorption, $\text{C}_{70}^-(\text{OEG})_2-1$ had a broader and higher absorption in the visible region. As C_{60} and its derivatives exhibit a high degree of symmetry, the lowest energy transitions are formally dipole forbidden.^[9,10] In consequence, the reduced symmetry of C_{70} and its derivatives lead to a stronger absorption.^[9-11]

2.3. Solubility

The processability of fullerene derivatives is an important issue for realizing large area devices at industry scale. Environmental-benign and industrial relevant solvents like ethyl acetate and acetone are the first preferences as solvents. To study the solubility of the fullerene derivatives and PC₆₁BM as a reference material, 100 mg solid was added to 1 mL tetrahydrofuran (THF), or acetone, ethyl acetate or isopropyl alcohol. To make sure that the fullerenes dissolve as much as possible in the solvents, the solutions were shaken three days at room temperature using an overhead shaker. After centrifugation the supernatant was filtered out with a 0.2 μm syringe filter, the non-dissolved solid is weighed and was dried for three days in a vacuum dryer to remove the solvent. The solubility thus calculated with the weight of the residue is given as average of three measurements in Table 8-1.

Table 8-1: Calculated solubility in THF, acetone, ethyl acetate and isopropyl alcohol, via TGA determined decomposition temperature $T_{d, 5 \text{ wt\%}}$ and via SCLC method calculated electron mobility μ_e of PC₆₁BM, C₆₀-(OEG)₂-1, C₆₀-(OEG)₂-2 and C₇₀-(OEG)₂-1.

Fullerene derivative	solubility [mg/mL] in				$T_{d, 5 \text{ wt\%}}$ [°C]	$\mu_e^{\text{a)}}$ [cm ² V ⁻¹ s ⁻¹]
	THF	Ethyl acetate	Acetone	Isopropyl alcohol		
PC ₆₁ BM	2.7	1.0	0.5	0.7	441	(6.1 ± 0.4) × 10 ⁻⁴
C ₆₀ -(OEG) ₂ -1	>100	>100	42.1	5.4	281	(2.8 ± 0.2) × 10 ⁻²
C ₆₀ -(OEG) ₂ -2	>100	>100	>100	3.4	309	(1.9 ± 0.2) × 10 ⁻³
C ₇₀ -(OEG) ₂ -1	>100	84.4	32.0	1.8	289	-

^{a)} Fitted mobility at a representative field of 5.00 × 10⁶ V m⁻¹.

The swallow-tail oligo ethylene glycol chains are able to interact with polar groups of the solvent leading to a better solubility in such solvents compared to PC₆₁BM. Unlike PC₆₁BM (2.7 mg/mL), all the added 100 mg of the newly synthesized derivatives dissolved in 1 mL of tetrahydrofuran. In literature a solubility value of 1.8 mg/mL for PC₆₁BM in THF is reported.^[12] Typically the solubility values can vary slightly depending on the purity of the supplied PC₆₁BM and the measurement method. C₆₀-(OEG)₂-2, with longer swallow-tail oligo ethylene glycol groups in comparison to the other two derivatives, also showed solubilities beyond 100 mg/mL in ethyl acetate and acetone. In ethyl acetate, the solubility for C₆₀-(OEG)₂-1 was determined to be beyond 100 mg/mL, for C₇₀-(OEG)₂-1, it is 84.4 mg/mL and for PC₆₁BM 1.0 mg/mL. On the other hand the solubility in acetone is slightly reduced, for example, 42.1 mg of C₆₀-(OEG)₂-1 and 32.0 mg of C₇₀-(OEG)₂-1 were soluble in 1 mL acetone, while just 0.5 mg of PC₆₁BM could be

dissolved in 1 mL of acetone. The solubility was further reduced in isopropyl alcohol: $C_{60}-(OEG)_2-1$ and $C_{70}-(OEG)_2-1$ differ only in the attached fullerene core. As the smaller C_{60} core is better soluble in polar solvents compared to the more hydrophobic C_{70} core, also $C_{60}-(OEG)_2-1$ showed a better solubility as $C_{70}-(OEG)_2-1$ in the tested solvents. Changing the length of the oligo ethylene glycol group added to the C_{60} core, lead to a change in solubility, as well. $C_{60}-(OEG)_2-2$, that had a longer oligo ethylene glycol chain, showed better solubility in the polar aprotic solvents (THF, ethyl acetate and acetone) than $C_{60}-(OEG)_2-1$. Nevertheless, the solubility in the less polar and protic isopropyl alcohol is higher for $C_{60}-(OEG)_2-1$. All the three derivatives $C_{60}-(OEG)_2-1$, $C_{60}-(OEG)_2-2$ and $C_{70}-(OEG)_2-1$ can be dissolved in highly sufficient amounts in common solvents except isopropyl alcohol, which is a big achievement for eco-friendly processing.

2.4. Thermal characteristics

With thermogravimetric analysis we determined the decomposition temperature $T_{d, 5 \text{ wt\%}}$ (Figure 8-S3b) of the fullerene derivatives. Since oligo ethylene groups take up water, the fullerenes were dried by pre-heating at 120°C for 90 minutes, before starting the thermogravimetric analysis. $T_{d, 5 \text{ wt\%}}$ was determined to be 441 °C for $PC_{61}BM$, 281 °C for $C_{60}-(OEG)_2-1$, 309 °C for $C_{60}-(OEG)_2-2$ and 289 °C for $C_{70}-(OEG)_2-1$ (Table 8-1). Whereas the attached butyric acid methyl ester group of $PC_{61}BM$ was splits off at higher temperatures, the three synthesized fullerene derivatives released the malonate with the attached swallow-tail oligo ethylene glycol groups in the range of 280 to 300°C. Even though the thermal stability of these new derivatives are lower than that of $PC_{61}BM$, they are appreciably stable for any thin film applications.

2.5. Cyclic voltammetry

The reduction potentials of the synthesized fullerene derivatives were investigated by cyclic voltammetry. The obtained cyclic voltammograms are shown in Figure 8-S4. All compounds exhibit multi-reduction peaks as expected for fullerenes.^[13,14] The reduction reactions were completely reversible. Values calculated from half-wave potential of the first reduction peak are often inappropriately referred to as lowest unoccupied molecular orbital (LUMO). Here the term electron affinity (EA) is used instead, as suggested by Bredas.^[15] These EA values calculated relative to ferrocene as standard and by taking account of solvent effects need to be considered as a relative value and can be very well used for comparisons of different compounds under the same conditions of measurement.^[16,17] All investigated fullerene derivatives, $C_{60}-(OEG)_2-1$, $C_{60}-(OEG)_2-2$, $C_{70}-(OEG)_2-1$ and $PC_{61}BM$, showed an identical EA value of -4.1 eV. Thus, the EA value is not affected by the chemical structure of the attached group as well as by changing the fullerene

core from C₆₀ to C₇₀. Wudl et al. already reported that pure C₆₀ and C₇₀ exhibit the same first reduction wave potential and therefore the same EA values.^[18] By changing the methyl end group of PC₆₁BM, the influence of the chemical structure of the attached groups on the EA was investigated by Troshin et al.. In line with our results, they also did not observe any differences in EA values for their derivatives.^[19]

2.6. Electron mobility via SCLC

High charge carrier mobility values are desired from semiconductor materials as they directly influence the charge carrier extraction in electronic devices. Here the bulk electron mobilities (μ_e) of the derivatives were determined via space charge limited current (SCLC) method (Figure 8-2). For that, single carrier electron only devices were prepared with a layer stack of glass/ITO/ZnO/active layer/Ca/Al. The charge carrier mobilities were evaluated by fitting measured I–V characteristics using the Murgatroyd formula (Equation (1)).

$$J = \frac{9}{8} \epsilon_s \epsilon_0 \mu_0 \exp(0.89\gamma\sqrt{F}) \frac{V^2}{L^3} \quad (1)$$

Here J is the current density, ϵ_s the relative permittivity of the material, ϵ_0 the permittivity of vacuum, μ_0 the charge carrier mobility at zero field, γ the field dependence parameter, F the average electric field across the active layer, V the voltage across the active layer, and L the thickness of the polymer layer. For fitting, a typical value of 3.5 was assumed for ϵ_s as most organic semiconductors have dielectric constants in the range of 3-4. A small expected increase in ϵ_s after OEG substitution will reduce the final calculated mobility value by only that small proportional factor not by an order of magnitude. After fitting of two independent parameters (μ_0 and γ), an effective charge carrier mobility was determined from all devices at a same field, $F = 5 \times 10^6 \text{ V m}^{-1}$ using the Poole–Frenkel relationship (Equation (2)) as it allows a systematic comparison of electron transport in all the derivatives.

$$\mu(F) = \mu_0 \exp(\gamma\sqrt{F}) \quad (2)$$

It has been recommended that reporting charge mobility at a constant field summarizes the information in a single parameter and allows a straightforward charge mobility comparison across different materials.^[20] The field value, $F = 5 \cdot 10^6 \text{ Vm}^{-1}$, was chosen as it is a rather low electric field value which is usually present in solar cell devices at maximum power point and also for comparative purposes. The SCLC fits were good around this field value for all the I–V curves reported in this article. Precise film thicknesses were determined for the mobility

calculations via atomic force microscopy (AFM) by scanning over a scratched portion of the devices.

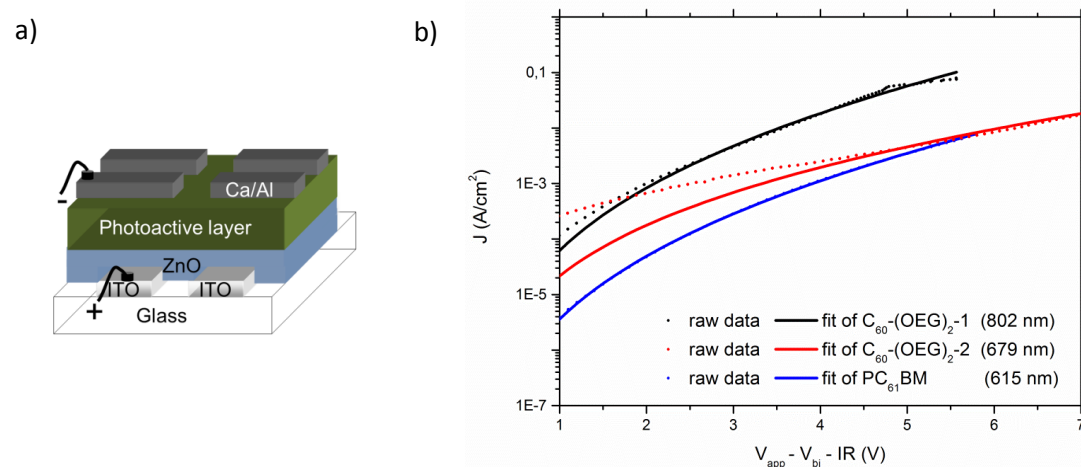


Figure 8-2: a) Schematic of electron-only device geometry and b) the I-V characteristics of $C_{60}-(OEG)_2-1$, $C_{60}-(OEG)_2-2$ and $PC_{61}BM$ films measured at room temperature in electron-only device configuration. The fits used for the calculation of the mobility are represented by solid lines. The corresponding film thicknesses are mentioned within the parentheses. The I-V characteristics were corrected for the voltage drop (IR) over the contacts.

The electron mobility values in Table 8-1 are averages obtained from three to five different devices varying in film thickness. The corresponding error in the mobility values is due to variation in measured film thicknesses. A complete table listing all film thicknesses and corresponding fitting parameters can be found in the supporting information (Table 8-S1). $C_{60}-(OEG)_2-1$ exhibited a bulk electron mobility of $(2.8 \pm 0.2) \times 10^{-2} \text{ cm}^2 \text{ V}^{-1} \text{ s}^{-1}$, which is around two orders of magnitude higher than that for the reference $PC_{61}BM$ ($(6.1 \pm 0.4) \times 10^{-4} \text{ cm}^2 \text{ V}^{-1} \text{ s}^{-1}$) material. In literature, the bulk electron mobility in the range of $\sim 10^{-3} \text{ cm}^2 \text{ V}^{-1} \text{ s}^{-1}$ has been reported for $PC_{61}BM$ via SCLC method.^[21,22] A little reduced electron mobility value for the reference $PC_{61}BM$ was obtained here, may be due to imperfect electrode interfaces. Nevertheless, the electron mobility of $C_{60}-(OEG)_2-2$ was determined to be $(1.9 \pm 0.2) \times 10^{-3} \text{ cm}^2 \text{ V}^{-1} \text{ s}^{-1}$. As the surface of $C_{70}-(OEG)_2-1$ films was too rough to get reliable thickness values (Rq: 13.8 nm, Ra: 9.96 nm on $20 \times 20 \mu\text{m}$, Figure 8-S5), it was not possible to determine its electron mobility with the SCLC method.

The fullerene derivatives with attached oligo ethylene glycol groups can interact intermolecularly to a higher degree compared to $PC_{61}BM$. This may lead to a more packed structure and hence to a higher electron mobility. As the mobilities of $C_{60}-(OEG)_2-1$ and $C_{60}-(OEG)_2-2$ differ one order of magnitude, the size of the attached swallow-tail oligo ethylene glycol groups seems to be influencing the electron mobility. It can be concluded that the bulkier attached groups limit the aggregation of the fullerene derivatives and in consequence limit the electron mobility.

Conclusion

In conclusion, three novel fullerene monoadducts have been synthesized via Bingel-Hirsch reaction. The reaction conditions were optimized for the mono-addition of a malonate with swallow-tail oligo ethylene groups to a C₆₀ core by using iodine instead of tetrabromomethane as halogenating agent and by tuning the stoichiometry of reagents. The fullerene derivatives were investigated for their optical properties, thermal stability, electron affinity and electron mobility and compared to the fullerene derivative, PC₆₁BM. The derivative based on C₇₀ showed the best absorption in the visible region due to its higher asymmetry. All three synthesized derivatives are thermally stable up to about 300 °C. Moreover, the novel C₆₀ and C₇₀ derivatives exhibit a higher solubility in non-chlorinated, non-toxic solvents such as THF, ethyl acetate and acetone compared to the reference PC₆₁BM. The bulk electron mobilities of the derivatives were measured via SCLC method and C₆₀-(OEG)₂-1 exhibited a very high electron mobility of $(2.8 \pm 0.2) \times 10^{-2} \text{ cm}^2 \text{ V}^{-1} \text{ s}^{-1}$, which is about two orders of magnitude higher than that determined for the reference PC₆₁BM ($(6.1 \pm 0.4) \times 10^{-4} \text{ cm}^2 \text{ V}^{-1} \text{ s}^{-1}$). Thus, the novel fullerene derivatives are promising candidates for applications in electronic devices by eco-friendly processing from non-toxic solvents. Furthermore, the derivatives can be very interesting for bioelectronic applications in aqueous electrolytes as they can swell in water due to the swallow-tail oligo ethylene glycol groups, but are not soluble in water.

Acknowledgement

We thank Markus Hund for the help with the AFM measurements. Financial support from DFG (GRK 1640) and the Bavarian State Ministry of Education, Science and Arts (SolTech) is kindly acknowledged. Martina M. Schmidt acknowledges the support from Elite Study program, Macromolecular Science at the University of Bayreuth.

References

- [1] H. Li, B. C.-K. Tee, J. J. Cha, Y. Cui, J. W. Chung, S. Y. Lee, Z. Bao, *J. Am. Chem. Soc.* **2012**, *134*, 2760.
- [2] M. A. Greaney, S. M. Gorun, *J. Phys. Chem.* **1991**, *95*, 7142.
- [3] P. Rapta, A. Bartl, A. Gromov, A. Staško, L. Dunsch, *ChemPhysChem* **2002**, *4*, 351.
- [4] F. Jahani, S. Torabi, R. C. Chiechi, L. Jan, A. Koster, J. C. Hummelen, L. J. A. Koster, J. C. Hummelen, *Chem. Commun.* **2014**, *50*, 10645.
- [5] S. Torabi, F. Jahani, I. Van Severen, C. Kanimozhi, S. Patil, R. W. A. Havenith, R. C. Chiechi, L. Lutsen, D. J. M. Vanderzande, T. J. Cleij, J. C. Hummelen, L. J. A. Koster, *Adv. Funct. Mater.* **2015**, *25*, 150.
- [6] C. Bingel, *Chem. Ber.* **1993**, *126*, 1957.
- [7] X. Camps, A. Hirsch, *J. Chem. Soc., Perkin Trans.* **1997**, *1*, 1595.
- [8] M. Prato, *J. Mater. Chem.* **1997**, *7*, 1097.
- [9] M. M. Wienk, J. M. Kroon, W. J. H. Verhees, J. Knol, J. C. Hummelen, P. A. van Hal, R. A. J. Janssen, *Angew. Chem. Int. Ed.* **2003**, *42*, 3371.
- [10] J. W. Arbogast, C. S. Foote, *J. Am. Chem. Soc.* **1991**, *113*, 8886.
- [11] J. P. Hare, H. W. Kroto, R. Taylor, *Chem. Phys. Lett.* **1991**, *177*, 394.
- [12] F. Machui, S. Langner, X. Zhu, S. Abbott, C. J. Brabec, *Sol. Energy Mater. Sol. Cells* **2012**, *100*, 138.
- [13] Q. Xie, E. Pérez-Cordero, L. Echegoyen, *J. Am. Chem. Soc.* **1992**, *114*, 3978.
- [14] L. Echegoyen, L. E. Echegoyen, *Acc. Chem. Res.* **1998**, *31*, 593.
- [15] J.-L. Bredas, *Mater. Horizons* **2014**, *1*, 17.
- [16] K. Gräf, M. A. Rahim, S. Dasb, M. Thelakkat, *Dye. Pigment.* **2013**, *99*, 1101.
- [17] I. Noviadri, K. N. Brown, D. S. Fleming, P. T. Gulyas, P. A. Lay, A. F. Masters, L. Phillips, *J. Phys. Chem. B* **1999**, *103*, 6713.
- [18] P.-M. Allemand, A. Koch, F. Wudl, Y. Rubin, F. Diederich, M. M. Alvarez, S. J. Anz, R. L. Whetten, *J. Am. Chem. Soc.* **1991**, *113*, 1050.
- [19] J. Y. Mayorova, S. L. Nikitenko, P. A. Troshin, S. M. Peregodova, A. S. Peregodov, M. G. Kaplunov, R. N. Lyubovskaya, *Mendeleev Commun.* **2007**, *17*, 175.
- [20] J. C. Blakesley, F. A. Castro, W. Kylberg, G. F. A. Dibb, C. Arantes, R. Valaski, M. Cremona, J. S. Kim, J.-S. Kim, *Org. Electron.* **2014**, *15*, 1263.
- [21] V. D. Mihailetschi, J. K. J. van Duren, P. W. M. Blom, J. C. Hummelen, R. A. J. Janssen, J. M. Kroon, M. T. Rispens, W. J. H. Verhees, M. M. Wienk, *Adv. Funct. Mater.* **2003**, *13*, 43.

- [22] H. Azimi, A. Senes, M. C. Scharber, K. Hingerl, C. J. Brabec, *Adv. Energy Mater.* **2011**, *1*, 1162.

Supporting Information

Experimental section

Methods

^1H - and ^{13}C -NMR spectra were measured on a Bruker Avance 250 spectrometer at 300 MHz. The spectra were calibrated according to the CDCl_3 signals (^1H : 7.26 ppm; ^{13}C : 77.16 ppm). Matrix assisted laser desorption/ionization time-of-flight mass spectrometry (MALDI-TOF MS) were performed on a Bruker Reflex III. It was measured in the positive polarized Reflector Mode. The spectrometer was calibrated with a polystyrol standard with *trans*-2-[3-(4-*t*-butylphenyl)-2-methyl-2-propenylidene]malononitrile (DCTB) as matrix and silver trifluoroacetate (AgTFA) as salt. For the synthesized fullerene derivatives *trans*-3-indoleacrylic acid (IAA) was used as matrix. No additional salt was needed.

A Jasco V670 spectrophotometer and a 1 cm thick quartz cuvette were used to record the UV-vis spectra.

To determine the solubility of the fullerene derivatives, 100 mg of each compound was weighted in an Eppendorf vial and 1 mL of each tested solvent (THF, acetone, ethyl acetate and isopropyl alcohol) were added. The sealed vials were shaken by an overhead shaker for three days at room temperature. After centrifugation for 15 minutes at 14000 rpm, the supernatant was filtered through a syringe filter with 0.2 μm pore size, weighed and dried in a vacuum dryer for three days to remove the solvent. Using the weight of the residue the solubility was calculated. Every fullerene derivative-solvent combination was measured three times to get an average value.

Thermogravimetric analysis was performed on a Mettler Toledo TGA/SDTA 851. The fullerene derivatives were measured in an aluminum oxide pan under nitrogen. First they were heated to 120 $^\circ\text{C}$. To remove water traces, they were kept at this temperature for 90 minutes. Afterwards, they were cooled to room temperature and measured to 700 $^\circ\text{C}$. The cooling/heating rate was 10 K/min.

The cyclic voltammetry measurements were performed with a standard three electrodes setup under nitrogen. As working electrode a platinum electrode with cross sectional area of 0.0314 cm^2 was used. The counter electrode was a platinum wire in a 0.1 M tetrabutylammonium hexafluorophosphate (Bu_4NPF_6) solution in dry dichloromethane. A silver wire in a 0.1 M AgNO_3 -solution in acetonitrile was used as reference electrode. The scan rate was set to 50 mV s^{-1} . Ferrocene served as internal standard.

For the space charge limited current measurements electron-only devices in diode configuration were prepared by first spin coating a zinc acetate solution (109.75 mg zinc acetate dehydrate,

30.5 μL ethanolamine and 1 ml methoxyethanol) onto cleaned substrates with patterned ITO electrodes, followed by 150 $^{\circ}\text{C}$ baking for 5 min in air to convert zinc acetate to zinc oxide. Subsequently, the substrates were transferred to a glovebox for the deposition of the active layer in a nitrogen environment. Fullerene films were prepared on these substrates by spin coating (different speeds) solutions containing 3.3 wt% fullerene derivative dissolved in 88.2 wt% CHCl_3 and 8.5 wt% dichlorobenzene were spin-coated under inert conditions using different spinning speeds. After annealing at 70 $^{\circ}\text{C}$ for 1 h, around 30 nm Ca followed by 100 nm Al were deposited as top contact layer. With a Keithley 2400 source meter unit I-V measurements were performed in dark under inert conditions. The thickness of the films was determined by using a commercial AFM (Dimension 3100 equipped with a NanoScope IV SPM controller from Veeco Instruments Inc.).

Before the I-V measurements, the electron-only devices were exposed to 100 mW cm^2 illumination for 3 min from an AM 1.5 class A solar simulator to improve the conductivity of the ZnO layer. After the light treatment, the I-V curves from the electron-only devices were found to be nearly symmetric around 0 V. Therefore, no built-in voltage correction was applied prior to the SCLC fitting. The contact resistance was determined from a reference device without fullerene layer and was found to be 27 Ω for the devices. For mobility evaluation, reverse bias voltages, that is, electron injection from ZnO was considered in the devices.

Synthesis

All solvents used for flash chromatography were distilled. All other chemicals were used as received from commercial suppliers.

Synthesis of 3,6,9,13,16,19-hexaoxahenicosan-11-ol

To diethylene glycol monomethyl ether (120 mL, 118.8 g, 0.89 mol) in a dried three-neck round-bottom flask with a dropping funnel and a reflux condenser sodium (14 g, 0.61 mol) was added in portions and stirred at 100 $^{\circ}\text{C}$ overnight. Afterwards epichlorohydrin (17.21 mL, 20.35 g, 0.22 mol) was added dropwise at 0 $^{\circ}\text{C}$. The reaction solution was stirred overnight at 50 $^{\circ}\text{C}$. At 0 $^{\circ}\text{C}$ the reaction was quenched with water. The organic phase was extracted with dichloromethane and dried over sodium sulfonate. After vacuum distillation the product yield was 61 %.

$^1\text{H-NMR}$ (300 MHz, CDCl_3): δ (ppm) = 1.16-1.24 (t, 6H), 3.45-3.70 (m, 24H), 3.92-4.02 (m, 1H), 7.26 (s, CDCl_3).

Synthesis of 2,5,8,11,15,18,21,24-octaoxapentacosan-13-ol

To triethylene glycol monomethyl ether (316.5 mL, 331.68 g, 2.02 mol) in a dried three-neck round-bottom flask with a dropping funnel and a reflux condenser sodium (27.6 g, 1.20 mol) was added in portions and stirred at 100 °C overnight. Afterwards epichlorohydrin (34.4 mL, 40.7 g, 0.44 mol) was added dropwise at 0 °C. The reaction solution was stirred overnight at 50 °C. At 0 °C the reaction was quenched with water. The organic phase was extracted with dichloromethane and dried over sodiumsulfonate. After vacuum distillation 2,5,8,11,15,18,21,24-octaoxapentacosan-13-ol was reached with a yield of 51 %.

¹H-NMR (300 MHz, CDCl₃): δ (ppm) = 3.38 (s, 6H), 3.45-3.70 (m, 28H), 3.91-4.03 (m, 1H), 7.26 (s, CDCl₃).

Synthesis of di(3,6,9,13,16,19-hexaoxahenicosan-11-yl)malonate

In a dried flask 3,6,9,13,16,19-hexaoxahenicosan-11-ol (9.723 mL, 9.732 g, 0.03 mol) and triethylamine (4.57 mL, 3.339 g, 0.033 mol) were dissolved in dried dichloromethane (90 mL). At 0 °C malonyl dichloride (1.5 mL, 2.175 g, 0.015 mol) was added dropwise. The reaction was stirred overnight at room temperature. With 0.1 M HCl the reaction was quenched and washed several times with water. The collected organic phase was neutralized with NaHCO₃ and dried over sodiumsulfonate. After evaporation of the solvent, the crude product was purified via silica gel column chromatography using a gradient of a dichloromethane:methanol mixture as eluent to obtain di(3,6,9,13,16,19-hexaoxahenicosan-11-yl)malonate in a yield of 73 %.

¹H-NMR (300 MHz, CDCl₃): δ (ppm) = 1.13-1.24 (t, 12H), 3.42 (s, 2H), 3.46-3.55 (q, 8H), 3.55-3.67 (m, 40 H), 5.11-5.20 (m, 2H), 7.26 (s, CDCl₃).

¹³C-NMR (300 MHz, CDCl₃): δ (ppm) = 15.3, 41.6, 66.8, 69.6, 70.0, 70.6, 70.8, 71.0, 72.8, 77.2 (CDCl₃), 166.2.

Synthesis of di(2,5,8,11,15,18,21,24-octaoxapentacosan-13-yl)malonate

Di(2,5,8,11,15,18,21,24-octaoxapentacosan-13-yl)malonate was prepared by following the procedure for di(3,6,9,13,16,19-hexaoxahenicosan-11-yl)malonate, except 2,5,8,11,15,18,21,24--octaoxapentacosan-13-ol was used instead of 3,6,9,13,16,19-hexaoxahenicosan-11-ol. Di(2,5,8,11,15,18,21,24-octaoxapentacosan-13-yl)malonate was reached in a yield of 59 %.

¹H-NMR (300 MHz, CDCl₃): δ (ppm) = 3.38 (s, 12H), 3.43 (s, 2H), 3.51-3.69 (m, 56H), 5.11-5.22 (m, 2H), 7.26 (s, CDCl₃).

Synthesis of [2,2'-(malonylbis(oxy))bis-(3,6,9,13,16,19-hexaoxahenicosan-11-yl)]-methano-1,2-dihydro[C₆₀]fullerene (C₆₀-(OEG)₂-1)

In a dried 1 L flask C₆₀ (1.0 g, 1.39 mmol) was solved in toluene (700 mL). Iodine (0.247 g, 0.97 mmol) and di(3,6,9,13,16,19-hexaoxahenicosan-11-yl)malonate (0.696 g, 0.97 mmol) were added. In 20 mL toluene solved DBU (0.296 g, 0.290 mL, 1.94 mmol) was added to the reaction solution dropwise and stirred overnight. Unreacted iodine was reduced with sodium thiosulfate. The organic phase was neutralized with 0.1 M HCl, washed with water and dried over sodiumsulfonate. After evaporation of the solvent, the crude product was purified via silica gel column chromatography using a gradient of a dichloromethane:acetone mixture as eluent. The product C₆₀-(OEG)₂-1 was freeze-dried and obtained in a yield of 55 %.

Additionally, C₆₀-(OEG)₂-1 was successfully synthesized and isolated using a C₆₀/malonate ratio of 1.0/1.0. The ratio of malonate/I₂/DBU was kept constant at 1/1/2. The yield amounted to 43 %.

¹H-NMR (300 MHz, CDCl₃): δ (ppm) = 1.08-1.29 (t, 12H), 3.46-3.55 (q, 8H), 3.55-3.72 (m, 32H), 3.79-3.84 (d, 8H), 5.43-5.57 (m, 2H), 7.26 (s, CDCl₃).

¹³C-NMR (300 MHz, CDCl₃): δ (ppm) = 15.3, 52.5, 66.8, 69.5, 69.9, 70.6, 70.7, 70.8, 71.0, 71.1, 71.6, 74.8, 77.2 (CDCl₃), 140.9, 141.9, 142.3, 143.0, 143.1, 143.2, 144.0, 144.7, 144.8, 145.0, 145.3, 145.4, 163.0.

MALDI-TOF MS: g/mol (%) = 1458.55 (100), 1474.53 (43).

Synthesis of [2,2'-(malonylbis(oxy))bis-(2,5,8,11,15,18,21,24-octaoxapentacosan-13-yl)]-methano-1,2-dihydro[C₆₀]fullerene (C₆₀-(OEG)₂-2)

C₆₀-(OEG)₂-2 was synthesized similar to C₆₀-(OEG)₂-1, except of using di(2,5,8,11,15,18,21,24-octaoxapentacosan-13-yl)malonate (0.813 g, 0.97 mmol). The product C₆₀-(OEG)₂-2 was obtained in a yield of 67 %.

¹H-NMR (300 MHz, CDCl₃): δ (ppm) = 3.31 (m, 12H), 3.45-3.65 (m, 48H), 3.73-3.80 (d, 8H), 5.37-5.50 (m, 2H), 7.26 (s, CDCl₃).

¹³C-NMR (300 MHz, CDCl₃): δ (ppm) = 52.5, 59.2, 69.5, 70.6, 70.7, 70.9, 71.5, 72.0, 74.8, 77.2 (CDCl₃), 139.2, 140.9, 141.9, 142.3, 143.0, 143.1, 143.2, 143.9, 144.7, 145.0, 145.2, 145.3, 145.4, 163.0.

MALDI-TOF MS: g/mol (%) = 1578.84 (100), 1594.82 (22).

Synthesis of [2,2'-(malonylbis(oxy))bis-(3,6,9,13,16,19-hexaoxahenicosan-11-yl)]-methano-1,2-dihydro[C₇₀]fullerene (C₇₀-(OEG)₂-1)

C₇₀-(OEG)₂-1 was synthesized like C₆₀-(OEG)₂-1, except of using C₇₀ instead of C₆₀. Additionally, several column chromatography steps were needed: Initially, a gradient of toluene:methanol mixture was used to remove unreacted C₇₀. Afterwards, a gradient of chloroform:methanol was used as eluent. At last, a column with a gradient of dichloromethane:acetone mixture served as eluent. After freeze-drying, C₇₀-(OEG)₂-1 was obtained in a yield of 32 %.

¹H-NMR (300 MHz, CDCl₃): δ (ppm) = 1.12-1.32 (m, 12H), 3.46-3.77 (m, 40 H), 3.77-3.89 (m, 8H), 5.39-5.51 (m, 2H), 7.26 (s, CDCl₃).

¹³C-NMR (300 MHz, CDCl₃): δ (ppm) = 15.3, 37.4, 66.8, 69.5, 69.9, 70.6, 70.7, 70.8, 70.9, 71.0, 74.9, 77.2 (CDCl₃), 130.9, 131.0, 132.9, 133.9, 137.0, 140.9, 141.6, 142.4, 142.9, 143.0, 143.6, 143.9, 144.0, 145.0, 146.0, 146.5, 147.1, 147.4, 147.6, 148.5, 148.6, 148.8, 149.2, 149.3, 149.4, 150.6, 150.8, 151.2, 151.4, 155.2, 162.9.

MALDI-TOF MS: g/mol (%) = 1578.47 (100), 1594.43 (16).

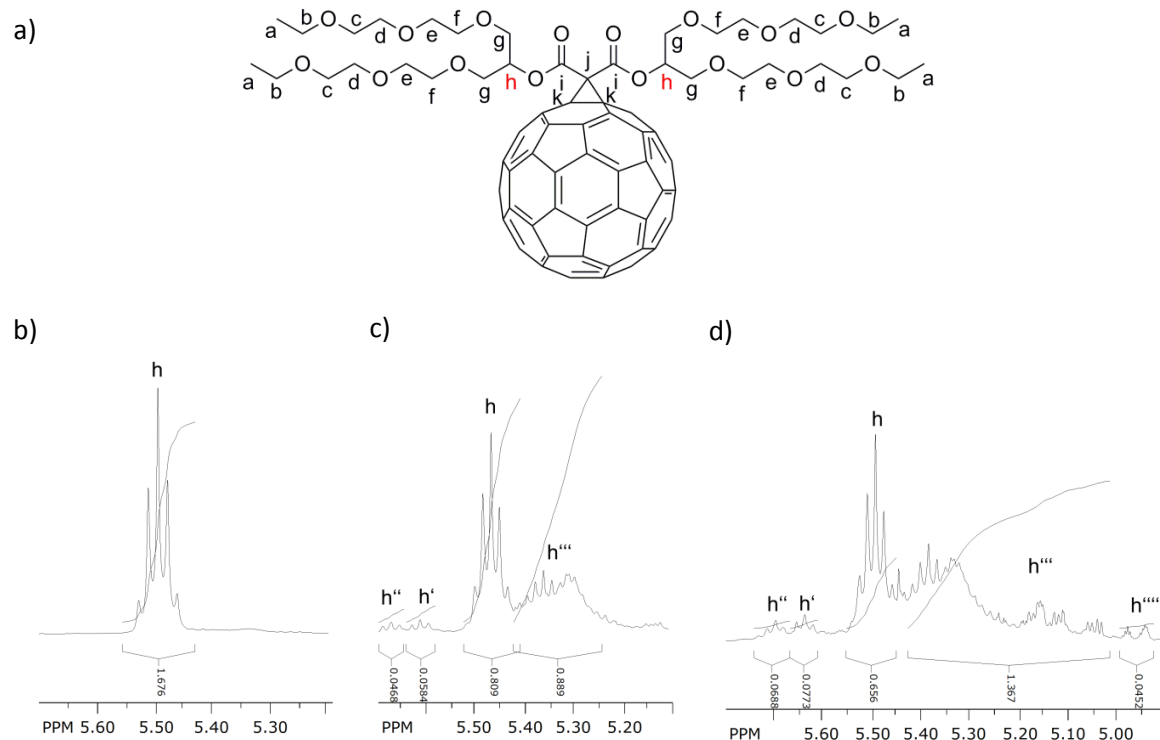


Figure 8-S1: $^1\text{H-NMR}$ segments of Bingel-Hirsch reaction product of malonate with R1 and C_{60} to $\text{C}_{60}-(\text{OEG})_2-1$ using iodine as halogenating reagent. a) shows the monoadduct $\text{C}_{60}-(\text{OEG})_2-1$ with labelled proton positions. The stoichiometric reactant ratio C_{60} :malonate amounts to b) 1.0:0.7, c) 1.0:1.0 and d) 1.0:1.2. Here, all $^1\text{H-NMR}$ sections were recorded after singular purification via conventional flash chromatography. The quintet h represents the fullerene monoadduct. h' , h'' , h''' and h'''' represent the proton signals of multiadducts at position h. The addition of all integrals on position h should ideally be 2 and therefore give some indication of the ratio monoadduct:multiadducts.

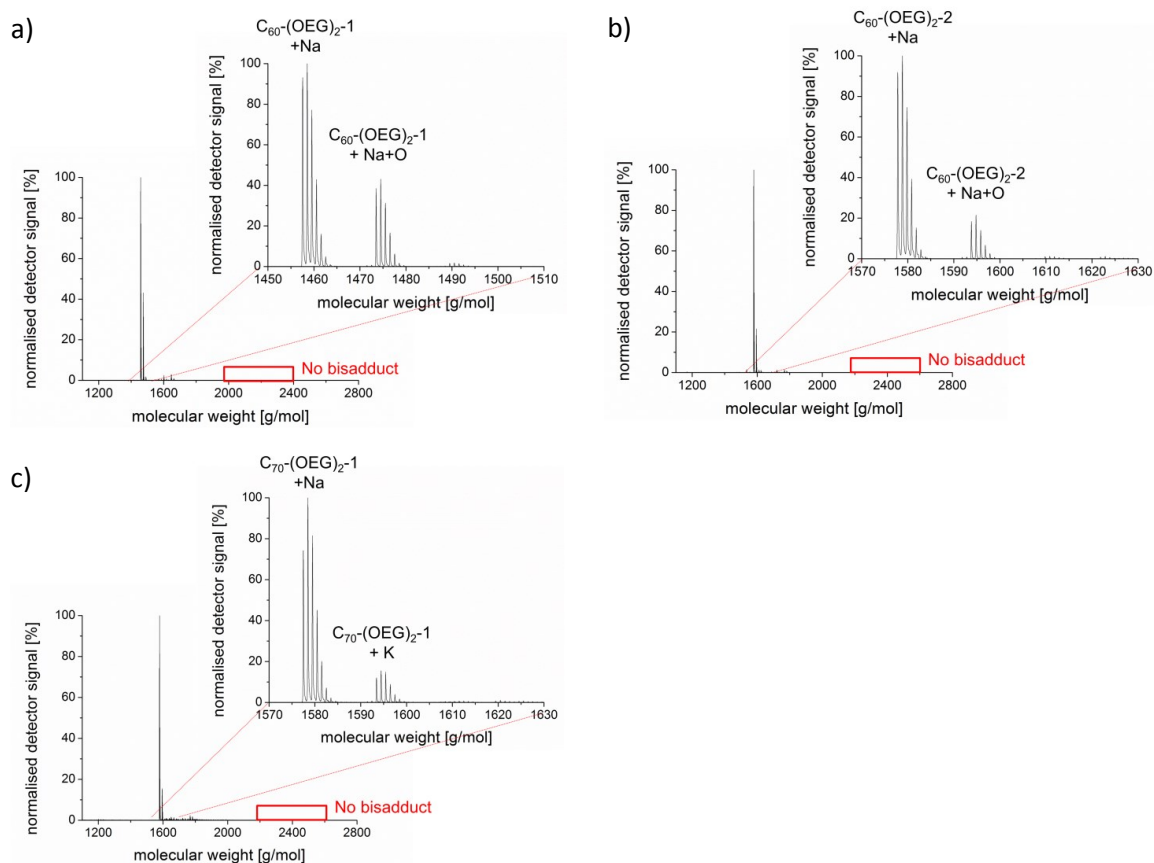


Figure 8-S2: MALDI-TOF spectra of a) $C_{60}-(OEG)_2-1$, b) $C_{60}-(OEG)_2-2$ and c) $C_{70}-(OEG)_2-1$. An enlarged section is shown in the inset. Here the isotopic splitting can be clearly seen. Attached sodium (Na) and potassium (K) ions derive from the used matrix (trans-3-indoleacrylic acid (IAA)).

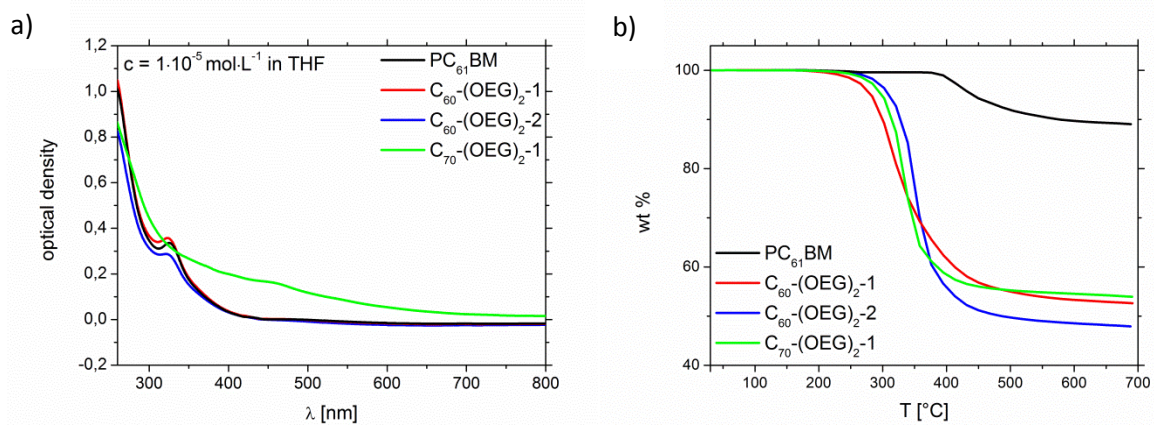


Figure 8-S3: a) UV-Vis absorption spectra of $1 \cdot 10^{-5} \text{ mol L}^{-1}$ solutions of $PC_{61}BM$, $C_{60}-(OEG)_2-1$, $C_{60}-(OEG)_2-2$ and $C_{70}-(OEG)_2-1$ in THF. b) Thermogravimetric analysis of $PC_{61}BM$, $C_{60}-(OEG)_2-1$, $C_{60}-(OEG)_2-2$ and $C_{70}-(OEG)_2-1$. Before measurement the fullerene derivatives were heated for 90 minutes at $120 \text{ }^\circ\text{C}$ to remove attached water.

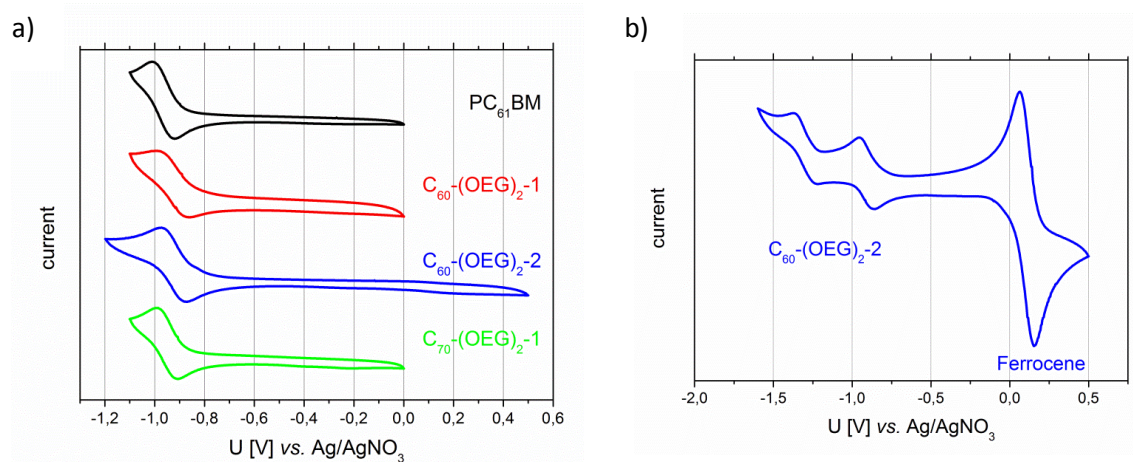


Figure 8-S4: a) Cyclic voltammograms of PC₆₁BM, C₆₀-(OEG)₂-1, C₆₀-(OEG)₂-2 and C₇₀-(OEG)₂-1 measured in DCM. Here, the first reduction peaks were recorded exclusively. b) Cyclic voltammogram of C₆₀-(OEG)₂-2 and the standard ferrocene. Typical multi-reduction peaks in CV observed for all fullerene derivatives.

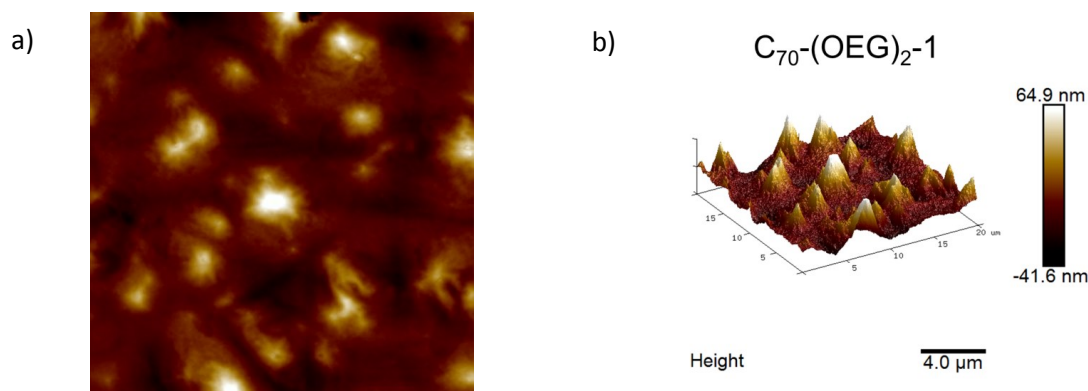


Figure 8-S5: a) Height AFM image (20x20 μm) of a C₇₀-(OEG)₂-1 film shown in 2D and b) 3D.

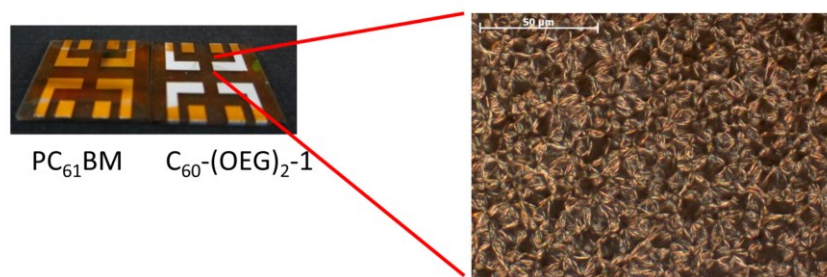


Figure 8-S6: Typical Image of an electron-only device of PC₆₁BM (left) next to one of C₆₀-(OEG)₂-1 (right). The magnification of a metal contact on C₆₀-(OEG)₂-1 was recorded using a microscope. Due to softness of the new derivative film, the top metal electrodes had a white appearance instead of the usual shiny metal appearance.

SCLC: Charge carrier mobility

The charge carrier mobilities were evaluated by fitting measured I–V characteristics using the Murgatroyd formula (Equation 1).

$$J = \frac{9}{8} \varepsilon_s \varepsilon_0 \mu_0 \exp(0.89\gamma\sqrt{F}) \frac{V^2}{L^3} \quad (1)$$

Here J is the current density, ε_s the relative permittivity of the material, ε_0 the permittivity of vacuum, μ_0 the charge carrier mobility at zero field, γ the field dependence parameter, F the average electric field across the active layer, V the voltage across the active layer, and L the thickness of the polymer layer. For fitting, a typical value of 3.5 was assumed for ε_s as most organic semiconductors have dielectric constants in the range of 3-4. A small expected increase in ε_s after OEG substitution will not reduce the final calculated mobility value considerably. After fitting of two independent parameters (μ_0 and γ), the charge carrier mobility was determined.

Table 8-S1: Listing of film thicknesses and fitting parameters for all the electron-only devices.

Active layer	Thickness [nm]	Fitted mobility [cm ² V ⁻¹ s ⁻¹]	Fitted gamma [V ^{-0.5} m ^{0.5}]	Mobility at 5 x 10 ⁶ Vm ⁻¹ [cm ² V ⁻¹ s ⁻¹]
PC ₆₁ BM	470	1.2 x 10 ⁻⁵	1.8 x 10 ⁻³	7.3 x 10 ⁻⁴
PC ₆₁ BM	615	1.4 x 10 ⁻⁶	2.6 x 10 ⁻³	4.7 x 10 ⁻⁴
PC ₆₁ BM	979	2.3 x 10 ⁻⁶	2.5 x 10 ⁻³	6.2 x 10 ⁻⁴
C ₆₀ -(OEG) ₂ -1	305	1.0 x 10 ⁻³	1.2 x 10 ⁻³	1.6 x 10 ⁻²
C ₆₀ -(OEG) ₂ -1	348	1.3 x 10 ⁻³	1.4 x 10 ⁻³	2.9 x 10 ⁻²
C ₆₀ -(OEG) ₂ -1	802	5.6 x 10 ⁻⁵	2.9 x 10 ⁻³	3.9 x 10 ⁻²
C ₆₀ -(OEG) ₂ -2	613	9.6 x 10 ⁻⁵	1.2 x 10 ⁻³	1.4 x 10 ⁻³
C ₆₀ -(OEG) ₂ -2	630	5.4 x 10 ⁻⁵	1.6 x 10 ⁻³	1.9 x 10 ⁻³
C ₆₀ -(OEG) ₂ -2	679	3.8 x 10 ⁻⁵	1.6 x 10 ⁻³	1.4 x 10 ⁻³
C ₆₀ -(OEG) ₂ -2	705	5.9 x 10 ⁻⁵	1.8 x 10 ⁻³	3.1 x 10 ⁻³

LIST OF PUBLICATIONS

- [1] “Controlled Synthesis of Water-Soluble Conjugated Polyelectrolytes Leading to Excellent Hole Transport Mobility”
by J. C. Brendel, M. M. Schmidt, G. Hagen, R. Moos, M. Thelakkat.
In *Chem. Mater.* **2014**, *26*, 1992-1998.
- [2] “A High Transconductance Accumulation Mode Electrochemical Transistor”
by S. Inal, J. Rivnay, P. Leleux, M. Ferro, M. Ramuz, J. C. Brendel, M. M. Schmidt, M. Thelakkat, G. G. Malliaras.
In *Adv. Mater.* **2014**, *26*, 7450-7455.
- [3] “Conjugated Polyelectrolyte Blend as Photonic Probe of Biomembrane Organization”
by E. Zeglio, M. M. Schmidt, M. Thelakkat, R. Gabrielsson, N. Solin, O. Inganäs.
In *ChemistrySelect* **2016**, *1*, 4340-4344.
- [4] “Conjugated Polyelectrolyte Blends for Highly Stable Accumulation-Mode Electrochemical Transistors”
by E. Zeglio, M. M. Schmidt, M. Thelakkat, R. Gabrielsson, N. Solin, O. Inganäs.
In *Chem. Mater.* **2017**, *29*, 4293-4300.
- [5] “Smaller Counter Cation for Higher Transconductance in Anionic Conjugated Polyelectrolytes”
by M. M. Schmidt, M. ElMahmoudy, G. G. Malliaras, S. Inal, M. Thelakkat.
In *Macromol. Chem. Phys.* **2017**, 1700374.

ACKNOWLEDGEMENT

At this point, I want to sincerely thank everybody who contributed directly or indirectly to the success of this thesis.

First, I want to thank my supervisor, Prof. Dr. Mukundan Thelakkat. Thanks a lot for the confidence in me and the interesting PhD topic. Your openness to scientific discussions, your critical point of view and your plain-spoken personality account very much for the success of this thesis. Furthermore, I want to thank you for the well-equipped lab space and the freedom in planning and realizing my studies. Thanks a lot for supporting my visits to conferences and seminars and for helping me in planning my internship at the Centre Microélectronique de Provence.

Thanks to the Research Training Group 1640 “Photophysics of Synthetic and Biological Multichromophoric Systems“ of the German research community and the elite study program Macromolecular Science for the financial support. This allowed me to visit seminars and conferences as well as my research stay in France.

I want to thank Prof. Dr. George Malliaras for the good collaboration and the possibility to work for three months in his group. I have learned a lot at this time and really enjoyed my stay. Some big thanks go also to his group, which received me heartily and took good care of me at all times. At this point I want to give special thanks to Dr. Sahika Inal. Thanks a lot for the collaboration and that you always freed some time for my questions. Thank you that you taught me the basics of bioelectronics. A further thank you to Dr. Mohammed ElMahmoudy for the pleasant time together in a shared office and the help with the measurement and analysis of QCM data. Dr. Anna Maria Pappa is thanked for the OECT substrates.

Sincere thanks to Prof. Dr. Olle Inganäs and Dr. Erica Zeglio for the fruitful collaboration on polyelectrolyte blends.

I thank the collaborators and colleagues at the University of Bayreuth for the cooperation and many fruitful discussions. In this connection, the chair of MC1 is thanked especially. Without you, a lot of things would not have been possible.

Thanks to Chetan Raj Singh for the help with the analysis of the mobility measurement data and for the many fruitful discussions. Thanks a lot for always having time and an open ear for my questions. Dr. Beate Förster is heartily thanked for the EDX/WDX measurements. These had answered a lot of my scientific questions and contributed significantly to this work. Many thanks

for your support. Sebastian Gödrich and his supervisor Prof. Dr. Georg Papastavrou is thanked for QCM measurements and discussions around that topic. Markus Hund is thanked for the introduction and support at the AFM, Paul Reichstein and Tina Weller for the size exclusion chromatographic measurements. Dr. Christoph Hunger and Dr. Tanaji Gujar is thanked for the pleasant office atmosphere. A great thanks to Martina Fried, Sandra Ganzleben and Jutta Failner for the supply of distilled solvents and for sharing their experiences. I want to thank Christina Wunderlich, Petra Weiss and Claudia Geier that I was allowed to come to you with every problem and for the help with all the administrative issues. Jonas Mayer and Alexander Kern are gratefully acknowledged. Thanks a lot for the help with many provisional measurement setups. I really enjoyed working with both of you! A lot of things would not have been possible without your creative ideas and solutions. Many thanks go to all members of the Research Training Group 1640. I was feeling very well as part of the Group and learned a lot. The conversations with PhDs and professors of different disciplines contributed to the success of this thesis. My former student apprentices Florian Dressel, Martin Rieß, Andreas Frank, Philip Schmode, Tobias Maur and Teresa Menzel is thanked for their effort in the lab.

A debt of gratitude is owed to my longstanding companions at the University of Bayreuth, Sebastian Gödrich, Isabel Wittmann, Annika Eckhardt, Stefen Czich, Daniel Weiß, Christina Saller, Hubertus Burchardt, Christoph Hunger and Johannes Brendel. The time in Bayreuth would not have been as well without all of you. Many thanks for the many common, especially joyful hours! You made my time in Bayreuth to an also privately worthwhile time! I hope, we will stay in touch even though our ways are leading in many different directions now.

Heartily thanks go to my parents Christa and Karlheinz, as well as to my siblings Simone and Florian. I can always rely on all of you! My godparents, Margarete and Hartmut Bauer, are also especially thanked. Thanks a lot, that I can come to you every time and that you are always there for me. Every one of you is an important part of my life. To this also Stefan belongs. Many thanks to you, that I always can count on you and that you manage to make me laugh again in almost every situation. A heartily thanks to all of you that you were and will be on my side in good as well as in difficult times. All of you give me a lot of strength.

I want to single out my father Karlheinz Schmidt, to whom I dedicate this thesis. Thanks a lot, that you always supported me and gave me freedom to take my decisions. Many thanks, that you always believed in me, even when I started to doubt. You are in many ways my hero and I am proud to be your daughter. I miss you!

DANKSAGUNG

An dieser Stelle möchte ich allen herzlich danken, die direkt oder indirekt zum Erfolg dieser Arbeit beigetragen haben.

Der erste Dank gilt meinem Betreuer, Prof. Dr. Mukundan Thelakkat. Vielen Dank für das mir entgegengebrachte Vertrauen und das spannende Promotionsthema. Deine Bereitschaft zu wissenschaftlichen Diskussionen, Deine kritische Betrachtungsweise und Deine stets offene Art haben sehr zum Gelingen dieser Arbeit beigetragen. Des Weiteren möchte ich mich für den sehr gut ausgestatteten Laborplatz und die großen Freiheiten bei der Planung und Umsetzung meiner Forschungsarbeiten bedanken. Danke, dass Du mir viele Konferenz- und Seminarbesuche ermöglicht und mich bei der Planung meines Forschungsaufenthalts an dem Centre Microélectronique de Provence unterstützt hast.

Bei dem Graduiertenkolleg 1640 „Photophysics of Synthetic and Biological Multichromophoric Systems“ der Deutschen Forschungsgemeinschaft und dem Elitenetzwerk Bayern bedanke ich mich für die finanzielle Unterstützung. Diese Förderung ermöglichte mir sowohl Besuche von Seminaren und Konferenzen als auch meinen Forschungsaufenthalt in Frankreich.

Bei Prof. Dr. George Malliaras möchte ich mich besonders für die gute Zusammenarbeit und die Möglichkeit drei Monate in seinem Arbeitskreis zu verbringen bedanken. Ich habe sehr viel in dieser Zeit gelernt und habe mich sehr wohl gefühlt. Seiner Arbeitsgruppe möchte ich danken, dass ich von ihnen herzlich aufgenommen wurde und sie sich jederzeit gut um mich gekümmert haben. Dabei möchte ich besonders Dr. Sahika Inal herausheben. Vielen Dank, dass ich mit Dir zusammen arbeiten durfte und Du Dir stets für meine Fragen Zeit genommen hast. Danke, dass ich so viel von Dir lernen durfte. Dr. Mohammed ElMahmoudy möchte ich für die gute Zeit im gemeinsamen Büro und für seine Unterstützung bei der Messung und Auswertung von QCM Daten danken. Dr. Anna Maria Pappa gilt ein besonderer Dank für die zur Verfügung gestellten OECT Substrate.

Meinen Kooperationspartnern Prof. Dr. Olle Inganäs und Dr. Erica Zeglio danke ich für die erfolgreiche und interessante Zusammenarbeit bezüglich Polyelektrolyt-Blends.

Den Kooperationspartnern und Kollegen an der Universität Bayreuth danke ich für die sehr gute Zusammenarbeit und viele hilfreiche Diskussionen. Hierbei sei auch der Lehrstuhl MC 1 besonders erwähnt. Ohne Euch wäre vieles nicht möglich gewesen.

Chetan Raj Singh möchte ich für die Unterstützung bei der Auswertung von Mobilitätsmessungen danken und für die vielen hilfreichen Diskussionen. Vielen Dank, dass Du

Dir für mich und meine Fragen immer Zeit genommen hast. Bei Dr. Beate Förster bedanke ich mich für die EDX/WDX Messungen. Diese Messungen haben viele meiner wissenschaftlichen Fragen beantworten können und maßgeblich zum Erfolg dieser Arbeit beigetragen. Herzlichen Dank für Deine Unterstützung. Sebastian Gödrich und seinem Betreuer der Doktorarbeit, Prof. Dr. Georg Papastavrou, möchte ich für die Unterstützung durch QCM Messungen danken.

Ein herzlicher Dank geht auch an Markus Hund für die Einweisung und Unterstützung am AFM, und Paul Reichstein und Tina Weller für GPC Messungen. Dr. Christoph Hunger und Dr. Tanaji Gujar möchte ich für die gemeinsame Bürozeit danken. Ein großes Dankeschön geht an Martina Fried, Sandra Ganzleben und Jutta Failner für die Bereitstellung destillierter Lösungsmittel und das Teilen Ihres Erfahrungsschatzes. Vielen Dank an Christina Wunderlich, Petra Weiss und Claudia Geier, dass ich mit Problemen jeglicher Art zu Euch kommen durfte und Ihr mich stets bei administrativen Angelegenheiten unterstützt und angeleitet habt. Des Weiteren möchte ich Jonas Mayer und Alexander Kern danken. Vielen Dank, dass Ihr mir bei vielen provisorischen Messaufbauten geholfen habt. Es hat mir sehr viel Spaß gemacht mit Euch zu arbeiten! Vieles wäre ohne Eure kreativen Ideen und Lösungen nicht möglich gewesen. Den Mitgliedern des Graduiertenkollegs 1640 möchte ich ebenfalls meinen besonderen Dank aussprechen. Ich habe mich in GRK immer sehr wohl gefühlt und habe viel gelernt. Der Austausch mit Doktoranden und Professoren aus verschiedenen Fachrichtungen hat sehr zum Gelingen dieser Arbeit beigetragen. Meinen ehemaligen Praktikanten Florian Dressel, Martin Rieß, Andreas Frank, Philip Schmode, Tobias Maur und Teresa Menzel sei für ihren Einsatz im Labor gedankt.

Meinen langjährigen Wegbegleitern an der Universität Bayreuth, Sebastian Gödrich, Isabel Wittmann, Annika Eckhardt, Steffen Czich, Daniel Weiß, Christina Saller, Hubertus Burchardt, Christoph Hunger und Johannes Brendel möchte ich einen besonderen Dank aussprechen. Ohne Euch wäre die Zeit in Bayreuth nicht so schön geworden! Danke, für die vielen gemeinsamen, vor allem lustigen Stunden! Ihr habt meine Zeit in Bayreuth zu einer auch privat sehr wertvollen Zeit gemacht! Ich hoffe, wir bleiben in Kontakt auch wenn wir nun in viele Richtungen verstreut sind. Einen herzlichen Dank richte ich an meine Eltern Christa und Karlheinz, sowie an meine Geschwister Simone und Florian. Auf Euch kann ich mich immer verlassen. Meinen Pateneltern, Margarete und Hartmut Bauer sei ebenfalls besonders gedankt. Danke, dass ich jederzeit zu Euch kommen kann und Ihr immer für mich da seid. Ihr seid ein wichtiger Teil meines Lebens. Zu diesem gehört auch Stefan. Vielen Dank, dass auf Dich immer Verlass ist und Du mich in nahezu jeder Situation wieder zum Lachen bringst. Ein herzliches Dankeschön, dass Ihr auch in schwierigen Zeiten immer an meiner Seite wart und seid. Ihr alle gebt mir sehr viel Kraft.

Der größte Dank gilt meinem Vater Karlheinz Schmidt, dem diese Doktorarbeit gewidmet ist. Vielen Dank, dass Du mich immer unterstützt hast und mir in meinen Entscheidungen jegliche Freiheit gewährt hast. Danke, dass Du immer an mich geglaubt hast, auch wenn ich selbst an mir gezweifelt habe! Du bist in vielerlei Hinsicht ein großes Vorbild für mich und ich bin stolz darauf, Deine Tochter zu sein. Ich vermisse Dich!

ERKLÄRUNG

nach der Promotionsordnung für die Bayreuther Graduiertenschule für Mathematik und Naturwissenschaften (BayNAT) vom 15.September 2017

(§ 9 S. 11 Nr. 3)

Hiermit versichere ich eidesstattlich, dass ich die Dissertation selbständig verfasst und keine anderen als die von mir angegebenen Quellen und Hilfsmittel benutzt habe. Ich habe die Dissertation nicht bereits zur Erlangung eines akademischen Grades eingereicht und habe nicht bereits diese oder eine gleichartige Doktorprüfung endgültig nicht bestanden.

(§ 9 S. 11 Nr. 4)

Hiermit erkläre ich, dass ich keine Hilfe von gewerblichen Promotionsberatern bzw. -vermittlern oder ähnlichen Dienstleistern weder bisher in Anspruch genommen habe noch künftig in Anspruch nehmen werde.

(§ 9 S. 11 Nr. 7)

Hiermit erkläre ich mich damit einverstanden, dass die elektronische Fassung meiner Dissertation unter Wahrung meiner Urheberrechte und des Datenschutzes einer gesonderten Überprüfung unterzogen werden kann.

(§ 9 S. 11 Nr. 8)

Hiermit erkläre ich mich damit einverstanden, dass bei Verdacht wissenschaftlichen Fehlverhaltens Ermittlungen durch universitätsinterne Organe der wissenschaftlichen Selbstkontrolle stattfinden können.

Bayreuth, den 28.05.2018

Martina Schmidt